Ping Guo Thesis

ABSTRACT

This thesis relates to a study of two deep excavations in Gold Coast, one at Surfers Paradise and the other at Southport, the depth of the excavations are 11.65 and 9.7m respectively. Both excavations are supported by secant piled wall. At the excavation in the Surfers paradise, only the upper part of the secant piled wall was reinforced and the bottom part below (14.5m and extending to 27m) was not reinforced and functioned mainly as a cut off wall. The main subsoil at both sites is sand with different degree of denseness. Five distinct layers of subsoil are identified and modelled inn this study. Peat layer was encountered in one excavation at the Surfers paradise site. Three rows of anchors were used at the Surfers Paradise excavation while only one row was used at Southport.

SPT tests were the only source of data available for the estimation of the geotechnical parameters needed in this study. As such, various well established correlations of the SPT with the engineering properties were critically studied and adopted.

The design analysis of the excavations was based on the well known WALLAP Program which is based on a spring beam concept and relies on limit analysis as well. The current study used a continuum approach and the user- friendly PLAXIS program. Both the WALLAP and the PLAXIS analysis are found to give similar results in the case of the bending moment of the support wall and the shear force. For the excavation at the Southport site where the support wall terminates at the rock layer, both analyses gave similar results. However at the Surfers Paradise site where the support wall was only reinforced for the upper part, the wall deflections were different; the PLAXIS values are higher by an order of 30-35 percent; the shear force and bending moment diagrams are reasonable the same.

At the Surfers Paradise site, a layer of peat was encountered. The analyses were somewhat difficult with this peat layer as its engineering properties estimated from STP will not be very reliable.

CHAPTER 1

INTRODUCTION

This thesis relates to a study of deep excavations in Gold Coast at two sites one in Surfers Paradise and the other in Southport. The project at Surfers Paradise is called the Circle on Cavill and the one at Southport is called the Sundale. The Circle on Cavill has two tower blocks 70 stories and 40 stories respectively. It also included a four level basement for car parks. The deepest depth of excavation is about 11.7. The Sundale project includes a tower building 30 stories high and a basement of two and three levels. The depth of excavation at the Sundale site is about 9.7m.

For both sites, the basement walls were constructed with secant piles. The diameter of the secant piles at the Circle on Cavill site is 600 mm, while the centre to centre spacing of the hard pile is 850mm. At the Sundale site 500mm secant piles were used as the basement support and the centre to centre distance of the hard pile is 800mm. The typical soil profile at Gold coast as established in this study is an upper layer of loose to medium dense sand varying in thickness from 4 to 5m. This layer is designated as Layer A in this thesis. Below this layer is a second layer of dense to very dense sand named as Layer B. This layer varied in thickness from about 9m to 11m. The third layer is peat and it is called Layer C its, thickness varied from 4 to 5m. The fourth layer is again dense to very dense sand varying in thickness from 5 to 8m. This fourth layer named Layer D is followed by a fifth Layer called Layer E and this is sandy clay varying in thickness from 5m to 9m. Below the sandy clay is the rock formation. At the Circle on Cavill site altogether 16 borehole data was available while at the Sundale site 8 borehole data are analysed. From these data idealized soil profile models were established.

Secant piled wall overcomes effectively the problem of the lacking of water tightness by its interlocking with contiguous bored piles. The secant piled walls offer the advantages of increased construction alignment flexibility, increased wall stiffness and can be installed in difficult ground conditions.

In the last two decades the geotechnical engineering practice began to rely on numerical analysis and a continuum approach in which the deformations of the soil and adjoining structures can be evaluated using various computer softwares. The design of these support walls at both sites were made with the WALLAP computer software by the designers and the contractors. WALLAP is widely used software developed by Borin (1988). It is very common to use this program in retaining wall analysis and the program allows to model the process of wall excavation, dewatering, placement of surcharge and the instalment of anchors. Three levels of anchors were used at the excavation in Circle on Cavill and only one level of anchor was used at the Sundale site.

In the analysis of retaining structures, two approaches are often used for modelling. One of them is the spring beam method and the WALLAP program is based on the spring beam method. The second method of the use of continuum approach softwares such as PLAXIS, CRISP, FLAC etc are now well known. Among these PLAXIS has recently been adopted internationally and is also continuously researched and updated. In this thesis the 2D plane strain version of PLAXIS is used for a detail analysis of the excavations at the Circle on Cavill and Sundale. An important feature to note is at both sites, the water table is high and also the subsoil is predominantly sand.

Well documented case histories are available in the literature of deep excavations in sand and also with water table close to the surface. Many factors influence significantly the results of numerical prediction , such as the of appropriate soil parameters, the dewatering, the surcharge from surrounding buildings, the stiffness of the wall, the anchor pre-stress and the anchor spacing, etc. In common design, engineers adopt worst consideration to obtain the conservative results. Field measurement is not common in Gold Coast considering the factors of cost and subsoil conditions encountered in Gold Coast.

The objectives of this thesis are:

- The establishment of the sub-soil profile model for Surfers Paradise and Southport in Gold Coast.

- The establishment of reliable geotechnical soil models for deep excavation analysis

- Perform PLAXIS analysis for the performance of the excavation and compare the results with the WALLAP Analysis

The layout of the thesis is an introductory chapter followed by Chapter 2 on the literature pertinent to deep excavation problems in subsoil conditions similar to Gold coast. The review also incorporated the advantages and disadvantages of different wall support systems, such as the use of sheet piled walls and diaphragm walls as well. The selection of appropriate wall system, a brief note is also made on the anchor characteristics. There are many factors which influence the excavation practice of which the lateral wall movements and the settlement of adjacent soil layers are quite important. Also presented in the review are the general pattern of ground movements, the lateral earth pressure distribution on walls, pore water pressure distribution, the prestress in anchors and the bending moment of the walls.

In Chapter 3 numerical methods and their salient features are presented. Contained in some detail are the important aspects of the WALLAP Program and the PLAXIS Software. The WALLAP program incorporates a limit equilibrium approach and as such safety factors can be deduced and the program can present envelopes of bending moment and shear forces in addition to the lateral deformation. The PLAXIS program has novel

features such as automatic mesh generation, ability to include interfaces, anchors, geogrids etc. Also, a wide choice of soil and rock models is available including, elastic, elastic-plastic. Visco-elastic-plastic behaviour in soils and jointed rock behaviour in rocks. Soft soil models and hardening models can also be incorporated in PLAXIS. The analysis can be in the undrained or drained mode. Coupled analysis can also be performed to incorporate time dependent consolidation phenomenon.

CHAPTER 2

LITERATURE REVIEW

2.1 General

In this section as review of the literature on excavations in soils is presented. It includes details of the secant piled wall support system and a comparison with other support system such as the sheet piled wall and diaphragm wall. It appears that the secant piled wall types are more appropriate for deep excavation practice in Gold Coast where the water table is high. A notable feature in Gold coast is for deep excavations strutted and braced excavations are not used and all excavations have the use of anchors. This type of support system gives adequate space inside the excavation for construction activities without any obstruction by internal struts and bracings. Thus a review is also made on the use of anchors in deep excavations. The other aspects discussed in this chapter are the various factors which influence the excavation behaviour, the lateral movement of secant piled wall during excavation, the general pattern of ground movement, the bending moment of retaining walls, the lateral earth pressure distribution, the pore water pressure distribution, the anchor arrangement and pre-stress.

2.2 Secant piled wall and other support systems.

In both the deep excavations studied in this thesis at Circle on Cavill and Sundale sites, secant piled wall support system was used. It is thus appropriate to compare such a support system with other traditional support systems. At the Gold coast sites ground water table is high and often dewatering is used to lower the water table in the excavation zone. Further, the subsoil conditions are predominantly sand. As such water tightness of the support system is quite important. Secant piles wall overcomes effectively the problem of lacking of watertightness happened in contiguous bore piles wall by interlocking which is just suitable for condition of high ground water; thus it is the most common type adopted in Gold Coast.

Secant pile walls are formed by constructing intersecting reinforced concrete piles, which are called " hard and soft " pile or "male or female " pile system, as shown in Figure 2.1 Every second pile is reinforced and constructed from full-strength concrete, the intermediate piles are not reinforced, and are sometimes constructed of a "soft" concrete. The hard or male piles are reinforced with either steel rebar or with steel beams and are constructed by either drilling under mud or auguring. Pile overlap is typically in the order of 80 mm (Bowles, 1993).

The secant piled wall offers the advantage of increased construction alignment flexibility, increased wall stiffness and can be installed in difficult ground conditions. Of course the

cost is high compared to sheet piled wall support system. Also waterproofing can be difficult at the joints and at deep depths the verticality tolerance can be compromised as well. The pile type can be adjusted in stiffness and strength by choosing suitable pile diameter. However, the disadvantage of secant piles wall is lack of durability of soft piles for permanent construction. (Malcolm Puller, 1996).

A brief note on the sheet-piled wall and diaphragm wall support systems is also presented here. Sheet pile wall is commonly used as temporary retaining wall system in shallow excavations due to its lower stiffness compared to other types of retaining wall such as diaphragm wall, contiguous bored piles or secant pile. It is suitable for the subsoil that "N" value is lower than 50 or else it would be difficult to achieve the required penetration. The selection of sheet pile depends on the requirement of the flexural strength and strength to resist driving. Driving of sheet piles in loose sandy soils can results in settlements in adjacent ground. Some seepage is expected pass through the interlocking steel sheet piling if there is a difference in hydraulic head. Diaphragm wall offers the most efficient watertightness compared to other wall types. It causes minimum noise and vibration disturbance. However, it is not suitable for highly collapsible soil during trenching. Meanwhile, it cost much higher to maintain the equipment compared to secant pile wall, so that it is not popular used in Gold Coast.

Construction sequence of secant piled wall and the selection of support systems.

In the construction of secant piled wall support system, first a concrete guide wall about 1m thick and of a width 400 to 600 mm (larger than the pile diameters) was constructed. The female piles are then drilled. After hardening, the male piles are drilled; during this process the drilling removes segments of the female piles so an interlock is obtained. The selection of retaining wall type and support system is usually made on the basis of the foundation of adjacent properties and services, designed limits on wall and retained ground movements, subsoil conditions and ground water level, working space requirements and site constraints, cost and time of construction, flexibility of the layout of the permanent works, local experience and available construction plant and the maintenance of the wall and support system in permanent condition.

Cantilevered, strutted and tied back support of excavation walls

The above retaining wall types can be further divided into three major categories according to the form of support provided as shown in Figure 2.2; cantilevered or unbraced wall (usually for shallow excavation), strutted or braced wall and tied -back or anchored wall. Table 2.1 from Institution of Structural Engineers (1975) lists the advantages and disadvantages of each support system. The factors involve in the selection of a support system for a deep excavation as suggested in Navy Design Manual by US Navy (1982) are summarized in Table 2 .2. Although ground anchor system can be used in unobstructed excavation in centre of the site, there are still some factors should be considered (Gue and Tan, 1998): permanents ground anchors always pose great problems in maintenance in long term. Refer BS 8081: 1989 for details; if the local authorities require temporary ground anchors to be removed after use, then remove of temporary

ground anchors may pose some problems if the system has not been proven at site to be fully removable; approval from the adjacent owners should be acquired if there is encroachment of ground anchors into adjacent properties; leakages and loss of fine through drill holes additional precautionary measures in the construction.

2.3 Anchors

Tieback anchors comprise a barrel anchorage located either in a bearing layer which is tensioned at the front face of the wall. The part of the anchors surrounding soil is frequently called the "fixed length", while the "free length" transmits forces from the fixed length through the anchor load to the wall. In order to minimize wall movement and ground settlement tieback anchors are designed to achieve the highest stiffness possible with economical considerations, which is especially common in deep excavation. Tieback capacity depends on the vertical and horned on surcharge conditions. Typical tieback spacing ranges from 2m to 4m in the vertical, and from 1.5m to 4.6m in the horizontal direction. All tiebacks are required to be proof-tested to an excess percentage of their final lock-off load, which usually ranged from 120 to 150%. Regroutable tiebacks are most commonly used because their capacity can be increased by regrouting (to meet test requirements) without having to drill a new anchor hole (Bowles, 1993).

A tieback is made by first drilling a hole with an auger and then placing a bar (tendon) in the hole, then concrete is poured in the hole and then connect with wall is made (Fig 2.3) Different types of augers are used to drill the tieback holes. The choice of the drilling method depends on the soil/rock conditions on the site. Drilling should be done carefully since inadequate procedures can cause significant soil losses. The bi-product of drilling is removed by flushing the hole with air, water, or slurry. Significant soil losses through the tiebacks cause significant settlements even if the retaining walls do not move towards the excavation. For stability reasons, the fixed anchor should be located beyond the active zone of movements (Kempfert, 1994). As a result, tieback anchors is not suitable for the sites congested where there are adjacent underground utilities or when adjacent owners do not grant permission to drill them under their properties.

2.4. Factors Influencing the Excavation Behaviour

Mana and Clough (1981) studied the movement behaviour of supporting system and adjacent ground during excavation by using finite element method, and the result was compared with monitoring measurements on the field. This study shows influencing factors of the excavation behaviours and concluded as follows: factor of safety against basal heave (depends on the embedment depth of the retaining walls and soil strength); stiffness of the supporting system (include the stiffness of strut and retaining wall); preloading of strut; excavation geometry; construction period (time effect). The study defined that the time during excavation may influence the displacement behaviour of the wall, especially in the soft to medium stiff clay layers.

O'Rourke (1981) proposed that during site preparation, ground movements might be caused by: relocating and underpinning of utilities; de-watering; construction of the excavation wall; pre-loading of strut. Yin ,Barry and Chan (1998) mentioned that the influential factors for deep excavation can be summarized as follows: effects of stress changes within the subsoil; dimensions of the excavation; soil properties; initial horizontal stresses within the soil; groundwater conditions and changes to them;. stiffness of the sheeting and the bracing system; effects of pre-loading in bracing and anchoring; construction methods and construction workmanship.

The study by Chan (1998) focused on the factors like soil properties, initial horizontal stress within the soil, groundwater conditions and changes to them and stiffness of sheeting and bracing system for typical excavations in frictional soils using FLAC program. The results were mentioned as follows: the horizontal displacement of sheet piled (vertical soil settlement, total strut load, shear force and bending moment) is factors such as friction angles,) SPT "N" value, dilation angle, sheet pile stiffness, horizontal strut stiffness, and vertical strut spacing; decreasing the distance between the vertical strut is the most effective method to reduce horizontal displacement; increasing the depth of excavation results in large displacement.

Briaud and Kim (1998) use beam-column methods to analyse tie-back wall, they found the factors that influence the bending moments and deflection predictions the most are the coefficient of active earth pressure Ka and the bending stiffness of the wall EI. The other parameters such K_0 and K_p have little influence.

2.5 Lateral Movement of Secant Piled Wall During Excavation

Clough and O'Rourke (1990) indicated that the pattern of the wall movement could simply be divided into three types: (1) cantilever movement (2) deep inward movement (3) cumulative of cantilever movement and deep inward movement. Most of the excavation movements are of type (3). As shown in Figure 2.4. During the initial stage of excavation and before the installation of strut support or anchorage application, the wall deforms as a cantilever deflection. When the excavation is going deeper, the upper wall movement is restrained by installation of excavation support or stiffening of existing support members, deep inward movement of the wall occurs, and latter movement of the wall is the combination of cantilever and deep inward components (cumulative movement).

Ting and Chan (1991) mentioned that measurements of vertical movements can reflect the horizontal movements which may lead to the practical correlation of wall deflection and its settlement at top. Clough et al. (1989) introduced the charts of computing maximum horizontal wall deformation shown in Figure 2.5. This method relates system stiffness $\rho_s = (EI /\gamma_w h^4)$, where EI is he bending stiffness of the wall, h is the average vertical spacing between support levels and γ_w is the unit weight of water. And factor of safety against basal heave to the maximum horizontal wall movement. Kemfert et al. (1994) analysed the damage occurred due to the deformation of the anchor-soil block system in a deep excavation in South Germany. In this paper, the soil block between the

wall and the middle of the bonded length of the anchor is assumed to act as a soil confined in a cofferdam. The governing horizontal deflection of the cofferdam is the sum of the following deflection components: horizontal deflection of the cofferdam due to excavation (relief of stresses); horizontal deformation due to shear under and within the cofferdam; horizontal deformation due to bending of the cofferdam; horizontal deflection due to other influence such as anchor prestressing, yielding and bending of the anchor, bending of the wall, reduction of the earth pressure at rest, and the interaction between the soil block and the anchor.

Hight and Higgins (1994) pointed out the influence of the wall stiffness on its horizontal displacements and on the ground deformation at proximity (Figure 2.6). The problem corresponds to the theoretical study of the behaviour at short term of a deep excavation (in London). The wall (1m breadth) is characterized by a reference stiffness of E = 28 GPa.

Kempner, et al (1994) presented analytical approaches to determine the horizontal movement of the soil-anchor-wall-system. The soil block between the wall and the middle of the bonded length of the anchor is assumed to act as a soil confined in a cofferdam. The governing horizontal deflection of a cofferdam is the sum of the following deflection components: horizontal deflection of the cofferdam due to excavation (relief of stress); horizontal deformation due to shear near the cofferdam; horizontal deformation due to shear within the cofferdam; horizontal deformation due to bending of the cofferdam; horizontal deflection due to other influences such as anchor prestressing, yielding and bending of the anchor, bending of the wall, reduction of the earth pressure at rest, and the interaction between the soil block and the anchor.

2.6 General Pattern of Ground Movement

Peck (1969) summarized the relationship between total ground settlements behind sheet piled wall and presents a graphical prediction of soil settlement adjacent to the excavation, taking into account of soil type, depth of excavation and distance from excavation (see Figure 2.7). From the figure, the maximum settlement of the first zone (Sand or Hard clay) is around (1%)H, while the excavation in soft clay will have the maximum settlement of (1to 3%)H or even larger. However at that time, the sheet piled wall was used in the study. The figure plotted for the sheet piled wall, cannot reflect the influence of the various other types of walls (such as the secant piled wall) and their rigidity on the settlement behaviour during excavation.

O'Rourke (1981) illustrated that the ground movements caused by braced excavations are related to the deflection patterns at the excavation wall (see Figure 2.8). The parameter C_d was termed as the coefficient of deformation, defined as:

$$C_d = S_w / (S_w + S_w') \qquad \text{Eq. 2.1}$$

S_w = Wall deflection in cantilever mode
S_w' = Wall deflection caused by bulging inward

As cantilever-type movements are allowed to dominate during the excavation phase. The above case histories indicate that the lateral movements of the wall increase with the coefficient C_d. It also shows if the wall is firmly braced at an early stage of excavation, the inward deflection of the wall would lead to horizontal movements that are significantly less than the settlements. Clough and O'Roourke (1990) combined the proposed settlement curves from several studies as stated earlier and concluded the results in a dimensionless plot as shown in Figure 2.9. For the sand and stiff clay layers, the settlement curve may be bounded by a trapezoidal shape and with the maximum ground settlement within the range of (0 ~0.75)H from the wall. Through the trapezoidal curve is capable to distinguish between the settlement curve in soft clay and sandy soil layers, it is unable to specify the settlement near to the wall that is the most critical problem.

Generally, the types of ground movement can be summarized into two shapes (triangular and groove). For the triangular shape, the prediction suggested by Peck (1969) and Ou et al (1993) in ground movement correspond to this type of movement. The prediction suggested by Clough (1990) and Moh et al. (1990) in ground movement correspond to the trough shape.

2.7 Bending Moment of Retaining Wall

There are three types of wall bending moment calculation (Karlsrud, 1986) which can be obtained from (1) earth pressure measurement; (2) rebar strain gauges; (3) inclinometer (curvature of lateral movement curve). Karlsrud (1986) used the Studenterlunden subway system case in Oslo as an example to calculate the wall bending moment, and comparison was made between the above three different methods of bending moment calculation, as shown in Figure.2.10 . It is clear that the results obtained by using second and third methods are closer to each other, while the results from the first method is obviously smaller; especially with the increasing of excavation depth, the differences is obviously smaller, especially with the increasing of excavation depth, the differences become much significant.

Multiple anchoring may be carried out in order to restrict the maximum bending moment in high walls, or to limit lateral wall deformations. Methods of designing multiple anchored wall can be found in James and Jack (1974), Hanna (1980), Hong Kong Geoguide 1 (1982), and Fleming et al. (1985).

Potts and Day (1990) stated that both experimental work (e.g., Rowe,1952) and more recent numerical work (.g., Potts and Fourie,195) indicate that under the same operating conditions stiffer walls attract larger bending moment than more flexible walls (Addenbrooke, et al. 2000).

2.8. Lateral Earth Pressure Distribution

Peck (1969) back-calculated the collected loading measurement of in-situ props and condensed into semi-empirical apparent earth pressure envelopes as shown in Figure 2.11. In fact, the apparent earth pressure diagram could not fully represent the real distribution of lateral earth pressure at any vertical section in a cut; by the way, the exact lateral earth pressure can be measured by earth pressure cell installed. Dibiagio (1972) analyzed the field monitoring data of Telefonhuset case in Oslo. After the final stage of excavation, the lateral earth pressure at active side of the all was larger than the Rankine earth pressure for depth less than 9m, whereas for the following depth, the measured earth pressure became less than the Rankine earth pressure (see Figure 2.12).

Karlsrud (1981) based on the Studenterlunden subway system case in Norway to describe the distribution of the active and passive earth pressure at various depths of excavation. Conclusion was made that the active earth pressure tends to decrease with the increasing of the excavation depth, but at shallow depth, the active earth pressure is larger than the Rankine active earth pressure. On the other hand, passive earth pressure decrease obviously with the depth and measurement of lateral earth pressure is getting larger than the vertical overburden pressure, (γZ).

Liao and Neff (1990) proposed the lateral earth pressure distribution on the wall, and the influences of OCR and pattern of wall movement during excavation, as shown in Figure 2.13, From the figure, lateral earth pressure of normally consolidated clay on the active side of the wall is smaller than lateral earth pressure at rest (K_o), but larger than that in active condition (Ka). For Over-consolidated clay, the lateral earth pressure distribution is more or less same as that of normally consolidated clay, but the distribution curve is more alike a trapezoidal.

2.9 Pore Water Pressure Distribution

Finno and Nerby (1990) have carried out a detailed study in pore water pressure on braced excavation in Chicago HDR-4 test section. The final depth of the excavation was 8.23m with installation of 19m steel sheet pile. Due to the installation of sheet pile, excess pore pressure increases significantly, incorporating the disturbance to the initial stress condition of soil surrounding. Figure 2.14 and Figure 2.15 show the behavior of excess pore water pressure around the excavation during and after sheet pile driving. Followed by Finno and Harahap (1991), an excavation analysis has been carried out by using finite element method, as shown in Figure 2.16, and the result of the analysis varied much with that of field measurement. This may probably be due to large deformation at the back of wall incorporated with the failure of soil.

The effective stress decreases during the excavation process with dissipation of excess pore pressure (usually negative) and may increase with time. In addition, the ultimate value of effective stresses will depend on the amount of stress relief that has been caused by movements during the construction process and the degree of lateral constraint imposed by the wall on soil during the dissipation of excess pore pressure. For sand, most

of the design method of excavation support implicitly assumes that the excavation is dewatered and that there is a significant lowering of the groundwater table behind the braced retaining wall; in cases where relatively impermeable concrete diaphragm walls are used, this assumption may not be valid.

Hsi and Small (1992) indicated that when the excavations are performed below the water table, ground movement is caused by stress release and seepage flow. A drawdown of the groundwater surface often occurs in long excavation period or in permeable materials and the consolidation of soil around the excavation takes place.

Ou and Lai (1994) performed a numerical analysis of deep excavation in layered sandy (Hyperbolic model) and clayey soil deposit (Modified Cam-Clay models). In the analysis, a simulation of dewatering process during excavation was proposed and the dissipation of negative excess pore-water pressure during the actual elapsed time for each construction phase was also modelled. Through parametric studies, the pore-water pressures in the passive zone experience an abrupt decrease immediately after excavation and then gradually recovers with elapsed time. However, it does not experience significant change in the active zone during excavation. The conclusion was made that some degree of dissipation of negative excess pore-water pressure actually occurs during the intermediate excavation stages. This may cause the soil swelling at passive zone of excavation, and hence lead to decrease of the wall deflection and ground surface settlement. Figure 2.17 shows the results of predicted deformation of the retaining wall during excavation by considering the effect of consolidation is smaller than that predicted by undrained analysis. On the other hand, the results indicated that for the case of short period construction and absence of drained material in the clayey layer, the excavation behaviour could be simulated as undrained analysis.

Schweiger and Freiseder (1997) performed the finite element calculations considering process to predict deformations due to deep excavations in soft soils. The lowering of the water table, achieved by vacuum wells inside the excavation, was modelled simply by increasing the unit weight of the soil (loss of buoyancy) in the appropriate area and applying the resulting water pressure on the wall as external load.

2.10 Anchor Arrangement and Pre-stress

Clayton et al (1993) found the use of ground anchors acts to spread ground movement further back from the wall. Settlement adjacent to the wall will depend to some extent on the level of prestress applied to the anchors, and the position of the top row of anchor. The first row of anchors will not normally exceed 4-5 m in depth.

Kempfert (1994) advanced that the ground surface movement behind the wall are governed by the displacement and deformation of the soil block between the back of the wall and the middle point of the fixed length of the ground anchors. The horizontal deflection at the top of the wall would have been reduced by 60% by increasing the anchor lengths by 9 m for the unfavourable ground water position, which almost avoid

the damage, have occurred. And the foundation of the building is better lie fully before the bonded part of the anchor instead of behind it.

Briaud et at (1999) used a three-dimensional nonlinear finite-element analysis to study the influence of various design decision for tie-back wall. There factors included the location of the first anchor, the length of the tendon unbonded zone, the magnitudes of the anchor forces, the embedment of the soldier pile and the stiffness of the piled wall. He found the best position for the first anchor appears to be between 1.2m and 1.5m below the top of wall, but in current practice the first anchor tends to be placed deeper than that. Significant deflections can accumulate during this step, and it is very difficult to eliminate them by further construction. Longer unbounded length particularly for the first anchor leads to somewhat smaller deflections. Cheney's unbonded length for an anchor is equal to the length from the wall to the failure surface plus 1.5m or one-fifth of the wall height, whichever is greater. The failure surface is taken as the plane having a $45^0 + \Phi /2$ angles with the horizontal starting at the bottom of the wall. The magnitude of the anchor loads is the most important factor influencing all variables. It has a direct influence on deflections and bending moments. In the tie-back wall, engineer use the proposed k versus (u_{top}/H) relationship to select anchor lock-off loads that will approximately generate a chosen deflection (see Figure 2.18), where k is the earth pressure coefficient. The use of the k versus (u_{top}/H) relationship should be limited to cases that are similar to the cases used to generate that relationship. Zero deflection can be reached for a constant pressure diagram with pressure intensity equal to $0.4\gamma H$. This pressure is 2 times larger than Terzaghi and Peck's intensity of $0.65K_a\gamma H$.

CHAPTER 3

NUMERICAL METHODS

3.1 Introduction

In the last two decades, the numerical modelling of retaining walls has become increasingly common. Associated with this design activity have been an increase in the monitoring of structures during construction, and an increase in the use of more sophisticated in-situ and laboratory soil-testing methods (Clayton, 1993). Numerical modelling, although often complex, has become more widely used because of:

- Advantages of speed, giving an opportunity to look at a number of different design options.
- The ability it gives to the designer to make predictions which cannot be made in other ways, in particular, the need to predict ground movements around inner-city excavations has been a major consideration.

Several types of computer programs are readily available, these are:

- Computer implementation of wedge/slice methods (e.g. to carry out Coulomb wedge or Sharma non-circular analyses, to determine the force applied to the wall).
- Winkler spring models. Here the soil is modelled either as a series of isolated horizontal springs, or as springs with some form of interconnection, such as WALLAP and FREW.
- Continuum models. These include finite element, boundary element and finite difference numerical approximations. In the case of finite element analysis, the geometry of the soil and the support system (wall, anchors, and props) are approximated by discrete elements, (such as, PLAXIS, CRISP). In the case of the finite difference method, the continuum is divided into areas between regular spaced points, (for example, FLAC).

There is a growing trend in practice to design tieback walls by using the Winkler springs model (Halliburton 1968; Matlock et al, 1981). This computer-based solution is used to predict the bending moment, the axial load, and the deflection profiles of the piles after the anchor loads have been chosen. Compared to the simple pressure diagram approach, the beam-column approach leads to deflection predictions and to improved bending moment profiles; however, the predicted deflections are not as reliable as the bending moments because the model ignores the mass movement of the soil. The finite-element method (FEM) represents another level of sophistication that better models the components involved (Clough, 1984).

The FEM has been used for the analysis of anchored retaining structures by Clough et al. (1972), Tsui (1974), Huder (1976), Desai et al (1986), and Fernandes and Falcao (1988). Contributions on the simulation of the excavation process with the FEM have been made

by Goodman and Brown (1963), Ishihara (1970), Christian and Wong (1973), Chandrasekaran and King (1974), Ghaboussi and Pecknold (1984), and Brown and Booker (1985), Heliu, (1991) and Tanseng (1997).

3.2 WALLAP (WALL ANALYSIS PROGRAM)

WALLAP is a widely used commercial package, available from Geosolve (London) and described by Borin (1988). It has been specifically designed for routine retaining wall design, and implements a number of factors of safety. The program allows the user to model the process of wall excavation, dewatering, placing of surcharge, and the introduction of anchors. Complex water pressure profiles can be defined, providing for steady seepage, submergence and perched water-tables.

3.2.1 Analysis methods

WALLAP offers two separate types of analysis within the one program:

1) Limit Equilibrium Analysis:
   Calculation of Factors of Safety according to one of the following methods:
   -CP2
   -BSC Piling Handbook
   -Burland-Potts
   -Strength factor method

2) Bending moment and Displacement Analysis:
   Modelling of the stage by stage development of forces and wall movements as construction proceeds.

3.2.2 Material models

The wall and soil are modelled as a beam and springs. Two springs models are available:

- Subgrade reaction analysis (for routine design);
- 2-D Finite Element analysis (for a more rigorous approach).

3.2.3 Analysis features

The analysis includes the following features:

- Elastic soil behaviour
- Active and Passive limits
- Effect of construction sequence
- Strut pre-stressing
- Finite length of the wall
- Simple non-linear elastic soil model (optional)
- Soil below the wall (2-D FE analysis only)
- Soil arching (2-D FE analysis only)

The analysis produces an economical design which automatically takes account of any moment reduction due to fixed length support.

The program offers a simple way of modelling the non-linear elastic behaviour which is characteristic of real soil. Hydrostatic or non-hydrostatic Water Pressure Profile may be defined on both sides of the wall. Thus it is possible to model a variety of complex conditions including: seepage, submerged ground, perched water tables and uplift pressures under structures. Strut or anchors can be installed at up to 20 levels and may be pre-stressed. Strut can also be removed after installation.

3.2.4 Parameters in WALLAP

For soil stratums, the following soil parameters are specified:

- Unit weight, γ
- At rest earth pressure coefficient, K_0
- Active and passive earth pressure coeffients, K_a and K_p
- Consolidation state (OC or NC)
- Drained or Undrained soil type
- Cohesion, c
- Soil modulus, E
- Poisson's Ratio, ν

The program offers advice on the selection of values of earth pressure coeffients and soil modulus. The program can calculate earth pressure coefficient from values of soil frictions, wall friction and backfill angle given by the users.

3.2.5 Output

Output from the program consists of:

- Limit equilibrium factors of safety (for cantilever and singly-propped walls only);
- Wall displacement v. depth profile;
- Bending moment, shear force, and earth pressure distributions;
- Anchor loads

To estimate wall movements, WALLAP uses finite elements to model the structural wall, but a Winkler spring model for the soil (Bowles, 1974). In the simplest soil model of homogeneous isotropic linear elastic continuum, at least two parameters are needed (E and v, or G and K) to fully define the soil. The stiffness of the soil is characterized by the modulus of subgrade reaction K_h (usually expressed in terms of force/area/displacement, or pressure per unit displacement) which is the spring constant. The stiffness of the springs must be obtained from experience, since there is no direct relationship between Young's modulus and subgrade reaction (Terzaghi, 1955). Typical ranges of K_h can be obtained from the literature but great care is required owing to the problem-dependent nature of the parameters (Clayton et al., 1993). Values appropriate for strips, rafts, lateral piles and flexible walls are all different. The other input parameters required in WALLAP are initial horizontal stress applied to the wall, and the active and passive earth-pressure coefficients, which are used to calculate the limiting values of horizontal effective stress.

The calculation starts with a wall with balanced horizontal forces applied to it. Spring forces are progressively set to zero, from the top of the wall towards the final depth of excavations, and at the same time the spring stiffness are progressively halved, to model the reduction in support on the excavated side of the wall. As a result of the load imbalance, horizontal wall displacement and bending take place. Proping or anchoring is simulated by the addition of springs at the required stiffness and levels, as modelling of excavation proceeds. (Clayton et al, 1993).

Due to simplifications imposed by the Winkler method, wall is the only component providing distribution of forces, since inter-spring shear is not included in this type of soil model. Winkler spring approximations do not yield the same wall displacements as are given by the more sophisticated types of models. For example, Brook and Spence (1992), who compared the result from WALLAP and FLAC, and concluded that lower stiffness, must be used in Winkler spring models to achieve displacements comparable with those predicted by continuum models (Clayton et al, 1993). For over consolidated soils the value of K_0 can be much higher and in the case of very stiff clays can be in excess of 2. Vaues can be obtained from pressure meter tests or from published papers such as Burland, et al.(1979).

3.3 PLAXIS

3.3.1 Introduction

PLAXIS grew out of research conducted at Delft University of Technology in the late 1970's on the use of finite element methods for geotechnical design. PLAXIS Version 8 is a 2D finite element packaged intended for the two-dimensional analysis of deformation and stability in geotechnical engineering. Geotechnical applications require advanced constitutive models for the simulation of the non-linear and time dependent behaviour of soils. Since soil is a multi-phase material, special procedures are required to deal with hydrostatic and non-hydrostatic pore pressures in the soil. Many tunnel and excavation project involve the modelling of structures and the interaction between the structures and the soil. PLAXIS is equipped with special features to deal with the numerous aspects of complex geotechnical structures. Some of features are listing as follows:

Graphical input of geometry model: The input of soil layers, structures, construction stages, loads and boundary conditions is based on convenient CAD drawing procedures, which allows for a detailed modelling of the geometry cross-section (see Figure 3.1). From this geometry model, a 2D finite element mesh is easily generated.

Automatic mesh generation: PLAXIS allows for automatic generation of unstructured 2D finite element meshes with options for global and local mesh refinement. The 2D mesh generator is a special version of the Triangle generator, which was developed by Sepra. Quadratic 6-node and 4^{th} order 15 node triangular elements are available to model the deformations and stresses in the soil (see Figure 3.2). And Figure 3.3 shows the generated mesh in a standard excavation model.

Plates: Special beam elements are used to model the bending of retaining walls, tunnel linings, shells, and other slender structures. The behaviour of these elements is defined using a flexural rigidity, a normal stiffness and an ultimate bending moment. Interface element is an important element to model soil structure interaction which can be used to simulate the thin zone of intensely shearing material at the contact between structural element and the surrounding soil. Plates with interface may be used to perform many realistic analyses of geotechnical structures (Prakoso & Kulhawy, 2001).

Interfaces: Joint elements are available to model soil-structure interaction. For example, these elements may be used to simulate the thin zone of intensely shearing material at the contact between a wall and the surrounding soil. Values of interface friction angle and adhesion are not generally the same as the friction angle and cohesion of the surrounding soil. The thin-layer interface has been used by previous research such as Clough and Denby (1977); Finno and Harahap (1991) etc.

Anchors: Elastoplastic spring elements are used to model anchors and struts. The behaviour of these elements is defined using a normal stiffness (EA) and a maximum force. A special option exists for the analysis of prestressed ground anchors and excavation supports.

Geogrids: Geogrids (or geotextiles) are often used in practice for the construction of reinforced embankments or soil retaining structures. These elements can be simulated in PLAXIS by the use of special tension elements. It is often convenient to combine these elements with interfaces to model the interaction with the surrounding soil.

Pore pressure: Complex pore pressure distributions may be generated on the basis of a combination of phreatic level or direct input of water pressures. As an alternative, a steady-state groundwater flow calculation can be performed to calculate the pore pressure distribution in problems that involve steady flow or seepage. In addition, PLAXIS distinguishes between drained and undrained soils to model permeable sands as well as nearly impermeable clays. Excess pore pressures are computed during plastic calculation when undrained soil layers are subjected to loads. Undrained loading situations are often decisive for the stability of geotechnical structures.

Automatic loading stepping: The PLAXIS program can be run in an automatic step size and automatic time step selection mode (Figure 3.4). This avoids the need for users to select suitable load increments for plastic calculations and it guarantees an efficient and robust calculation process.

Calculation facilities: The staged construction facility has been extended to allow for the activation and change of external loadings. This system improves the possibilities of varying external loads and combining individual loads with excavation or construction stages. In addition, a new and more robust calculation kernel has been implemented for steady-state groundwater flow calculations. Consolidation calculations have been extended to allow for staged construction in time and also for large deformation effects.

Structural elements have been improved by the inclusion of an enhanced plasticity formulation for plates and anchors

Presentation of results: The PLAXIS postprocessor has enhanced graphical features for displacing computational results. Values of displacement, stress, strains and structure behaviour can be obtained from the output tables. Plots and tables can also presented by MS EXCEL™ by using the provided data. In additional, animations are now available with this latest package, the animations include displacements and forces in structural elements. A report Generator has been implemented to provide a report of input data and output results that can be further edited in MS Word™.

3.3.2 Material Models

PLAXIS supports various models to simulate the behaviours of soil and other soil continua. A short introduction of the available model is given as below:

1) **Linear elastic model (LE)**
   This model represents Hook's law of isotropic linear elasticity. The model involves two elastic stiffness parameters, namely Young's modulus (E), and Poison's ratio (ν). While linear elastic model is very limited for the simulation of soil behaviour, it is primarily used for modelling structure element in the soil.

2) **Mohr-Coulomb model (MC)**
   This model is used as a first approximation of soil behaviour in general. The model involves five parameters, namely Young's modulus (E), Poison's ratio (ν), the cohesion (c), the friction angle (φ), and the dilatancy angle (ψ). Beside this five model parameters, initial soil conditions play an essential role in most soil deformation problems. Initial horizontal soil stresses have to be generated by selecting proper K_0-values

3) **Jointed Rock model (JR)**
   This is an anisotropic elastic-plastic model where plastic shearing can only occur in a limited number of shearing directions. This model can be used to simulate the behaviour of stratified or jointed rock.

4) **Hardening-Soil model (HS)**
   This is an elastoplastic type of hyperbolic mode, formulated in the framework of friction hardening plasticity. Moreover, the model involves compression hardening to simulate irreversible compaction of soil under primary compression. This second-order model can be used to simulate the behaviour of sands and gravel as well as softer types of soil such as clays and silts.

5) **Soft Soil model (SS)**
   This is a Cam Clay type model that can be used to simulate the behaviour of soft soils like normally consolidated clays and peat. The model performs best in situations of primary compression.

6) **Soft-Soil-Creep model (SSC)**
   This is a second order model formulated in the framework of visco-plasticity. The model can be used to simulate the time-dependent behaviour of soft soils like normally consolidated clays and peat. The model includes logarithmic compression.

7) **User-defined soil model**
   This facility allows user to implement a wide range of constitutive soil models to simulate the problem of soil-structures. Such models must be programmed in FORTRAN, then complied as a Dynamic Link Library (DLL) and then added to the PLAXIS program directory.

For cases where the high quality soil parameter are not known with any great certainty, the use of Mohr-Coulomb model (MC) is more appropriate than the sophisticated model available in PLAXIS. Moreover, the MC model and HS model are often used to simulate the hard soils such as compacted soils and over-consolidated clays while the SS model is usually used to simulate the soft soils such as normally consolidated clay and lightly over-consolidated soils.

3.3.3 Types of material behaviour – Material Type

In principle, all model parameters in PLAXIS are meant to represent the effective soil response, i.e. the relation between the stresses and strains associated with the soil skeleton. An important feature of soil is the presence of pore water. Pore pressures significantly influence the soil response. To enable incorporation of the water-skeleton interaction in the soil response PLAXIS offers for each soil model a choice of three types of behaviours:

1) **Drained behaviour:**
   This setting means no excess pore pressure generated. This is clearly the case for dry soil and also for full drainage due to a high permeability (sand) and /or low rate of loading. This option may also be used to simulate long term soil behaviour without the need to model the precise history of undrained loading and consolidation.

2) **Undrained behaviour:**
   This setting is used for a full development of excess pore pressures. Flow of pore water can sometimes be neglected due to a low permeability (clays, peat) and/or a high rate of loading. All effective model parameters should be entered here.

3) **Non-porous behaviour:**
   Using this setting neither initial nor excess pore excess pressures will be taken into account in soil of this type. Applications may be suitable for modelling of concrete or structural behaviour, as well as interface. Non-porous behaviour is often used in combination with the linear elastic model.

3.3.4 Calculations

In the reality of geotechnical engineering practice, a project of calculation phase is the activation of a particular loading at a certain time, the simulation of a construction stage, the introduction of a consolidation period, the calculation of a safety factor, etc. Each calculation phase is generally divided into numbers of calculation steps because the non-linear behaviour of the soil requires loadings to be applied in load steps.

PLAXIS allows for a different type of finite element calculations, including a plastic calculation, a consolidation analysis, Phi-c reduction (Safety analysis), and Dynamics calculation. The first three types of calculations (Plastic, consolidation, Phi-c reduction) optionally allow for the effects of large displacements being taken into account. This is termed Updated mesh. The different types of calculations are explained as follows:

1) **Plastic Calculation**

   A plastic calculation should be selected in order to carry out an elastic-plastic deformation. The stiffness matrix in the plastic calculation is based on the original undeformed geometry. This type of calculation is used in many practical geotechnical applications. In general, a plastic calculation does not take time effects into account, except when the Soft Soil Creep model is used. Considering the quick loading of water-saturated clay-type soils, a plastic calculation may be used for the limiting cases of fully undrained behaviour using the undrained option I the material data sets. On the other hand, the settlements at the end of consolidation can be assessed by performing a fully drained analysis. This will give a reasonably accurate prediction of the final situation, although the precise loading history is not followed and the process of consolidation is not dealt with explicitly.

2) **Consolidation Analysis**

   A consolidation analysis should be selected when it is necessary to analyse the development and dissipation of excess pore pressures in water-saturated clay-type soils as a function of time. PLAXIS allows for true elastic consolidation analyses. In general, a consolidation analysis without adding loading is performed after an undrained plastic calculation. It is also possible to apply loads during a consolidation analysis, but there are some limitations in PLAXIS on the types of loading that can be considered in a consolidation analysis. The first limitation is that it is not possible to perform a staged construction calculation with simultaneous consolidation. Activation or deactivation of clusters and structures must therefore be applied in a proceeding undrained plastic calculation. Another limitation is that the iteration process will not converge as the structure approaches failure. This means that a consolidation analysis cannot be used to analyse failure conditions. Finally, a consolidation analysis in PLAXIS cannot be

performed in the framework of large deformation theory (updated mesh analysis) and can therefore not be used after an updated mesh calculation.

3) Updated Mesh Analysis

An updated mesh analysis is a plastic calculation where effects of large deformations are taken into account. This type of calculation should be considered when deformations are to be expected that significantly influence the shape of the geometry. This stiffness matrix in an updated mesh analysis is asked on the deformed geometry. In addition, a special definition of stress rates is adopted that include rotation terms. These calculation procedures are based on an approach known as an Updated Lagrange formulation. For most applications the effects of large deformations are negligible so that a normal plastic calculation is sufficiently adequate, but there are circumstance under which it is may be necessary to take these effects into accounts. Typical applications are the analysis of reinforced soil structures, the analysis the collapse load of large offshore footing and the study of projects involving soft soils where large deformations can occur.

3.3.5 Output

The PLAXIS postprocessor has enhanced graphical features for displacing computational results. Values of displacement, stress, strains and structure behaviour can be obtained from the output tables. Plots and tables can also presented by MS EXCEL^{TM} by using the provided data. In additional, animations are now available with this latest package, the animations include displacements and forces in structural elements. A report Generator has been implemented to provide a report of input data and output results that can be further edited in MS Word.

3.3.6 Preliminaries on Material Modelling.

A material model is a set of mathematical equations that describes the relationship between stress and strain. Material models are often expressed in a form in which infinitesimal increments of stress are related to infinitesimal increments of strain. All material models implemented in PLAXIS are based on a relationship between the effective stress σ', and the strain ε'. In the following section it is described how stresses and strains are defined in PLAXIS. The basic stress-strain relationship is formulated as well.

3.3.6.1 Stress and Strain

In plan strain condition, according to Terzaghi's principle, stress in the soil are divided into effective stresses,

$$\sigma = \sigma' + \sigma_w \qquad \text{Eq.3.1}$$

Where, σ' is effective stress, and σ_w is pore pressure.

Strains are decomposed into elastic and plastic components for elastoplastic models used in PLAXIS:

$$\varepsilon = \varepsilon^e + \varepsilon^p \qquad \text{Eq.3.2}$$

Where, ε is strain, ε^e is elastic strain and ε^p is plastic strain

3.3.6.2 On the Initials Stresses

In over-consolidated soils the coefficient of lateral earth pressure is larger than for normally consolidated soils. This effect is automatically taken into account for advanced soil models when generating the initial stress using the K0-procedure. The procedure that is followed here is described below.

Consider a one-dimensional compression test, during unloading the sample behaves elastically and the incremental stress ratio, is according to Hooke's Law, given by (see Figure 3.5)

$$\frac{\Delta\sigma'_{xx}}{\Delta\sigma'_{yy}} = \frac{K_0^{NC}\sigma_p - \sigma'^0_{xx}}{\sigma_p - \sigma'^0_{yy}} = \frac{K_0^{NC} OCR\sigma'^0_{yy} - \sigma'^0_{xx}}{(OCR-1)\sigma'^0_{yy}} = \frac{v_{ur}}{1-v_{ur}} \qquad \text{Eq.3.3}$$

Where, K_0^{NC} is the stress ratio in the normally consolidated state;

σ'^0_{yy} is effective horizontal stress;

σ'^0_{xx} is effective vertical stress;

$\Delta\sigma'^0_{yy}$ is horizontal incremental stress ratio;

$\Delta\sigma'^0_{xx}$ is vertical incremental stress ratio;

σ_p is the greatest vertical stress reached previously;

OCR is the over-consolidation ratio;

v_{ur} is small Poisson's ratio.

Hence, the stress ratio of the over-consolidated soil sample is given by:

$$\frac{\sigma'_{xx}}{\sigma'_{yy}} = K_0^{NC} OCR - \frac{v_{ur}}{1-v_{ur}}(OCR-1) \qquad \text{Eq.3.4}$$

The parameters in above equations are same with previous definitions.

The use of a small Poisson's ratio, will lead to a relatively large ratio of lateral stress and vertical stress, as generally observed in over-consolidated soils. However, the Eq.3.4 is only in the elastic domain, because the formula was derived from Hooke's law of elasticity. If a soil sample is unloaded by a large amount, resulting in a high degree of over-consolidation, the stress ratio will be limited by the Mohr-Coulomb failure condition.

3.3.7. The Mohr-Coulomb Model (Perfect-Plasticity)

3.3.7.1 Elastic Perfectly-Plastic Behaviour:

Plasticity is associated with the development of irreversible strains. In order to evaluate whether or not plasticity occurs in a calculation, a yield function, f, is introduced as a function of stress and strain. A yield function can often be presented as a surface in principal stress space. A perfectly-plastic model is a constitutive model with a fixed yield surface, i.e. a yield surface that is fully defined by model parameters and not affected by (plastic) straining. The basic principle of elastoplasticity is that strain rates are decomposed into an elastic part and a plastic part:

$$\varepsilon = \varepsilon^e + \varepsilon^p \qquad \underline{\dot{\varepsilon}} = \underline{\dot{\varepsilon}}^e + \underline{\dot{\varepsilon}}^p \qquad \text{Eq.3.5}$$

Where, ε is strain, ε^e is elastic strain and ε^p is plastic strain; $\underline{\dot{\varepsilon}}$ is strain rates, $\underline{\dot{\varepsilon}}^e$ is elastic strain rate and $\underline{\dot{\varepsilon}}^p$ is plastic strain part.

Hooke's law is used to relate the stress rates to the elastic strain rates (see Figure 3.6),

$$\underline{\dot{\sigma}} = \underline{\underline{D}}^e \underline{\dot{\varepsilon}}^e = \underline{\underline{D}}^e (\underline{\dot{\varepsilon}} - \underline{\dot{\varepsilon}}^p) \qquad \text{Eq.3.6}$$

Where, $\underline{\dot{\sigma}}$ is stress rate, $\underline{\underline{D}}^e$ is the elastic material matrix according to Hooke's law, and $\underline{\dot{\varepsilon}}$ and $\underline{\dot{\varepsilon}}^p$ are same with previous definition.

According to the classical theory of plasticity (Hill, 1950), plastic strain rates are proportional to the derivative of the yield function with respect to the stresses. This means that the plastic strain rates can be represented as vectors perpendicular to the yield surface. This classical form of the theory is referred to as associated plasticity. However, for Mohr-Coulomb type yield functions, the theory of associated plasticity leads to an over-prediction of dilatancy. In general, the plastic strain rates are written as:

$$\underline{\dot{\varepsilon}}^p = \lambda \frac{\partial g}{\partial \sigma'} \qquad \text{Eq.3.7}$$

Where λ is the plastic multiplier, g is a plastic potential function denoted as non-associated plasticity, $\underline{\dot{\varepsilon}}^p$ is plastic strain, σ' is effective normal stress.

For purely elastic behaviour λ is zero, whereas in the case of plastic behaviour λ is positive:

$$\lambda = 0 \quad \text{for:} \quad f < 0 \qquad \text{or} \qquad \frac{\partial f^T}{\partial \underline{\sigma}'} \; \underline{\underline{D}}^e \; \underline{\dot{\varepsilon}} < 0 \qquad \text{(Elasticity)} \qquad \text{Eq.3.8 a}$$

$$\lambda > 0 \quad \text{for:} \quad f = 0 \quad \text{or} \quad \frac{\partial f^T}{\partial \underline{\sigma}'} \underline{\underline{D}}^e \dot{\underline{\varepsilon}} > 0 \quad \text{(Plasticity)} \qquad \text{Eq.3.8 b}$$

Where f is a yield function to estimate whether or not plasticity occurs in a calculation, λ is the plastic multiplier, $\underline{\underline{D}}^e$ is the elastic material matrix , $\dot{\underline{\varepsilon}}$ is strain rates, σ' is effective normal stress.

These equations may be used to obtain the following relationship between the effective stress rates and strain rates for elastoplasticity (Smith & Griffith, 1982;Vermeer & Borst, 1984).

3.3.7.2 Formulation of the Mohr-Coulomb Model

The Mohr-Coulomb yield condition is an extension of Coulomb's friction law to general states of stress. In fact, this condition ensures that Coulomb's friction law is obeyed in any plane within a material element. The full Mohr-Coulomb yield condition consists of six yield functions when formulated in terms of principal stresses (Smith & Griffith, 1982):

$$f_{1a} = \frac{1}{2}(\sigma'_2 - \sigma'_3) + \frac{1}{2}(\sigma'_2 + \sigma'_3)\sin\varphi - c\cos\varphi \le 0 \qquad \text{Eq.3.9 a}$$

$$f_{1b} = \frac{1}{2}(\sigma'_3 - \sigma'_2) + \frac{1}{2}(\sigma'_3 + \sigma'_2)\sin\varphi - c\cos\varphi \le 0 \qquad \text{Eq.3.9 b}$$

$$f_{2a} = \frac{1}{2}(\sigma'_3 - \sigma'_1) + \frac{1}{2}(\sigma'_3 + \sigma'_1)\sin\varphi - c\cos\varphi \le 0 \qquad \text{Eq.3.9 c}$$

$$f_{2b} = \frac{1}{2}(\sigma'_1 - \sigma'_3) + \frac{1}{2}(\sigma'_1 + \sigma'_3)\sin\varphi - c\cos\varphi \le 0 \qquad \text{Eq.3.9 d}$$

$$f_{3a} = \frac{1}{2}(\sigma'_1 - \sigma'_2) + \frac{1}{2}(\sigma'_1 + \sigma'_2)\sin\varphi - c\cos\varphi \le 0 \qquad \text{Eq.3.9 e}$$

$$f_{3a} = \frac{1}{2}(\sigma'_2 - \sigma'_1) + \frac{1}{2}(\sigma'_2 + \sigma'_1)\sin\varphi - c\cos\varphi \le 0 \qquad \text{Eq.3.9 f}$$

Where, $f_{1a} \sim f_{3a}$ are yield functions, $\sigma'_1, \sigma'_2, \sigma'_3$ are principal stresses, φ is friction angle and c is the cohesion.

These yield functions together represent a hexagonal cone in principal stress space as shown in Figure 3.7. In addition to the yield functions, six plastic potential functions are defined for the Mohr-Coulomb model:

$$g_{1a} = \frac{1}{2}(\sigma'_2 - \sigma'_3) + \frac{1}{2}(\sigma'_2 + \sigma'_3)\sin\psi \qquad \text{Eq.3.10 a}$$

$$g_{1b} = \frac{1}{2}(\sigma'_3 - \sigma'_2) + \frac{1}{2}(\sigma'_3 + \sigma'_2)\sin\psi \qquad \text{Eq.3.10 b}$$

$$g_{2a} = \frac{1}{2}(\sigma'_3 - \sigma'_1) + \frac{1}{2}(\sigma'_3 + \sigma'_1)\sin\psi \qquad \text{Eq.3.10 c}$$

$$g_{2b} = \frac{1}{2}(\sigma'_1 - \sigma'_3) + \frac{1}{2}(\sigma'_1 + \sigma'_3)\sin\psi \qquad \text{Eq.3.10 d}$$

$$g_{3a} = \frac{1}{2}(\sigma'_1 - \sigma'_2) + \frac{1}{2}(\sigma'_1 + \sigma'_2)\sin\psi \qquad \text{Eq.3.11 e}$$

$$g_{2a} = \frac{1}{2}(\sigma'_2 - \sigma'_1) + \frac{1}{2}(\sigma'_2 + \sigma'_1)\sin\psi \qquad \text{Eq.3.12 f}$$

Where, $g_{1a} \sim g_{3a}$ are six plastic potential functions, $\sigma'_1, \sigma'_2, \sigma'_3$ are principal stresses, ψ is the dilatancy angle. This parameter is required to model positive plastic volumetric strain increments (dilatancy) as actually observed for dense soils.

3.3.7.3 Basic Parameters of the Mohr-Coulomb Model

General

The Mohr-Coulomb model requires a total of five parameters, which are generally familiar to most geotechnical engineers and which can be obtained from basic tests on soil samples. These parameters with their standard units are listed below:

E	:	Young's modulus	[kN/m^2]
ν	:	Poisson's ratio	[-]
φ	:	Friction angle	[°]
c	:	Cohesion	[kN/m^2]
ψ	:	Dilatancy angle	[°]

Young's Modulus, (E)

PLAXIS uses the Young's modulus as the basic stiffness modulus in the elastic model and the Mohr-Coulomb model, but some alternative stiffness moduli are displayed as well. A stiffness modulus has the dimension of stress. The values of the stiffness parameter adopted in a calculation require special attention as many geo-materials show a nonlinear behaviour from the very beginning of loading. In soil mechanics the initial slope is usually indicated as E_0 and the secant modulus at 50% strength is denoted as E_{50} (see Figure 3.8). For materials with a large linear elastic range it is realistic to use E_0, but for loading of soils one generally uses E_{50}. E_{ur} is needed instead of E_{50} when unloading problems involved.

For soils, both the unloading modulus, E_{ur}, and the first loading modulus, E_{50}, tend to increase with the confining pressure. Hence, deep soil layers tend to have greater stiffness than shallow layers. Moreover, the observed stiffness depends on the stress path that is followed. The stiffness is much higher for unloading and reloading than for primary

loading. Also, the observed soil stiffness in terms of a Young's modulus may be lower for (drained) compression than for shearing. Hence, when using a constant stiffness modulus to represent soil behaviour one should choose a value that is consistent with the stress level and the stress path development. In particularly PLAXIS offers a special option for the input of a stiffness increasing with depth.

Poisson's ratio, (υ)

Standard drained triaxial tests may yield a significant rate of volume decrease at the very beginning of axial loading and, consequently, a low initial value of Poisson's ratio (ν_0). For some cases, such as particular unloading problems, it may be realistic to use such a low initial value, but in general when using the Mohr-Coulomb model the use of a higher value is recommended.

In many cases one will obtain ν values in the range between 0.3 and 0.4. In general, such values can also be used for loading conditions other than one-dimensional compression. For unloading conditions, however, it is more common to use values in the range between 0.15 and 0.25.

While for clay soil Poulos and Davis (1980) suggested that the following typical ranges of values of υ_s`:

Stiff over-consolidated clays:	0.1~0.2 (average: 0.15)
Medium clays:	0.2~0.35 (average: 0.3)
Soft normally consolidated clays:	0.35~0.45 (average: 0.4)

For cohesionless soil, values of Poisson's ration, υ_s, obtained from triaxial tests generally lie between 0.25 and 0.35 at relatively low stress levels. An average value of 0.3 is reasonable when no test data are available (Poulos and Davis, 1980)

Cohesion, (c)

The cohesive strength has the dimension of stress. PLAXIS can handle cohesionless sands ($c = 0$), but some options will not perform well. To avoid complications, it is thus often recommended to enter a low value of cohesion (use c>0.2 kPa) (Brinkgrev, 2002).

Friction angle, (φ)

The friction angle largely determines the shear strength by means of Mohr's stress circles. The Mohr-Coulomb failure criterion proves to be better for describing soil behaviour than the Drucker-Prager approximation, as the latter failure surface tends to be highly inaccurate for axisymmetric configurations.

Dilatancy angle, (ψ)

Apart from heavily over-consolidated layers, clay soils tend to show little dilatancy ($\psi \approx 0$). The dilatancy of sand depends on both the density and on the friction angle. For quartz sands the order of magnitude is $\psi \approx \varphi - 30°$. For φ-values of less than 30°, however, the angle of dilatancy is mostly zero. A small negative value for ψ is only realistic for extremely loose sands.

Interface strength, (R_{inter})

An elastic-plastic model is used to describe the behaviour of interfaces for the modelling of soil-structure interaction. The coulomb criterion is used to distinguish between elastic behaviour, where small displacements can occur within the interface, and plastic interface behaviour when permanent slip may occur.

For the interface to remain elastic the shear stress τ is given by:

$$|\tau| < \sigma_n \tan\varphi_i + c_i \qquad \text{Eq.3.13}$$

Where, τ is the elastic shear stress, σ_n is the elastic normal stress, φ_i and c_i are the friction angle and cohesion (adhesion) of the interface.

For plastic behaviour τ is given by:

$$|\tau| = \sigma_n \tan\varphi_i + c_i \qquad \text{Eq.3.14}$$

where τ is the elastic shear stress, σ_n is the plastic normal stress, φ_i and c_i are the friction angle and cohesion (adhesion) of the interface.

The strength properties of interfaces are linked to the strength properties of a soil layer. Each data set has an associated strength reduction factor for interface (R_{inter}). The interface properties are calculated from the soil properties in the associated data set and the strength reduction factor by applying the following rules:

$$c_i = R_{inter} Csoil \qquad \text{Eq.3.15}$$

$$\tan\varphi_i = R_{inter} \tan\varphi_{soil} \leq \tan\varphi_{soil} \qquad \text{Eq.3.16}$$

$$\psi_i = 0^o \; for Ri_{nter} < 1, otherwise, \psi_i = \psi_{soil} \qquad \text{Eq.3.17}$$

Where, R_{inter} *is an* associated strength reduction factor for interface. φ_i and c_i are the friction angle and cohesion (adhesion) of the interface. ψ is the dilatancy angle.

Real interface thickness, (δ_{inter})

The real interface thickness, δ_{inter} is a parameter that represents the real thickness of a shear zone between a structure and the soil. The value of δ_{inter} is only of importance when interfaces are used in combination with the Hardening Soil Model. The real interface thickness is expressed in the unit of length and is generally of the order of a few times the

average grain size. This parameter is used to calculate the change in void ratio in interfaces for the dilatancy cut-off options.

3.3.8 Material Data Sets for Structural Elements

Plates are used to model the behaviour of slender walls, plates or thin shells. Distinction can be made between elastic and elastoplastic behaviour.

3.3.8.1 Material Data Sets for Plates

Stiffness properties, EA and EI

For elastic behaviour an axial stiffness, EA, and a flexural rigidity, EI, should be specified as material properties. For both axisymmetric and plane strain models the values of EA and EI relate to a stiffness per unit width in the out-of-plane direction. Hence, the axial stiffness, EA, is given in force per unit width and the flexural rigidity, EI, is given in force length squared per unit width. From the ratio of EI and EA an equivalent thickness for an equivalent plate (d_{eq}) is automatically calculated from the equation:

$$d_{eq} = \sqrt{12\frac{EI}{EA}} \qquad \text{Eq.3.18}$$

Where EA is axial stiffness, EI is flexural rigidity. d_{eq} is equivalent thickness for an equivalent plate.

For the modelling of plates, PLAXIS uses the Mindlin beam theory. This means that, in addition to bending, shear deformation is taken into account. The shear stiffness of the plate is determined from:

$$\text{Shear stiffness} = \frac{5EA}{12(1+\nu)} = \frac{5E(d_{eq} \bullet 1m)}{12(1+\nu)} \qquad \text{Eq.3.19}$$

In which, EA is axial stiffness, E is young's modulus of plate, d_{eq} is equivalent thickness for an equivalent plate, ν is Poisson's ratio.

This implies that the shear stiffness is determined from the assumption that the plate has a rectangular cross-section. In the case of modelling a solid wall, this will give the correct shear deformation. However, in the case of steel profile element, like sheet-pile wall, the computer shear deformation may be too large. For steel profile element, d_{eq} should be at least of the order of a factor 10 times smaller than the length of the plate to ensure negligible shear deformation.

Poisson's ratio

In addition to the above stiffness parameters, a Poisson's ratio, ν, is required. For thin structures with a certain profile or structures that are relatively flexible in the out-of-plane direction (like sheet pile wall), it is advisable to set Poisson's ratio to zero. For real massive structures (like concrete wall), it is more realistic to enter a true Poisson's ratio of the order of 0.15.

Since PLAXIS consider plates (extending in the out-of-plane direction) rather than beams (one-dimensional structures), the value of Poisson's ratio will influence the flexural rigidity of the plate as follows:

$$\text{Input value of flexural rigidity:} \quad EI$$

$$\text{Observed value of flexural rigidity:} \quad \frac{EI}{1-\nu^2}$$

The stiffness effect of Poisson's ratio is caused by the stresses in the out-of-plane direction (σ_{zz}) and the fact that strains are prevented in this direction.

Weight

In a material set for plates a specific weight can be specified, which is entered as a force per unit area. For relatively massive structures this force is, in principle, obtained by multiplying the unit weight of the plate material by the thickness of the plate. Note that in a finite element model, plates are superimposed on a continuum that therefore "overlap" the soil. To calculate accurately the total weight of soil and structures in the model, the unit weight of the soil should be subtracted from the unit weight of the plate material. For sheet-pile walls the weight (force per unit area) is generally provided by the manufacturer. This value can be adopted directly since sheet-pile walls usually occupy relatively little volume.

3.3.8.2 Material Data Sets for Geogrids

Geogrids are flexible elastic elements that represent a grid or sheet of fabric. Geogrids cannot sustain compressive forces. The only property in a geogrid data set is the elastic axial stiffness, EA, entered in units of force per unit width. The axial stiffness, EA, is usually provided by the geogrid manufacturer and can be determined from diagrams in which the elongation of the geogrid is plotted against the applied force in a longitudinal direction. The axial stiffness is the ratio of the axial force per unit width and the axial strain.

$$EA = \frac{F}{\Delta l / l} \qquad \text{Eq.3.20}$$

Where, EA is axial stiffness, Δl is the elongation and l is the length.

3.3.8.3 Material Data Sets for Anchors

A material data set for anchors may contain the properties of node-to-node anchors as well as fixed-end anchors. In both cases the anchor is just a spring element. The major anchor property is the axial stiffness, EA, as per anchor in the unit of force and not per unit width in the out-of-plane direction. To calculate an equivalent stiffness per unit width, the out-of-plane spacing, L_s, must be entered. If the material type is selected as elastoplastic, two maximum anchor forces, $F_{max,tens}$ (maximum tension force) and $F_{max,comp}$ (maximum compression force) can be entered in the unit of force (also per anchor). In the same way as the stiffness, the maximum anchor forces are divided by the out-of-plane spacing in order to obtain the proper maximum force in a plane strain analysis. If the material type is set to elastic, the maximum forces are set to 1E+05 units.

3.3.9 Deformation Theory

The basic equations for the static deformation of a soil body are formulated with the framework of continuum mechanics. A restriction is made in the sense that deformation are considered to be small. The continuum description is dispraised according to the finite element methods. The static equilibrium of a continuum can be formulated as:

$$L^T \sigma + p = 0 \qquad \text{Eq.3.21}$$

Where, σ is the spatial derivatives of the six stress components, p is three components of the body forces, L^T is the transpose of a different operator, defined as:

$$L^T = \begin{bmatrix} \frac{\partial}{\partial x} & 0 & 0 & \frac{\partial}{\partial y} & 0 & \frac{\partial}{\partial z} \\ 0 & \frac{\partial}{\partial y} & 0 & \frac{\partial}{\partial x} & \frac{\partial}{\partial z} & 0 \\ 0 & 0 & \frac{\partial}{\partial z} & 0 & \frac{\partial}{\partial y} & \frac{\partial}{\partial x} \end{bmatrix} \qquad \text{Eq.3.22}$$

In addition to the equilibrium equation, the kinematic relation can be formulated as:

$$\varepsilon = L^T u \qquad \text{Eq.3.23}$$

Where ε is the six strain components, and u is the spatial derivatives of the three displacement components.

The combinations of above equations would lead to a second-order partial differential equation in the displacements.

3.3.10 Groundwater Flow Theory

3.3.10.1 Basic Equations of Steady Flow

Flow in a porous medium can be described by Darcy's law. Considering flow in a vertical x-y-plane the following equations apply:

$$q_x = -k_x \frac{\partial \phi}{\partial x}$$
$$q_y = -k_y \frac{\partial \phi}{\partial y} \qquad \text{Eq.3.24}$$

Where q_x is the specific discharge in horizontal direction and q_y is the specific discharge in vertical direction respectively.

The equations express that the specific discharge, q, follows from the permeability, k, and the gradient of the groundwater head. The head, ϕ, is defined as follows:

$$\phi = y - \frac{p}{\gamma_w} \qquad \text{Eq.3.25}$$

Where ϕ is the total head, y is the vertical position, p is the stress in the pore fluid (negative for pressure) and γ_w is the unit weight of the pore fluid.

For steady flow the continuity condition applies:

$$\frac{\partial q_x}{\partial x} + \frac{\partial q_y}{\partial y} = 0 \qquad \text{Eq.3.26}$$

where, q_x and q_y are same with Eq.3.24.

Equation.3.26 expresses that that there is no net inflow or outflow in an elementary area, as illustrated in Figure 3.9. .

3.3.10.2 Finite Element Discretisation

The groundwater head in any position within an element can be expressed in the values at the nodes of that element:

$$\phi(\xi, \eta) = \underline{N}\underline{\phi^e} \qquad \text{Eq.3.27}$$

Where $\underline{N}$ s the vector with interpolation functions and ξ and η are the local coordinates within the element.

The specific discharge is based on the gradient of the groundwater head. This gradient can be determined by mean of the $\underline{B}$-matrix, which contains the spatial derivatives of the interpolation functions. In order to describe flows for saturated soil (underneath the phreatic line) as well as non-saturated soil (above the phreatic line), a reduction function K^r is introduced in Darcy's law (Desai, 1976; Bakker, 1989):

$$q_x = -K^r k_x \frac{\partial \phi}{\partial x} \qquad q_y = -K^r k_y \frac{\partial \phi}{\partial y} \qquad \text{Eq.3.28}$$

Where, ϕ is total head, and K^r is reduction function in the range between 1 and 10^{-4}.

The function is described using a log-linear relation:

$$K^r = 10^{-4h/h_k} \qquad 10^{-4} \le K^r \le 1 \qquad \text{Eq.3.29}$$

or

$$^{10}\log(K^r) = -\frac{4h}{h_k} \qquad \text{Eq.3.30}$$

Where h is the pressure head and h_k is the pressure head where the reduction function has reached the minimum of 10-4. In PLAXIX h_k has a default value of 0.7m (independent of the chosen length unit) (see Figure 3.10).

In the numerical formation, the specific discharge, q is written as:

$$\underline{q} = -K^r \underline{\underline{R}}\underline{\underline{B}}\underline{\phi}^e \qquad \text{Eq.3.31}$$

Where,

$$\underline{q} = \begin{bmatrix} q_x \\ q_y \end{bmatrix} \quad \text{and} \quad \underline{\underline{R}} = \begin{bmatrix} k_x & 0 \\ 0 & k_y \end{bmatrix} \qquad \text{Eq.3.32}$$

From the specific discharges in the intergration points, $\underline{q}$, the nodal discharges Q^e can be intergrated according to:

$$Q^e = -\int \underline{\underline{B}}^T \underline{q} dV \qquad \text{Eq.3.33}$$

in which $\underline{\underline{B}}^T$ is the transpose of the B-matrix. On the element level the following equations apply:

$$Q^e = \underline{\underline{K}}^e \underline{\phi}^e \qquad \text{with:} \qquad \underline{\underline{K}}^e = \int K^r \underline{\underline{B}}^T \underline{\underline{B}} dV \qquad \text{Eq.3.34}$$

On a global level,

$$Q = \underline{\underline{K}}\underline{\phi} \qquad \text{Eq.3.35}$$

in which $\underline{\underline{K}}$ is the global flow matrix and Q contains the prescribed discharges that are given by the boundary conditions.

CHAPTER 4

METHODOLOGY

4.1 Introduction

This chapter contains the details of methodology adopted in the thesis work, including the description of the two excavation projects, the subsoil model, the geotechnical model adopted and the numerical simulations.

4.2 Description of Projects

4.2.1 Soil Profiles and Excavation details

Soil profilers and other relevant details are obtained for the Circle on Cavill project in Surfers Paradise and the Sundale project in Southport. Circle on Cavill has the deepest excavation 11.65m depth with three rows of anchors, and the Sundale project include a 9.7m deep excavation with one row of anchor. The descriptions of the two projects are presented below:

4.2.2 Circle on Cavill Project

4.2.2.1 Site Condition

This project site is located in Cavill Avenue, Surfers Paradise, Gold Coast (Figure 4.1). It consists of the construction of 2 towers; north tower is 40 stories and the south tower is 70 stories. Both structures have 4 basements for car parks. There is an adjacent two-story building on the north-west of the construction site seated on piled foundation as shown in Figure 4.2 .

All together 16 boreholes are carried out at this site. All boreholes were done with solid flight auger drilling and continued by rotary drilling with water and mud (bentonite and polymer) circulation. SPT were undertaken at typically 3m depth intervals in each borehole to the depth where peat was encountered and then at typically 1.5m intervals thereafter over the non-cored sections of the boreholes. Water pressure testing in the cored sections of selected boreholes comprised single packer tests undertaken at the completion of core drilling. Pressure testing was also undertaken in the cored sections of the selected boreholes.

Multi-anchored and single-anchored secant pile walls are used to support the excavation and no field measurement are adopted in the project for consideration of cost and soil conditions.

4.2.2.2. Soil Conditions

The subsoil conditions at the project site are shown in Figure 2.1, the details of the subsurface conditions are presented below:

- Upper Aquifer: About 14 meters thick loose to medium dense sand to the water table then medium dense to very dense sand. Laboratory testing indicates that these sands have a very low fine content (percentage passing the 0.075mm sieve) in the order of 2% to 5%.
- Peat-layer: Encountered at elevation from around RL.-10.8 to RL.-14.30, the thickness of peat is 3.5 meters with low permeability.
- Lower Aquifer: Approximate 3.8m thick very dense sand with high elastic soil modulus.
- Lower "Clayey" layer: Inconsistent layer of stiff to very stiff silty/sandy clay and or very stiff to hard silty clay underlain by or interbedded with medium dense sand. Commences at elevation RL -18.1 and finish at RL. -27.5 with a thickness of 9.4m.
- Basement "Gravelly" Layer: Clayey/sandy Gravel typically dense to very dense. Commences at elevation RL-27.5 and finishes at RL.-30.0 with a thickness of 2.5m.
- Argillite and in places Greywacke rock: Commences at elevation RL -30.0 to RL-36.0 where borehole stops. Typical high strength rock but significant fractured.
- Groundwater lever was encountered at RL -1.00.

For the current research on section A with the maximum excavation depth 11.65m was selected. Borehole BH2 was investigated; it was drilled up to 40m depth. Simplified subsoil of BH2 is shown in Figure 4.3(a). Detailed borehole records are given in Appendix A.

4.2.2.3. Secant Piles and Anchors

The photos of the excavation at the Circle on Cavill site during construction are shown in Figure 4.3 (b) and Figure 4.3(c).The diameter of constructed cast secant piled wall is 600mm and the spacing between the centres of the hard piles is 850mm.The toe of the wall is embedded into stiff sandy clay at a depth 27 m below the ground level, but reinforcements of hard pile stop just above the peat layer, which means the top 14.5m reinforced pile wall take bending moment and shear forces, the lower 12.5m non-reinforced pile wall does not take bending moment, only act as cut-off wall to prevent the groundwater seepage (see Figure 4.4) The supported excavation is for four basements. The maximum excavation depth was set to be 11.65 m and three levels of anchors were adopted to construct the basements with conventional bottom up construction method. Figure 4.5 shows the anchored secant pile wall system.

4.2.3 Sundale Excavation Project

4.2.3.1. Site Conditions

The site is located between Queen Street, Brighton Parade and Health Street, Southport. The mouth of the Nerang Rive (into the Gold Coast Broadwater) is located approximately 50 to 75m to the east of the site. Regional topography comprises slightly elevated areas to

the west and north of the site sloping down across the site towards the mouth of the Nerang River and the Broadwater. The development includes 8 stages, and each stage has some high rise buildings with different number of stories. The researched target in this thesis belongs to stage B2, which has a 30 story tower residential building with possible commercial ground floor suspended over two to three levels of basement car parks. Eight boreholes and 1 groundwater monitoring well investigation were set up in stage B2 (Figure 4.6). A single row of anchored secant piled wall was adopted in the excavation and no field measurement is carried out.

4.2.3.2 Soil Conditions

The subsoils at Sundale is shown in Figure 4.7, it comprised about 1m thickness of fill which include sand and some gravels, then about 4 m thick loose to medium or dense sand with high modulus underlain by a 3 m thick very stiff clay to a depth of 8 m, and the borehole eventually terminating in a rock layer. The ground water level is about RL 1.2 m. The deepest excavation section is at section A as shown in the site plan, the simplified borehole BH2 is investigated and detailed borehole information are presented in Appendix B.

4.2.3.3 Secant Piles & Anchors

The diameter of the constructed cast in –situ secant piled wall is 500mm and spacing between the centres of the hard piles is 800mm. The toe of wall is embedded into rock layer at a depth 11 m below the ground level. The wall was designed for construction of three basements. The maximum excavation depth was set to be 9.7 m and one level of anchor was adopted to construct the basements with conventional bottom up construction method. Figure 4.8 shows the elevations and cross sections of the secant piled wall.

4.3 STANDARD PENTRATION TEST (SPT) RESULTS

4.3.1. Introduction

The standard penetration tests (SPT) was performed in the two projects because it can advance through hard stratum compared to the CPT. According to the borehole reports supplied by the special geotechnical company, the SPT tests followed the same procedure at both projects:

A standard 50mm diameter thick-walled split tube sampler is driven up to 450mm into the ground from the bottom of the borehole by a 63.5kg mass hammer with 760mm free-fall. The blows required to penetrate each 150mm (or part of) are recorded. Where the full 450mm penetration is achieved the total blows over the final 300mm are recorded as the “N” value for the test.

4.3.2 Corrected SPT Test Results

Schmertmann and Palacios (1979) showed that measured SPT blow counts are inversely proportional to the energy ratio for blow counts less than 50. Seed et al. (1985) and Skempton (1986) subsequently proposed that measured blow counts should be corrected to the value that would have been recorded if a standard amount of energy had been transmitted through the rods. A standard value of 60% of the hammer potential energy has been adopted because it is the historical average measured for most drill rigs and operators. The energy corrected SPT blow count (N_{60}) SPT is calculated as follows:

$$N_{60} = \frac{E_m C_B C_S C_R N}{0.60} \qquad \text{Eq.4.1}$$

Where:

N_{60} = SPT N value corrected for field procedures
E_m = hammer efficiency (from Table 4.2)
C_B = Borehole diameter correction (from Table 4.3)
C_S = sample correction (from Table 4.3)
C_R = rod length correction (from Table 4.3)
N = measured SPT N value

The SPT data also may be adjusted using an overburden correction that compensates for the effects of the effective stress. Deep test in a uniform soil deposit will have higher N values that shallow tests in the same soil. So the overburden correction adjusts the measured N values to $(N1)_{60}$ (Liao and Whitman, 1985):

$$(N1)_{60} = N_{60} C_N = N_{60} \sqrt{\frac{100kPa}{\sigma_z'}} \qquad \text{Eq.4.2}$$

Where, $(N_1)_{60} = N_{60}$ value corrected to a reference stress of one atmosphere ;
C_N = correction factor for overburden pressure.
σ_z' = Vertical effective stress at the test location.

Although Liao and Whitman didn't place any limits on this correction, it is possibly best to keep $(N_1)_{60} \leq 2N_{60}$. This limit avoids excessively high $(N_1)_{60}$ values at shallow depth. A simple correction chart has been proposed by Tomlinson (1969) base on the work by Gibbs and Holtz (1957) and is reproduced in Figure 4.9.Peck and Bazara, (1969), and Peck, Hanson and Thornburn, (1974) also corrected the N value for the influence of vertical effective overburden pressure shown in Figure 4.9.

The corrected SPT N values of the two projects are given in Table 4.4 **and** Table 4.5 respectively and in Figure 4.10 and Figure 4.11 respectively.

4.4 SOIL PARAMETERS

4.4.1 Unit Weight, γ_{unsat}, γ_{sat}

The unit weight of cohesionless is difficult and costly to determine in the laboratory. Bowles (1996) presented empirical values for unit weight of granular soil based on SPT

at about 6m depth and normally consolidated as given in Table 4.6. Huybrechts et al (2004) published Table 4.7 to estimate the unit weight of soil.

PLAXIS implicit that the saturated weight of sand is generally around 20 kN/m^3 whereas the unsaturated weight can be significantly lower, depending on the degree of saturation.

4.4.2. Relative Density *Dr*

The relative density of sands may also be estimated from N_{60} (see Jamiokowski et al, 1988, Skempton 1986) as

$$D_r = 100\left(\frac{N_{60}}{60}\right)^{0.5} \qquad \text{Eq.4.3}$$

Where, N_{60} = Penetration resistance normalized to an effective energy delivered to the drill rod at 60 percent of theoretical free-fall energy, blows/300 mm.

Where Dr $\geq$ 35 percent, N_{60} should be multiplied by 0.92 for coarse sands and 1.08 for fine sands. Jamiolkowski et al (1988) also demonstrated the relationship between Dr and N_{60} given in Table 4.8.

4.4.3. Friction Angle, $\bar{\phi}$

The angle of friction determines the shear strength as shown in Figure 4.12. SPT test can be one of the methods to estimate the friction angle of cohesionless soil. Table 4.9 summarised the research on correlation of friction angle to SPT N value. Huybrechts et al (2004) presented a method to estimate the friction angle for cohesionless soil and cohesive soil as given in Table 4.9 to Table 4.10 as well.

Peck *et al* (1974) also provided a more conservative correlation as shown in Figure 4.13. Schmertmann (1975) and Carter & Bentley (1991) proposed the relationship between N value and the effective friction angle $\bar{\phi}$ as shown in Figure 4.14 and Figure 4.15 respectively. Meanwhile, Stroud (1989) replotted all the available data to obtain the variation of $\bar{\phi}$ versus $(N_1)_{60}$ for different OCR as shown in Figure 4.16.

4.4.4. Dilation angel, ψ

In order to shear sand, the grains must physically ride over each other. This requires the sand to expand in the direction perpendicular to the shear. This expansion is known as dilation. When the soil is loose, the shearing process will actually cause contraction rather than dilation, as the sand particles readily bed in to a denser structure. Sands can display behaviour between these two extremes depending on the particular relative density.

Apart from heavily over-consolidated layers, clay soils tend to show little dilation (≈0). Rock dilation also tends to be zero. The dilation of sand depends on both the density and

on the friction angle. For quartz sands, the order of magnitude is $\psi = \varphi - 30^0$. For φ-value of less than 30°, the angle of dilation is almost zero. A small negative value for the angle of dilation is only realistic for extremely loose sands (CUR 195). Table 4.11. shows the typical values for dilation angles in the manual published with the FLAC program (2000).

4.4.5 Young's modulus E

According to the manual of WALLAP, the Young's modulus E of normally compacted cohesionless soil increase linearly from zero at ground level and is related to its density. Terzaghi (1954) suggested the E values given in Table 4.12. For over-consolidated (compacted) cohesionless soil the E values are approximately proportional to the corrected SPT N value according to the equation:

$$\text{Young's modulus (kN/m}^2\text{)} = \text{F x SPT N value} \qquad \text{Eq.4.4}$$

where F is in the range 2000 to 6000 for retaining walls in sands and gravels.

Table 4.13 presents the ranges of E values published by former researchers, including Kulhawy and Mayne (1990), Das (1994) Bowles (1996) and Huybrechts et al (2004).

4.4.6 Poisson's ratio (υ)

The selection of a Poisson's ratio is particularly simple when the elastic model or Mohr-Coulomb model is used for gravity loading. For this type of loading PLAXIS should give realistic ratios of

$$K_0 = \frac{\sigma_h}{\sigma_v} \qquad \text{Eq.4.5}$$

As both models will give the well-know ratio of

$$\frac{\sigma_h}{\sigma_v} = \frac{\nu}{(1-\nu)} \qquad \text{Eq.4.6}$$

For one-dimensional compression it is easy to select a Poisson's ratio that gives a realistic value of K_0. Hence, υ is evaluated by matching K_0.

In many cases one will obtain υ values in the range of 0.3 to 0.4. In general, such values can also be used for loading conditions other than one-dimensional compression. For unloading condition, however, it is more common to use values in the range between 0.15 and 0.25. Bowles (1993), Das (1994), Huybrechts (2004) gives the range for Poisson's ratio, υ as presented in Table 4.14

4.4.7 The coefficient of earth pressure at rest, K_o

The coefficient of earth pressure at rest K_0 was proposed by Jaky (1974), it is not a constant soil parameter but depend on the stress history (OCR) of the soil. However, K_0 can be assumed to be constant and less than unity for normally consolidated soils. When soil becomes over-consolidated, the value of K_o increases and becomes larger depending on the OCR values.

Schmidt, (1966), Mayne & Kulhawy, (1982), Hayat (1992) and Michalowski (2005) researched on this parameter intensively. There are some empirical relationships to obtain K_0 as given below:

For perfect elastic materials (Mohr-Coloumb Model)

$$K_0 = \frac{\nu'}{1-\nu'} \qquad \text{Eq.4.7}$$

Where, υ' = Poisson's ratio.

Normally consolidated loose sand (Jaky, 1944)

$$K_0 = 1 - \sin\bar{\phi} \qquad \text{Eq.4.8}$$

Dense compacted sand (Sherif et al, 1984)

$$K_0 = (1 - \sin\bar{\phi}) + 5.5x\left[\frac{\rho_{compact}}{\rho_{\min}} - 1\right] \qquad \text{Eq.4.9}$$

Where,

$\rho_{compact}$ = actual compacted dry density;

$\rho_{\min}$ = minimum dry density (loosest state) of the sand.

Normally consolidated clays (Brooker & Lreland, 1965)

$$K_0 = 0.95 - \sin\bar{\phi} \qquad \text{Eq.4.10}$$

Over-consolidated sand and clays (Mayne and Kulwahy, 1982)

$$K_{0(OC)} = K_{0(NC)} OCR^{\sin\phi'} \qquad \text{Eq.4.11}$$

Typical values of K_0 are given in Table 4.15 (Mayne and Kulwahy, 1982). According to the above empirical formulae, the K_0 values for the soils at the two project sites are tabulated in Table K0.

4.4.8 Active pressure coefficient K_a and Passive pressure coefficient K_p

According to the Mohr- Coloumb theory, the active pressure coefficient K_a and passive pressure coefficient K_p are given by

$$K_a = \frac{1-\sin\phi'}{1+\sin\phi'}, \qquad K_p = \frac{1+\sin\phi'}{1-\sin\phi'} \qquad \text{Eq.4.12}$$

Meanwhile, WALLAP program manual provides the empirical values for K_p as given in Table 4.16 (Caquot and Kerisel,1949).

4.4.9. Permeability,K_x and K_y

PLAXIS distinguishes horizontal permeability K_x and vertical permeability K_y since in some soil type, for example peat, there can be a significant difference between horizontal and vertical permeability.

For the Circle of Cavill project e permeability tests were conducted. (see Appendix C). Table 4.17 gives the typical values of permeability as presented by Duncan (2001).

Finally, based on SPT Test results, details of soil parameters for the two projects can be obtained. Because the soil parameters needed in PLAXIS and WALLAP are different, so they are tabulated in two Tables for each project from Tables 4.18 to Table 4.21 respectively.

4.5. NUMERICAL SIMULATION

4.5.1 Boundary Conditions

The first step to in any numerical simulation is to determine where to place the boundaries so that their influence on the results will be minimized, i.e. How far is far enough? The two programs had different clues. The next section addresses this issue.

4.5.1.1 Depth of model

The boundary effect was studied while using a linear elastic soil. The bottom of the mesh is best placed at a depth where the soil becomes notably harder. The distance from the bottom of the excavation to the hard layer, is called D_b (see Figure 4.17) . It was shown (Lim and Briaud 1996) that when using a linear elastic soil in the simulation, D_b had a linear influence on the vertical movement of the ground surface at the top of the wall but comparatively very little influence on the horizontal movement of the wall face.

A value of D_b equal to 9 m or 1.2 times the wall height was usually used. This value of *Db* came from the instrumented case history used to calibrate the FEM model (Briaud & Lim, 1999**).** In PLAXIS model, take depth of model is three times of excavation depth, i.e.:

1) Circle of Cavill project :
Depth of model = 2 x 11.65 +11.65 = 34.95m, take 40m. (Fix boundary exists 40m below the ground surface)

2) Sundale Project:
Depth of model = 2 x 8.9 +8.9 = 26.7 m, take 30m. (Fix boundary exists 30m below the ground surface).

In the WALLAP model, Frankie Piling company take fix boundary at the toe of the reinforced pile wall, that means the depth of model as the length of the reinforced pile, i.e. 14.5m for Circle on Cavill and 10.2 m for Sundale project .

4.5.1.2 Width of Model

Lim and Briaud (1996) did a separate study about the parameters H, W_e, B_e, and D_b *as* shown in Figure 2, they gave the appropriate values for W_e and B_e as

$$W_e = 3D_b$$
$$B_e = 3(H + D_b)$$

Beyond these values, W_e and B_e have little influence on the horizontal deflection of the wall due to the excavation of the soil. This confirms previous findings by Dunlop and Duncan (1970).

For PLAXIS, the B_e and W_e just take half of the width of excavation for wide excavation. So the total width of model is equal to the whole excavation width, i.e. 70 m.

According to WALLAP manual, the manual instruct the B_e should be between one and three times the wall depth, and *We* should be one and three times the wall depth for wide or asymmetrical excavation, so

Circle of Cavill project:
B_e = (1 ~ 3) x Depth of wall = (1 ~ 3) x 11.65 = 11.65 ~ 34.95, take 25 m
W_e = (1 ~ 3) x Depth of wall = (1 ~ 3) x 11.65 = 11.65 ~ 34.95, take 20 m
The width of boundary = B_e + W_e = 25 + 20 = 45 m

Sundale Project:
B_e = (1 ~ 3) x Depth of wall = (1 ~ 3) x 9.7 = 9.7 ~ 29.1, take 25 m
W_e = (1 ~ 3) x Depth of wall = (1 ~ 3) x 9.7 = 9.7 ~ 29.1, take 20 m
The width of boundary = B_e + W_e = 25 + 20 = 45 m

Therefore, the model set up by PLAXIS and WALLAP for Circle on Cavill and Sundale projects were shown from Figure 4.18 to Figure 4.21.

4.5.2. Simulations of Soil Layers

Soil strata are input (drawn in screen) according to different soil properties under Mohr-Coulomb theory. Excavation levels are also drawn in the screen to active or de-active stage constructions in calculation steps. Sand, Gravel and rock layers are considered as drained behaviour; and clay and peat are considered as undrained behaviour in short term and drained in long term. Comparisons between the results of drained and undrained for peat and clay was done in the results and discussion section.

Young's modulus E, which was found to be the most important parameter in the whole simulation, the elastic modulus for dense sand and peat have different effects on the performance of wall, so they are analysed separately.

For sand layers, there are lot of debates about the values of elastic modulus of very dense sand and rock. Frankie Piling Ltd took the E-value as 200 MPa according to empirical methods and WALLAP manual, but many references present different lower E-values. Considering the subsoil conditions of Gold Coast which is made up of mainly sand, a relatively higher E-value is possible for very dense sand and strong rock. To find out the effects of Young's modulus on the performance of the wall, a series of different E-values are given to very dense sand and rock layers to compare the results by numerical methods. For peat layer (this is only for Circle on Cavill project), it was found its stiffness has great effect to the deflected shape of the retaining wall, especially at the toe of the reinforced pile wall. Keeping the other parameters unchanged, simulation of different stiffness for the peat layer can determine the reasons for the deformation at the toe of the reinforced wall.

Since the Mohr-Coulomb model has limited application for the soil that shows an over-consolidated behaviour, it cannot reflect the over-consolidation ratio, the coefficient of lateral earth pressure at rest, K_o, has great influence on the performances of the wall as well. By assuming the over-consolidation ratio, a series of K_o values can be obtained to analyse their effects on the retaining walls.

Therefore the following factors and their range will be analysed to present the effects on the performances of the wall:

- E value of dense sand and rock
- E value of peat
- Drained and undrained status for peat and clay layer.
- Coefficient of lateral earth pressure at rest, Ko

The detailed ranges of the oil parameters will be given in next chapter on results and discussions

4.5.3. Simulations of Structural Elements

Secant piled wall is simulated as an impermeable beam. Anchors are modelled as Elasto-plastic spring elements and grouted body are modelled as special tension elements. There is another key point to be noted for the Circle on Cavill project:

The secant pile wall have two parts, the top 14.5m pile has reinforcement to take bending moments and shear forces; the lower 12.5 m pile has no reinforcement only with concrete (see Figure 4.4), so it acts as a cut-off wall to prevent groundwater flowing into the excavation zone , but it cannot bear bending moment and shear force. Therefore, the Young's modulus of the cut-off wall is different from the upper reinforced wall, so the piled wall was modelled as two elements in PLAXIS. For convenient analysis and

explanation, the upper part of the wall was named as Pile-1 and the lower part of the wall was named as Pile-2 in later sections.

The properties of all structural elements for the two projects are concluded in Table 4.22 and Table 4.23. The following factors of the structural elements are used to analysis the effects on the performance of wall.

- Stiffness of wall
- Pre-stress of anchor
- Length of anchor

The detailed ranges of structural elements are presented in the next chapter on results and discussions.

4.5.4. Construction Stages

The construction stages of the Circle of Cavill project and Sundale project are shown in Table 4.24 and Table 4.25 respectively.

4.5.5. Output

The following results are the output to analyse and compare the performance of the wall in different excavation stages or excavation height:

- Bending moments of wall ;
- Shear forces of wall ;
- Deflections of wall ;
- Settlement of ground surface.

CHAPTER 5

RESULTS AND DISCUSSIONS

5.1 General

Based on previous estimations for all parameters, the results from PLAXIS are presented and discussed in this chapter. The general contents of this chapter include:

- Present and analysis of output results of PLAXIS;
- Compare with the results of WALLAP and discuss the difference;
- Discuss the important effect factors on the performance of the retaining wall.

5.2 Soil Profile Model and Geotechnical Parameter Model

The sub-soil condition at the Circle on Cavill Project is as follows:

- Upper Aquifer- About 14 meters thick loose to medium dense sand to the water table then medium dense to very dense sand. Laboratory testing indicates that these sands have very low fines content (percentage passing the 0.075mm sieve) in the order of 2% to 5%.

- Peat-layer – Encountered at elevation from around RL.-10.8 to RL.-14.30, the thickness of peat is 3.5 meters with low permeability.

- Lower Aquifer – Approximate 3.8m thick very dense sand with high elastic soil modulus.

- Lower "Clayey" layer – Inconsistent layer of stiff to very stiff silty/sandy clay and or very stiff to hard silty clay underlain by or interbedded with medium dense sand. Commences at elevation RL -18.1 and finish at RL. -27.5 with a thickness of 9.4m.

- Basement "Gravelly" Layer- Clayey/sandy Gravel typically dense to very dense. Commences at elevation RL-27.5 and finishes at RL.-30.0 with a thickness of 2.5m.

- Argillite and in places Greywacke rock – Commences at elevation RL -30.0 to RL-36.0 where borehole stops. Typical high strength rock but significant fractured.

- Groundwater lever was encountered at RL -1.00.

The subsoils at Sundale is shown in Figure 4.7, it comprised about 1m thickness of fill which include sand and some gravels, then about 4 m thick loose to medium or dense sand with high modulus underlain by a 3 m thick very stiff clay to a depth of 8 m, and the borehole eventually terminating in a rock layer. The ground water level is about RL 1.2 m. The Geotechnical parameters used in the WALLAP and PLAXIS analysis are summarized in Tables 4.24 and Table 4.26

5.3 Parameters for Structural Elements

The parameters used for the structural elements are summarized in Table 4.28 and Table 4.29

5.4 Output of PLAXIS

5.4.1 General

The output of the standard PLAXIS models for the two excavations are presented in Appendix D, including deformed mesh, horizontal and vertical displacements, lateral earth pressures, pore pressures, and groundwater flow, etc. Their maximum values are presented in Table 5.1 for Circle on Cavill and Sundale projects.

5.4.2 Comments on PLAXIS Analysis in General

During the simulation, the input parameter such as Young's modulus, E', is found to be very sensitive to the performance of the wall, especially the E value of peat layer. In addition, Mohr-Coulomb Model is highly sensitive with respect to the coefficient of lateral earth pressure at rest, $K_{o;}$ thus the accurate estimation of these two parameters is most important.

The Mohr-Coulomb model has limited application for the soil that shows an over-consolidated behaviour, it cannot reflect the over-consolidation ratio. Furthermore, a good estimation of the interaction coefficient, R_{inter}, (strength reduction factor) is vital in modelling the roughness of interaction that relates the interface strength (wall friction and adhesion) to the soil strength (friction angle and cohesion). This factor can model the behaviour of the interaction between structures and soils (smooth and rough surface), and also to evaluate the relative movements and the associated deformation within the interface. In this simulation, R_{inter} is taken as 0.67 .

Besides, the selected mesh should not induce any boundary effects on the results. However, introducing a large geometry mesh may cause high computer effort and time, thus the optimization of the dimension of mesh becomes very important in the modelling.

5.5 Comparison of Results Between PLAXIS and WALLAP

WALLAP results presented here were supplied by the Frankie Piling Consultant Ltd that designed and constructed the secant piled wall system; the results included lateral

deflections, envelopes of bending moment and shear force. In the following section a comparison is made between the PLAXIS results and the WALLAP results for the two excavations.

Figures 5.1 and Figure 5.2 show the lateral wall movement at the final stage from WALLAP and PLAXIS for Circle on Cavil and Sundale projects. The lateral wall movements of Circle on Cavill are obviously different for the two type of analysis. Tables 5.2 and Table 5.3 summarize the extreme values between PLAXIS and WALLAP for Circle on Cavill and Sundale project. The reasons for the two values to be different for Circle on Cavill project are:

- WALLAP assumes a rigid boundary at the toe of reinforced wall (GL.-14.5m), i.e. it assumes that the toe of the reinforced wall is fixed and the subsoil below the toe of the reinforced wall has no effect on the upper part of the wall which is reinforced.
- In the PLAXIS analysis the whole length pile is taken into account; it was found that the deflection of the wall was affected greatly by the stiffness of the peat layer.
- Only the upper 14.5m of the wall is reinforced, so the concrete wall below the upper 14.5m has not enough stiffness to take the active pressure resulting during deformations and thus causes a stability problem.
- The peat layer is just below the toe of the reinforced part of the piled wall, because of its low stiffness, it cannot supply enough passive pressure to the concrete wall, so that peat and the concrete wall move forward together and magnify the deformation and increase the stability risk.

For the Circle on cavil project the depth of the reinforced portion of the wall and the peat stiffness are both important for the stability and deformations; hey are discussed in the next sections.

Figure 5.3 and Figures 5.4 summarize the envelopes of bending moments and shear forces from PLAXIS and WALLAP for both excavations. The results of WALLAP and PLAXIS match quite well, which means both computer programs, can be used to design the secant pile wall; and they can get the same order of results for the bending moments and shear forces. In the preliminary design of the retaining wall, WALLAP can have the same effects as PLAXIS to estimate the amount of reinforcement needed and the cross sectional property of the secant piled wall. However, WALLAP model ignored the subsoil condition below the toe of the reinforced part of the secant piled wall, which increases the potential to have more lateral movement in the results.

5.6 Effects of Construction Stages

Figure 5.5 shows the lateral wall movements at various excavation stages for Circle on Cavill. For Circle on Cavill, after installing the 1st anchor, the deflection of the wall above the excavation depth was controlled effectively, the movement at the top of the wall was almost zero, but the deflection of the wall below the excavation depth was still

not controlled. With the excavation depth increased from 7.6m to 10m, the deflection at the toe of reinforced wall increased faster and became larger than the value above the excavation depth. When the 3rd row of anchors was installed and the excavation depth was 11.65m, the maximum deflection point moved above the excavation depth, but the deflection at the "problem" point is still closed to the maximum value of the wall. The variation of the lateral wall movement with the construction stages reflected sufficiently the potential stability problem arising from not enough embedment of the reinforced wall.

Figure 5.6 summarize the deflections of the secant piled wall at different construction stages for the Sundale excavation. It is good to compare this performance at Sundale with the performance at the Circle on Cavill, because the wall seats on the rock layer in the Sundale Project and there is no stability problem at all. The behaviour of the wall obeys the basic rules of the performance of retaining walls. The maximum deflection of the wall is at the top of the wall, which is different from Circle on Cavill, because the position of the 1st row of anchors are deeper and up to GL.-2.7 m. Briaud et al (1999) found that the best position for the first row of anchors to be between 1.2m and 1.5m below the top of wall; but in current practice the first row of anchors tends to be placed at deeper than that recommended by Briaud et al (1999).

Figures 5.7 and Figure 5.8 summarize the variation of the settlement of the round surface at different stages excavation for the two projects. Surcharge from the adjacent building in Circle on Cavill project caused an additional 10mm settlement of ground surface. The ground surface settlement increases with the increasing of excavation depth. Figures 5.9 and Figure 5.10 show the relationships between the maximum settlement of the ground surface, the deflection of the wall and the excavation depth for both projects.

Figure 5.11 and Figure 5.12 present the changing of bending moments of the walls with the construction stages. The bending moments of the walls behave like beam. The maximum bending moment increase with the excavation depth.

According to the diagrams of the movements adjacent to braced excavation proposed by Peck (1969), the main subsoil of Circle on Cavill and Sundale projects belongs to firm sand (see Figure 5.13(a)), However, from the diagram of the normalized ground settlement profiles of different oil types published by Clough and O'Rourke(1990), the subsoil of Circle on Cavill shows properties similar to soft to medium clay (see Figure 5.13(b)), which is perhaps due to effect of the peat layer. The main subsoil of the Sundale excavation still belongs to sand according to the hypothesis of Clough and O'Rourke (1990).

5.7 Parametric Studies

5.7.1 Embedment Depth, D of Reinforced Cage

The effect of the wall embedment depth on the lateral wall movements, and maximum bending moments on the wall is investigated by the effect of the wall embedment depth for three depths: 2.85 m (D/H =0.25, H =11.65 m), 6.64m (D/H =0.57, H = 11.65

m), and 15.35 m (D/H =1.32, H =11.65 m). When the embedment depth is 6.64 m, the reinforced cage just stopped under the peat layer; when the embedment depth is 15.35m, the reinforced cage is continued for the whole 27m pile length.

Figure 5.14 and Figure 5.15 show the relationship between the predicted maximum lateral wall movements, the wall bending moments with the wall embedment depths. The maximum lateral wall movements tend to increase slightly with the increase of wall embedment ratio (D/H); but increasing the wall embedment depth is not that effective in reducing the maximum lateral wall movements. This observation is in agreement with the study carried out by Whittle & Hashash, (1992) and Poh & Wong, (1995), but the embedment depth of the reinforced wall should reach to a reasonable and safe depth to meet the requirement of the retaining wall.

5.7.2 Young's modulus, E for peat (only for Circle on Cavill project).

According to the previous analysis, the stability of the wall depends on the embedment depth of the reinforced wall and the stiffness of peat layer. Young's modulus of peat has become very sensitive to the performance of the wall as the bottom part of the wall in this project was not reinforced. Therefore the peat layer was replaced by very dense sand in the analysis and the modulus was taken as 200MPa in the analysis.

Figure 5.16(a) to (d) present the lateral wall movements for the two cases when the peat layer was present and the case when the peat layer was replaced with dense sand. The deflection of the wall in the peat layer is larger than the case when it is replaced with very dense sand: excavation depth is 7.6m. This difference increases with the increase of the excavation depth. When the excavation depth is 11.65m, the difference between their maximum lateral wall movement is about 25 mm, which proves that the stiffness of peat can influence the maximum lateral wall movement to a great extent.

Figures 5.17(a) to (d) compare the ground surface settlement for the case when the peat layer is present to the case when it is replaced in the analysis with very dense sand layer. The difference between the maximum ground surface settlements for the two cases is about 35 mm. That means the peat layer may lead to large ground surface settlement for the adjacent building; thus more care need to be taken in accommodating this large settlement in adjoining structures when such peat layer is encountered.

5.7.3 Young's modulus, E for dense sand

The Young's modulus for very dense sand layer was taken as 200MPa in the above standard PLAXIS and WALLAP analysis, however this high value caused lot of debates when the standard analysis was carried out, because this value is much higher when compared to those given in the published literature as referenced in the Methodology chapter. Therefore it was necessary to find the effect of the stiffness of the dense sand layer on the performances of the retaining wall system.

A series of Young's modulus values for the dense sand was taken as 200 MPa (designated E-200 in the analysis), 150MPa (designated E-150 in the analysis) and

100MPa (designated as E-100) for the Circle on Cavill project; these values are inferred from the related literature review in Chapter four. Figure 5.18 and Figure 5.19 summarize the lateral wall movements and ground surface settlements for Circle on Cavill excavation... The general deformed shape of the wall does not change with the variation of the Young's modulus of dense sand, but both maximum lateral wall movement and maximum ground surface settlements increases with the reduction of the stiffness of the dense sand. T he maximum lateral wall movements and ground surface settlements of E-200 are smaller (by about 15mm) than the case with E-100. The lateral wall movement and ground surface settlements for the cases E-200 and E-150 are close to each other. Figure 5.20 shows that the bending moment of the wall slightly increases with the Young's modulus of the dense sand. Figure 5.21 shows the relationships between the maximum lateral wall movements, the surface ground settlement contains the maximum lateral wall movements, the ground surface settlements and the bending moments for every case at every excavation depth.

5.7.4 Undrained and drained mode of analysis -for peat and clay layers

Analysis with undrained and drained modes for the performance of the peat and clay layers were done to check the behaviour of the wall in short-term and long-term conditions. The peat and clay layers are simulated under undrained mode the in short term case and in drained mode for the long term case. Figures 5.22 to Figure 5.25 show the deflections of the wall and the ground surface settlements for the two cases. The lateral wall movements and the settlements in the drained mode are both smaller than the undrained mode for both excavations; but the differences are not significant (see Table 5.6)

5.7.5 Effect of Wall stiffness

The stiffness of the secant pile wall is another parameter that affects the deformation pattern of the supported excavations. For bored piled wall system, the reduction factor adopted for the stiffness is also a controversial topic in Gold Coast engineering practice; varying from 50% (50%EI) to 70% (70% EI), and the full value(i.e. 100% EI) without any reduction. Thus, the influence of the wall stiffness on the performance of the secant piled wall was also investigated by adopting different cracked coefficients for the wall stiffness (EI) values. Also the stiffness of the wall was increased 10 times to enlarge the range of study as can be noted in Table 5.7 for the two excavations

Figures 5.26 and 5.27 summarize the lateral wall movement and surface ground settlement as influenced by the stiffness of wall at different excavation stages for the two projects. In general, the maximum lateral wall movements and the ground surface settlements decrease with increasing wall stiffness. However, the use of stiffer wall is not effective in reducing the maximum lateral wall movements as well as the maximum ground surface settlements. The maximum lateral wall movements were almost unchanged when the stiffness of the wall increased from 50%EI to 100% EI. This result is in agreement with the study carried out by Cheng and Tui (1990) and Wong and Poh (1995), who found that the wall stiffness is not effective in limiting the lateral

movements. However, when the stiffness of the wall was improved by 10 times, the maximum deflection of the wall reduced from about 60mm to about 40mm.

Similar phenomenon happened on the pattern of the ground surface settlements for the two excavations as shown in Figures 5.28 and 5.29. The coefficients for the cracked flexible stiffness of the pile do not influence the ground surface settlement a lot, however, when the stiffness of the wall increased by 10 times, the ground surface settlement reduced almost to half of the original values. Figures 5.30 and 5.31 show, the bending moment of the wall with different stiffnesses at each excavation depth for the two excavations. The bending moment of the wall increased with the increase in the f stiffness of the wall. Tables 5.9 and 5.10. contain the extreme values as caused by different stiffness of the wall for Circle on Cavill and Sundale excavations.

Clough and O'Rourke (1990) pointed out that in clay the effect of wall stiffness theoretically does not significantly affect the basal heave. Figure 5.38 shows the relationship between the maximum lateral wall movement and the stiffness of wall for Circle on Cavill project. With the increase of the system stiffness, δ_{hmax} /H keeps unchanged from the 30% EI to 100% EI, but reduce to about half the value at 500% EI. The risk of Basal Heave is low since the factor of safety against Basal Heave varied between 1.5 to 2.0.

5.7.6 Pre-stress of Anchor (only for Circle on Cavill)

To control the lateral wall movement analysis was performed by keeping the same EA value for anchors but increasing their pres-stress forces as shown in Table 5.11. Case A is the prestress value from the standard simulation, while Case B is for the case when the prestress is increased by 100 kN/m for the first row of anchors. Case C increases the prestress by 70kN/m for the 2nd row of anchors and by 60 kN/m for the 3rd row of anchors as compared to case B. The results of the lateral wall movements, ground surface settlements and bending moments of wall at each excavation depth for Circle on Cavill project are shown in Figures 5.33 to Figure 5.35 respectively. From these figures, it can seen that increasing the prestress by 100kN/m for the first row of anchors can reduce the lateral wall movement by 15mm at the top of the wall and by 10mm the ground surface settlement (Case B); but it cannot reduce the maximum deflection of the wall. However, increasing the prestress of the three anchors at same time (Case C), the maximum lateral wall movement can reduce by 10mm and the ground surface settlement can reduce by about 20 mm as compared to Case B at 11.65 m excavation depth. Figure 5.34 shows the effects of the pre-stress of the anchors on the bending moments of the wall. The Case B has the largest bending moment of 189.3 kNm/m than other two cases because its deformation is larger than the other two cases. Table 5.12 shows the extreme values for these three cases at different excavation depth.

5.7.7 Effect of the length of Anchor (only for Circle on Cavill)

Kempfert, H.G. (1994) found that the horizontal deflection at the top of the wall would be reduced by 60% by increasing the anchor length by 9 m for an unfavourable ground

water position, which almost avoid the damage which would have otherwise occurred. Therefore the length of anchors at the Circle on Cavil excavation was varied with length of anchors adopted in the analysis. Case L2 is an analysis where s the length of the first row anchor is increased by 3m based on the standard value used, and Case L3 is when the anchor lengths of the second row and third row are increased by 3m over and above the increase adopted in Case L2; Case L4 increases the length of the first row of anchor by an additional 3m as was used in Case L3.

Figure 5.36 summarize the lateral wall movements with the increase of the anchor lengths. Figure 5.37 shows that Case L2 and Case L3 have lower maximum ground surface settlements than Case L1 and Case L4. Case L4 did not result in reducing the maximum ground surface settlement effectively although its anchor length is the longest. Case L3 was able to reduce to 40%, the ground surface settlement than Case L1 where all three anchors were increased in length by 3m. Case L4 increases by 6m the length of the first row of anchors and by 3m for the 2^{nd} and 3^{rd} row of anchors; in this case the reduction in the maximum ground surface settlement is only 30%. Therefore it can be concluded that the ground surface settlement reduces with the increase in anchor length; but the anchor lengths should be within reasonable range to reduce the ground surface settlement more effectively.

CHAPTER 6

CONCLUSIONS AND RECOMMENDATIONS FOR FUTURE RESEARCH

Two secant piled wall deep excavations (Circle of Cavil and Sundale) predominantly permeable sandy soils at Gold Coast were analysed. In situ- tests data from Standard Penetration Tests were used to obtain the relevant geotechnical parameters using the correlations proposed by well known researchers.

PLAXIS software was used to analyse these excavations and the results were compared with the WALLAP analysis used in the design and construction control. A parametric study was conducted with the PLAXIS software to have greater understanding of the factors that control the performance of deep excavations. The conclusions are in three parts: one relates to the sub-soil layer modelling, the second part is on the geotechnical parameters chosen for the analysis and this part relates to the analysis using PLAXIS and its comparison with the WALLAP analysis.

6.1 Soil Layers

The general subsoil at Gold Coast established in this study is composed of five soil layers: The first layer is loose to medium sand layer varying in thickness from 4 to 5m; The second layer is dense to very dense sand layer varying in thickness from 9m to 11m; The third layer is peat layer whose thickness is from 4m to 5m; The fourth layer is very dense sand layer varying in thickness from 5m to 8m followed by the fifth layer, sandy clay varying in thickness from 5m to 9m, then final layer is rock. In situ SPT tests were done to obtain the soil parameters for these soil layers.

6.2 Soil Parameters

The soil parameters adopted during PLAXIS simulation for the two excavations are given in Tables 4.24 and Table 4.26. The stiffness of soil is especially sensitive to the performance of the secant pile wall system. The Young's modulus of the peat layer was found to have substantial effects on the wall movements and the settlement profiles.

6.3 PLAXIS Analysis and Comparison with WALLAP Analysis

The secant piled wall was in two parts at the Circle on Cavill site; the upper 14.5 m was reinforced and the lower 12.5m was not reinforced and functioned as a cut off wall. However, for the Sundale excavation the secant piled wall stopped at the rock layer and was reinforced for the full depth of 11m.

The WALLAP model only analysed the upper reinforced part of the secant piled wall at the Circle on Cavill excavation; thus the WALLAP analysis assumed a fixed boundary at

the toe reinforced portion of the wall at the Circle of Cavill excavation. This assumption in the WALLAP analysis at the Circle of Cavill excavation under-estimated the lateral wall movement at the bottom of the reinforced part of the wall. Bending moment and shear force diagrams are similar for both analyses. For the Sundale excavation both PLAXIS and WALLAP gave similar results for the wall deflection, bending moment and shear force.

The soil model used in the PLAXIS analysis in this study is based on Mohr-Coulomb yield function. Using such a model posed difficulties with the peat layer encountered at the Circle on Cavill excavation. The frication angle ($\bar{\phi}$), the coefficient of earth pressure at rest (K_o), and the Young's modulus (E) were hard to decide for the peat layer in this PLAXIS simulation. The soft-creep-model in software PLAXIS is more suitable to analyse the soft soil like peat in future work.

The conclusions reached from the extensive parametric study conducted with the PLAXIS analysis will now be presented

- The wall embedment depth is not effective in reducing the maximum lateral wall movement for both excavations.

- The low stiffness of the peat layer seems to increase the lateral wall movement by an additional 25mm and the surface settlement also by additional 35mm for the Circle on Cavill excavation.

- The lateral wall movement and the surface settlement at the Circle on Cavill excavation is greatly influenced by the modulus value, E of the very dense sand layer and are about 15mm when the modulus is 200 MPa. The bending moment of the wall increased with the Young's modulus of this very dense sand layer

- The effect of the cracking in the wall and the subsequent reduction in the stiffness do not seem to influence the wall movement, bending moment and shear force.

- Increase in the pres-stress values of the anchors reduced the lateral movement of the wall.

The increase in length of the anchors reduced the lateral wall movements and the settlement, and there appear to be a critical length beyond which further increase in the anchor length has no effect on the wall movement or the surface settlement. increasing 6m for first row anchor and increasing 3m for other two anchors only can reduce about 30% of horizontal wall displacement and ground surface settlement.

6.4 Recommendations for Future Research

The following recommendations are suggested for future research on deep excavations.

- Geotechnical parameters are obtained both from SPT and CPT (Cone penetration test) and a decision be made on the reliability of the parameters to be used in deep excavation analysis.
- Refined soil models based on elasto-plastic theories should be used rather than the simple Mohr Coulomb model.
- The performance of anchored excavations should be compared with strutted or braced type of excavations.
- 3D analysis be conducted and the results are used to calibrate the simple 2D Plane strain analysis as conducted in this study.

REFERENCE

Addenbrooke, T.I., Potts, D.M. and Dabee, B. (2000), Displacement Flexibility Number for Multipropped Retaining Wall Design, Journal of Geotechnical and Geoenvironmental Engineering, ASCE, Vol.126, No.8, pp.718-726.

Bolton, M.D. (1986), The Strength and Dilatancy of Sands, Geotechnique, 36, No.1, 65-78.

Boone, S. J., and Crawford, A. M. (2000). Braced Excavation: Temperature, Elastic Modulus, and Strut Loads. Journal of Geotechnical and Geoenvironmental Engineering, Vol. 16, No. 10, pp. 870-881.

Bowles, J.E. (1993). Foundation Analysis and Design , 5th edit, Times Roman by Publication Services, Inc.

Bowles, J.E. (1996), Foundation Analysis and Design, 5th ed, America, The McGraw-Hill Companies, Inc.

Borin, D.L. (1989), Wallap - computer program for he stability analysis of retaining wall. Geosolove.

Briaud and Kim, (1998). Beam –Column Method for Tieback wall, Journal of Geotechnical and Geoenvironmental Engineering, Vol. 124, No.1 .

Briaud, J.L. and Lim, Y.J. (1999). Tieback Walls in Sand : Numerical Simulation and Design Implications, Journal of Geotechnical and Geoenvironmental Engineering, ASCE, Vol. 125, No.2, pp.101-110.

Brooks, N.J. and Spence, J.F.(1992). Design and recorded performance of a secant retaining wall in Croyon. Proc. Int. Conf. Retaining Structures, Cambridge.

Brown, P.T., and Booker, J.R. (1985), Finite element analysis of excavation, Res. Rep.No. 532, School of Civil and Mining Engineering, University of Sydney, Sydney, Australia

BS 8081 (1989), Code of Practice for Ground Anchorage. British Standard Insituation, London.

Charn, J.C., Chi, S.Y., Wang, C.C., Lin, C.C. and Tsay, M.S.(2006) Development of Case History Database and Back-Analysis of Soil Parameters for Deep Excavation in Taipei Basin.

Day, R.A., Potts, D.M.(1998), The effect of interface properties on retaining wall behavior, John Wile & Sons, Ltd.

Caspe,5 M (1996), Surface Settlement Adjacent to Braced Open Cuts, J.Soil Mech. And Foundation Div, ASCE, Vol. 92, No. SM4, July, pp 51-59.

Chandrasekaran, V.S. and King, G.J.W. (1974). Simulation of excavation using finite element, J. Geotech. Engrg. Div., ASCE 100 (9), 1086-1089.

Chou, N. S., and Su, C. K. (1990). Exteral Stability of a Reinforced Warth Wall Consructed Over Soft Clay. Design and Performance of Earth Retaining Structures. ASCE., pp. 394-408.

Christian, J.T., and Wong, I.H. (1973). Erros in simulating excavation in elastic media by elements. Soils and Found., Tokyo, 13, 1-10.

Clayton, C.R.I., Militisky, J., and Woods, R.I. (1993), Earth Pressure and Earth-Retaining Structures, 2nd edition, chapman & Hall, UK, pp. 285.

Cloough, G.W., Weber, P.R., and Lamont, J.(1972). Design and observation of a tie-back wall. Proc., ASCE Spec. Conf., Perf. of Earth and Earth Supported Struct., Vol. 1, ASCE, New York, 1367-1389.

Clough, G.W., Smith, E.M., and Sweeney, B.P.(1989), Movement control of excavation supports systems by iterative design, Foundation engineering, current principles and practices, K. H. Kulhawy, ed., Vol. 2, pp.869-884.

Clough, G.W. and O'Rourke, T.D. (1990), Construction-induced Movements of Insitu Walls, Proceedings, Design and Performance of Earth Retaining Structures. ASCE Special Conference, Ithaca, New York, pp. 439-470.

C, Y.Ou and C, H.Lai (1993), Finite-element analysis of deep excavation n layered sandy and clayey soil deposit, Canadian Geotechnical Journal, 31, pp. 204-214.

Day, R.A., Potts, D.M.(1998), The effect of interface properties on retaining wall behavior, John Wile & Sons, Ltd.

Desai, C.S., Muqtadir, A., and Sheele, F.(1986). Interaction analysis of anchor-soil system. J.Geotech. Engrg., ASCE, 112(5), 537-553.

Dibiagio, E. and Roti, J.A. (1972), Earth Pressure Measurements on a Braced Slurry Trench Wall in Soft Clay, European Conference Soil Mechanics and Foundation Engineering, 5. Madrid.Proceeding, Vol.1,pp. 473-483.

Fernandes, M.M., and Falcao, J.C.B. (1988), The nonlinear behavior of ground anchors and its consideration in finite element analysis of tied-back walls, Proc.Num. Meth in Geomech., Balkema, Rotterdam, The Netherlands, 1243-1248.

Finno, R.J. and Nerby, S.M. (1989), Saturated Clay Response During Braced Cuts Construction, J.Geotech. Eng., ASCE, Vol. 115, No.8, pp.1065-1084.

Gan C.H. (1997), Review and Analysis of Ground Movements of Braced Excavation in Bankok Subsoil using Diaphragm wall, M.Eng. Thesis, Asian Institute of Technology.

Ghaboussi, J., and Pecknold. D.A.(1984), Incremental finite element analysis on geometrically altered structure. Int. J. Number. Methods in Engrg., 20, 2051-2064.

Goodman, R.E., and Brown, C.B. (1963). Dead load stresses and instability of slopes. J.Soil Mech. and Found.Div., ASCE, 89(3).

Hayat, T. M. (1992). "The coefficient of earth pressure at rest." PhD thesis, Univ. of Illinois at Urbana-Champaign, Urbana, Ill.

Heliun, R. (1991), Analysis of Diaphragm Wall by Finite Element Method, M.Sc. Course in Foundation Engineering, The University of Birmingham.

Hight, D.W. & Higgins, K.G.(1994) An approach to the prediction of ground movements in engineering practice. Background and application, International sysmposium on Pre-Failure Deformation characteristic of Geomaterials, Sapporo, Japan.

Hunder,K.J. (1976). Deformation and earth pressure. Proc. Panel Discussion, 6th ECSMFE, Vol.4, 37-40.

Huybrechts, N., Vos, M.D., Whenham,V., WP 3 (2004). Design Tools, Part 1: Use of Finite Element Method in Geotechnical Design.

Hsi, J.P. and Small, J.C. (1992), Analysis of Excavation in An Elasto-Piastic Soil Involving Drawdown of the Water Table, Computers and Geotechnics, 13, pp. 1-19.

Ishihara, K. (1970). Relations between process of cutting and uniqueness of solution, Soils and Found., Tokyo, 10 (3), 50-65.

Jiang, M.J., Yu, H-S, Harris, D. (2004) Discrete element modeling of deep penetration in granular soil, John Wile & Sons, Ltd.

KARLSRUD, K. (1986), Perfomance Monitoring of Deep Supported Excavations in Soft Clay, Fouth International Geotechnical Seminal Field Instrumentation and Insitu Measurements, Singapore, pp.187-202.

Kempfert, H.G. Gebreselassie, B. Raithel, M. , Stroh, D. (1974). "Berechnung verankerter Baugruben nach der Finite Elemente Methode". Mitteilungen der Versuchsanstalt für Bodenmechanik und Grundbau, TH Darmstadt, Heft 13.

Kempfert, H.G. Gebreselassie, B. Raithel, M. ,Ulrichs, K.R. (1981). "Untersuchungen über das Trag- und Verformungsverhalten verankerter Schlitzwände in rolligen Böden". Die Bautechnik, pp. 142.

Kempfert, H.G. and Gebreselassie, B. and Raithel, M. (1994). Damage from Deep, Multi-Tied Excavation due to Deformation of the Anchor-Soil Block System, Holzmann Bautechnik GmbH.

Kempfert, H.G. Gebreselassie, B. Raithel, M., Nendza, H., Klein ,K. (1974). "Bodenverformung beim Aushub tiefer Baugruben". Straße Brücke Tunnel 9; pp. 231.

Lim, Y., and Briaud, J-L.(1996). Three dimensional non linear finite element analysis of tieback walls and soil nailed wall under piled bridged abutment. Rep.to the Federal Highway Administration and the Texa Department of Transportation, Department of Civil Engineering, Texas A & M University, College Station, Tex.

Mana, A.I. and Clough, G.W. (1981), Prediction of Movements for Braced Cur in Clay, Journal of Geotechnical Engineering Division, ASCE, Vol. 107, No.6, pp.759-777.

Mayne, P. W., and Kulhawy, F. H. (1982). "*K*0– OCR relationship in soil." *J. Geotech. Eng. Div., Am. Soc. Civ. Eng.*, 108(6), 851–872.

Mesri, G., and Hayat, T. M. (1993). "The coefficient of earth pressure at rest." *Can. Geotech. J.*, 30, 647–666.

Michalowski, R.L. (2005). Coefficient of Earth Pressure at Rest, ASCE, Journal of Geotechnical and Geoenvironmental Engineering, Vol. 131, No. 11, November,1,

NAVFAC, 1986, Foundations and Earth Structures (DM-7.02), Washington, D.C. Department of the US Navy.

O'Rourke, T.D. (1981), Ground Movements Caused by Braced Excavations, Journal of Geotechnical Engineering division, ASCE, Vol.107, No.6, pp.1159-1177.

Osman, A.S., and Bolton, M.D.(2004), Avoiding Excessive Displacements: A New Design Approach For Retaining Wall, Department of Engineering, Cambridge University, Uk.

Ou, C.Y, Hsieh, P.G. and Chiou, D.C. (1993), Characteristics of Ground Surface Settlement during Excavation, Can. Geotech.J., Vol. 30, No.5, pp758-767.

Ostermayer, H., and Scheele, F. (1977). ''Research on ground anchors in noncohesive soils.'' *Proc., Special Session No. 4, 9th Int. Conf. on Soil Mechanics and Foundation Engineering*, 92–97

Peck, R.B. (1969), Deep Excavation and Tunneling in Soft Ground, Proc. Of the 7" Int. Conf. on Soil Mechanics and Foundation Engineering;, Mexico, State of the Art Volume, pp.225-290.

Peck, R.B.& Bazaraa, A.R.S.(1969), Discussion of " settlement of spread foundation", Journal of Soil Mechanics and Foundation Division, ASCE, SM3.

Poh, T.Y. Wong, I.H. and Chandrasekaran, B.(1997), Performance of Two Propped Diagram Walls in Stiff Residual Soil, J.Performance of Construction Facilities, Vol.11, No.4, pp.190-199.

Rampello,S., Tamagnini, C. and Calabrese, C.,(1992), Observed and Predicted Response of a Braced Excavation in Soft to Medium Clay, Predictive Soil Mechanics, Proceedings of the Wroth Memorial Symposium Catherine's college, Oxford, pp.544-561.

Rowe, P.W., (1955) "Sheet pile walls encastre at the anchorage", *Institution of Civil Engineers, Proceedings*, part 1, vol 4.

Schmertmann, J.H. (1975). Statics of SPT. Journal of the Geotechnical Engineering Division, ASCE, **105**(GT5): 655–670.

Schmidt, B. (1966). "Earth pressures at rest related to stress history .Discussion." *Can. Geotech. J.*, 3(4), 239–242.

Schmidt, B.(1966). "Earth pressures at rest related to stress history.Discussion." *Can. Geotech. J.*, 3(4), 239–242.

Schweiger,H.F. and Freiseder (1997), Deep Excavations in Soft Ground-In-Situ Measurements and Numerical Predictions, 14 International Conference on Soil Mechanics and Foundation Engineering, Congress centrum, Hamburg, Germany, 6-12 Septermber.

Seed, H.B., Tokimatsu, K., Harder, L.F., and Chung, R.M. (1985).Influence of SPT procedures in soil liquefaction resistance evaluations.Journal of the Geotechnical Engineering Division, ASCE, **111**(GT12): 1425–1445.

Skempton, A.W. (1986). Standard penetration test procedures and effects in sands of overburden, relative density, particle size, aging and overconsolidation. Géotechnique, **36**(3): 425–447.

Stroud, M.A.1989, The standard Penetration test-its application and interpretations. Penetration testing in the UK, Tomas Telford, London, 29-49.

Tephraksa,W. Thasnanipan, N. and Tanseng, P.(1999). Analysis of lateral wall movement for deep excavation in Bangkok Subsoil, Civil and Environmental Engineering Conference, Vol.2, Part 1, Bangkok, Thailand.

Tsui, Y. (1974). A fundamental study of tie-back wall behavior, PhD thesis, School of Engineering, Duke University, Durham, N.C.

Wyllie, D.C.(1999), Foundations on Rock, 2nd, E & FN Spon, London, pp. 53.

Tables

Table 2.1 Advantages and disadvantages of each support system.

Name	Typical EI (MPa/m)		Advantages	Disadvantages
Steel sheeting	142	14155	(1) Can be impervious (2) Easy to handle and construct (3) Low initial cost	(1) Limited stiffness (2) Inerlocks can be lost in hard driving or in gravelly soils
Soldier pile and lagging	315	18873	(1) Easy to handle and construct (2) Low initial cost (3) Can be driven or augered	(1) Wall is pervious (2) Requires care in placement of lagging
Cast-in-place concrete slurry wall	45296	361742	(1) can be impervious (2) High stiffness (3) Can be part of permannent structure	(1) High initial cost (2) Special contrator required to construct (3) Extensive slurry disposal needed (4) Surface can be rough
Precast concrete slurry	45296	361742	(1) can be impervious (2) High stiffness (3) Can be part of permanent structure (4) Can be prestressed	(1) High initial cost (2) Specialty contractor required to construct (3) Slurry disposal needed (4) Very large and heavy members must be handled for deep systems (5) Permits some yielding of subsoils
Cylinder Pile Wall	18087	157279	(1)Secant piles impervious (2) High stiffness (3) Highly specialized equipment not needd for tangent piles (4) Slurry not needed	(1) High initial cost (2) Secant piles require special equipment

Table 2.2 Factors in the selection of a support system for a deep excavation (US Navy, 1982)

	Requirement	Lends itself to Use of	Downgrades Utility of	Comment
1	Open excavation area	Tiebacks or rakers or cantilerer walls (shallow excavation)	Crosslot struts	-
2	Low initial cost	Soldier pile or sheetpile walls; combined soil slope with wall	Diaphram walls, cylinder pile walls	-
3	Use as part of permanent structure	Diaphragm or cylinder pile walls	Sheetpile or soldier pile wall	Diaphragm wall most common as permanenet wall
4	Deep, soft clay subsurface conditions	Strutted or raker supported diaphragm or cylinder pile walls	Tiebacks, flexible walls	Tieback capacity not adequate in soft clays
5	Dense, gravelly sand	Soldier pile, diaphragm or clay subsoils	Sheetpile walls or cylinder pile	Sheetpile lose interlock on hard driving
6	Deep, over-consolidatied clays	Struts, long tiebacks or combination tie-back	Short tiebacks	High lateral stresses ar relieved in O.C.soils and lateral movements may be large and extend deep into soil
7	Avoide dewatering	Diaphragm walls, possibly sheetpile walls in soft subsoils	Soldier pile wall	Soldier pile wall is pervious
8	Minimize movemenets	High preloads on stiff strutted or tie-back wall	Flexible walls	Analyze for stability of bottom of excavation
9	Wide excavation (greater than 20m wide)	Tiebacks or rakers	Crosslot struts	Tieback preferable except in very soft clay subsoils.
10	Narrow excavation (less than 20m wide)	Crosslot struts	Tiebacks or rakers	Struts more economical but tiebacks still may be preferred to keep excavation open

Table 4.1. Two researched excavation projects in Gold Coast

Parameters	Unit	Excavation Project Name	
		Circle on Cavill	Sundale
Excavation width	(m)	70.0	34.0
Excavation depth	(m)	11.7	9.7
Embedment depth	(m)	2.9	1.3
Diameter of pile	(m)	0.6	0.5
Anchor	(row)	3.0	1.0
Spacing of anchors	(m)	2.4	2.4

Table 4.2. SPT hammer efficiencies (Clayton, 1990)

Country	Hammer Type	Hammer Release Mechanism	Hammer Efficiency E_m
Argentina	Donut	Cathead	0.45
Brazil	Pin weight	Hand dropped	0.72
China	Automatic	Trip	0.60
	Donut	Hand dropped	0.55
	Donut	Cathead	0.50
Colombia	Donut	Cathead	0.50
Japan	Donut	Tombi trigger	0.78-0.85
	Donut	Cathead 2 turns + special release	0.65-0.67
UK	Automatic	Trip	0.73
US	Safety	2 turns on cathead	0.55-0.60
	Donut	2 turns on cathead	0.45
Venezuela	Donut	Cathead	0.43
Gold Coast, AU	Automatic	Trip	0.73

Table 4.3. Borehole, sampler, and rod correction factors (Skempton, 1986)

Factor	Equipment Variables	Value
Borehole diameter factor, C_B	65-115 mm	1.0
	150 mm	1.05
	200 mm	1.15
Sampling method factor, C_S	Standard sampler	1.00
	Sampler without liner	1.20
Rod length factor, C_R	3 – 4 m	0.75
	4-6 m	0.85
	6-10 m	0.95
	>10 m	1.00

Table 4.4 Summarised average SPT *N*, N_{60}, $(N_1)_{60}$ of Circle on Cavill

Layer No.	Soil Layers	Thickness (m)	Bulk Density, γ (kN/m^3)	Effective density, γ' (kN/m^3)	Measured, SPT N-Value	Corrected SPT-*N* value, N_{60}	Vertical effective stress , σ_z'	Total vertical stress, $\Sigma(\sigma_z')$	overburden stress corrected N-value, $(N_1)_{60}$
1	Loose sand	2.3	17	7	3	3	16	16	7
2	Md sand	3.0	18	8	24	22	24	40	35
3	Vd Sand up	9.5	19	9	50	46	86	126	41
5	Peat	3.5	16	6	8	7	21	147	6
4	Vd sand low	3.8	19	9	50	46	34	181	34
5	Sandy clay	9.4	19	9	22	20	85	265	12
6	Clay Sand Gravel	2.5	18	8	50	46	20	285	27
7	Strong Argillite	6.0	22	12	50	46	72	357	24

Table 4.5 Summarised average SPT *N*, N_{60},, $(N_1)_{60}$ of Sundale

Layer No.	Soil Layers	Thickness (m)	Bulk Density, γ (kN/m3)	Effective density, γ' (kN/m3)	Measured, SPT N-Value	Corrected SPT-*N* value, N_{60}	Vertical effective stress , σ_z'	Total vertical stress, $\Sigma(\sigma_z')$	Overburden stress corrected N-value, $(N_1)_{60}$
1	Fill	1.1	16	6	10	9	6.6	7	36
2	Loose sand	1.5	17	7	10	9	10.5	17	22
3	Md sand	2.6	18	8	33	30	20.8	38	49
4	V st clay	3	20	10	24	22	30	68	27
5	EW S' stone	7.6	22	12	50	46	91.2	159	36

Table 4.6 Empirical values for φ, Dr, and unit weight of granular soils based on the SPT at about 6m depth and normally consolidated (approximately, $\varphi = 28^0+15^0Dr(+2^0)$, Bowles,1996)

Description		**Very loose**	**Loose**	**Medium**	**Dense**	**Very dense**
Relative density, Dr		0	0.15	0.35	0.65	0.85
SPT, $N_{70'}$	fine	1-2	3-6	7-15	16-30	-
	medium	2-3	4-7	8-20	21-40	>40
	coarse	3-6	5-9	10-25	26-45	>45
Friction angle, φ	fine	26-28	28-30	30-34	33-38	<50
	medium	27-28	30-32	32-36	36-42	
	coarse	28-30	30-34	33-40	40-50	

Table 4.7. Bulk density & friction angle & cohesion for soil (Huybrechts, 2004)

Soil	Loose		Compacted		Loose or compacted		Friction Angle,φ		Cohesion,c
	bulk density	Weight density	bulk density	Weight density	Submerged density	Submerged weight density	Loose	Compacted	
	(kg/m^3)	(kN/m^3)	(kg/m^3)	(kN/m^3)	(kN/m^3)	(kN/m^3)	(^{o})	(^{o})	(kN/m^2)
Fine sand	1750	17.5	1900	18.6	1050	10.3	30	35	0
Coarse sand	1700	16.7	1850	18.2	1050	10.3	35	40	0
Gravel	1600	15.7	1750	17.2	1050	10.3	35	40	0
Peat	-	-	1300	12.8	300	3	-	5	5
River mud	1450	14.2	1750	17.2	1000	9.8	-	5	5
Loamy soil	1600	15.7	2000	19.6	1000	9.8	-	10	10
Silt	-	-	1800	17.7	800	7.9	-	10	10
Sandy clay	-	-	1900	18.6	900	8.8	-	0	15 to 40
Very soft clay	-	-	1900	18.6	900	8.8	-	-	< 20
Soft clay	-	-	1900	18.6	900	8.8	-	-	20 to 40
Firm clay	-	-	2000	19.6	1000	9.8	-	-	50 to 75
Stiff clay	-	-	2100	20.6	1100	10.8	-	-	100 to 150
Very stiff clay	-	-	2200	21.6	1200	11.8	-	-	> 150

Table 4.8. Relative density versus N_{60} (Jamiolkowski et al.1988)

Sand	D_r, (%)	N_{60}
Very Loose	0-15	0 - 3
Loose	15-35	3 - 8
Medium	35-65	8 - 25
Dense	65-85	25 - 42
Very Dense	85-100	42 -58

Table 4.9. : Relative Density Dr and SPT and Friction angle φ'

Soil Type	Relative Density	SPT N_{60}	Friction Angle φ', degree			
	Dr (%)	Terzaghi and Peck	Meyerhof	Peck, Hanson and Thornburn	Meyerhof	Kulhawy and Mayne
		-1967	-1974	-1974	-1956	2004
Very Loose	< 20	< 4	< 30	< 29	< 30	25
Loose	20- 40	4 -10	30 - 35	29 - 30	30 - 35	28
Medium	40- 60	10 -30	35 - 38	30 - 36	35 - 40	30
Dense	60- 80	30 - 50	38 - 41	36 - 41	40 - 45	36
Very Dense	> 80	> 50	41 - 44	> 41	> 45	41

Table 4.10 Friction angle φ' for Cohesive soil (Huybrechts, 2004)

Description	Ip (%)	Undrained c (kPa)	φ' (^{0})
Very soft	> 80	< 20	15
Soft	80	20 - 40	15
Firm	50	50- 75	20
Stiff	30	100- 150	25
Very stiff	15	> 150	30

Table 4.11. Typical values for dilation angle (FLAC,2000)

Soil type	Dilation angle, Ψ(^{0})
Dense sand	15
Loose sand	<10
Normally consolidated clay	0
Granulated and intact marble	12-20
Concrete	12

Table 4.12. Approximate values of Young's modulus E (Terzaghi,1954)

Young's modulus, E		Unit	Relative density, Dr		
			loose	medium	dense
Cohesionless soil	Dry or moist sand	kPa/m	880	2800	7100
	Submerge sand	kPa/m	560	1800	4600
Cohesive soil	Undrained shear strength	kPa	20-40	40-75	75-150
	Young's Modulus	kPa	1600-6000	6000-20000	20000-75000

Table 4.13. Young's modulus E

Soil Type	Bowles, 1996	Das, 1994	Kulhawy and Mayne, 1990	Huybrechts, 2004
Clay				
Very soft	2-15	-	-	1 - 5
Soft	5-25	2-4	1.5 – 4	5 - 20
Medium	15-50		4 – 8	20 - 50
Hard	50-100	6-14	8 – 20	50 -100
Sandy	25-250	-	-	25 - 200
Shale	-	-	-	100 - 200
Sand				
Silty	5-20	-	-	-
Loose	10-25	10 -27	10 – 20	10 - 25
Medium			20 – 50	
Dense	50-81	34 - 69	50 – 100	25 - 100
Sand and gravel				
Loose	50-150	-	-	-
Dense	100-200	-	-	100 - 200
Shale	150-5000	-	-	-

Table 4.14. Poisson ratio, υ

Soil Type	Huybrechts, 2004	Bowles, 1993	Das, 1994
Clay saturated	0.5	0.4-0.5	-
Unsaterated clay	0.35 to 0.4	0.1-0.3	-
Soft clay	-	-	0.15-0.25
Medium clay	-	-	0.2-0.5
Sandy clay	-	0.2-0.4	-
Silt	0.3 to 0.35	0.3-0.35	-
Rock	0.1 to 0.4	0.1-0.3	-
Silty sand	0.15-0.35	-	0.2-0.4
Loose sand	0.1 to 0.3	-	0.2-0.4
Medium sand	-	-	0.25-0.4
Dense sand	0.3 to 0.42	-	0.3-0.45
Clay	0.2 to 0.4	-	-
commonly used	-	0.3-0.4	-

Table 4.15. Typical values of Ko (Mayne and Kulwahy, 1982)

Soil Type	K_0
Loose sand	0.35
Dense sand	0.6
NC Clays	0.5-0.6
Lightly OC Clay	1
Heavily OC Clay	3

Table 4.16. Tables of values of horizontal component of K_p (Caquot and Kerisel,1949)

Soil friction angle (degrees)	wall friction angle, φ (degrees)							
	0	5	10	15	20	25	30	35
10	1.42	1.55	1.62	–	–	–	–	–
15	1.7	1.88	2.05	2.12	–	–	–	–
20	2.04	2.28	2.55	2.77	2.83	–	–	–
25	2.46	2.85	3.21	3.57	3.85	3.89	–	–
30	3	3.56	4.07	4.63	5.16	5.53	5.56	–
35	3.69	4.48	5.3	6.14	6.99	7.83	8.41	8.36
40	4.6	5.78	7.03	8.37	9.75	11.3	12.7	13.8
45	4.83	7.58	9.58	11.8	14.3	16.9	19.7	22.5
50	7.55	10.2	13.5	17.4	21.9	26.9	32.6	38.9

Table 4.17. Typical values of permeability (Duncan ,2001)

Soil type	**Permeability, k (cm/sec.)**
Coarse sand	$>10^{-1}$
Fine sand	10^{-3}-10^{-1}
Silty sand	10^{-5}-10^{-3}
Silt	10^{-7}-10^{-5}
Clay	$<10^{-7}$

Table 4.18. Soil parameters used in PLAXIS for Circle on Cavill

No.	Soil Layer	$(N1)_{60}$	r_{sat}	r_{unsat}	E	K_0	Φ'	Ψ	*Kx*	*Ky*	v
			(kN/m^3)	(kN/m^3)	(Mpa)		(degrees)	(degrees)	(m/day)	(m/day)	
1	Loose sand	7	17	16	20	0.5	28	0	1.0368	1.0368	0.35
2	Md sand	35	18	17	70	0.45	39	9	4.32	4.32	0.35
3	Vd Sand up	41	19	18	200	0.33	45	15	0.259	0.259	0.35
5	Peat	6	16	15	10	0.658	20	0	0.00021	0.00042	0.35
4	Vd sand low	34	19	18	200	0.33	45	15	0.259	0.259	0.35
5	Sandy clay	12	18	17	62.5	0.515	29	0	0.00605	0.00605	0.35
6	Clay Sand Gravel	27	21	20	200	0.33	45	15	0.00605	0.00605	0.35
7	Strong Argillite	24	21	20	200	0.33	45	15	0.00017	0.00017	0.35

Note: Md : Medium dense; Vd : Very dense

Table 4.19. Soil parameters used in WALLAP for Circle on Cavill

No.	Soil Layer	$(N1)_{60}$	r_{sat}	E	K_0	Consol State	Ka	Kp	C
			(kN/m^3)	(Mpa)		NC/OC			(kPa)
1	Loose sand	7	17	20	0.5	OC	0.285	4.632	-
2	Md sand	35	18	70	0.45	OC	0.25	5.649	-
3	Vd Sand up	41	19	200	0.33	OC	0.168	10.72	-
5	Peat	6	16	10	1.5	OC	1	1	21
4	Vd sand low	34	19	200	0.33	OC	0.168	10.72	-
5	Sandy clay	12	18	62.5	0.33	OC	0.168	10.72	-
6	Sand Gravel	27	21	200	0.33	OC	0.168	10.72	-
7	Strong Argillite	24	21	200	0.33	OC	0.168	10.72	

Note: Md : Medium dense; Vd : Very dense; OC: over-consolidated

Table 4.20. Soil parameters used in PLAXIS for Sundale project

No.	Soil Layer	$(N_1)_{60}$	γ_{sat}	γ_{unsat}	E	K_0	Φ'	Ψ	*Kx*	*Ky*	υ
			(kN/m^3)	(kN/m^3)	(Mpa)		(degrees)	(degrees)	(m/day)	(m/day)	
1	fill	21	17	16	75	0.4	34	4	1.728	1.728	0.29
2	Loose sand	22	17	16	30	0.5	34	4	1.037	1.037	0.33
3	Md sand	49	18	17	75	0.4	37	7	0.173	0.173	0.29
4	V st clay	27	20	19	30	1.0	34.0	0.0	0.0216	0.0216	0.38
5	EW S' stone	36	22	21	200	0.5	41.5	0.0	0.0086	1.0086	0.33

Table 4.21. Soil parameters used in WALLAP for Sundale project

No.	Soil Layer	$(N_1)_{60}$	γ_{sat}	E	K_0	Consol State	Ka	Kp	c
			(kN/m^3)	(Mpa)		NC/OC			(kN/m^2)
1	fill	10	17	75	0.4	OC	0.258	5.56	
2	Loose sand	10	17a	30	0.5	OC	0.333	3.000	
3	Md sand	33	18	75	0.4	OC	0.258	5.56	
4	V st clay	24	20	30	1.0	OC	1.000	1.000	66.5
5	EW S' stone	>50	22	200	0.5	OC	1.000	1.000	266.4

Notes: Md = Medium dense;
V st = Very stiff

Table 4.22. The properties of structure element (Circle on Cavill)

Wall Type	E	I (50%)	EI	d	d_{eq}	A	EA	Weight	υ
	(kN/m^2)	(m^4/m) run	(kNm^2/m)	(m)	(m)	(m^2)	(kN/m)	(kN/m/m)	
Reinforced	3.00E+07	3.75E-03	1.13E+05	0.6	0.399	0.2826	8.48E+06	3.60	0.15
Cut-off	319754	3.75E-03	1.20E+03	0.6	0.399	0.2826	9.04E+04	3.60	0.15

	No.	Elev.	Spacing	A	E	Free Length	Inclination	EA	Pre-stress
		RL.	(m)	(m^2)	(kPa)	(m)	(degree)	(kN)	(kN)
Anchor	1	2.5	2.4	0.00043	2.00E+08	6	15	8.60E+04	350
	2	-2.0	2.4	0.00043	2.00E+08	6	15	8.60E+04	200
	3	-5.3	2.4	0.00043	2.00E+08	3	15	8.60E+04	100

	EA
	(kN)
Grout Body	1.00E+05

Notes: E = Young's modulus
I = Moment of initial
EI = Flexible stiffness of wall
EA = Axial stiffness of wall

d = Diameter of pile
d_{eq} = Equivalent diameter of pile
A = Area

Table 4.23. The properties of structure element (Sundale)

	E	I (50%)	EI	d	deq	A	EA	Weight	v
Wall	**(kN/m^2)**	**(m^4/m) run**	**(kNm^2/m)**	**(m)**	**(m)**	**(m^2)**	**(kN/m)**	**(kN/m/m)**	
	3.00E+07	1.10E-03	3.30E+04	0.5	0.001	0.19625	5.89E+06	13.0613447	0.15

	No.	Elev.	Spacing	A	E	Free Length	Inclination	EA	Pre-stress
Anchor		**RL.**	**(m)**	**(m^2)**	**(kPa)**	**(m)**	**(degree)**	**(kN)**	**(kN)**
	1.00E+00	1.20E+00	2.40E+00	0.000572	1.93E+08	5	1.50E+01	1.1E+05	500

	EA
Grout Body	**(kN)**
	1.00E+05

Notes: E = Young's modulus
I = Moment of initial
EI = Flexible stiffness of wall
EA = Axial stiffness of wall

d = Diameter of pile
d_{eq} = Equivalent diameter of pile
A = Area

Table 4.24. Construction stages of Circle on Cavill project

Stage No.	Excavate Depth	Stage description
1		Apply surcharge at RL. 4.00
2	2.2 m	Excavate to RL. 1.80 on passive side
3		Install first row anchor at RL.2.5
4	7.6 m	Excavate to RL-3.60 on passive side
		Dewatering
5		Install second row anchor at RL.-2.00
6	10.0 m	Excavate to RL.-6.00 on passive side
		Dewatering
7		Install third row anchor at RL -5.30.
8	11.65 m	Excavate to elevation -7.65 on passive side
		Dewatering

Table 4.25. Construction stages of Sundale project

Stage No.	Excavate Depth	Stage description
1		Apply surcharge at RL.3.80
2	3.3 m	Excavate to elevation 0.50 on passive side
		Dewatering
3		Install anchor at RL.1.20
2	9.7 m	Excavate to RL.-5.90 on passive side.
		Dewatering

Table 5.1. Maximum values from PLAXIS for the two projects

Extreme Values	Unit	Circle on Cavill	Sundale
Total Displacement	(mm)	74.69	23.17
Horizontal deflection	(mm)	65.4	21.45
Vertical deflection	(mm)	63.69	12.23
Bending moment	(kNm/m)	185.53	92.48
Shear force	(kN/m)	159.81	115.2
Velocity of groundwater	(mm/day)	10.01	29.47

Table 5.2. Comparison maximum values between PLAXIS and WALLAP for Circle on Cavill Project (final stage)

Circle of Cavil			PLAXIS	WALLAP
Maximum Lateral Wall Movement		(mm)	65.40	18.0
Maximum Ground Surface Settlement		(mm)	62.68	-
Maximum Bending Moment		(kNm/m)	185.53	159.90
Maximum Shear Force		(kN/m)	159.80	145.90
Anchor Forces	1	(kN/m)	177.5	150.96
	2	(kN/m)	139.21	151.83
	3	(kN/m)	98.473	139.54

Table 5.3. Comparison maximum values Between PLAXIS and WALLAP for Sundale Project (final stage)

Sundale		PLAXIS	WALLAP
Maximum Lateral Wall Movement	(mm)	21.07	22.00
Maximum Ground Surface Settlement	(mm)	12.44	-
Maximum Bending Moment	(kNm/m)	91.55	149.50
Maximum Shear Force	(kN/m)	115.43	143.8
Anchor Force	(kN/m)	213.00	228.00

Table 5.4. Maximum values from variations of Young's modulus of dense sand (Circle of Cavill)

Type	Excavation Depth (m)	Parameter Studies		
		E - 200	E-150	E- 100
Maximum lateral wall movement, δ_{hmax} (mm)	-2.2	6.2	6.3	6.6
	-7.6	18.0	21.7	27.7
	-10.0	33.8	37.7	46.0
	-11.7	65.4	69.9	78.8
Maximum ground surface settlement, δ_{vmax} (mm)	-2.2	11.3	11.9	13.1
	-7.6	18.8	21.0	26.3
	-10.0	33.8	37.6	45.6
	-11.7	62.7	66.3	75.3
Maximum wall bending moment, BM_{max} (kNm/m)	-2.2	49.1	48.7	48.8
	-7.6	73.2	77.0	84.5
	-10.0	154.4	146.5	139.2
	-11.7	185.5	170.9	152.2

Note: E-200 : Young's modulus of very dense sand is 200 MPa
E-150: Young's modulus of very dense sand is 150 MPa
E-100 : Young's modulus of very dense sand is 100 MPa.
δ_{hmax} : Maximum lateral wall movement
δ_{vmax}: Maximum vertical wall movement
BM_{max} : Maximum bending moment of the wall.

Table 5.5. Maximum values for undrained and drained peat and clay layers.

Project Name	Excavation Depth	Type		Undrained	Drained
Circle on Cavill	H = 11.65 m	δ_{hmax}	(mm)	65.40	56.28
		δ_{vmax}	(mm)	62.68	50.09
		BM_{max}	(kNm/m)	185.53	205.56
Sundale	H = 9.7 m	δ_{hmax}	(mm)	21.45	19.49
		δ_{vmax}	(mm)	12.23	10.65
		BM_{max}	(kNm/m)	92.48	98.93

Note :δ_{hmax} : Maximum lateral wall movement
δ_{vmax}: Maximum vertical wall movement
BM_{max} : Maximum bending moment of the wall.

Table 5.6. Variation of stiffness of wall for Circle on Cavill and Sundale

Wall type	Case No.	Stiffness of Wall, EI (kNm^2/m)	
		Circle on Cavill	Sundale
Reinforced secant pile Wall	50% EI	1.13E+05	3.30E+04
	70% EI	1.58E+05	4.62E+04
	100% EI	2.25E+05	6.60E+04
	500% EI	1.13E+07	3.30E+05

Table 5.7. Maximum values for different stiffness of wall (Circle on Cavill)

Results	Excavation Depth (m)	Parameter Studies			
		50% EI	70% EI	100% EI	500% EI
Maximum lateral wall movement, δ_{hmax} (mm)	-2.2	6.2	5.4	4.7	3.9
	-7.6	18.0	17.8	17.8	17.6
	-10.0	33.8	33.3	33.0	32.0
	-11.7	65.4	63.4	62.0	34.0
Maximum ground surface settlement, δ_{vmax} (mm)	-2.2	11.3	11.2	11.1	10.8
	-7.6	18.8	18.1	17.8	17.2
	-10.0	33.8	33.2	32.5	30.4
	-11.7	62.7	62.7	62.0	31.7
Maximum wall bending moment, BM_{max} (kNm/m)	-2.2	49.1	51.0	52.6	92.7
	-7.6	73.2	80.7	93.0	146.4
	-10.0	154.4	168.0	184.4	221.1
	-11.7	185.5	183.5	190.0	222.7

Table 5.8 Maximum values for different stiffness of wall (Sundale)

Results	Excavation Depth (m)	Parameter Studies			
		50% EI	70% EI	100% EI	500% EI
Maximum lateral wall movement, δ_{hmax} (mm)	-3.3	16.5	15.2	12.1	8.8
	-9.7	21.5	19.9	16.6	13.0
Maximum ground surface settlement, δ_{vmax} (mm)	-3.3	10.7	10.0	7.9	5.6
	-9.7	12.2	11.6	9.4	6.9
Maximum wall bending moment, BM_{max} (kNm/m)	-3.3	32.9	35.9	32.0	66.8
	-9.7	92.5	100.7	104.2	187.3

Note: 50% EI : Stiffness with 50% cracked coefficient of reinforced concrete pile
70% EI: Stiffness with 70% cracked coefficient of reinforced concrete pile
100% EI: Stiffness with 100% cracked coefficient of reinforced concrete pile
500% EI: Stiffness with 500% cracked coefficient of reinforced concrete pile

Table 5.9. Variation of anchor pre-stress

Anchor No.	Case No.		
	A	B	C
	(kN/m)	(kN/m)	(kN/m)
Anchor 1	146	250	250
Anchor 2	83	83	150
Anchor 3	42	42	100

Table 5.10. Maximum values for different anchor pre-stress (Circle on Cavill)

Results	Excavation Depth (m)	Case No.		
		A	B	C
Maximum lateral wall movement, δ_{hmax} (mm)	-2.2	23.3	6.2	6.2
	-7.6	28.0	17.8	17.8
	-10.0	56.2	33.5	33.6
	-11.7	84.6	63.1	54.1
Maximum ground surface settlement, δ_{vmax} (mm)	-2.2	26.1	11.3	11.3
	-7.6	33.4	17.1	17.1
	-10.0	49.4	32.3	30.6
	-11.7	61.2	57.3	47.7
Maximum wall bending moment, BM_{max} (kNm/m)	-2.2	45.3	49.1	49.1
	-7.6	68.4	92.4	92.4
	-10.0	81.7	151.6	128.6
	-11.7	103.3	189.3	160.4

Table 5.11. Variation of anchor length (Circle on Cavill)

Case No.	Anchor 1		Anchor 2		Anchor 3	
	Free (m)	Bonded (m)	Free (m)	Bonded (m)	Free (m)	Bonded (m)
L1	6	3	6	3	3	2
L2	9	4	6	3	3	2
L3	9	4	9	4	6	3
L4	12	5	9	4	6	3

Note: Free : Free length of anchor
Bonded: Bonded length of anchor

Figures

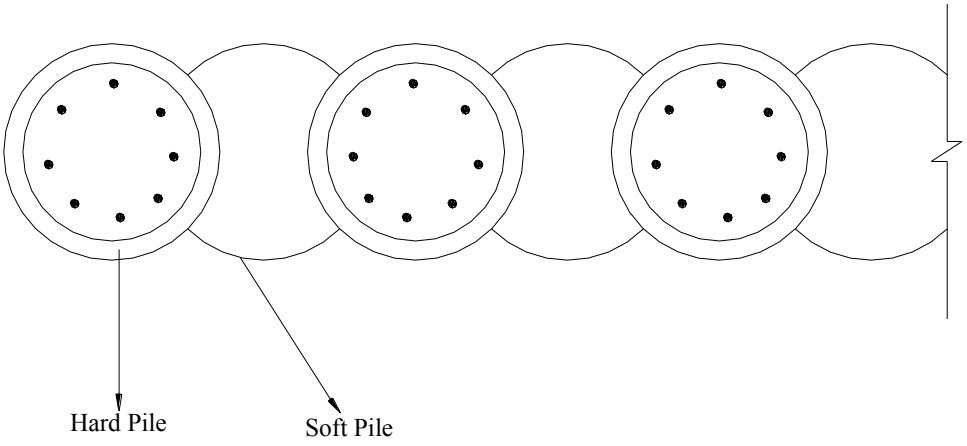

Figure 2.1. Secant pile wall cross section

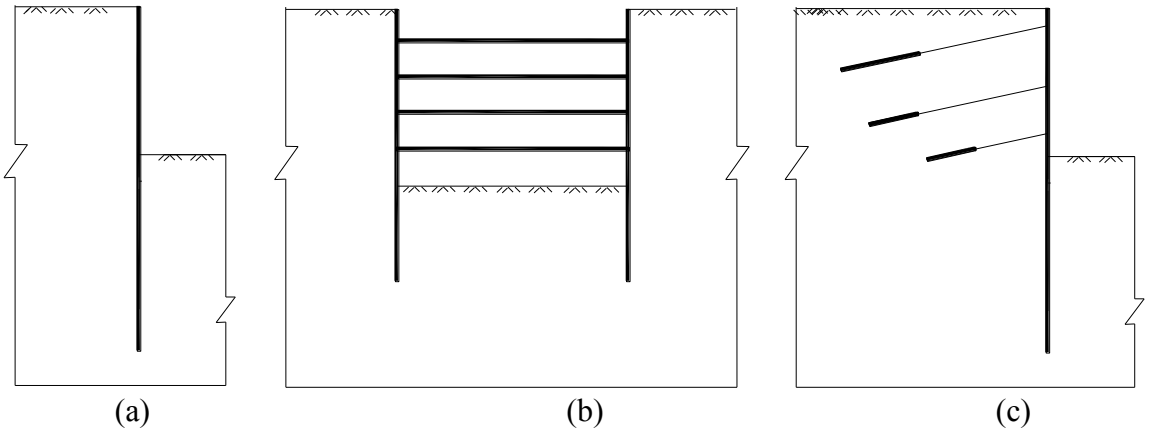

Figure 2.2. Three types of supported excavation systems.

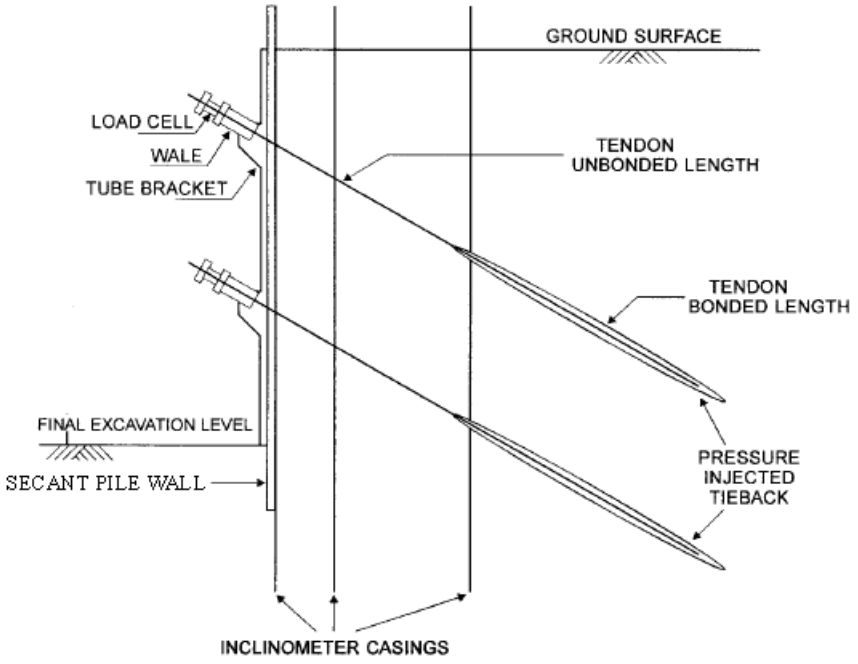

Figure 2.3. Tieback anchored system

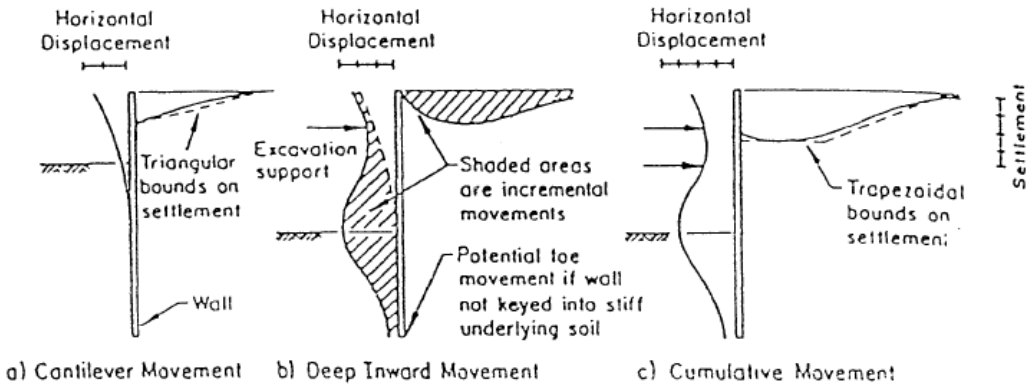

Figure 2.4. Typical profile of wall movement and ground settlement (Clough & O'Rourke, 1990)

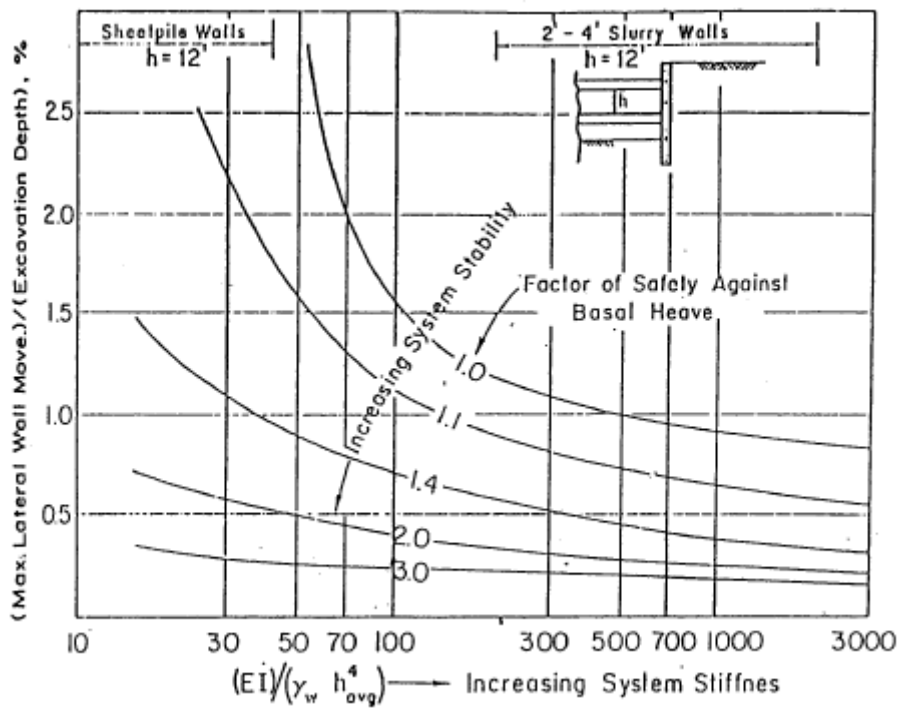

Figure 2.5. Theoretical relationship between maximum lateral wall movement, factor of Safety against basal heave and system Stiffness (Clough et al.,1989).

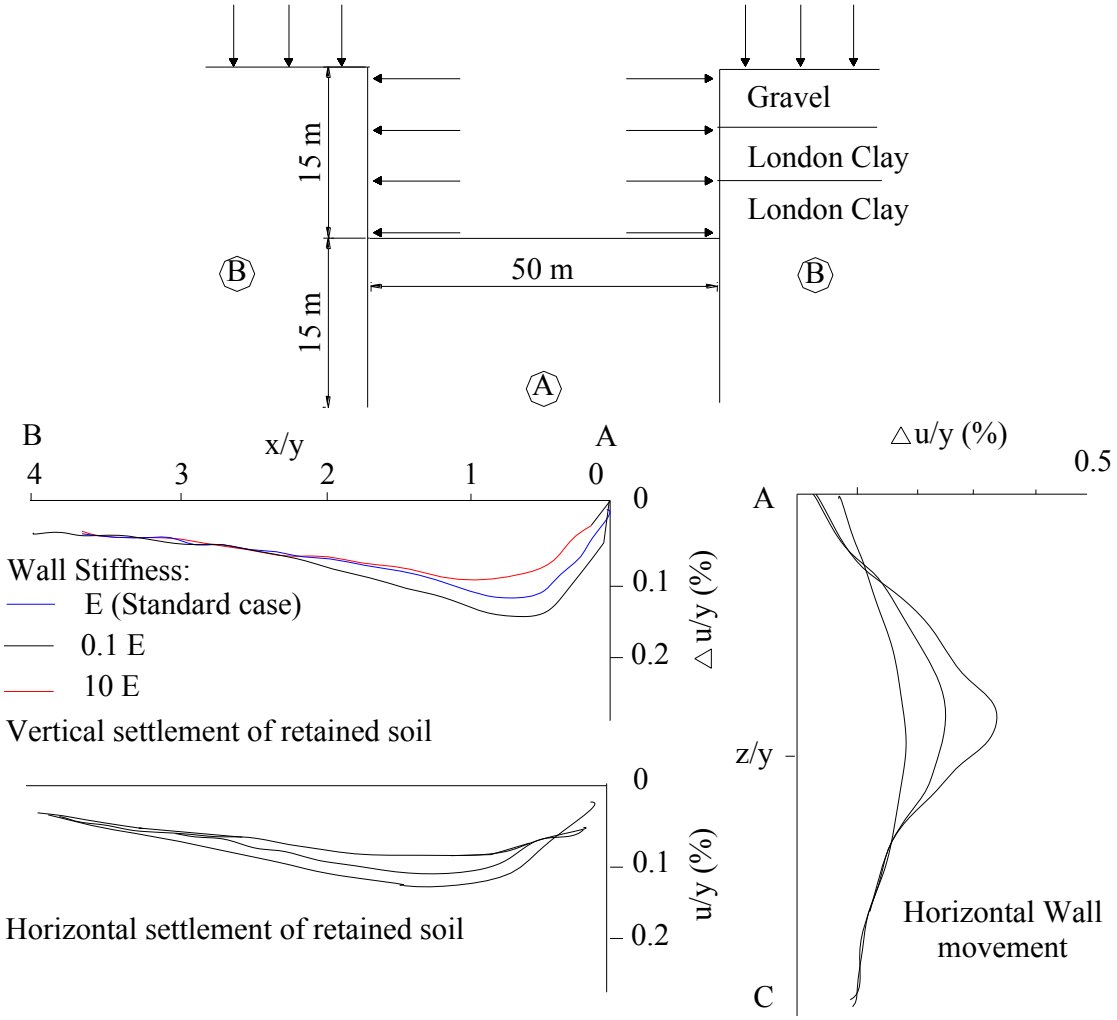

Figure 2.6. Influence of the stiffness of the walls (Hight and Higgins, 1994).

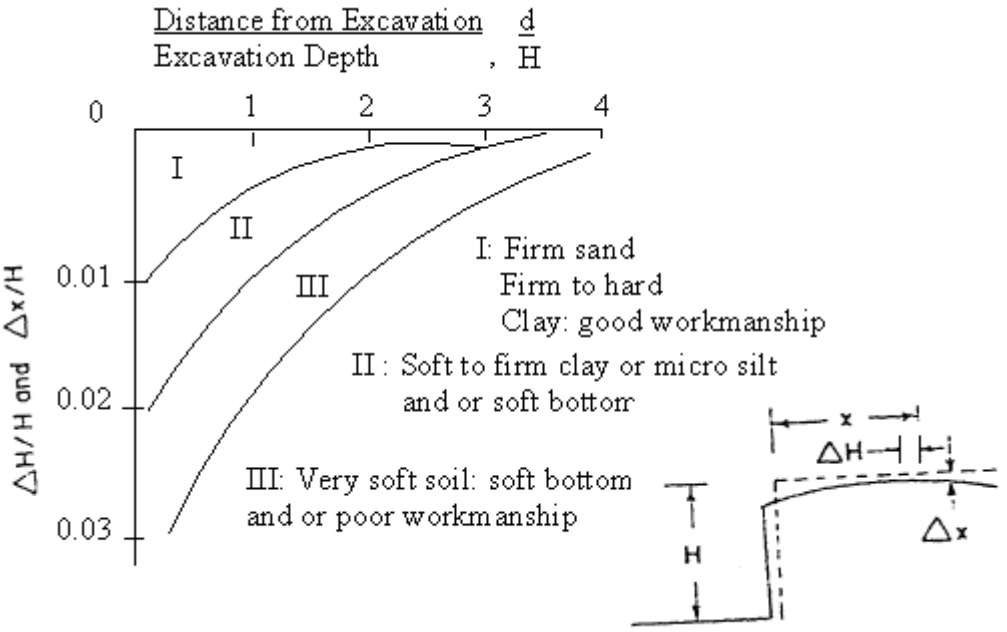

Figure 2.7. Movement adjacent to braced excavation (Peck, 1969)

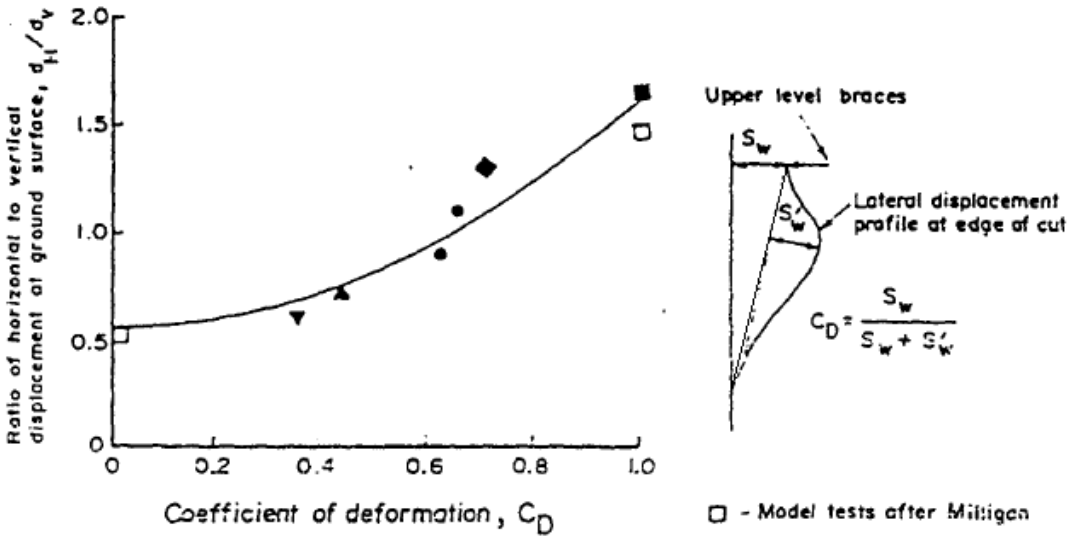

Figure 2.8. Relationship of "Movement Ratio" and coefficient of deformation (O'Rourke, 1981)

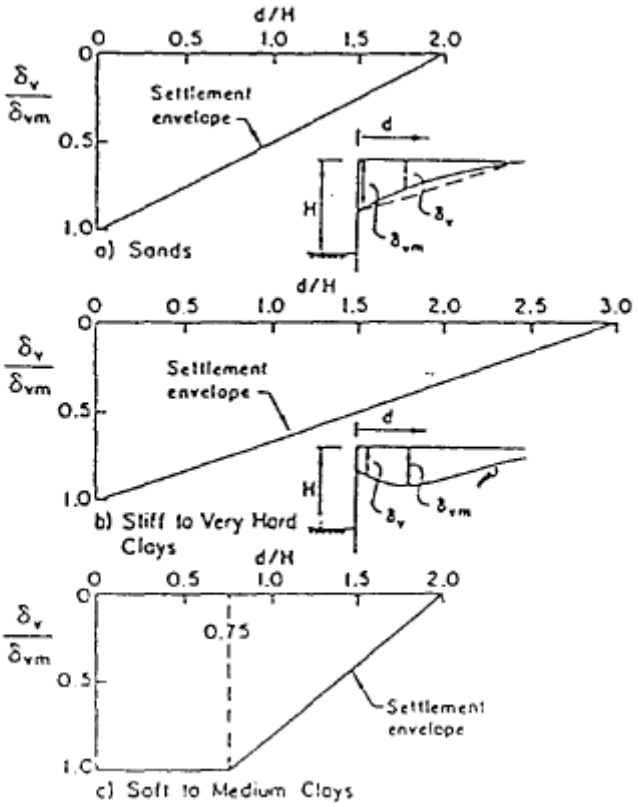

Figure 2.9. Normalized ground settlement profiles of various soil types (Clough & O'Rourke 1990)

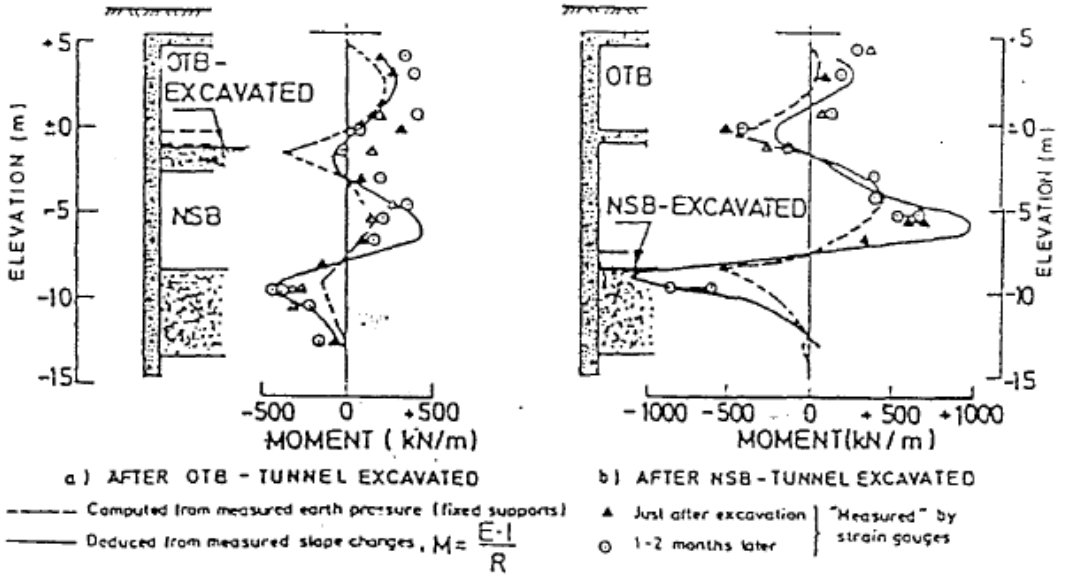

Figure 2.10. Derivation of wall bending moment with 3 different analysis methods (Karlsrud, 1986)

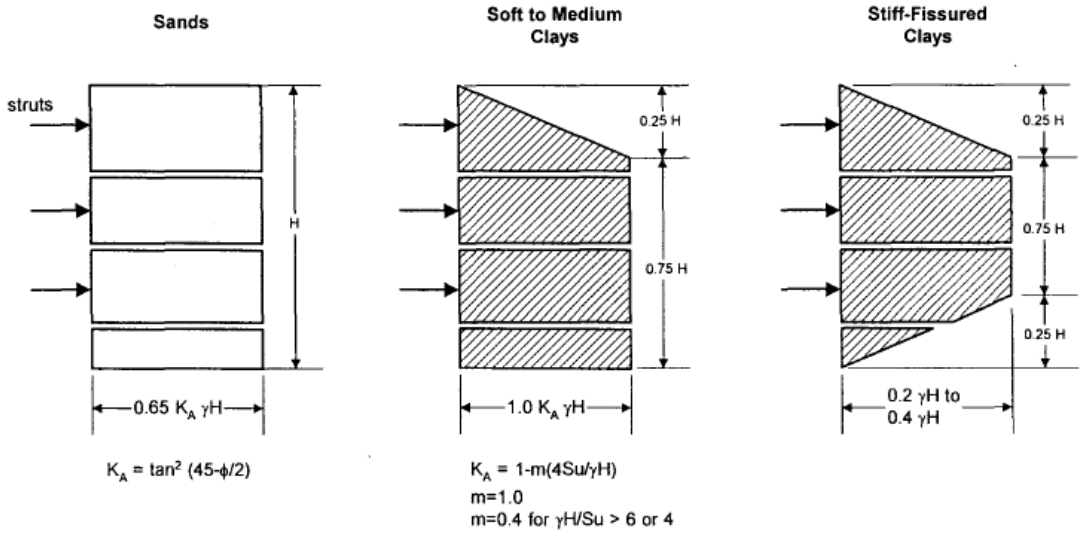

Figure 2.11. Apparent pressure diagram (Terzaghi and Peck, 1967)

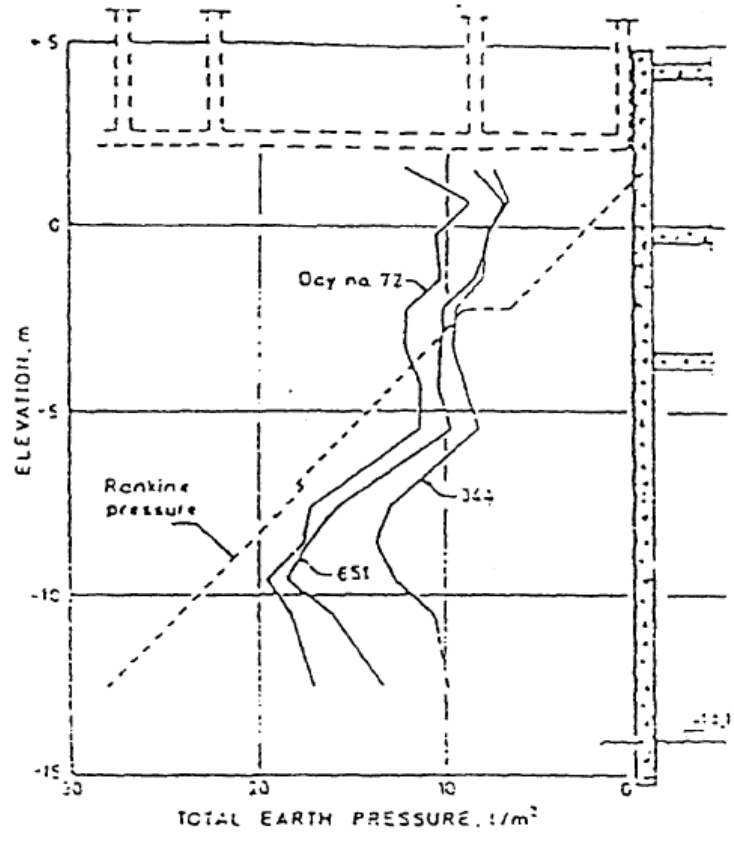

Figure 2.12. Distribution of lateral earth pressure in Oslo Telefonhuset (Dibiagio, 1972)

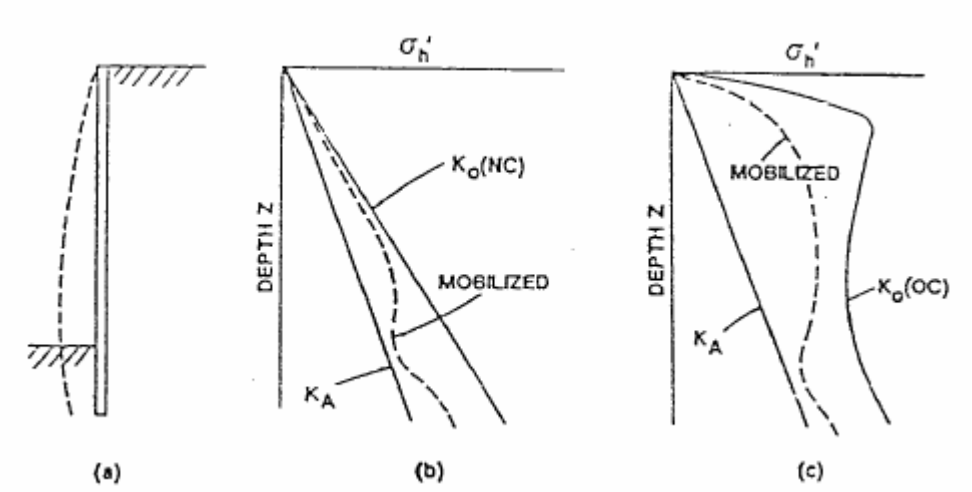

Figure 2.13. Lateral earth pressure distribution on the wall (Liao & Neff, 1990)

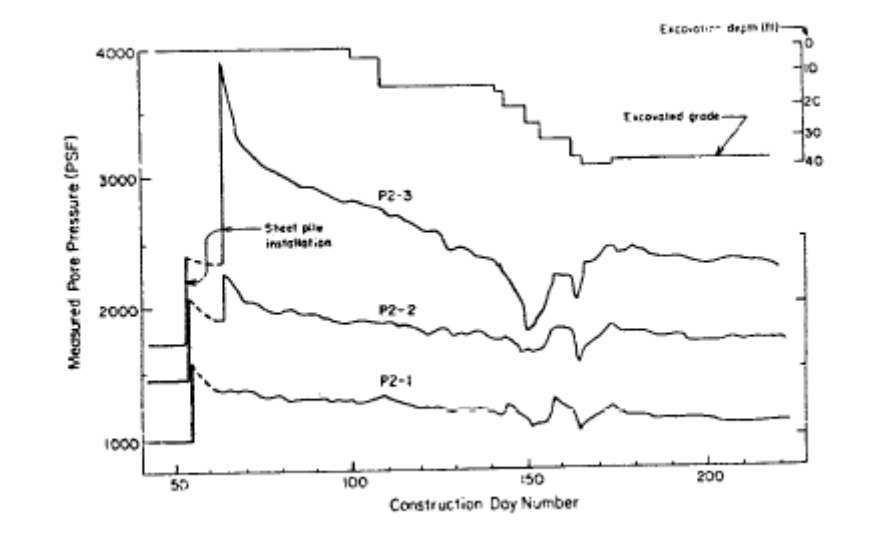

Figure 2.14. Pore water pressure during construction (1psf = 0.048Kpa)
(Finno & Coworkers, 1990)

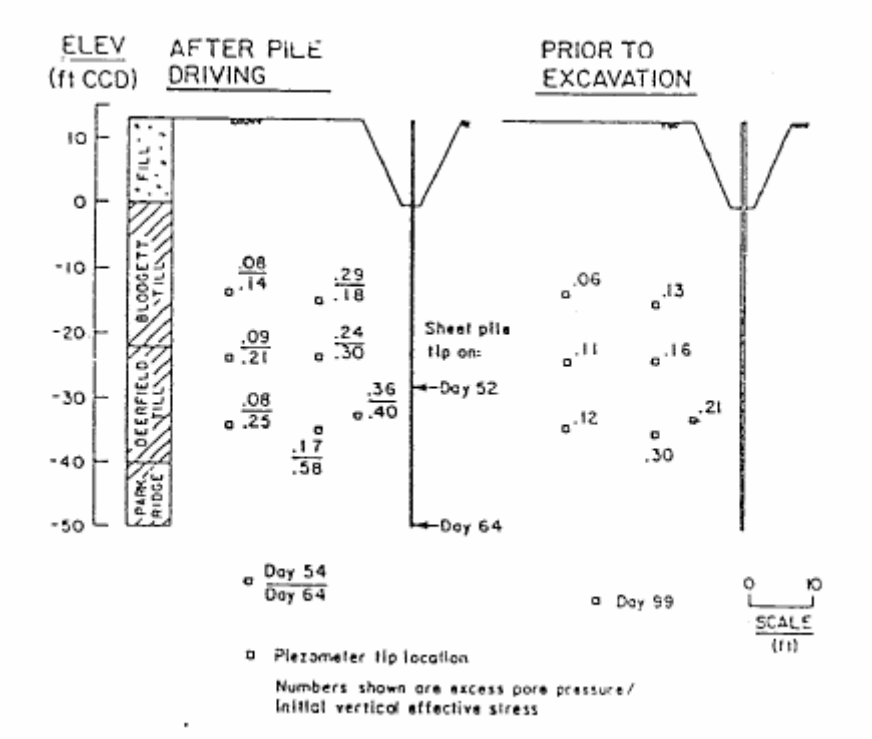

Figure 2.15. Normalized excess pore pressure during and after sheep-pile driving (Finno & Coworkers, 1990)

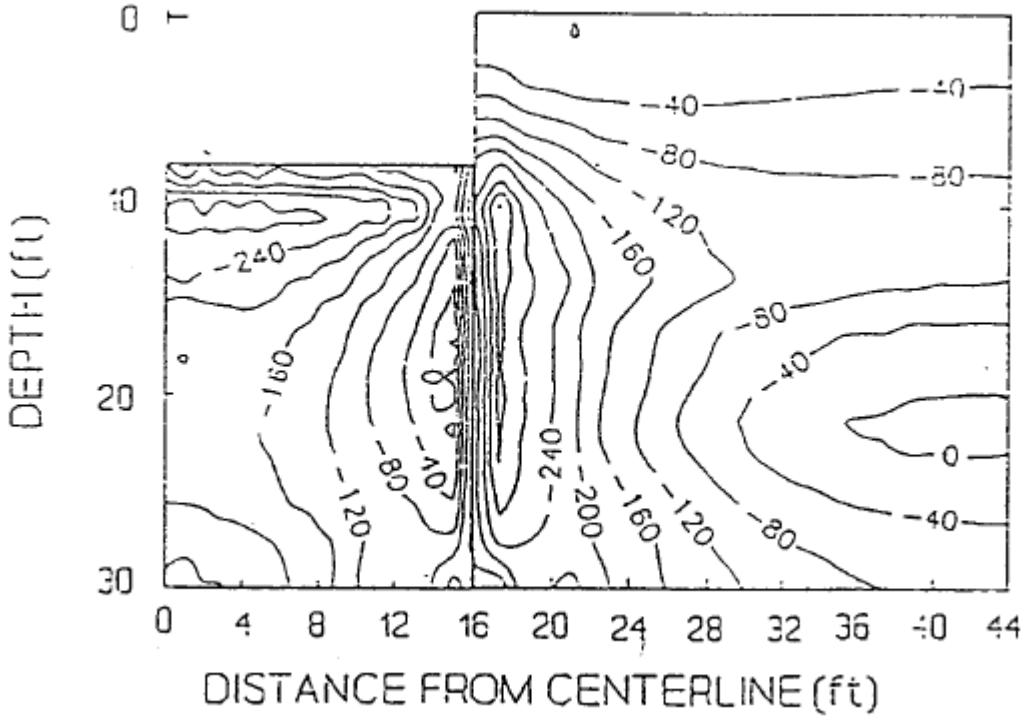

Figure 2.16 Pore water pressure distribution after excavation (Finno & Harahap, 1991)

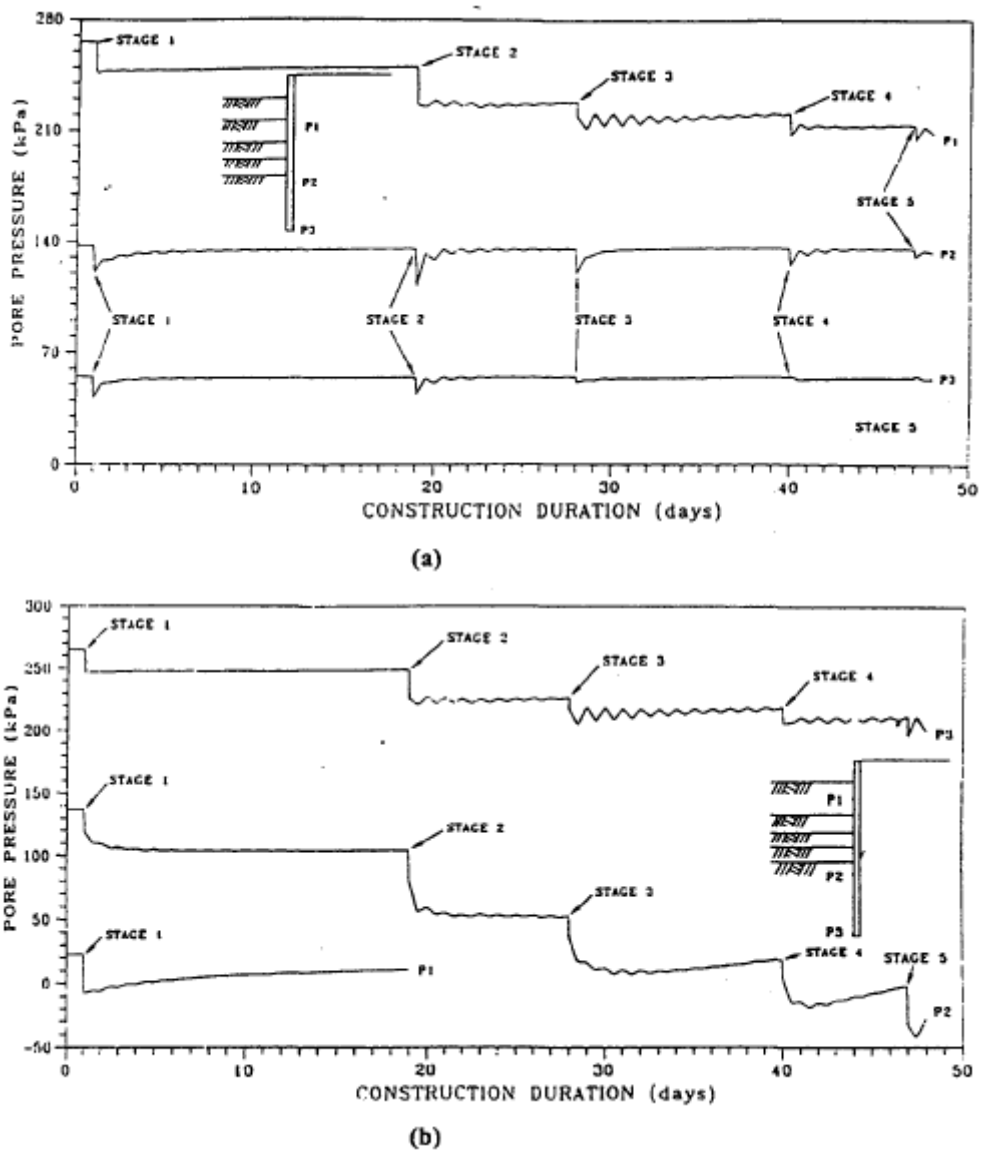

Figure 2.17. Variation of pore pressure on (a) the active side, (b) the passive side of the Retaining wall at Different stages. (after Ou,C.Y. and Lai, C.H, 1994)

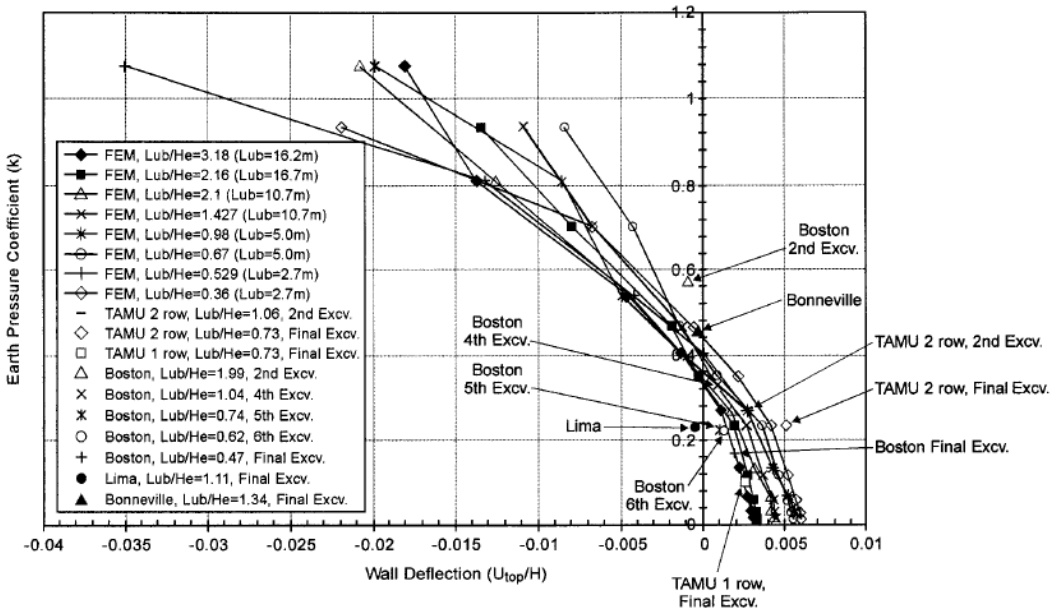

Figure.2.18. Influence of anchor force on deflection at top of wall (Briaud et at, 1999)

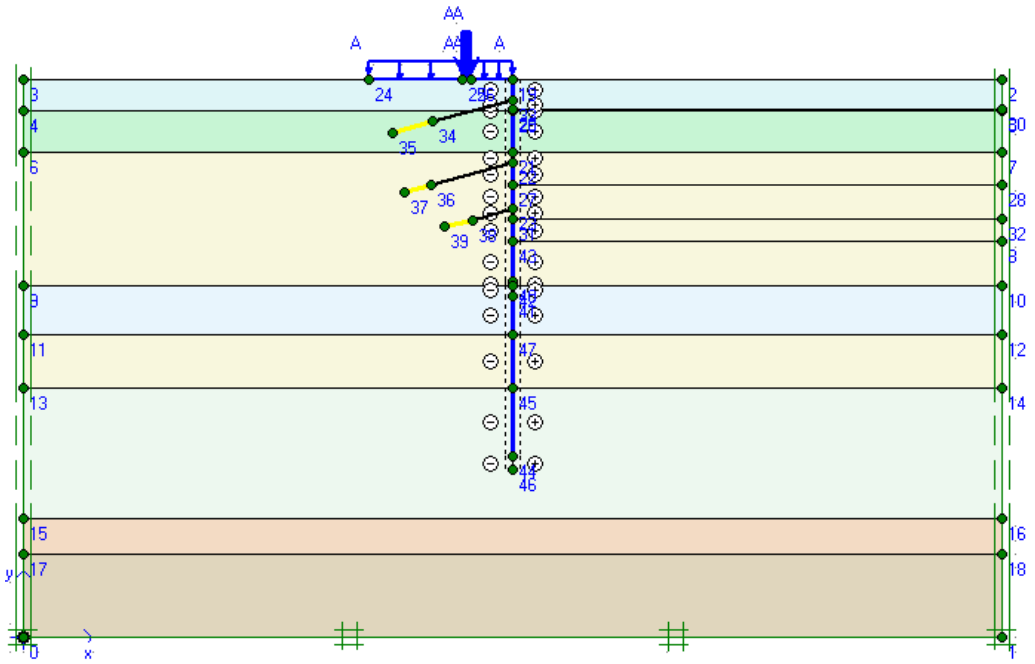

Figure 3.1. Detailed modelling of the geometry cross-section in PLAXIS

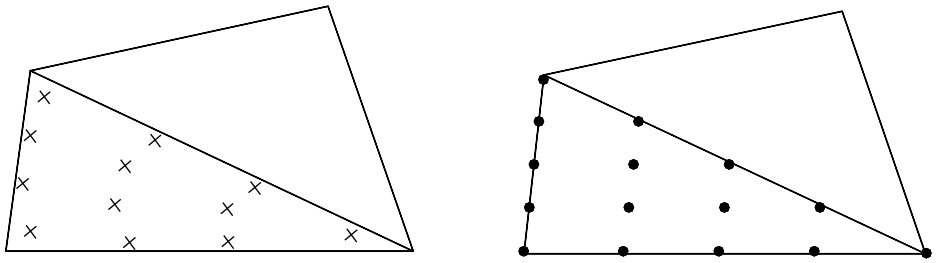

Figure 3.2. Position of nodes and stress points in soil elements

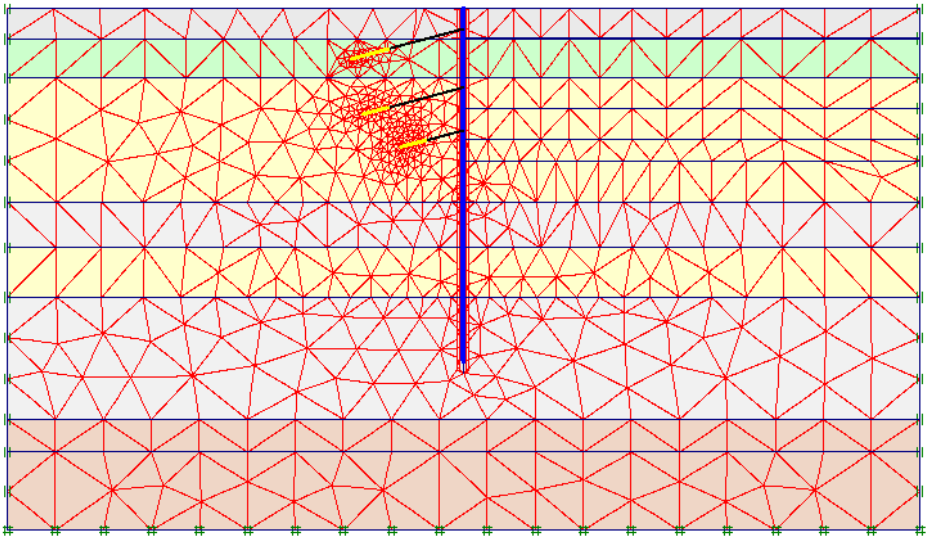

Figure 3.3 Generated mesh in the excavation model.

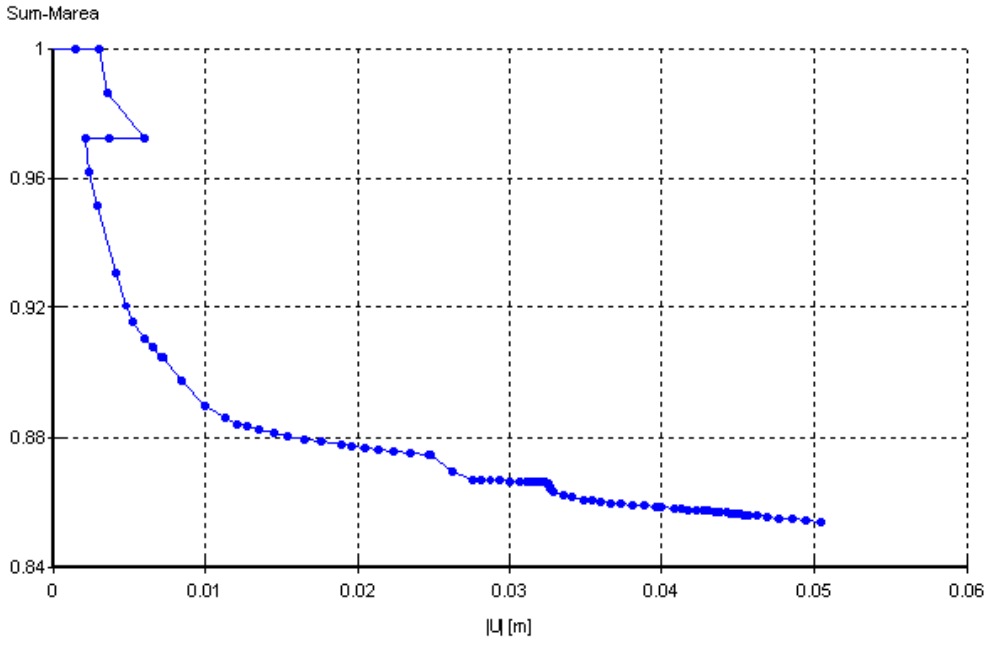

Figure 3.4 Automatic step deflection U(m) and automatic time step Sum-Marea selection mode

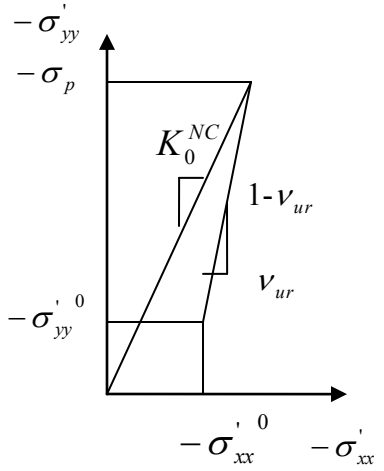

Figure 3.5 Over-consolidated stress state obtained from primary loading and subsequent unloading.

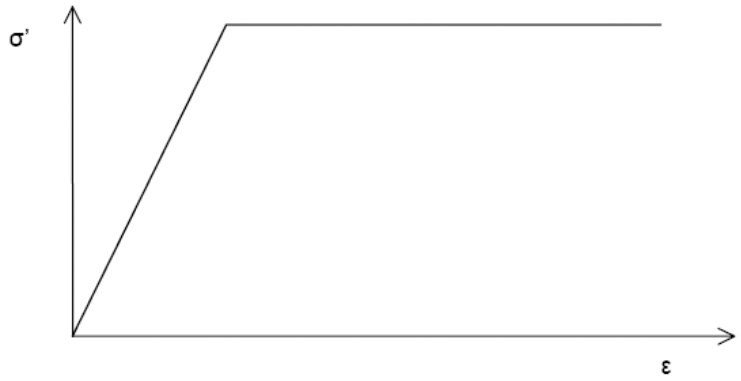

Figure 3.6 Basic idea of an elastic perfectly plastic model

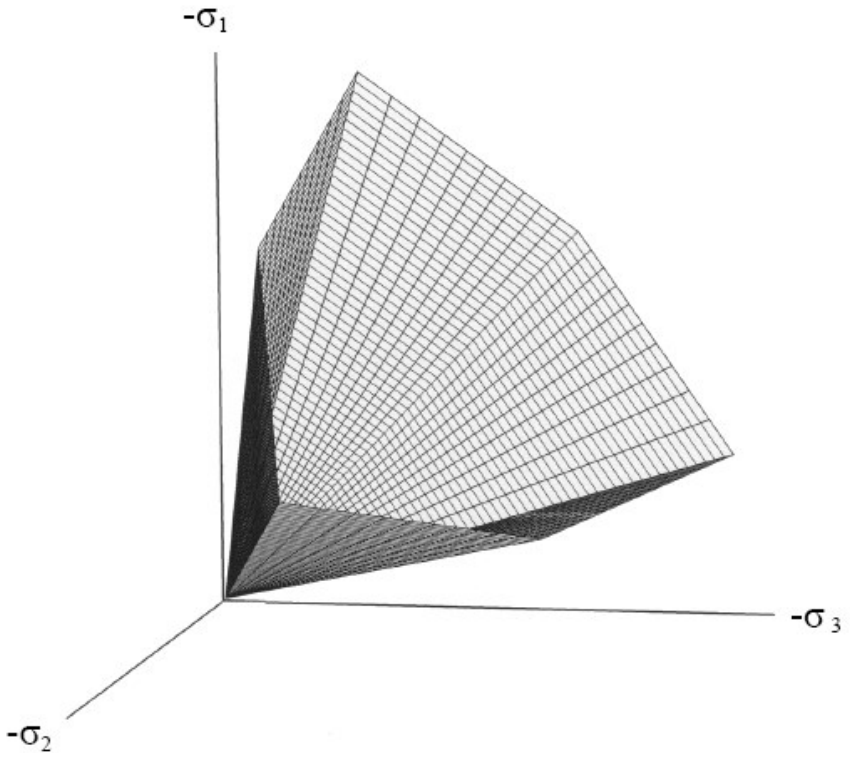

Figure 3.7 The Mohr-Coulomb yield surface in principal stress space (c = 0)

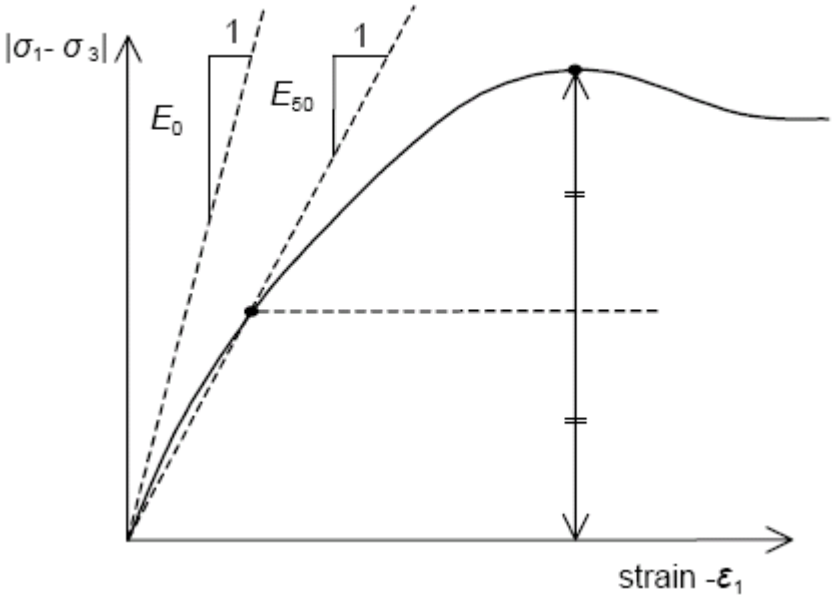

Figure 3.8. Definition of E_0 and E_{50} for Standard drained triaxial test results

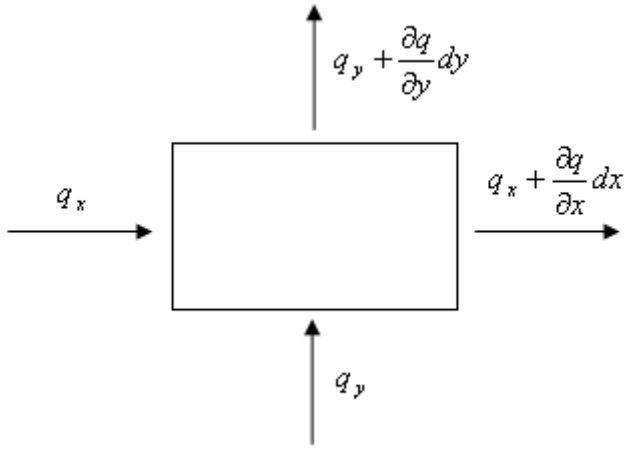

Figure 3.9. Illustration of continuity condition.

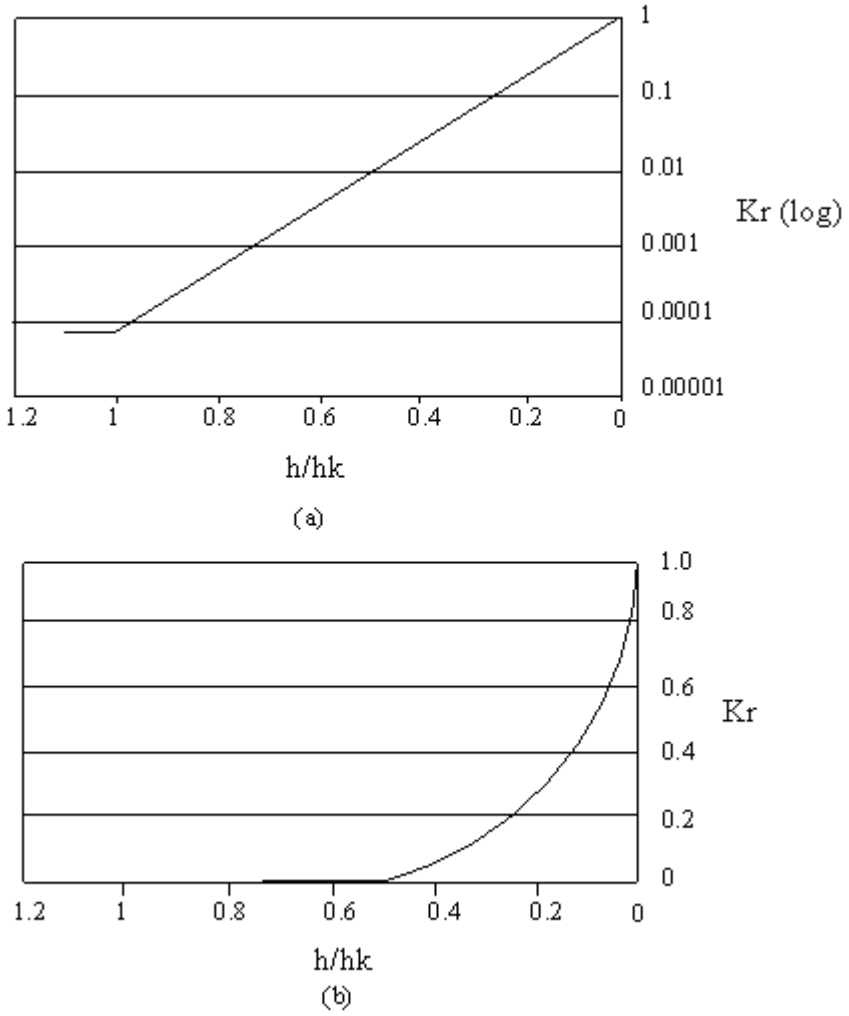

Figure 3.10 Adjustment of the permeability between saturated (a) and unsaturated (b) zones (K^r = ratio of permeability over saturated permeability)

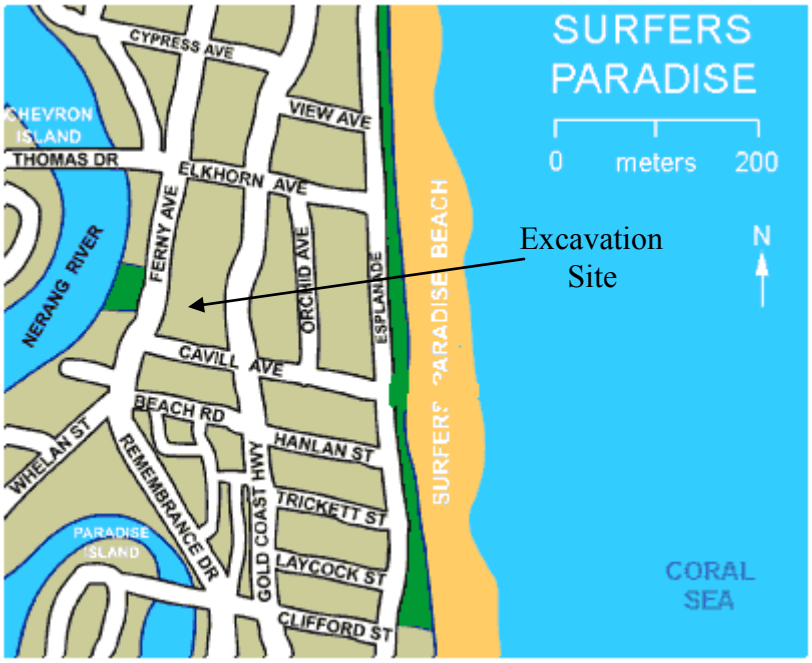

Figure 4.1 Location of Circle on Cavill project

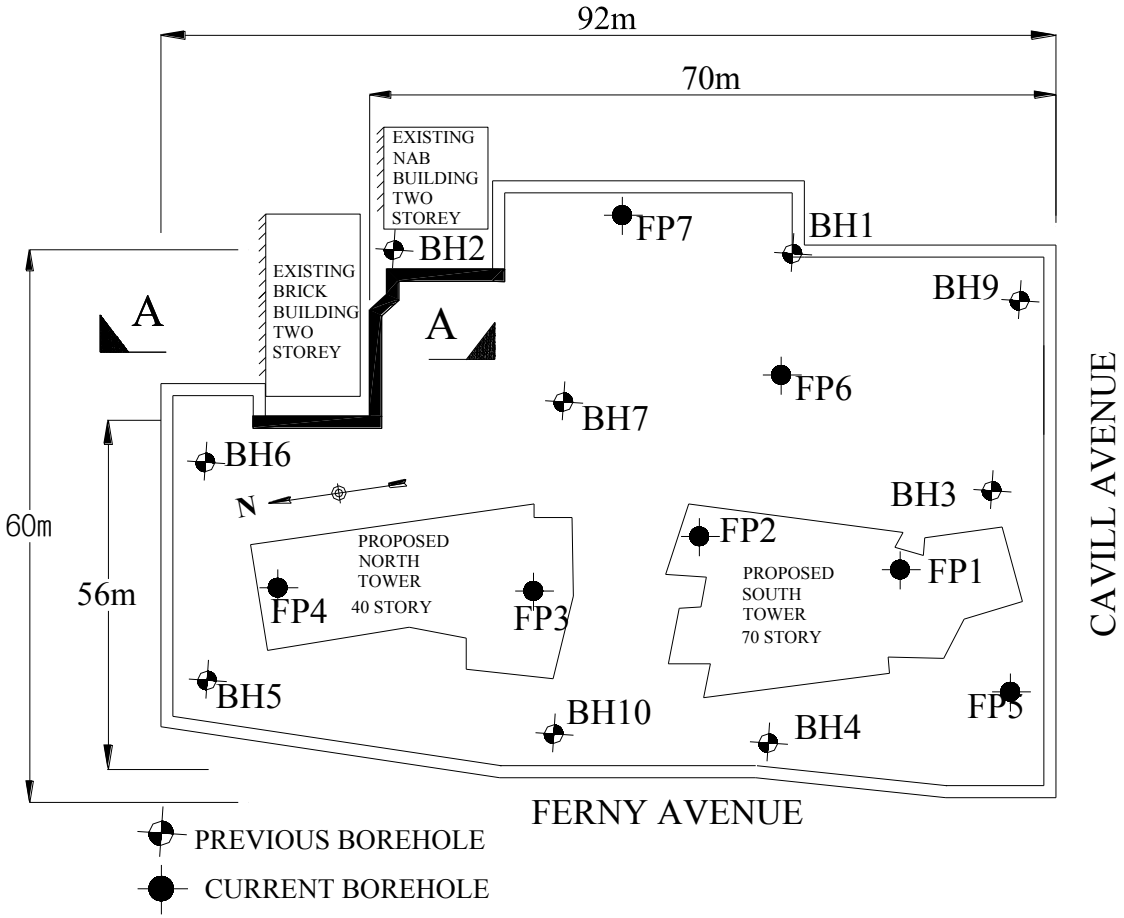

Figure 4.2 Site plan of Circle on Cavill project

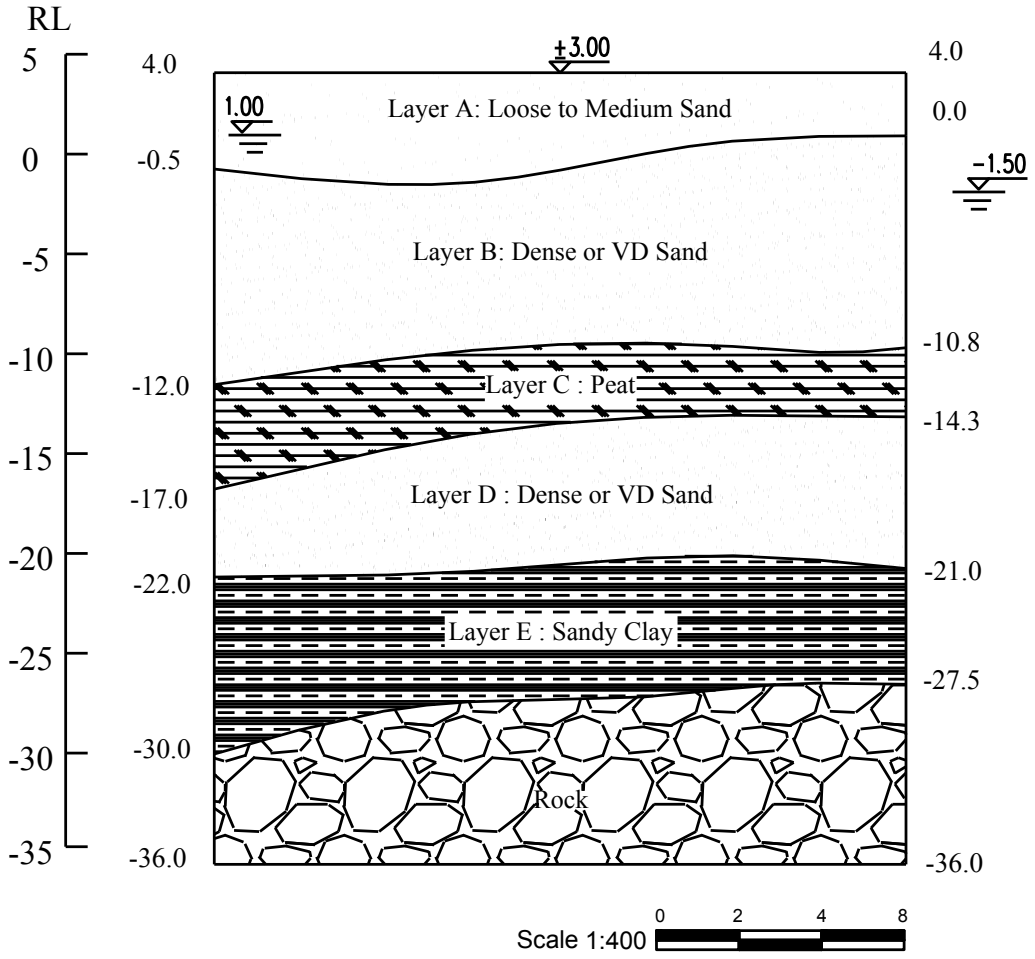

Figure 4.3(a) The subsoil condition of BH2 in Circle on Cavill

Figure 4.3(b) Excavation site of Circle on Cavill

Figure 4.3(c) Excavation site of Circle on Cavill

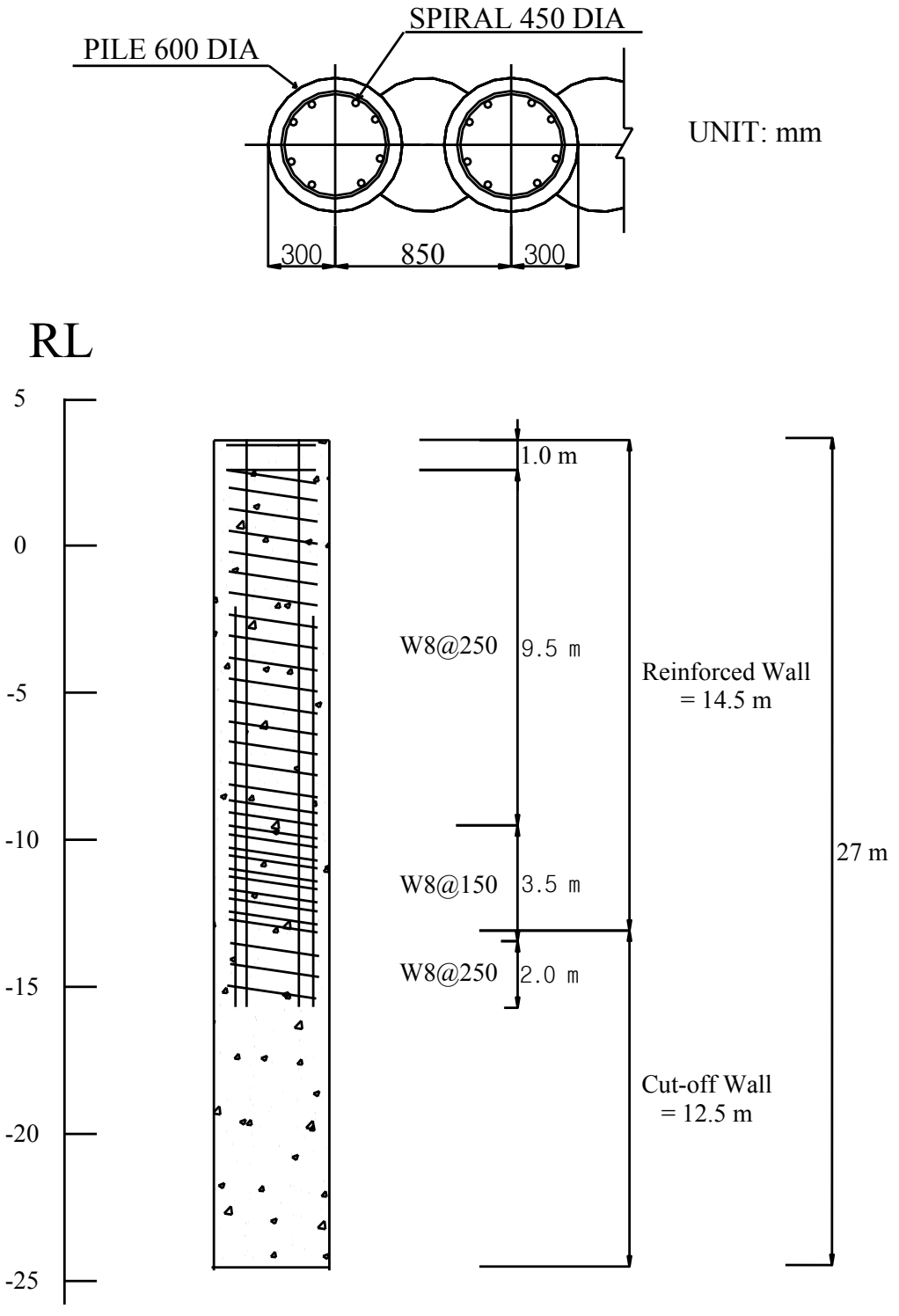

Figure 4.4. Details of secant pile wall for Circle on Cavill System.

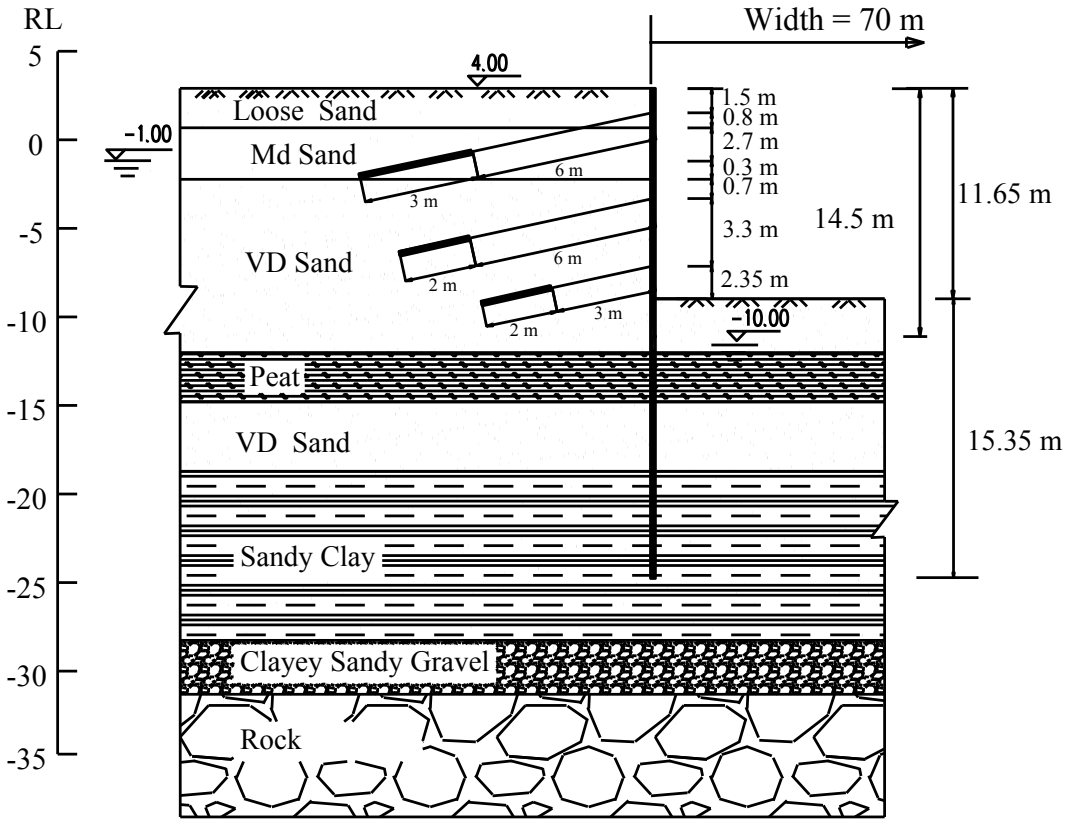

Note: VD = Very dense

Figure 4.5 Anchored secant pile system of Circle on Cavill System.

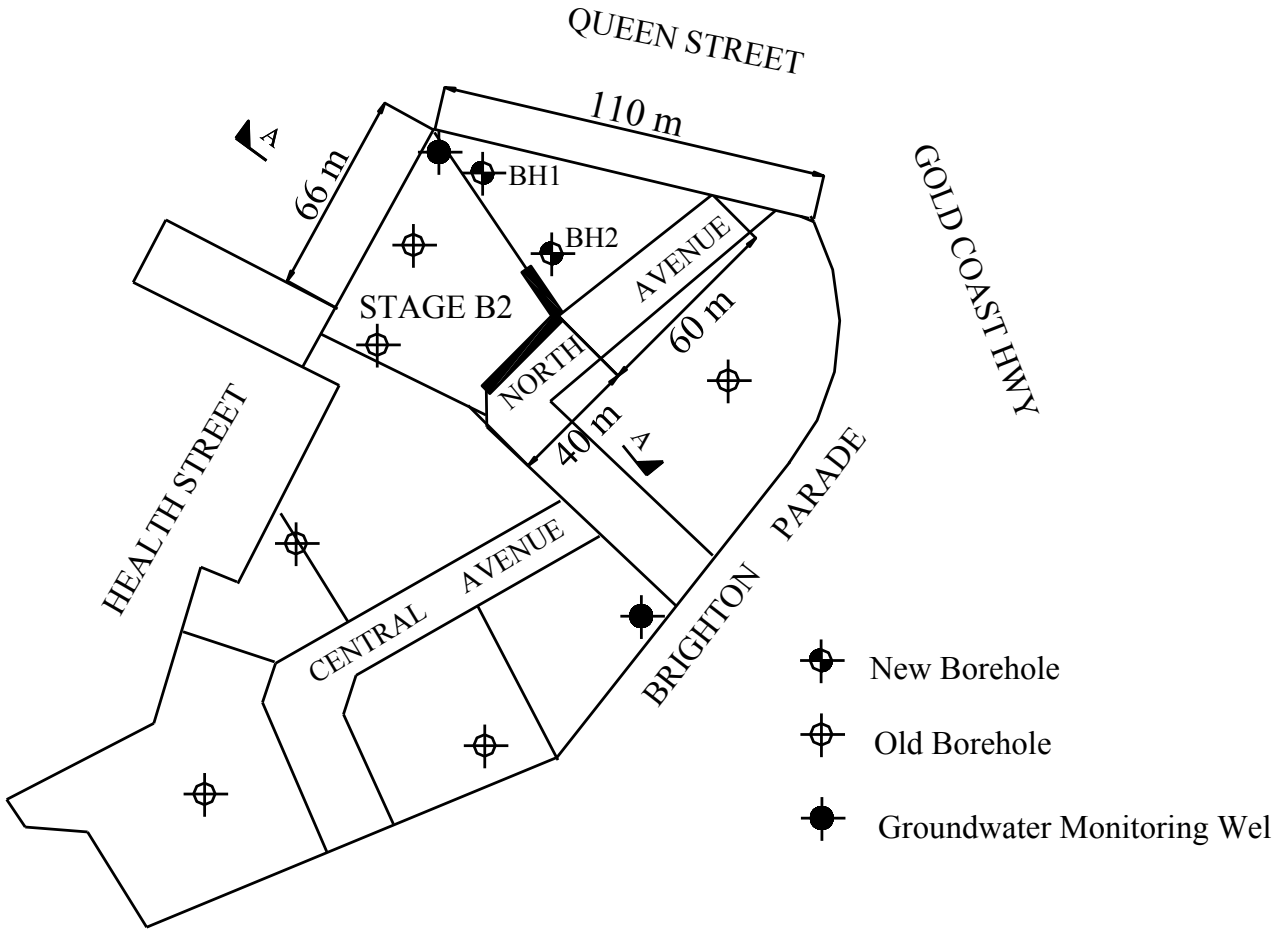

Figure 4.6. Site Plan of Sundale Project

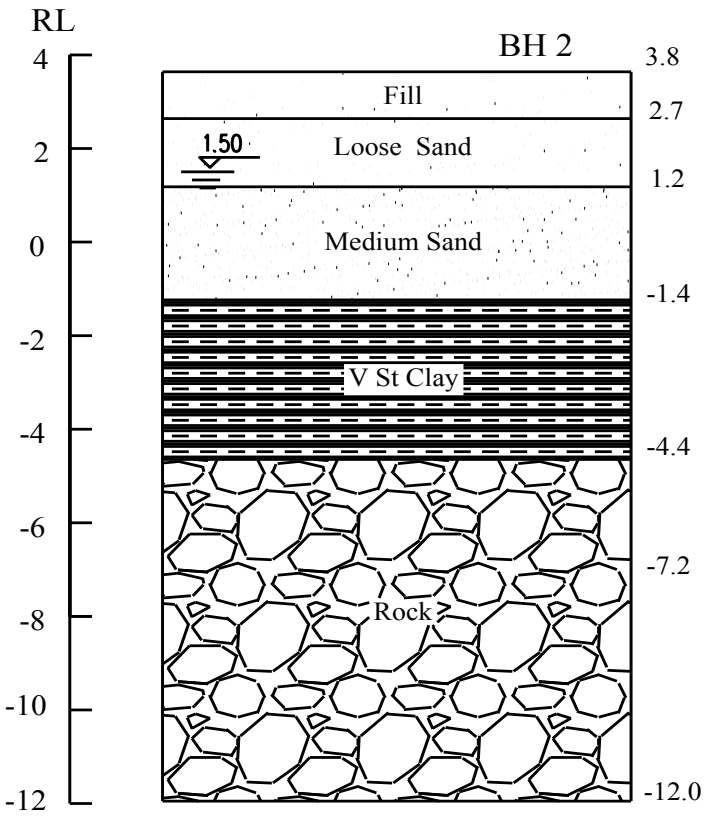

Figure 4.7 Subsoil condition of Sundale project

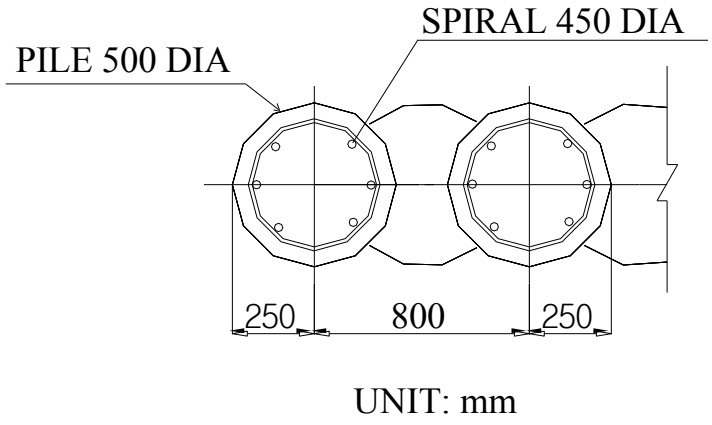

Figure 4.8(a). Details of secant pile wall of Sundale project

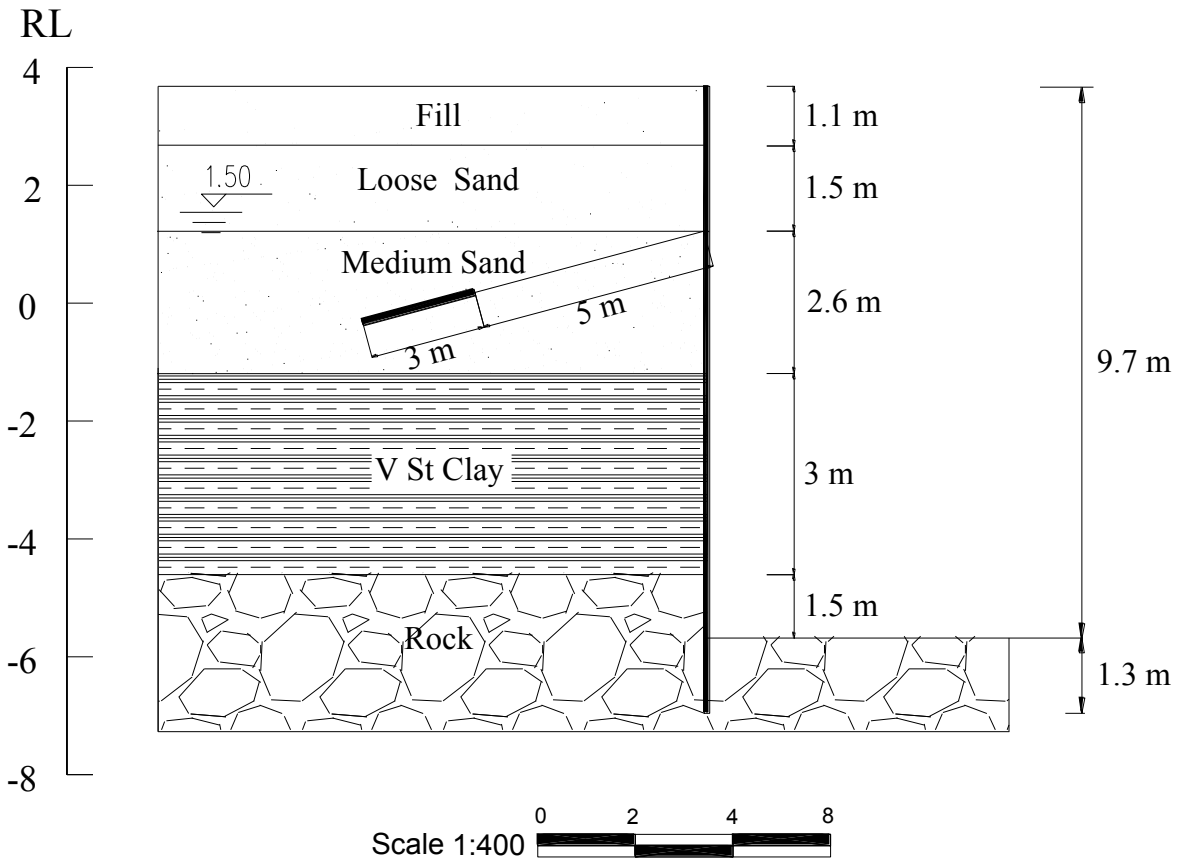

Figure 4.8(b). Anchored secant pile wall system of Sundale project

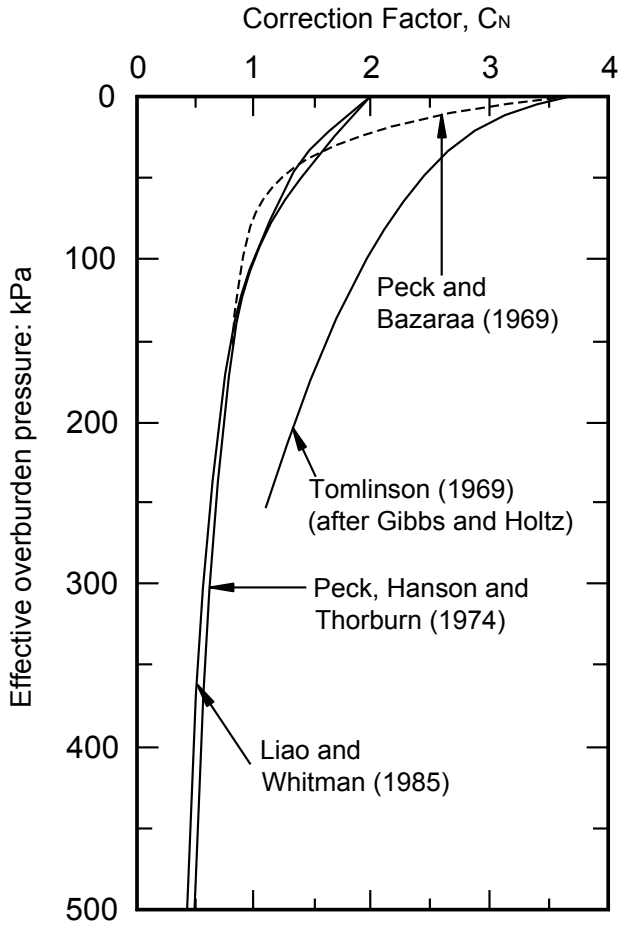

Figure 4.9. Correction factor influence for influence of effective overburden pressure on SPT "N" value, after Tomlinson (1969), Peck and Bazaraa (1969) and Peck, Hensan and Thorburn (1974).

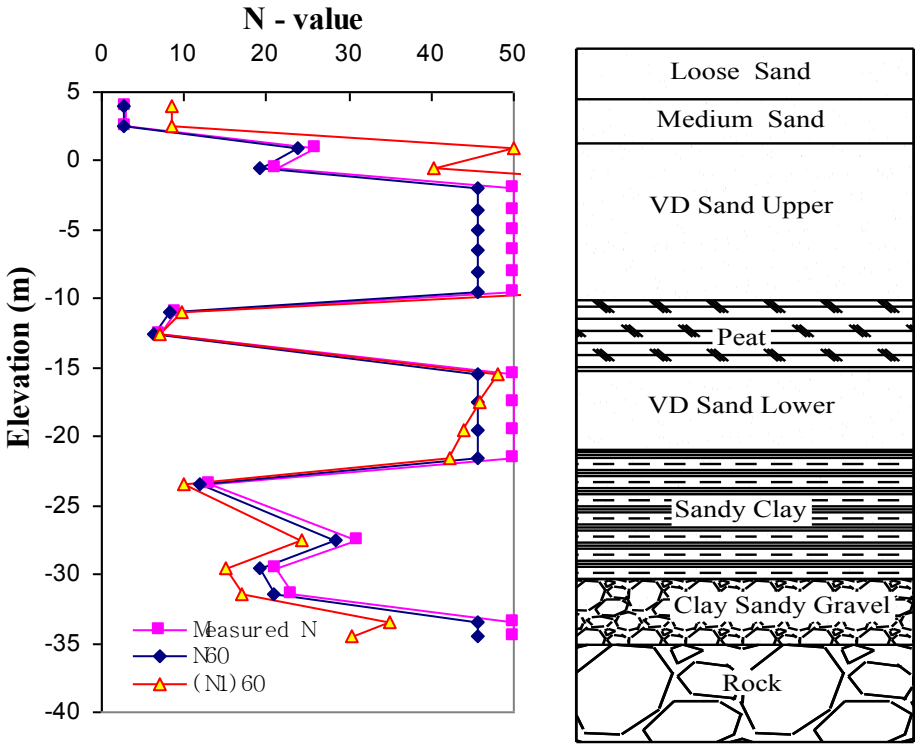

Figure 4.10. Corrected N value of Circle on Cavill

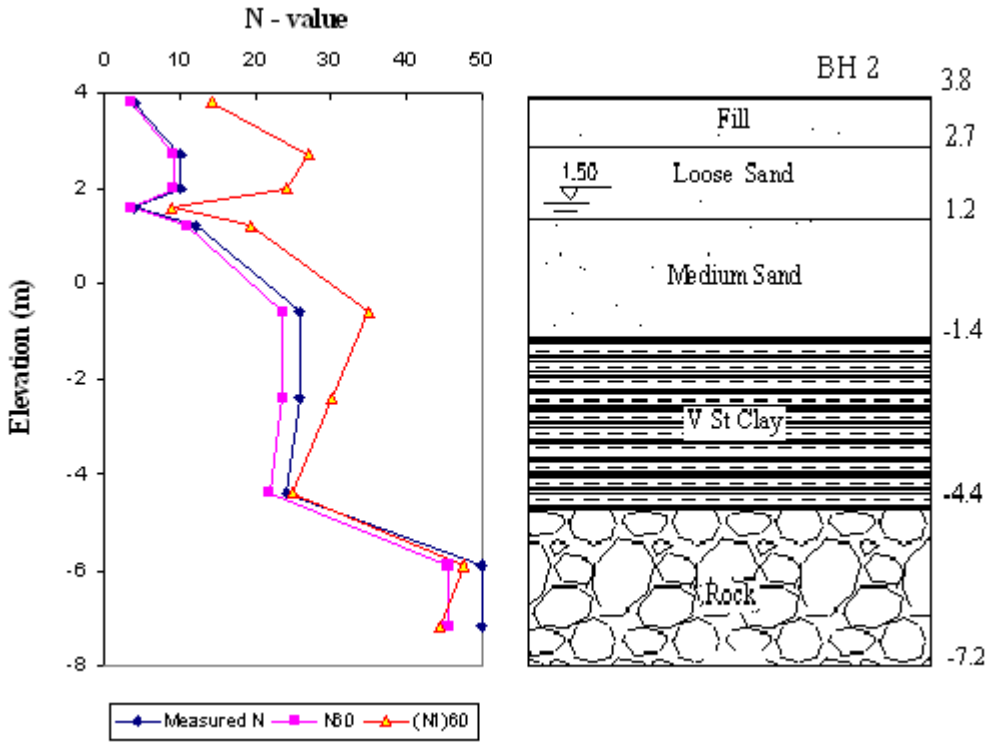

Figure 4.11. Corrected N value of Sundale project

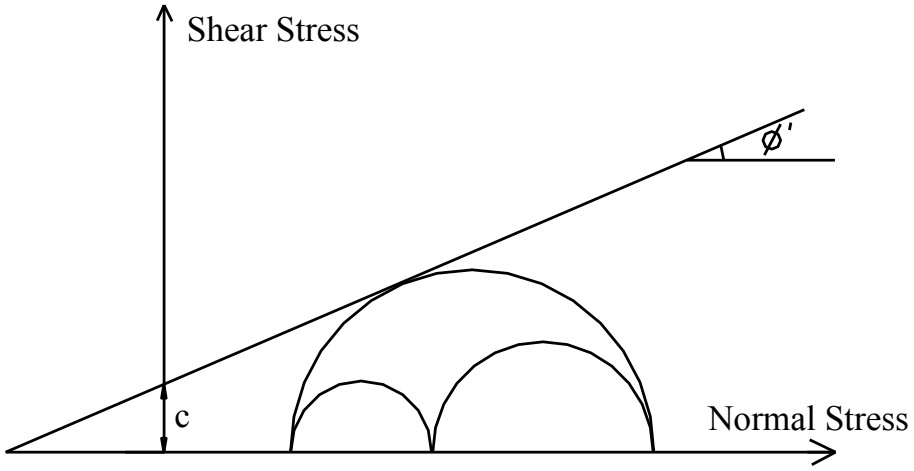

Figure 4.12. Stress circles at yield: one touches Coulomb's envelope

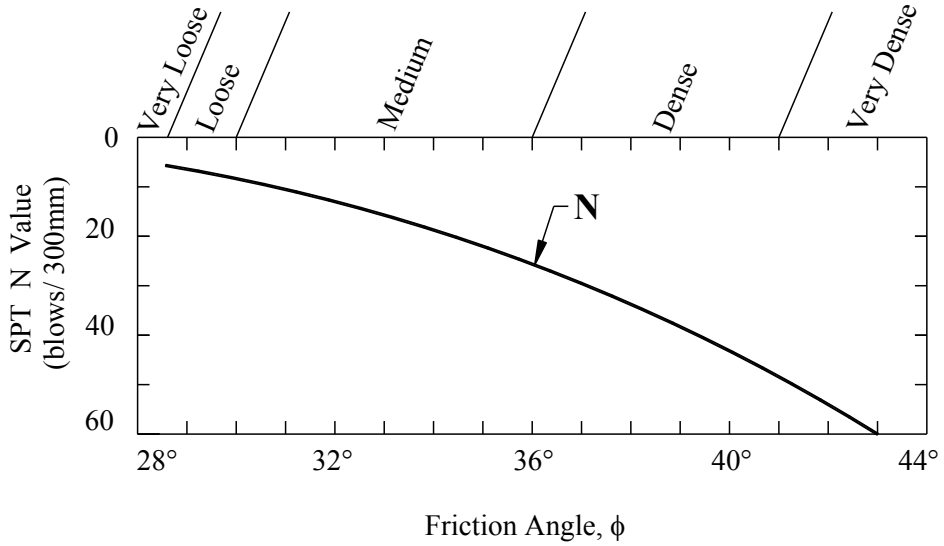

Figure 4.13. N versus ϕ (after Peck *et al*, 1974)

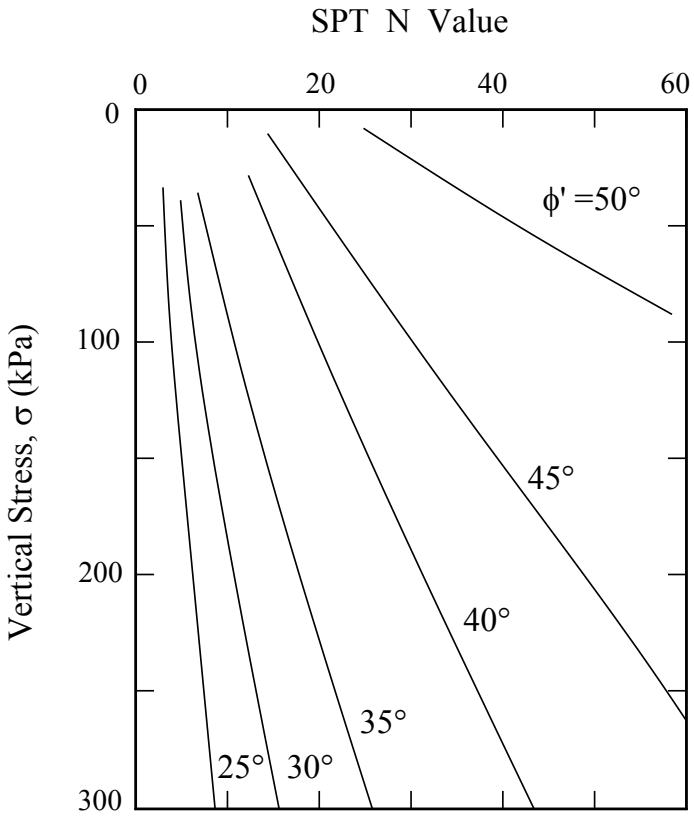

Figure 4.14. N versus ϕ` and overburden pressure (after Schmertmann, 1975)

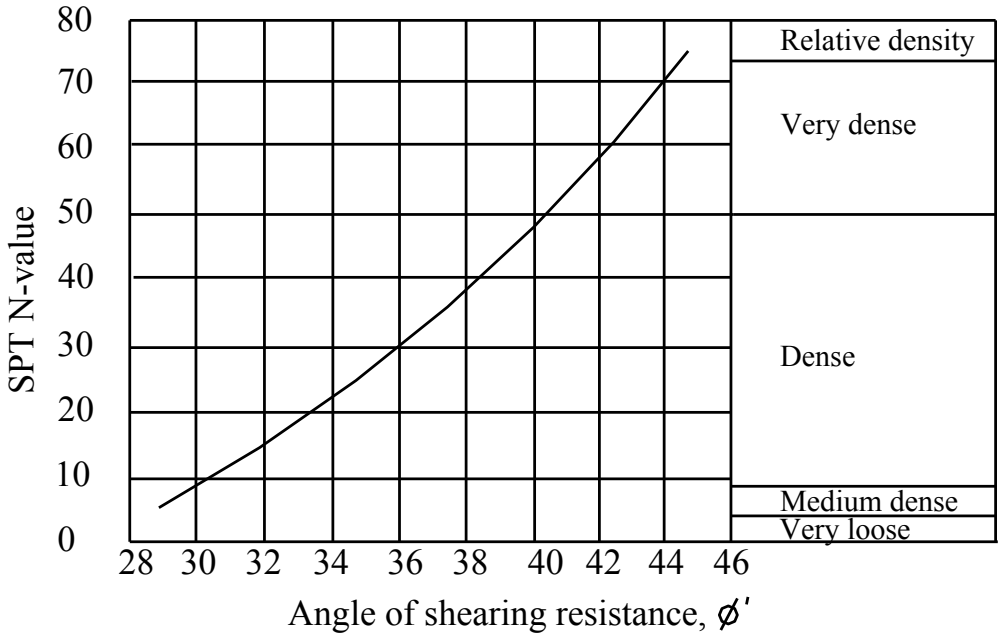

Figure 4.15. N versus ϕ` (after Carter & Bentley, 1991)

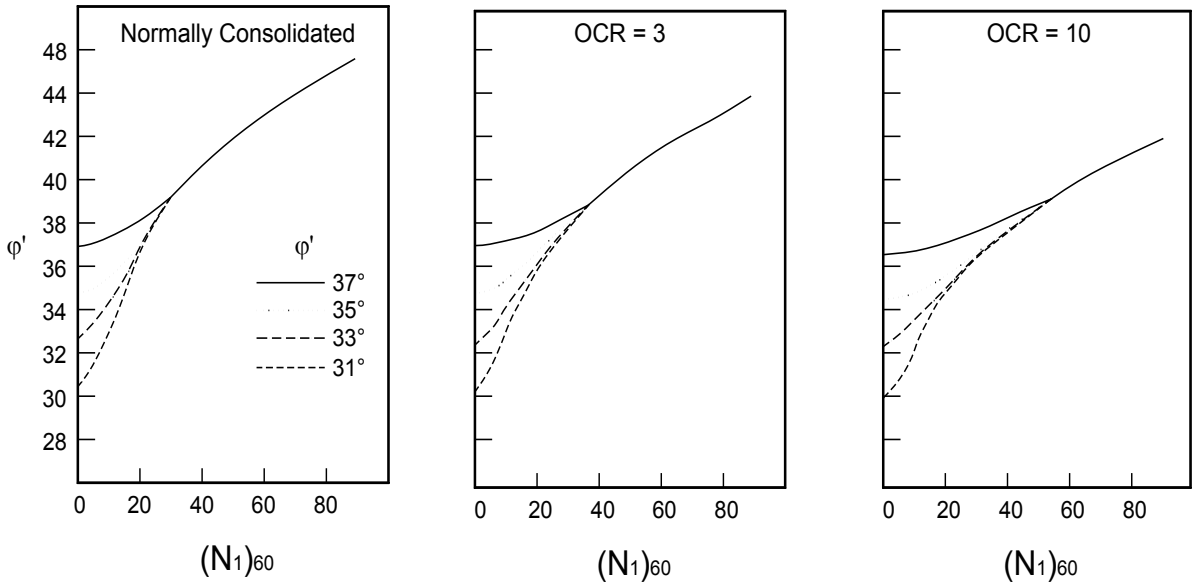

Figure 4.16. Variation of φ` and $(N_1)_{60}$ and OCR (Stroud, 1989)

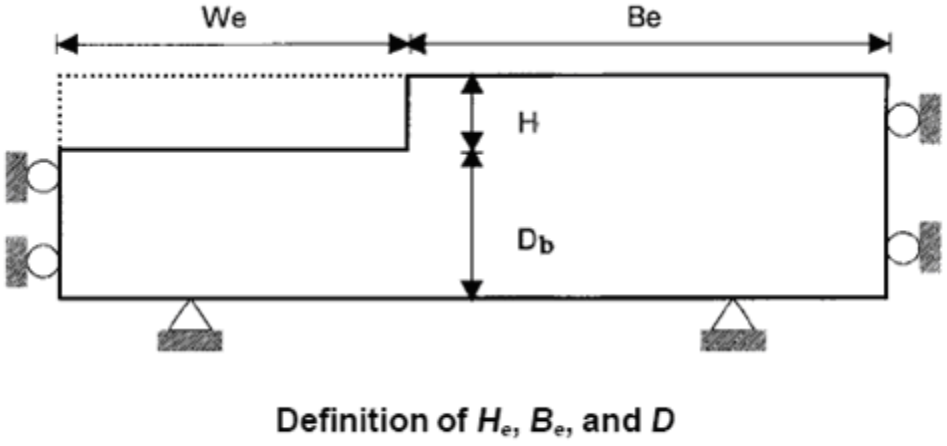

Figure 4.17. Defination of *H*e, *B*e and D (Briaud & Lim, 1999**).**

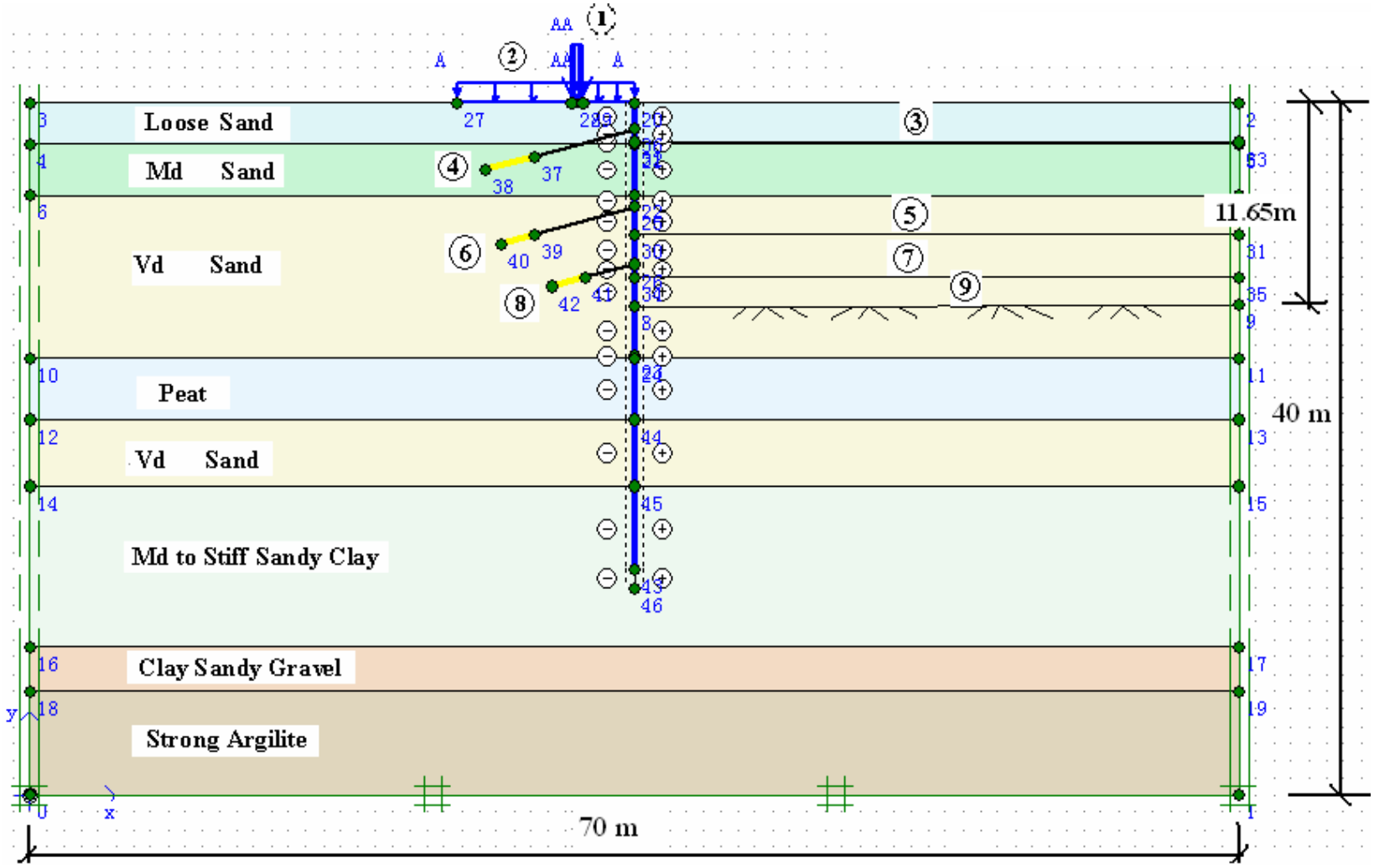

Figure 4.18. PLAXIS model for Circle on Cavill project.
(The numbers in circles represent the construction stages)

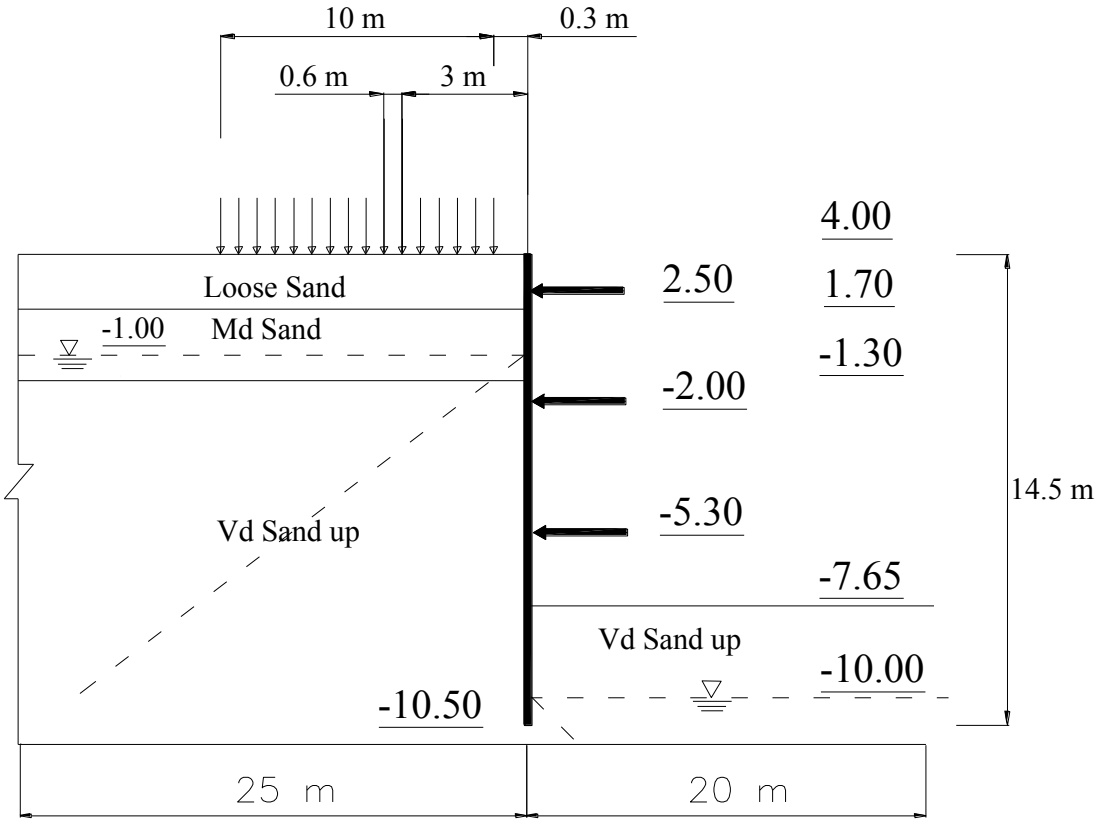

Figure 4.19 WALLAP model for Circle on Cavill project.

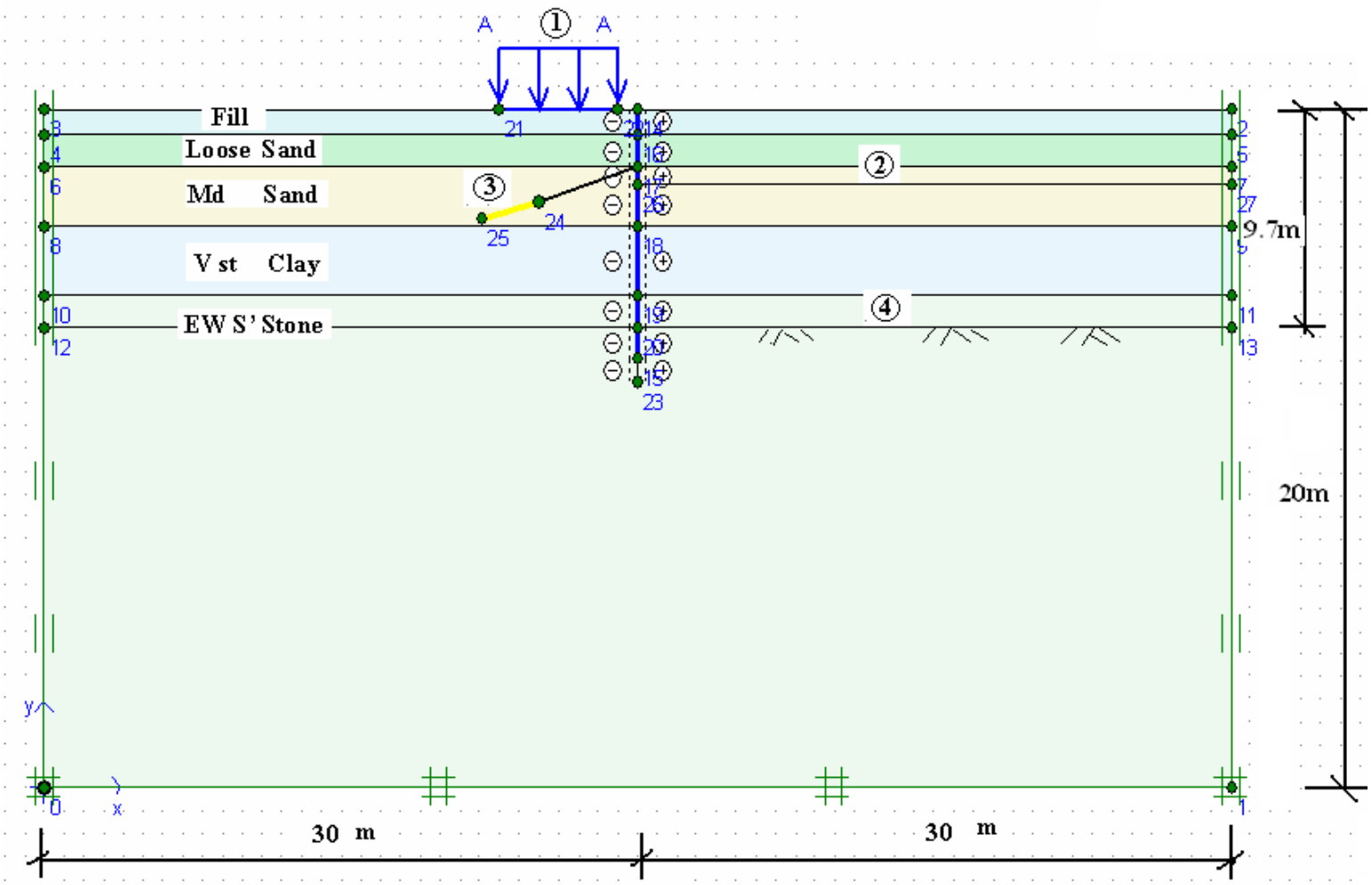

Figure 4.20 PLAXIS model for Sundale project.
(The numbers in circles represent the construction stages)

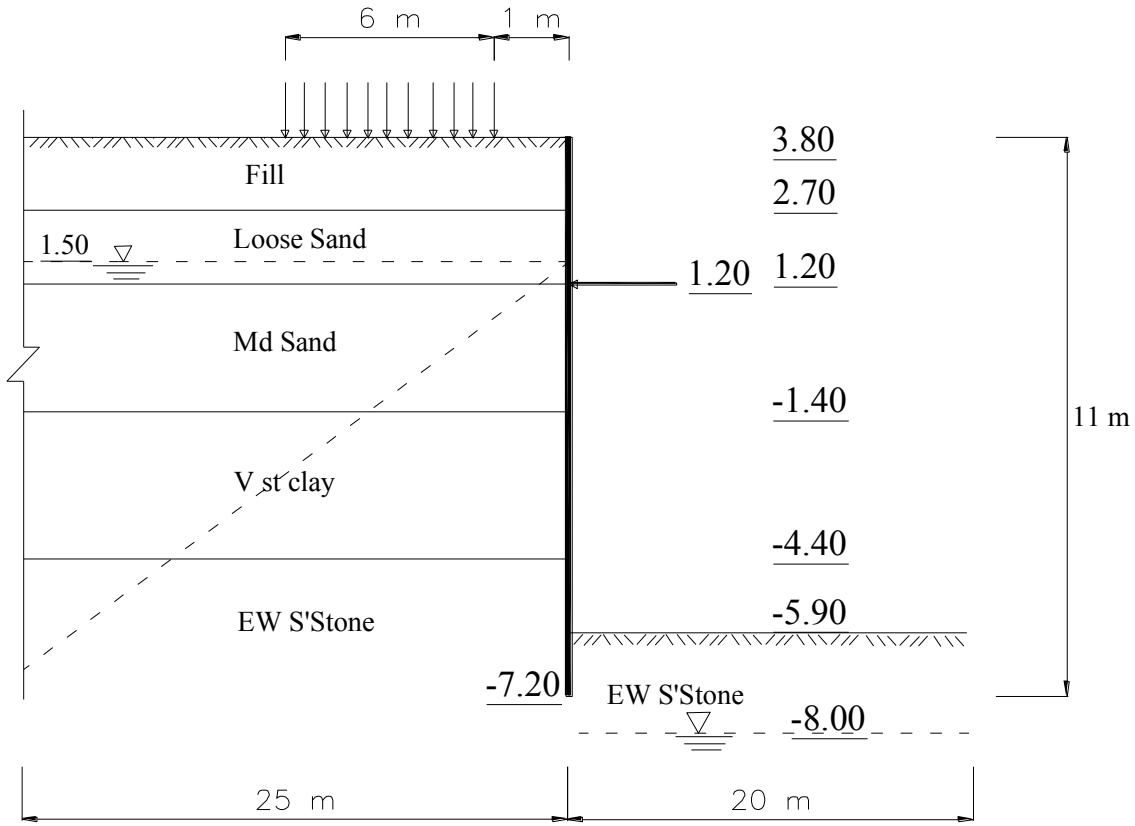

Figure 4.21 WALLAP model for Sundale project

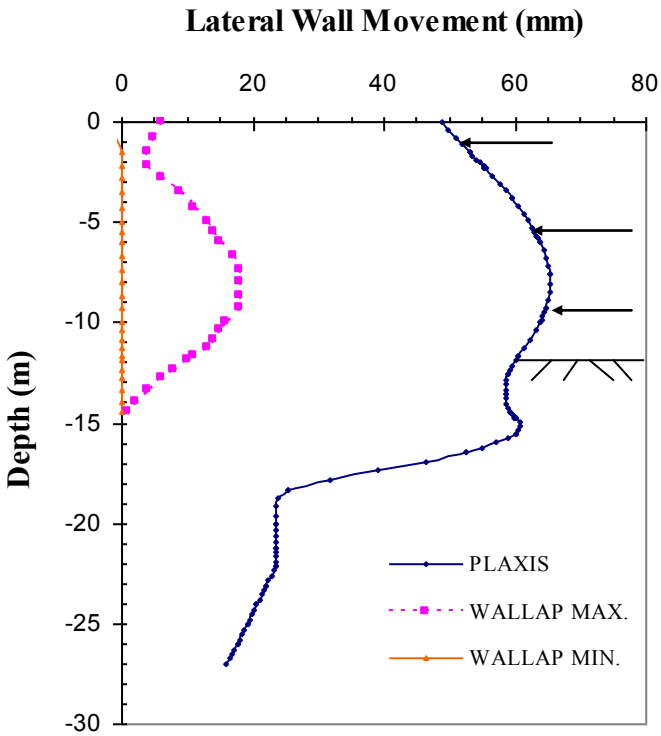

Figure 5.1 Comparison Lateral Wall Movement between WALLAP and PLAXIS (Circle on Cavill)

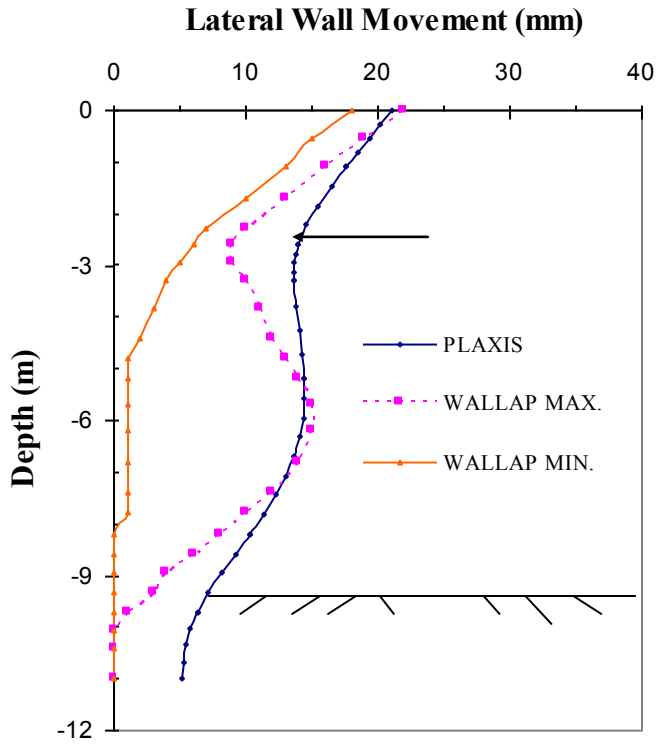

Figure 5.2 Comparison Lateral Wall Movement between WALLAP and PLAXIS (Sundale)

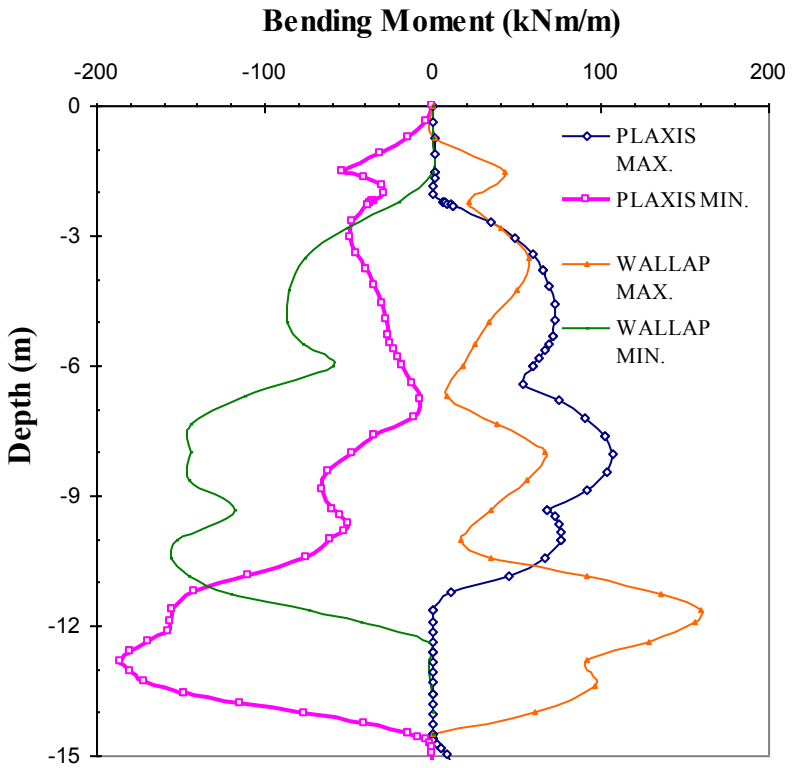

Figure 5.3(a). Compare Envelopes of Bending Moments between WALLAP and PLAXIS (Circle on Cavill)

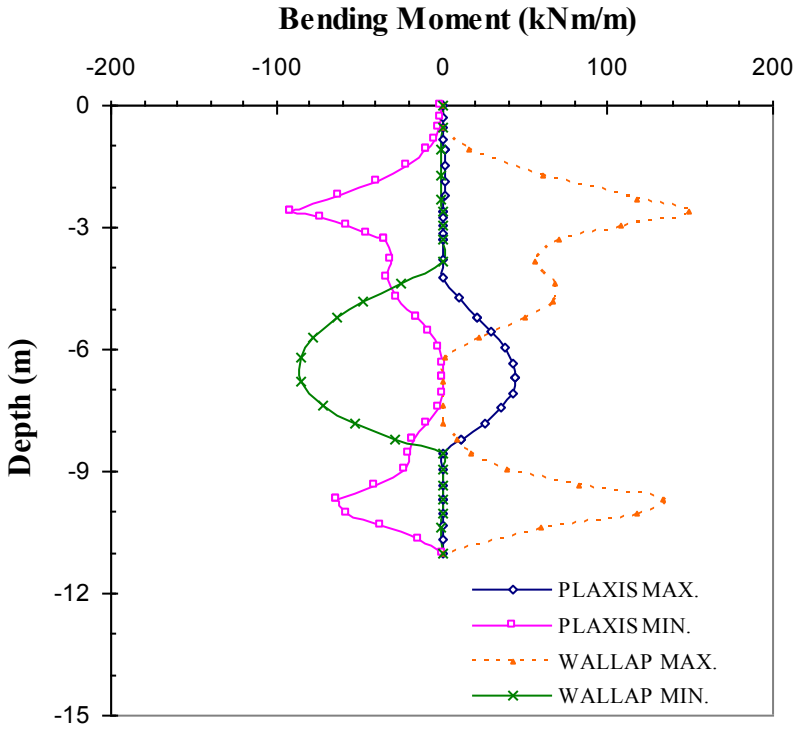

Figure 5.3(b). Compare Envelopes of Bending Moments between WALLAP and PLAXIS (Sundale)

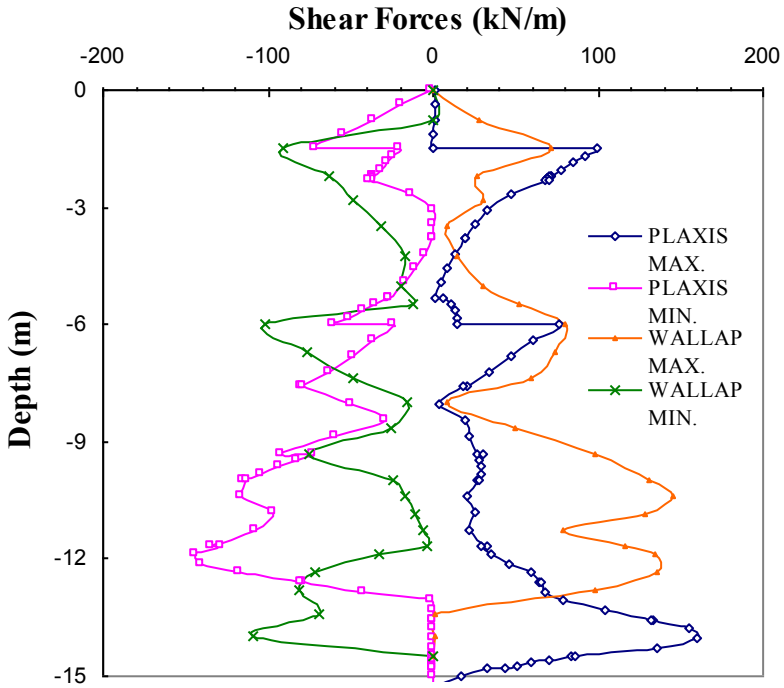

Figure 5.4(a). Compare Envelopes of Shear Forces between WALLAP and PLAXIS (Circle on Cavill)

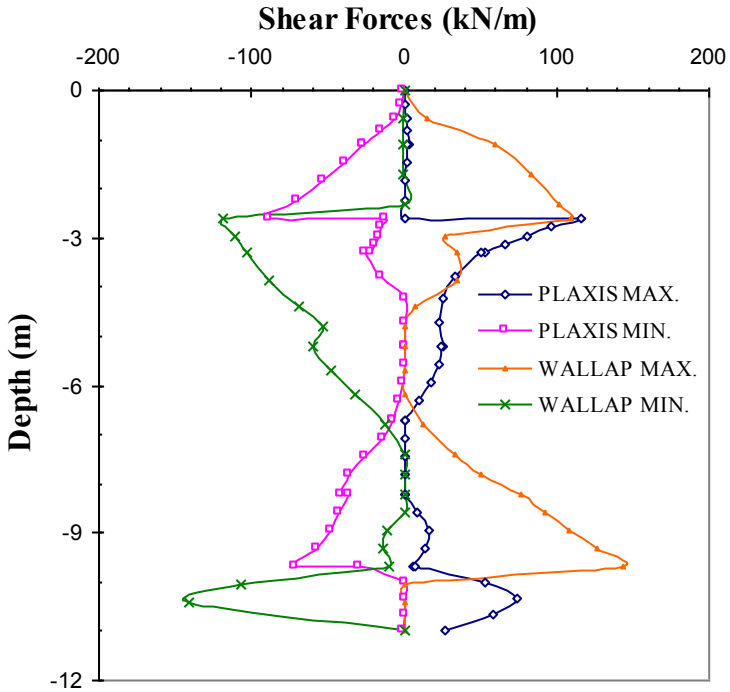

Figure 5.4(b). Compare Envelopes of Shear Forces between WALLAP and PLAXIS (Sundale)

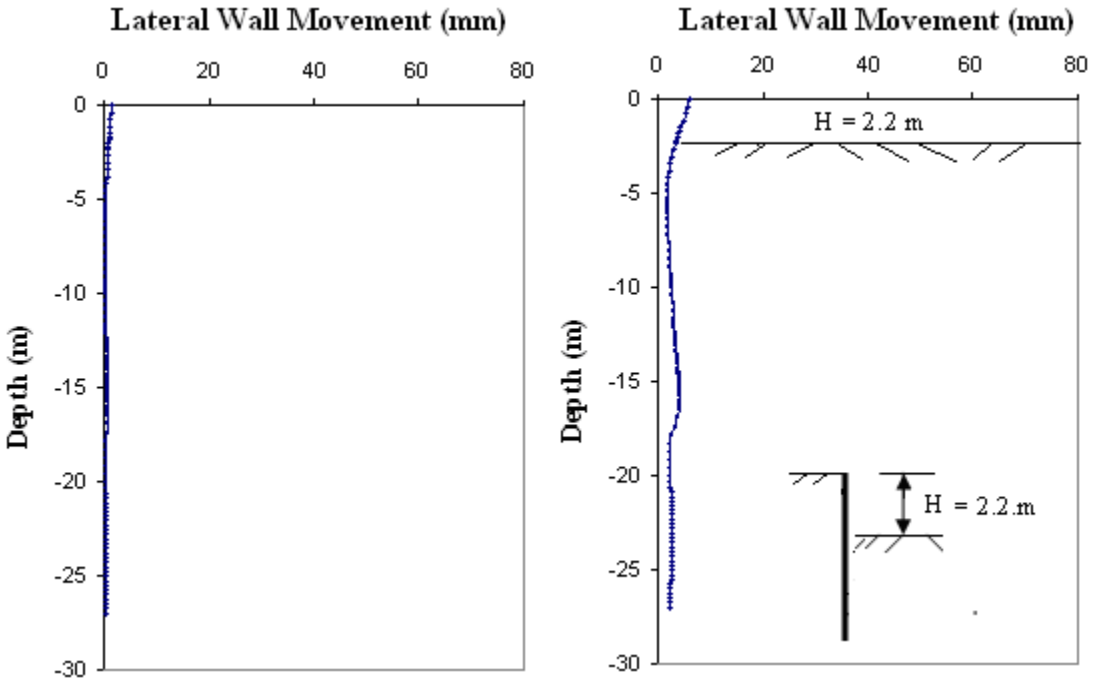

(a) Stage 1

(b) Stage 2

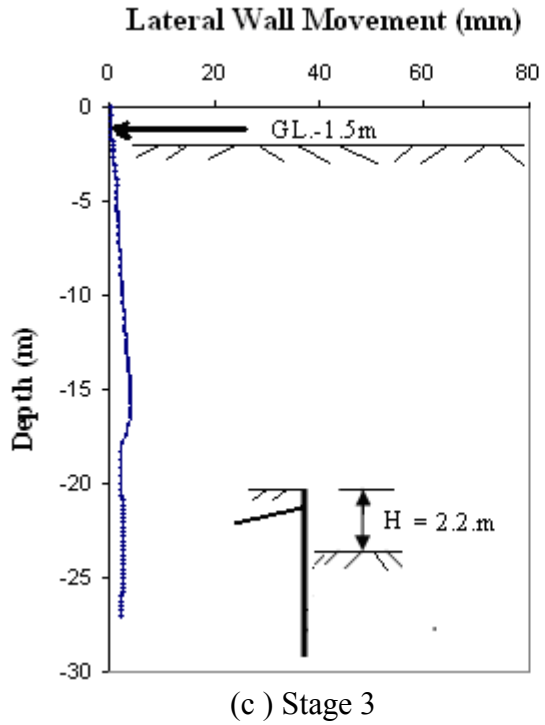

(c) Stage 3

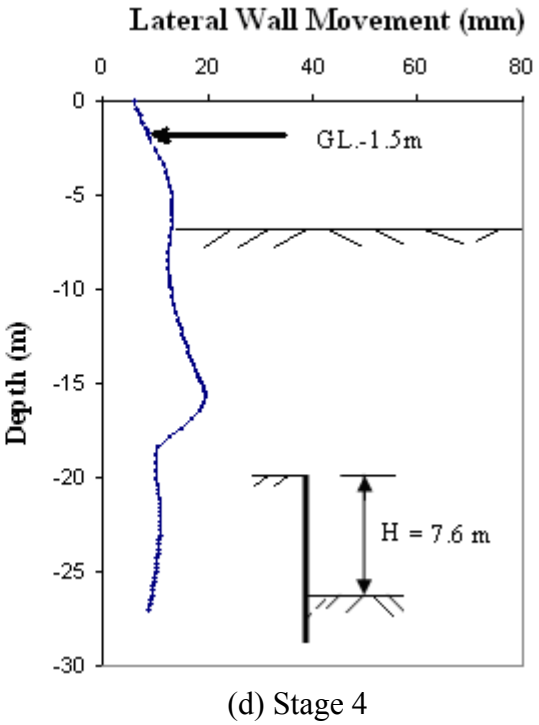

(d) Stage 4

Figure 5.5 (a) ~ (d), Lateral Wall Movement from Stage 1 to Stage 4 (Circle on Cavill)

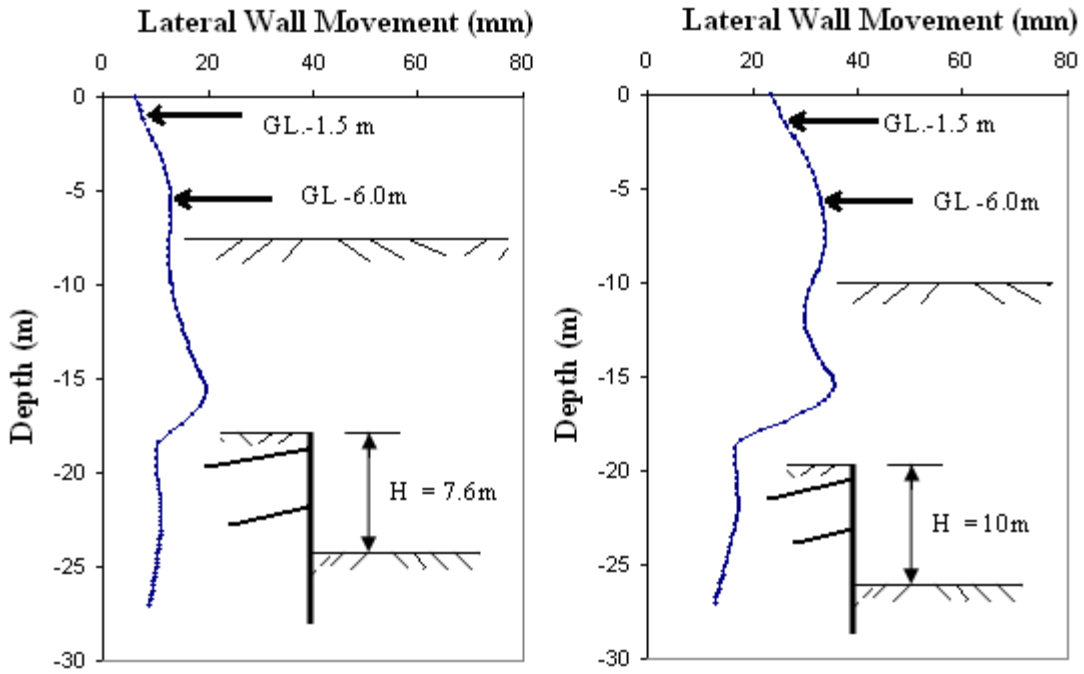

(e) Stage 5

(f) Stage 6

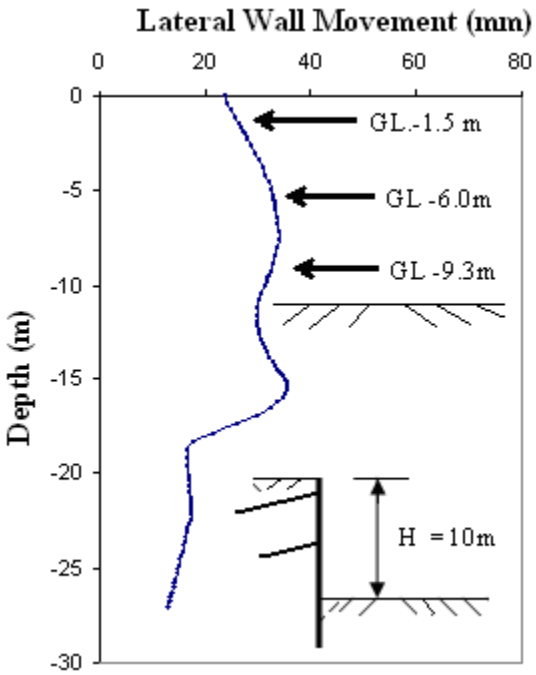

(g) Stage 7

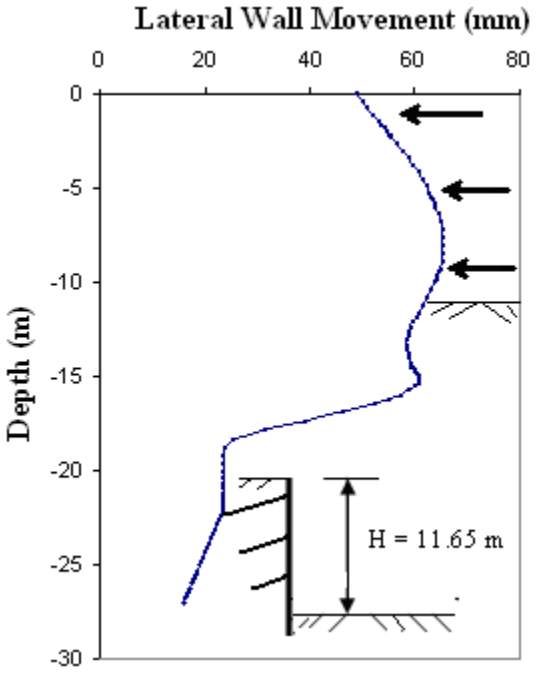

(h) Stage 8

Figure 5.5 (e) ~ (h), Lateral Wall Movement from Stage 5 to Stage 8 (Circle on Cavill)

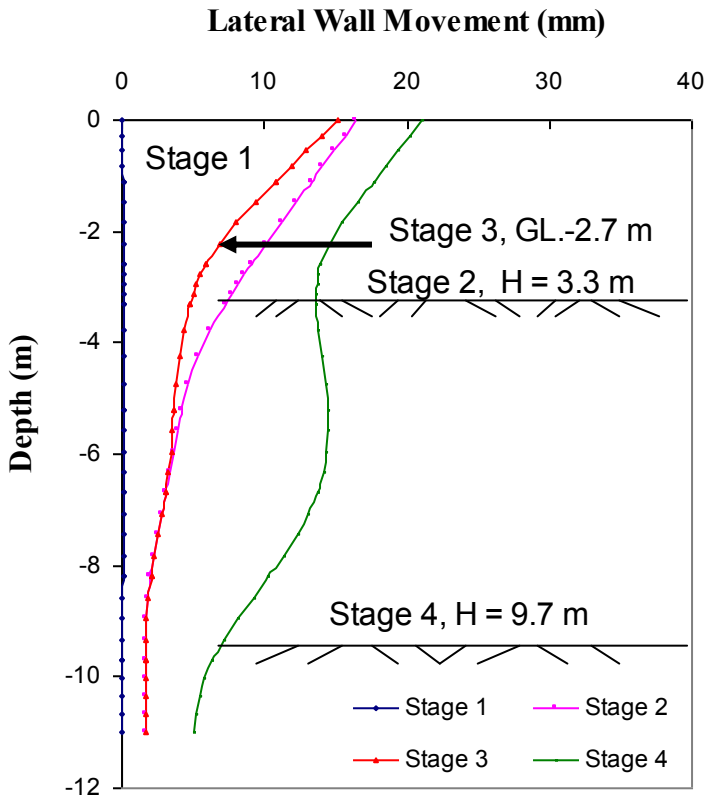

Figure 5.6 Lateral Wall Movement at Each Stage (Sundale)

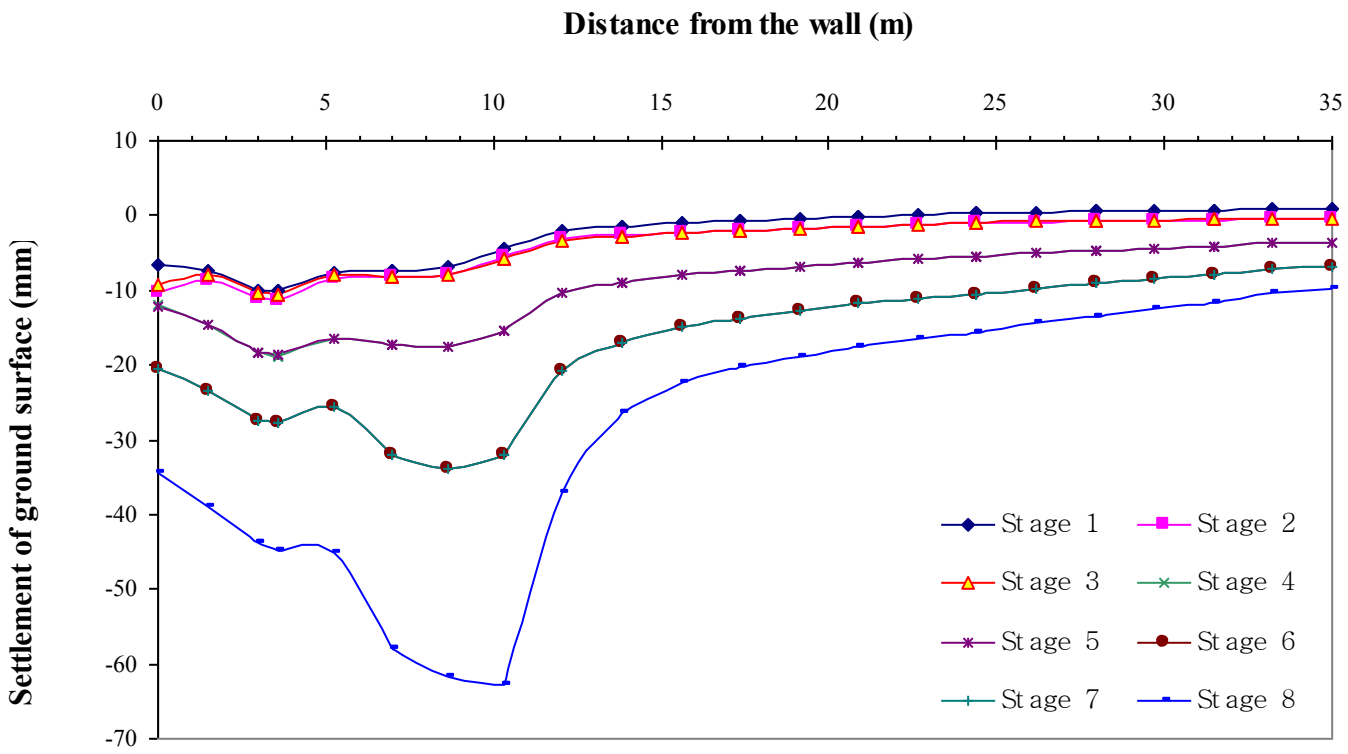

Figure 5.7. Ground Surface Settlement at Each Stage (Circle on Cavill)

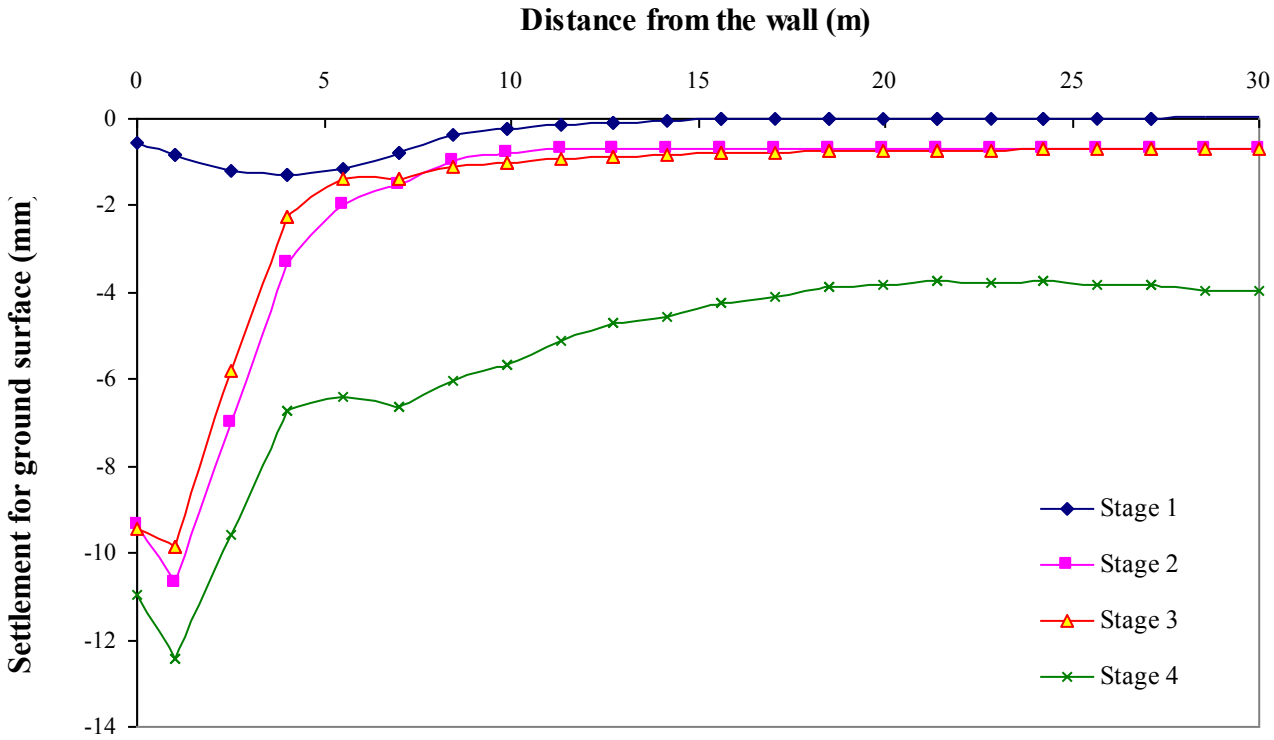

Figure 5.8. Ground Surface Settlement at Each Stage (Sundale)

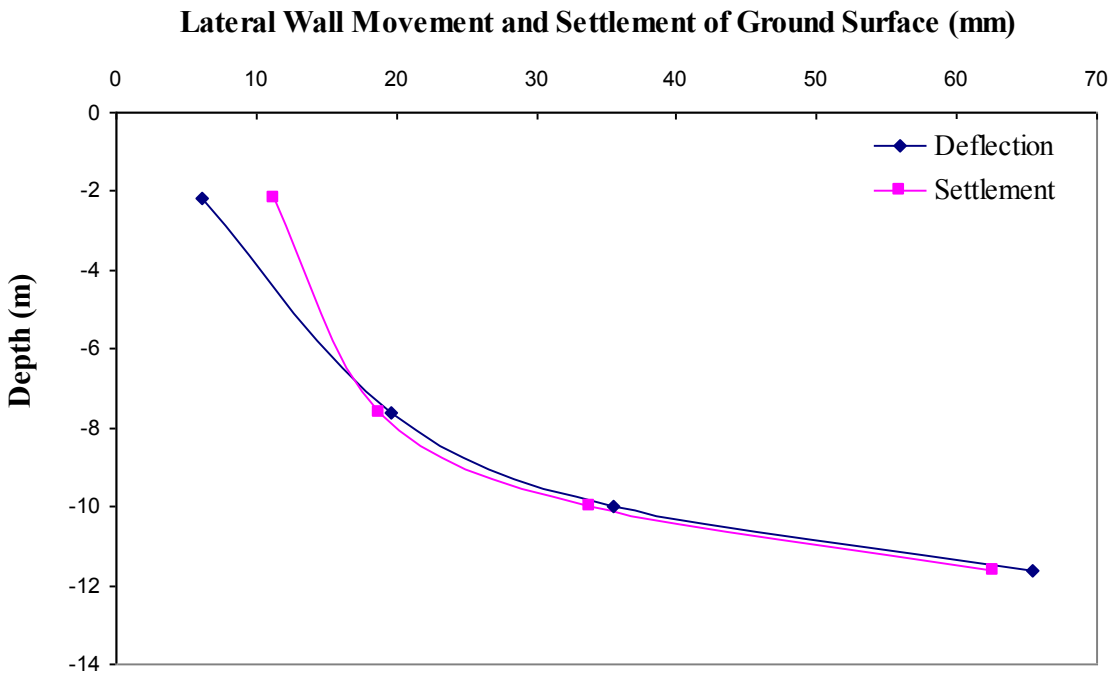

Figure 5.9. Relationships Between Lateral Displacement and Settlement of Ground Surface and Excavation Depth (Circle on Cavill).

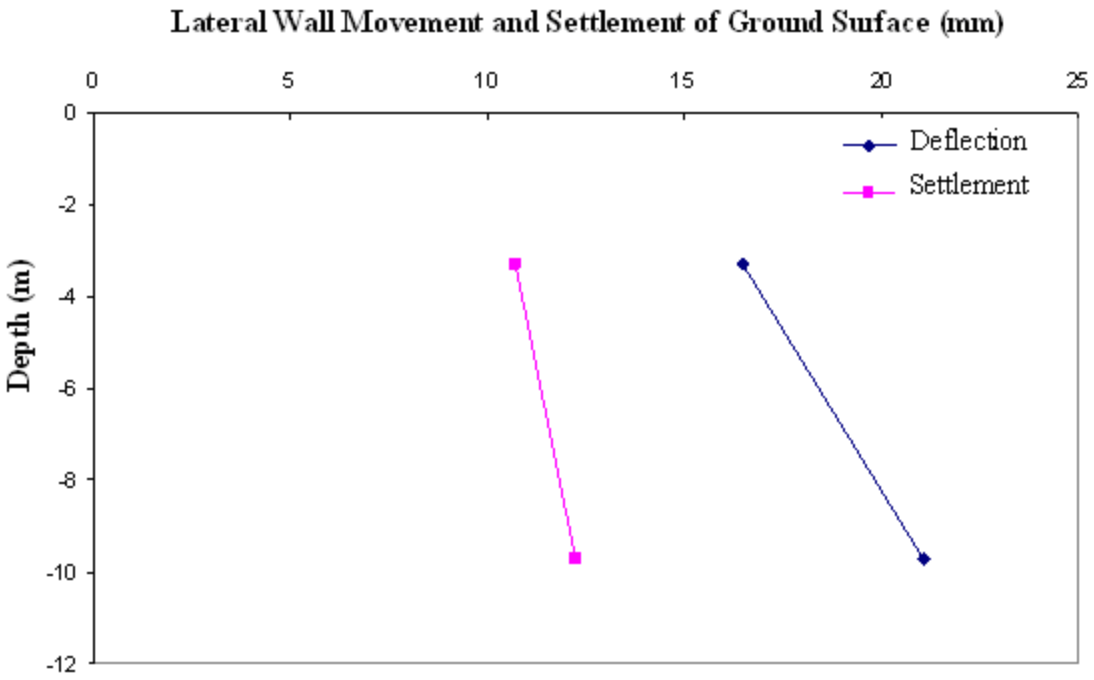

Figure 5.10. Relationships Between Lateral Displacement and Settlement of Ground Surface and Excavation Depth (Sundale)

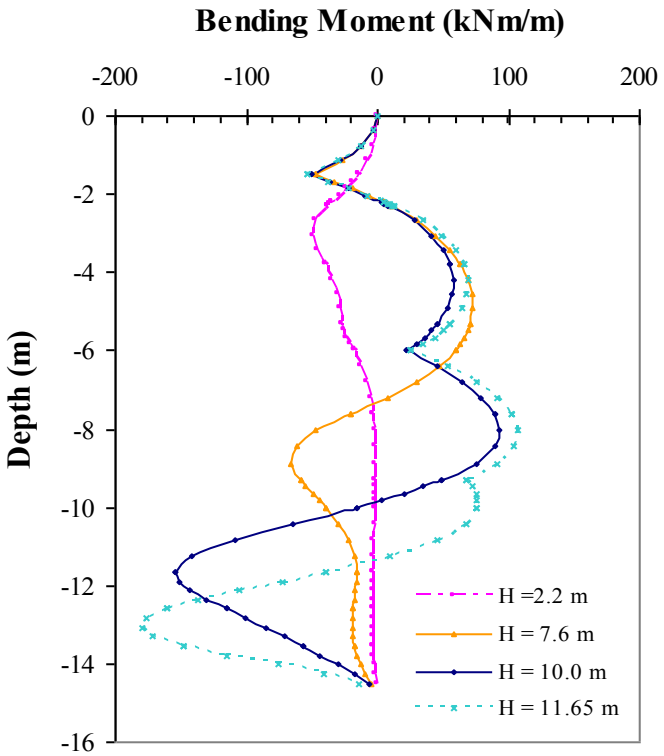

Figure 5.11. Bending Moments at different excavation depth (Circle on Cavill)

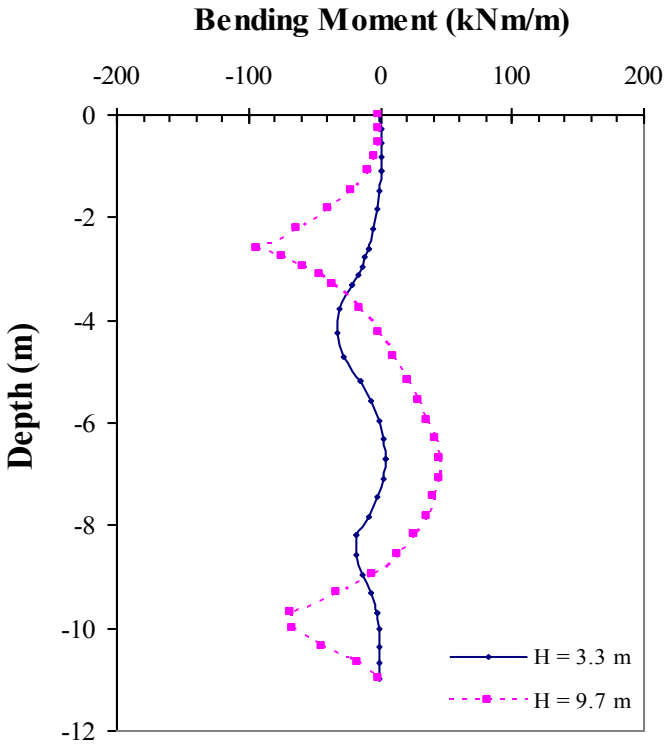

Figure 5.12. Bending Moments at different excavation depth (Sundale)

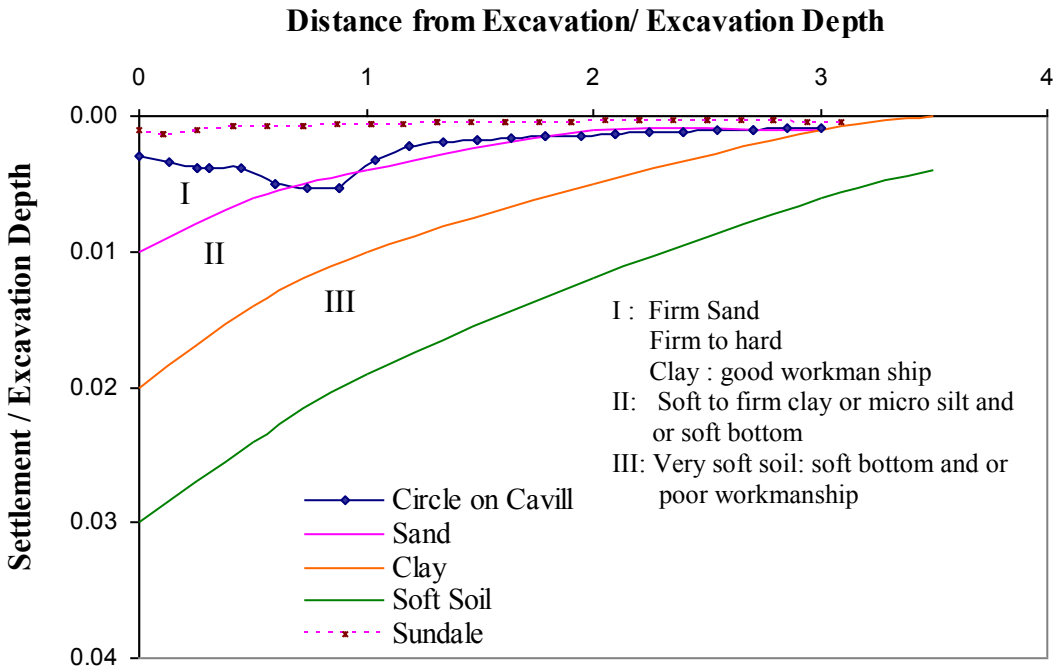

Figure 5.13(a). Movement adjacent to braced excavation (Peck, 1969)

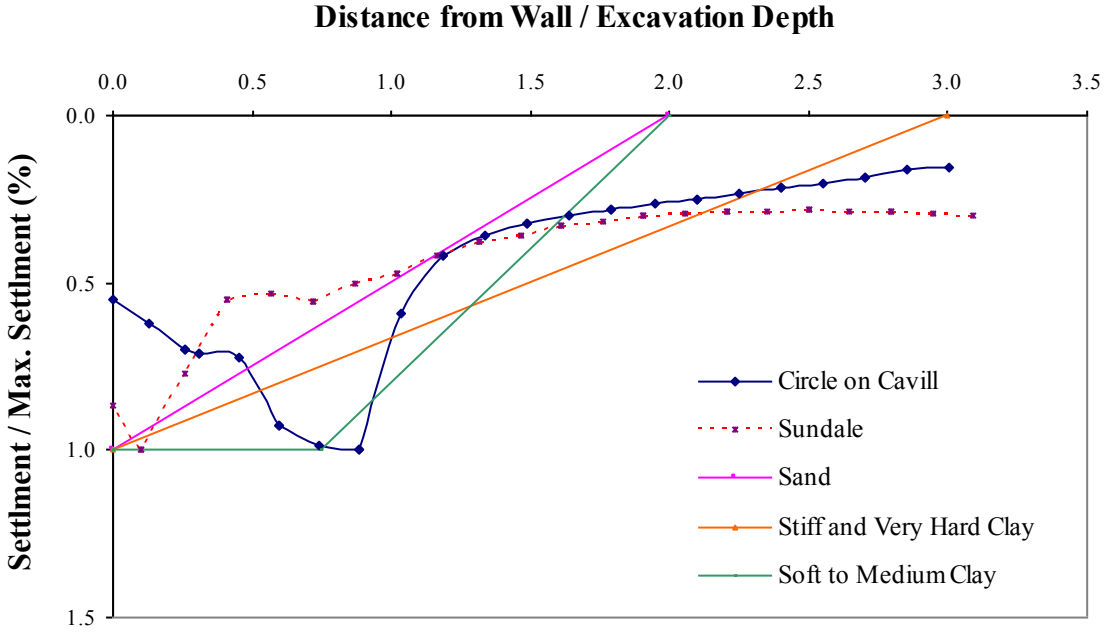

Figure 5.13(b). Normalized ground settlement profiles of various soil types (Clough and O'Rourke, 1990)

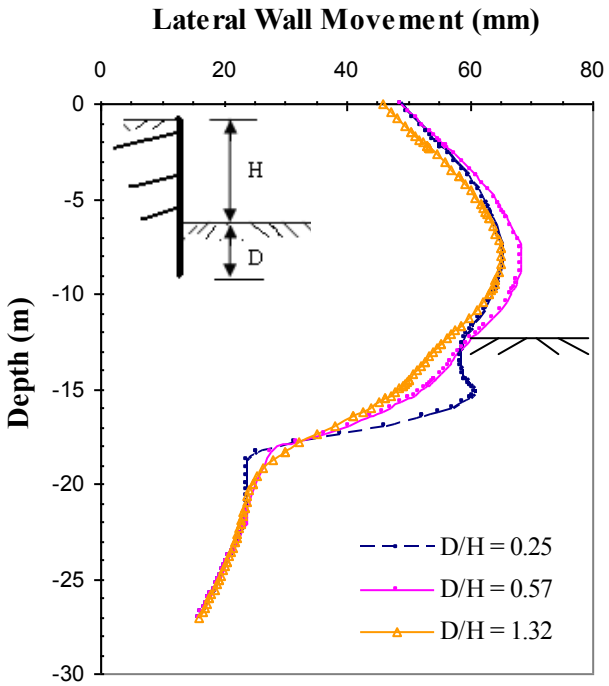

Figure 5.14. Effect of Embedment Depth on Lateral Wall Movement (Circle on Cavill)

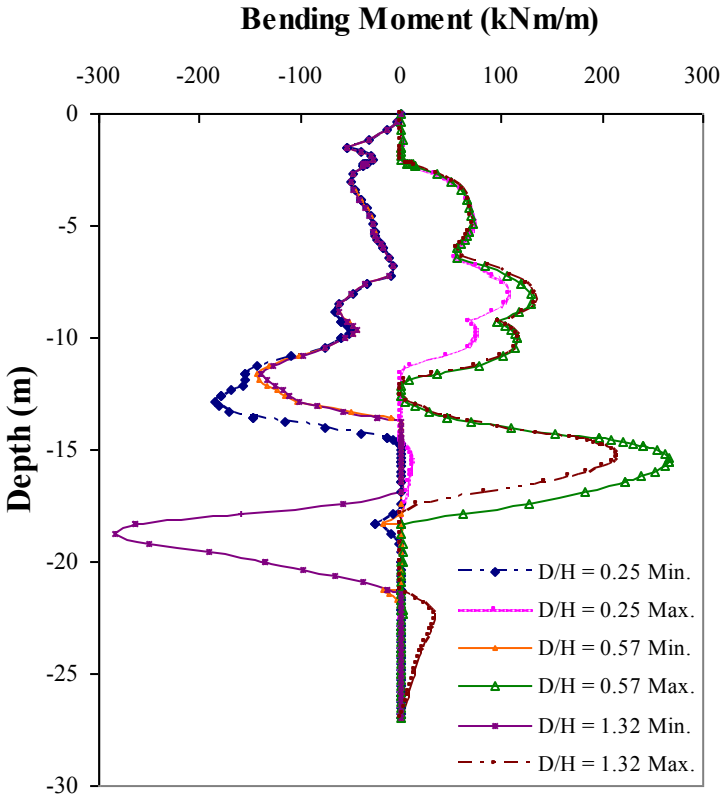

Figure 5.15. Effects of Embedment Depth on Envelopes of Bending Moments (Circle on Cavill)

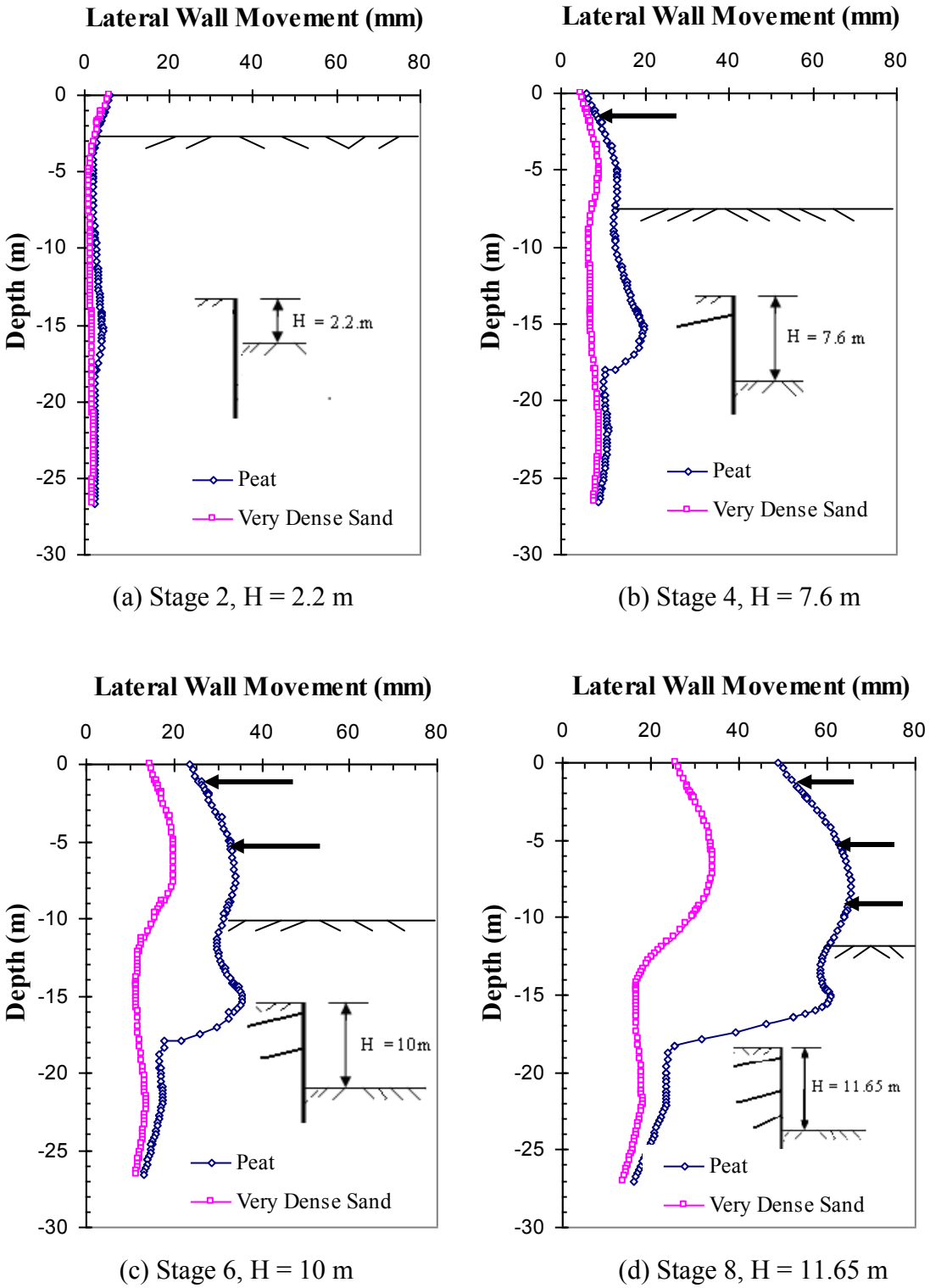

(a) Stage 2, H = 2.2 m

(b) Stage 4, H = 7.6 m

(c) Stage 6, H = 10 m

(d) Stage 8, H = 11.65 m

Figure 5.16 (a) ~ (d). Effects of Stiffness of Peat on Lateral Wall Movement at Different Excavation Depth (Circle on Cavill)

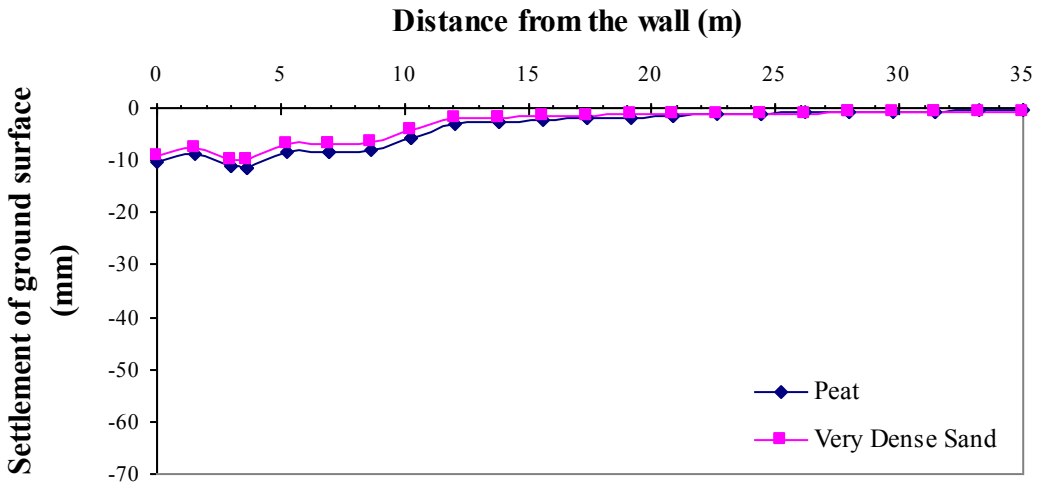

(a) Stage 2, H = 2.2 m

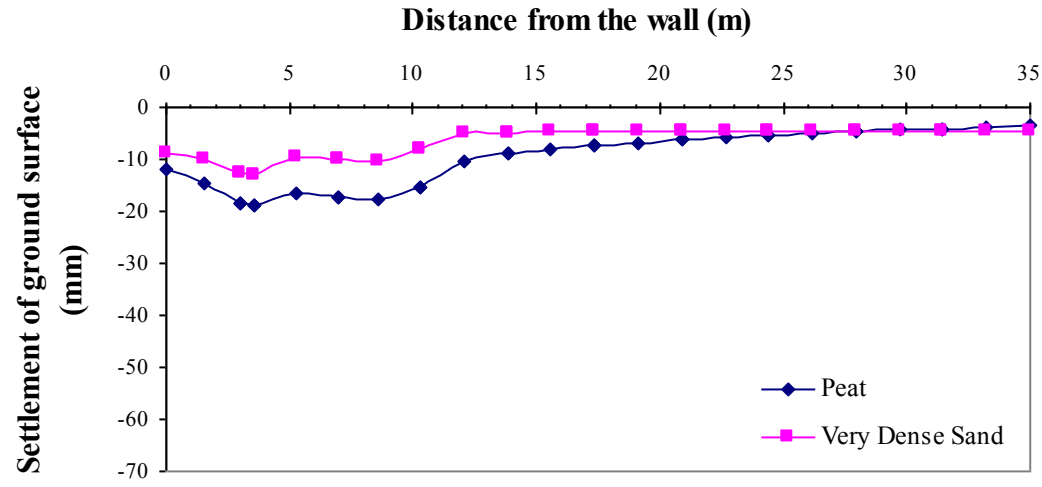

(b) Stage 4, H = 7.6 m

Figure 5.17(a)~(b). Effects of Stiffness of Peat for Ground Surface Settlement at Different Excavation Depth (Circle on Cavill)

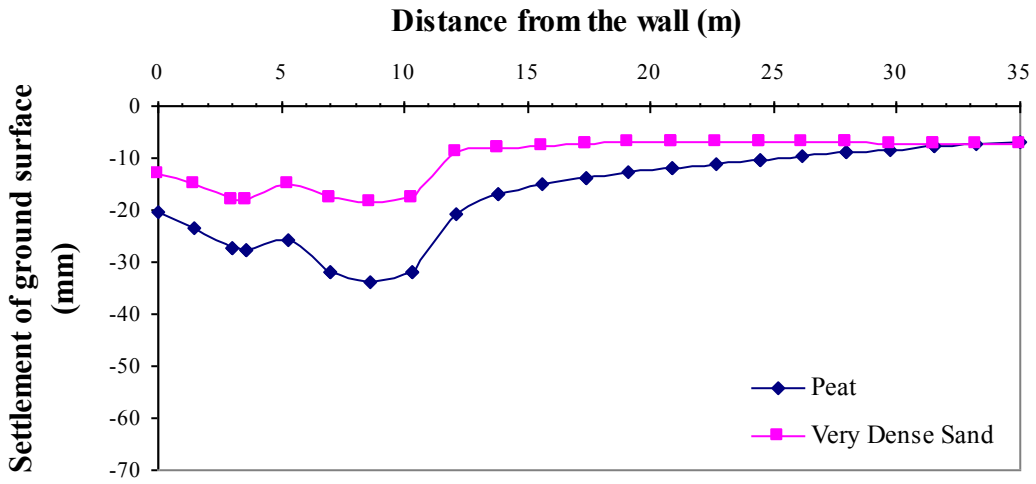

(c) Stage 6, H = 10 m

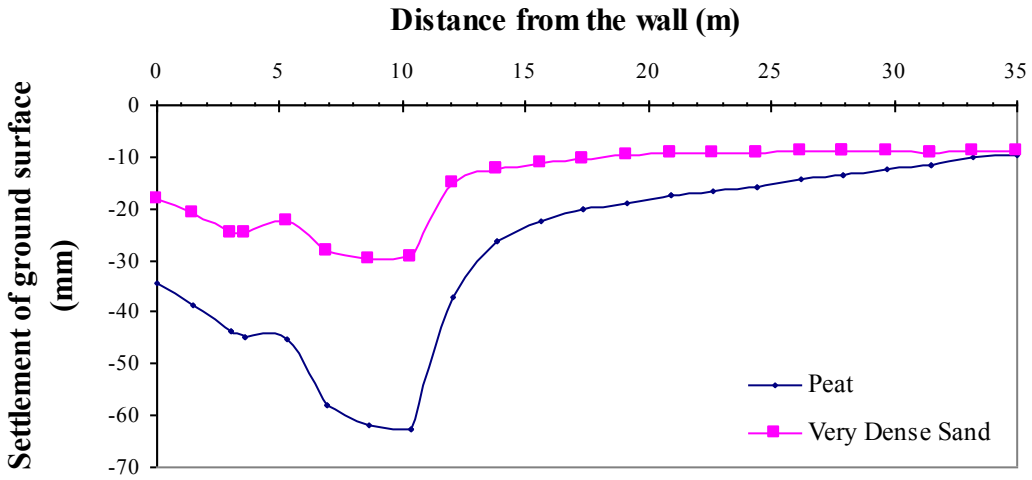

(d) Stage 8, H = 11.65 m

Figure 5.17(c) ~(d). Effects of Stiffness of Peat for Ground Surface Settlement at Different Excavation Depth (Circle on Cavill)

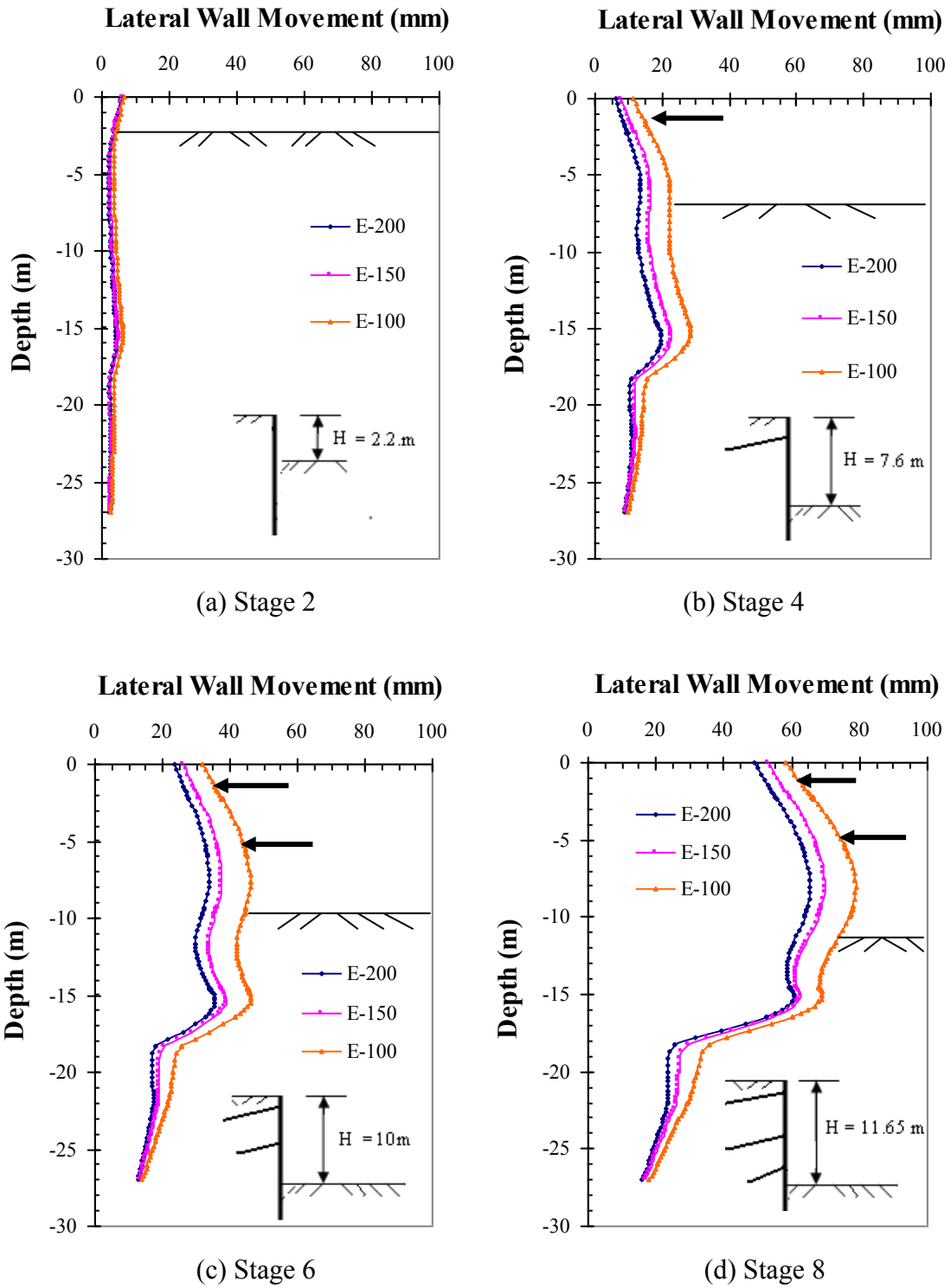

Figure 5.18. Effect of Stiffness of Dense Sand on Lateral Wall Movement at Different Excavation Depth (Circle on Cavill)

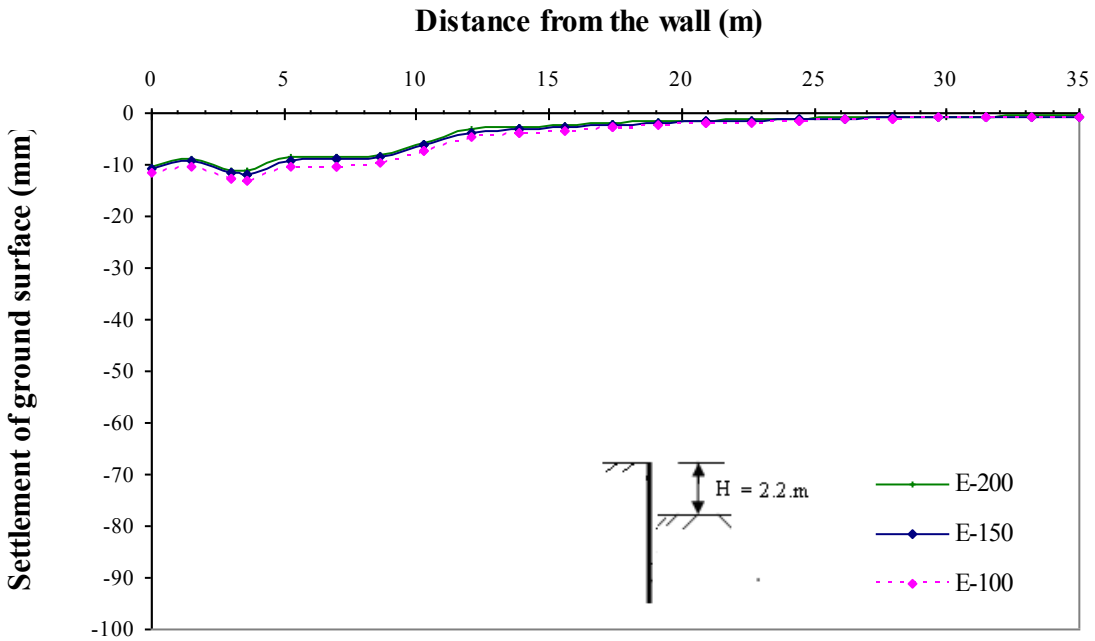

(a) Stage 2

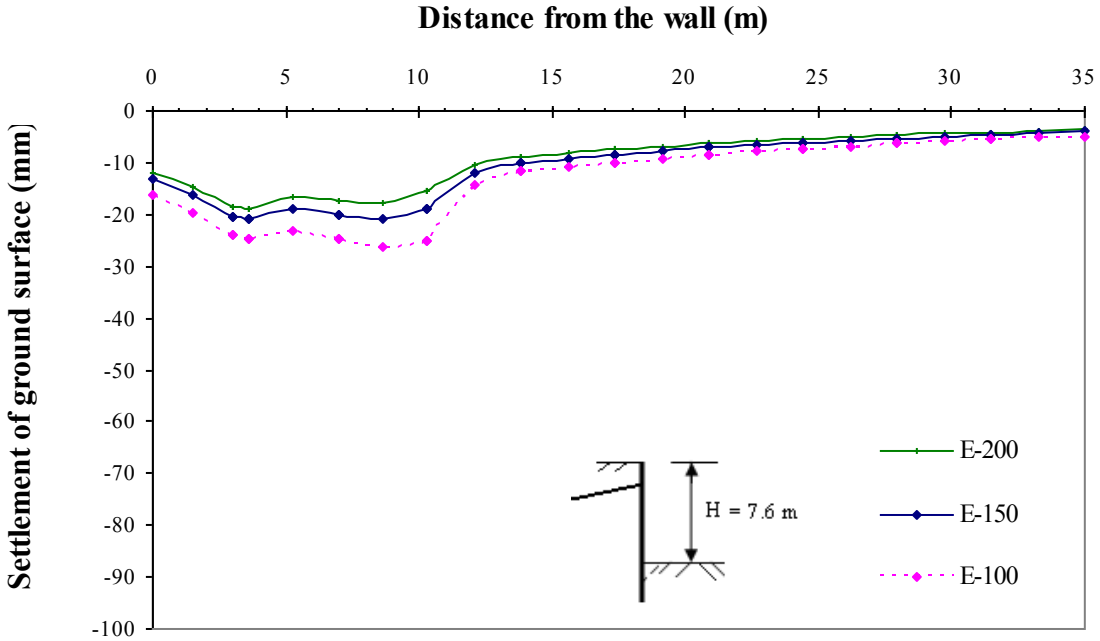

(b) Stage 4

Figure 5.19 (a) ~ (b). Effects of Stiffness of Dense Sand on Settlement of Ground Surface at Different Excavation Depth.(Circle on Cavill).

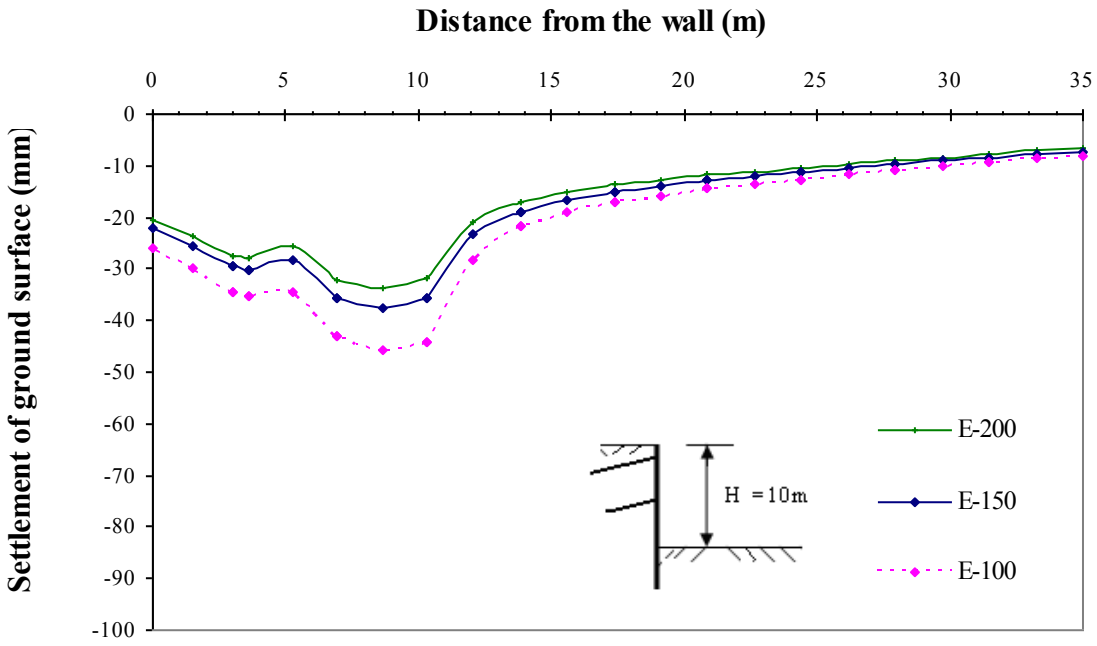

(c) Stage 6

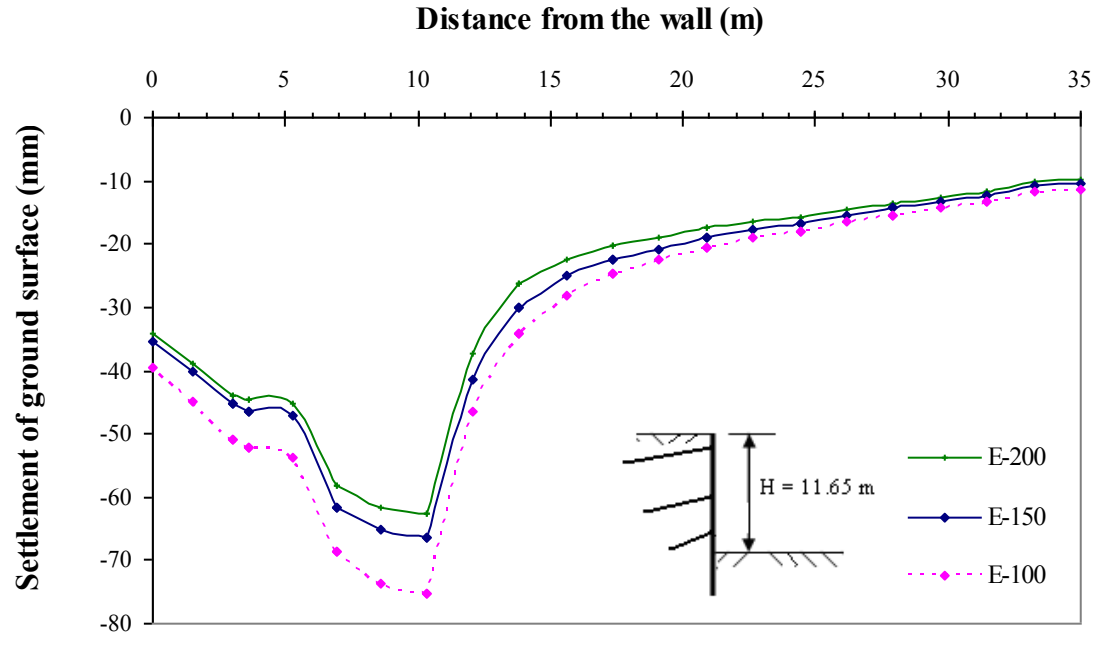

(d) Stage 8

Figure 5.19 (a) ~ (d). Effects of Stiffness of Dense Sand on Settlement of Ground Surface at Different Excavation Depth.(Circle on Cavill).

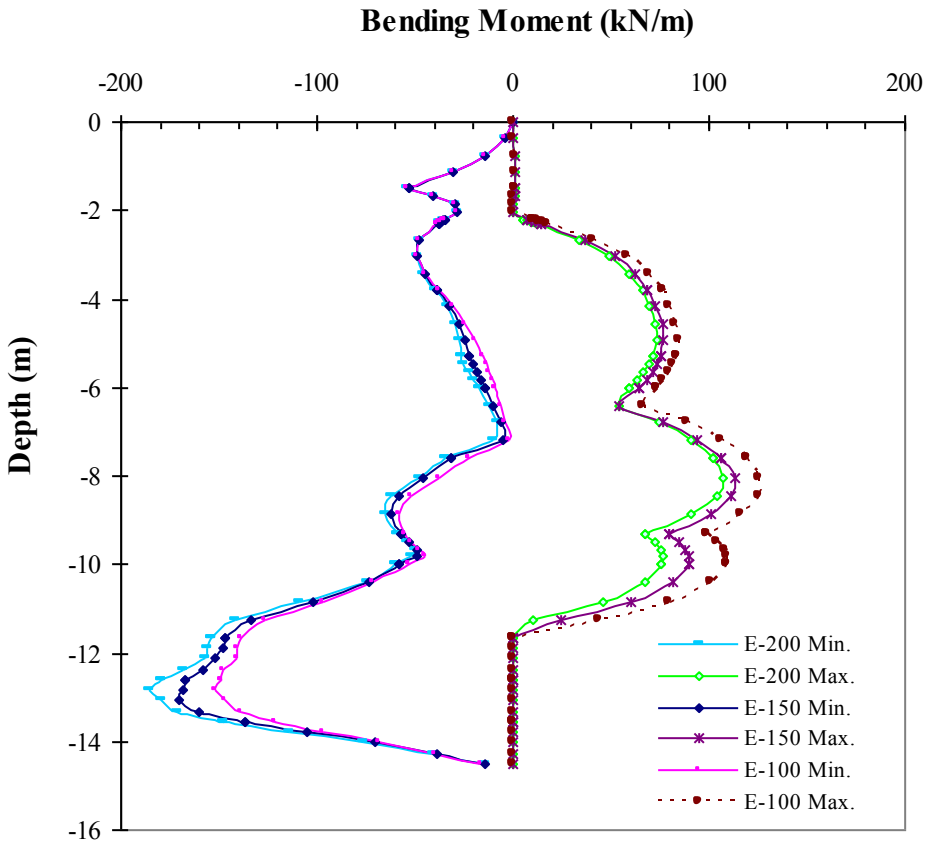

Figure 5.20. Envelopes of Bending Moments for Different E-value for Dense Sand Layers (Circle on Cavill project)

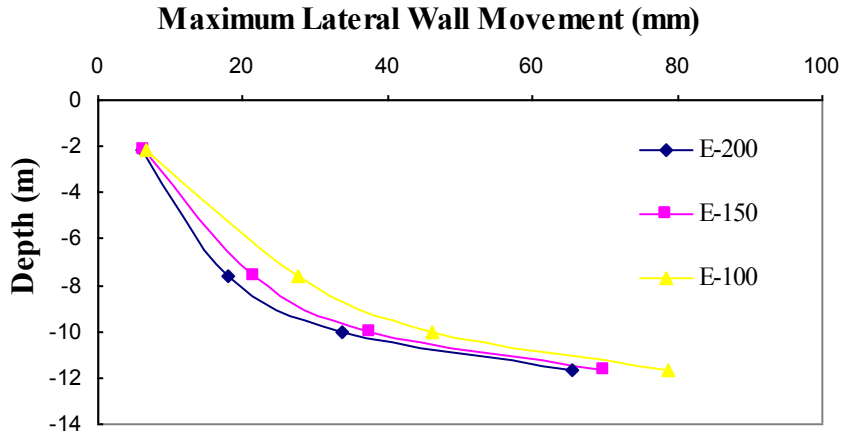

(a)

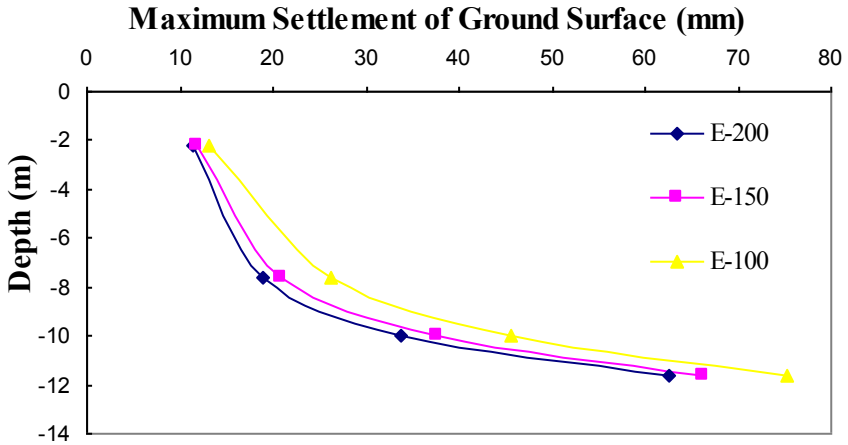

(b)

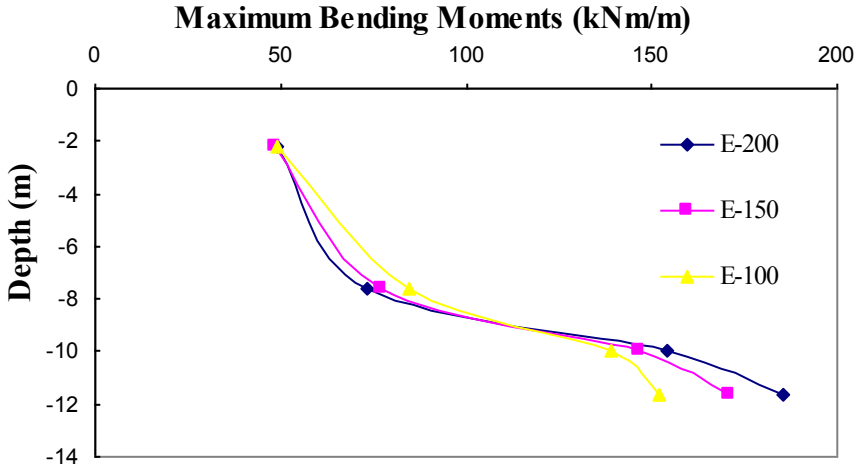

(c)

Figure 5.21(a) ~ (c). Relationship Between Maximum Values, Stiffness of Dense Sand Layers and Excavation Depth (Circle on Cavill)

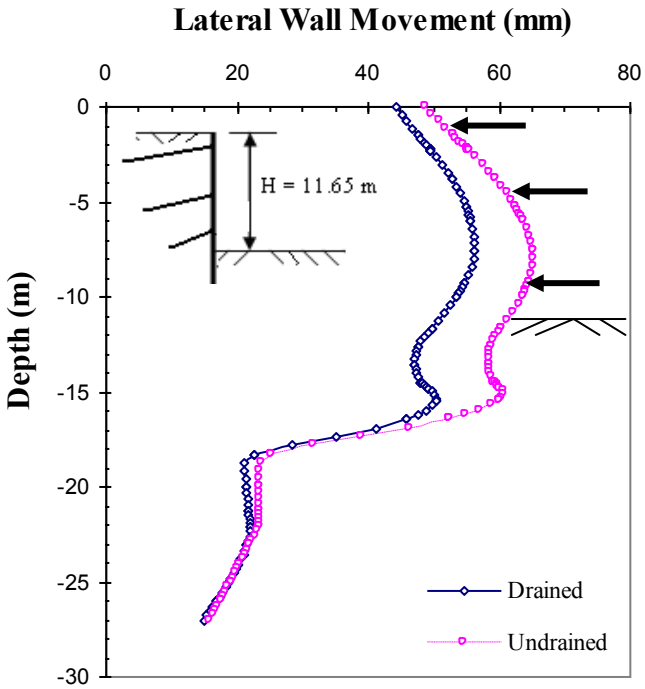

Figure 5.22 Comparison of Lateral Wall Movements for Drained and Undrained Peat and Clay layers (Circle on Cavill).

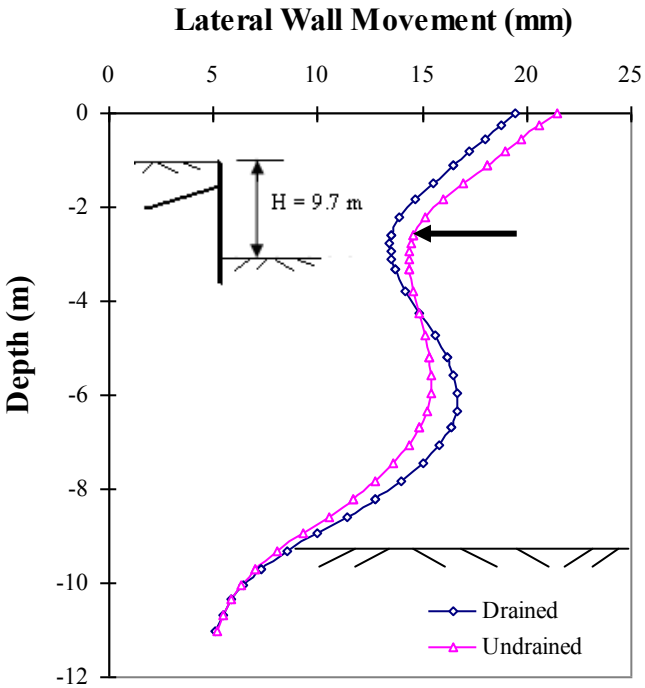

Figure 5.23 Lateral Wall Movements for Drained and Undrained Clay layers (Sundale Project).

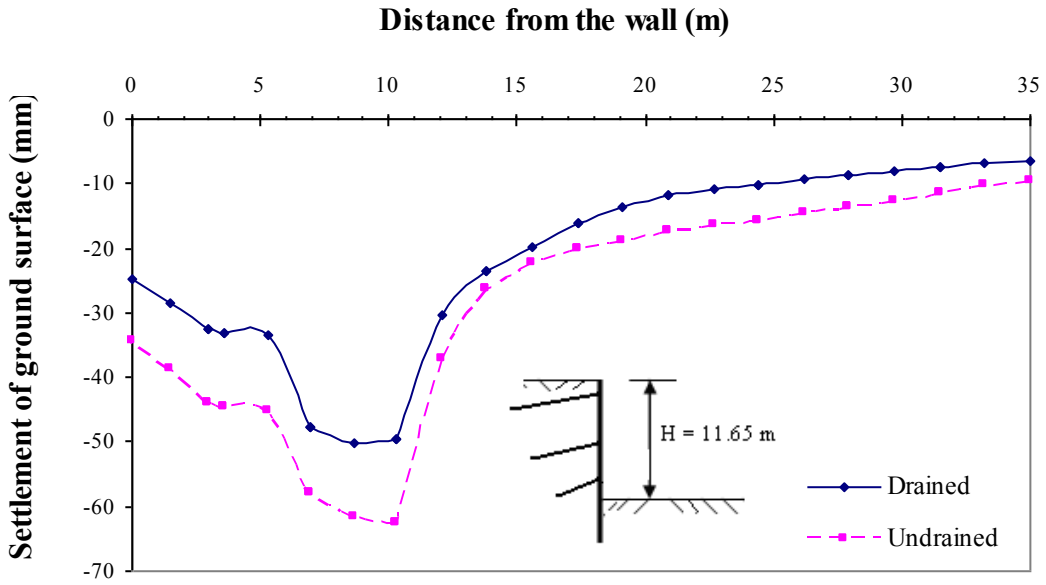

Figure 5.24. Settlement of ground surface for Drained and Undrained Peat and Clay layers (Circle on Cavill).

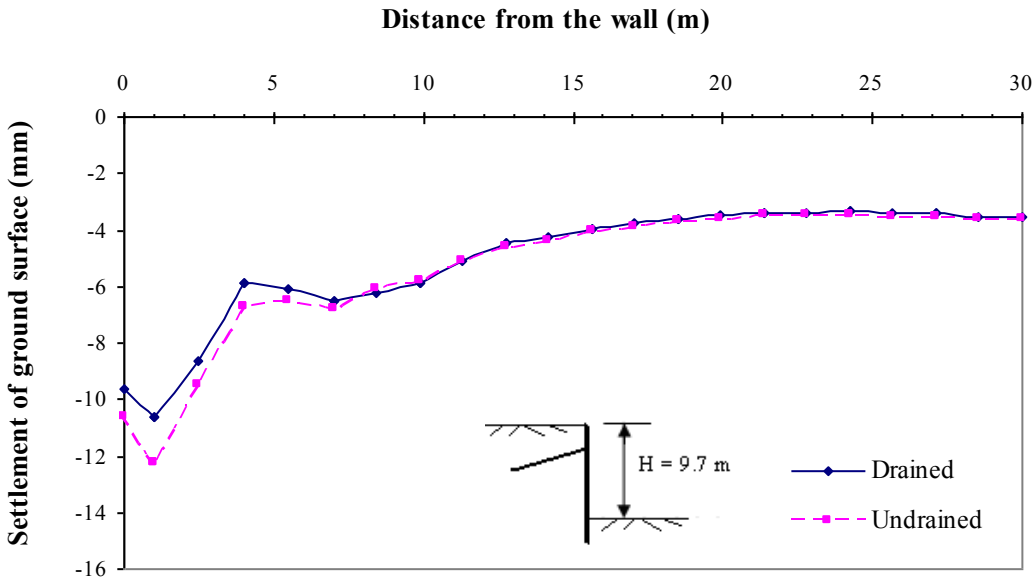

Figure 5.25. Settlement of ground surface for Drained and Undrained Clay layers (Sundale)

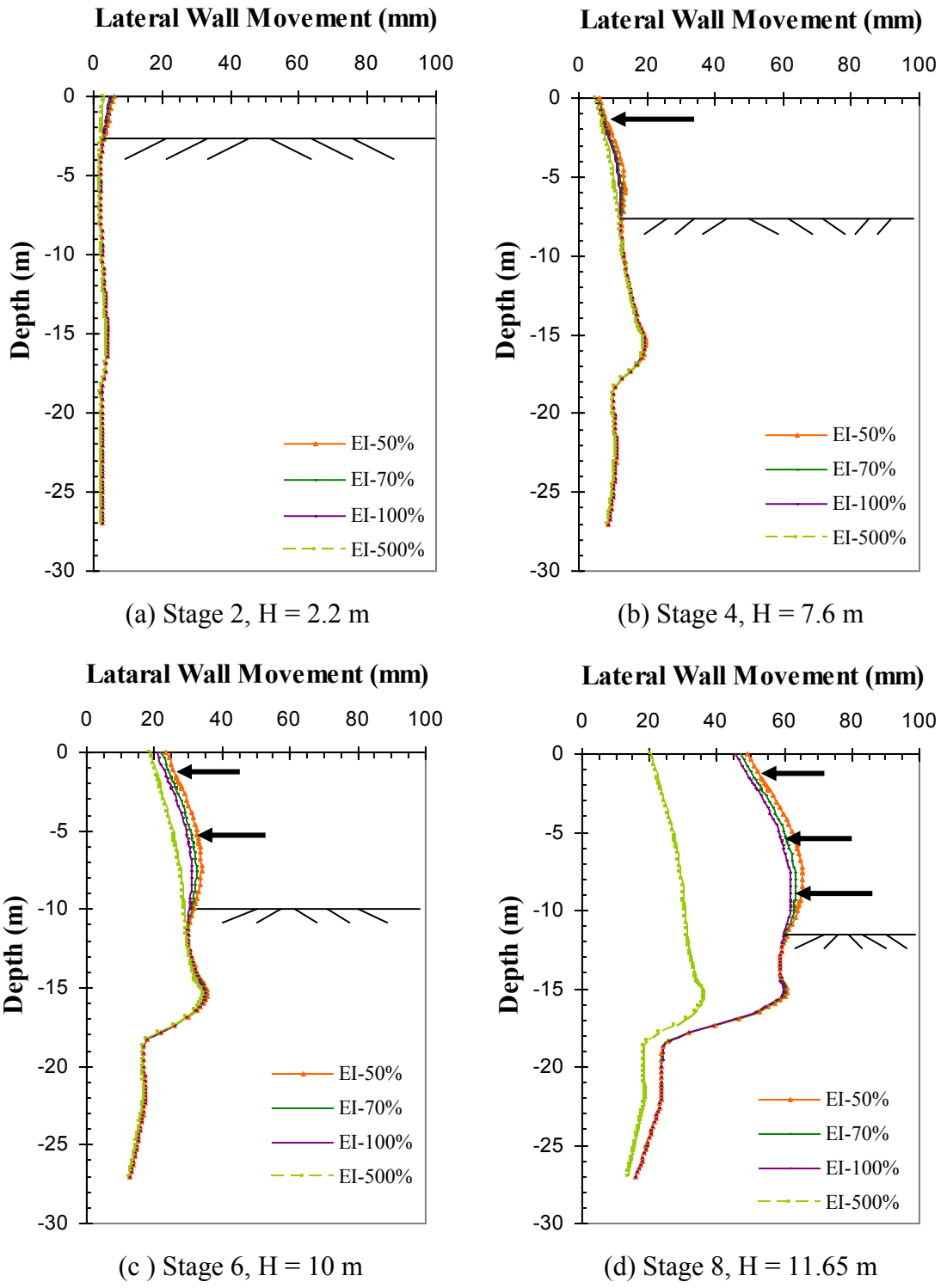

Figure 5.26. Effect of Stiffness of Wall on Lateral Wall Movement at Different Excavation Depth (Circle on Cavill)

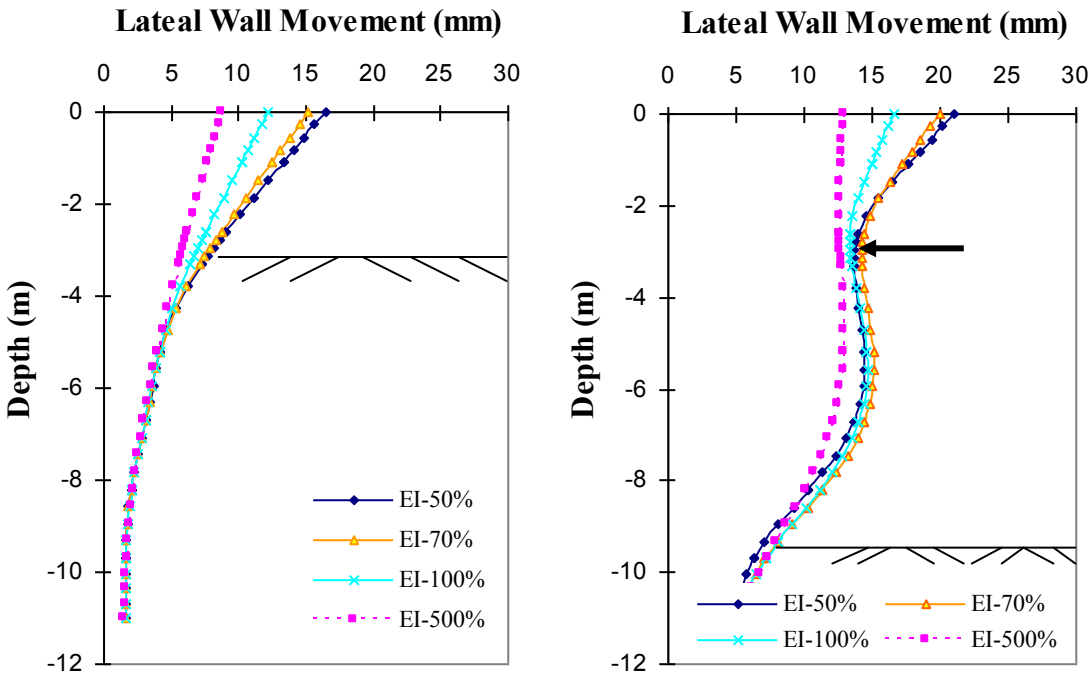

(a) Stage 2, H = 3.3 m (b) Stage 4, H = 9.7 m

Figure 5.27. Effect of Stiffness of Wall on Lateral Wall Movement at Different Excavation Depth (Sundale)

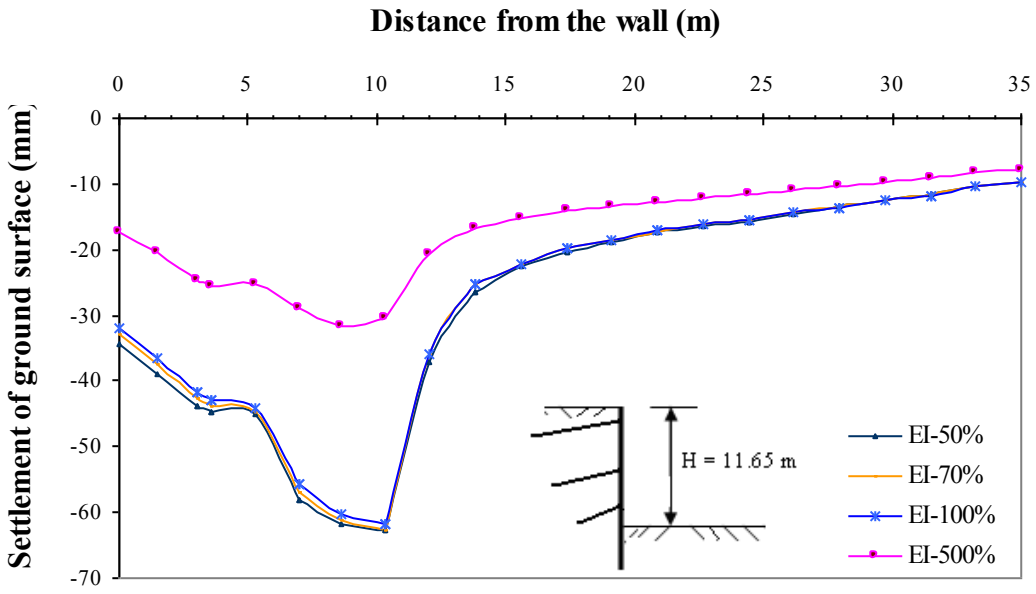

Figure 5.28. Ground Surface Settlement for Different Stiffness of Wall (Excavation Depth = 11.65m, Circle on Cavill)

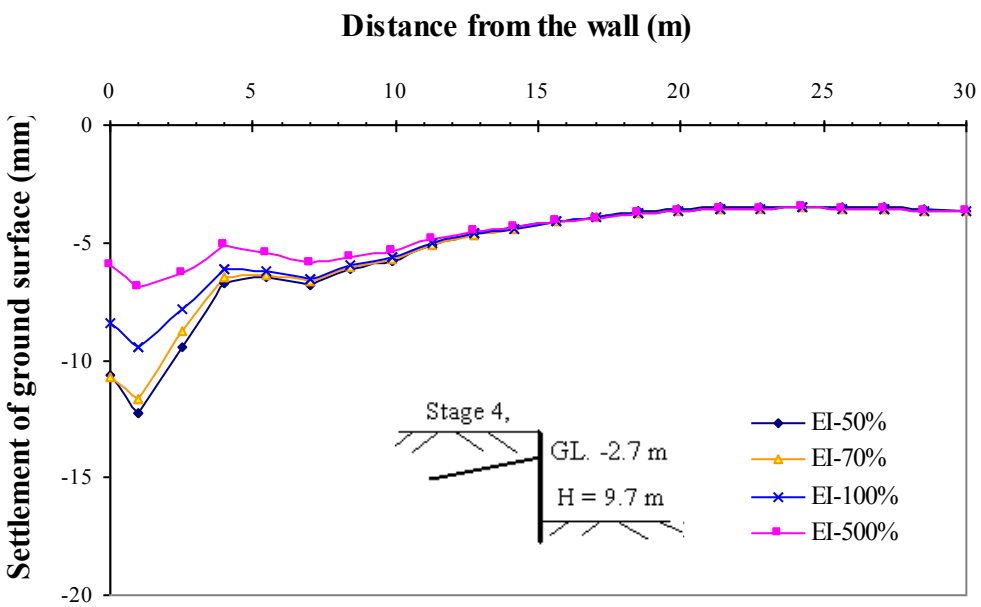

Figure 5.29. Ground Surface Settlement for Different Stiffness of Wall (Excavation Depth = 9.7m, Sundale)

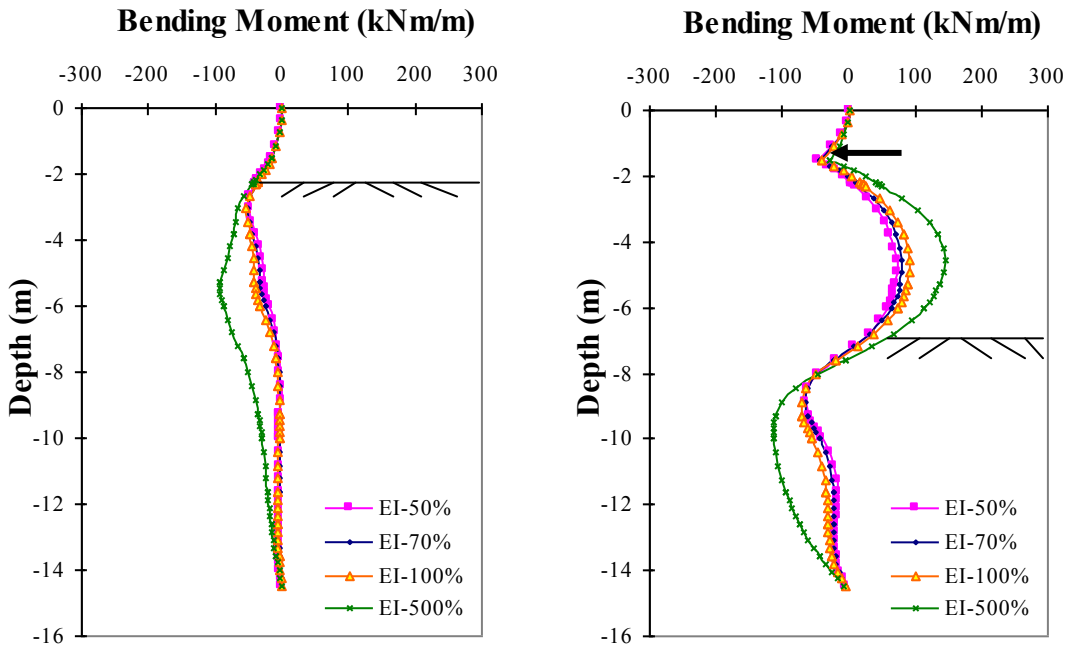

(a) Stage 2, H = 2.2

(b) Stage 4, H= 7.6 m

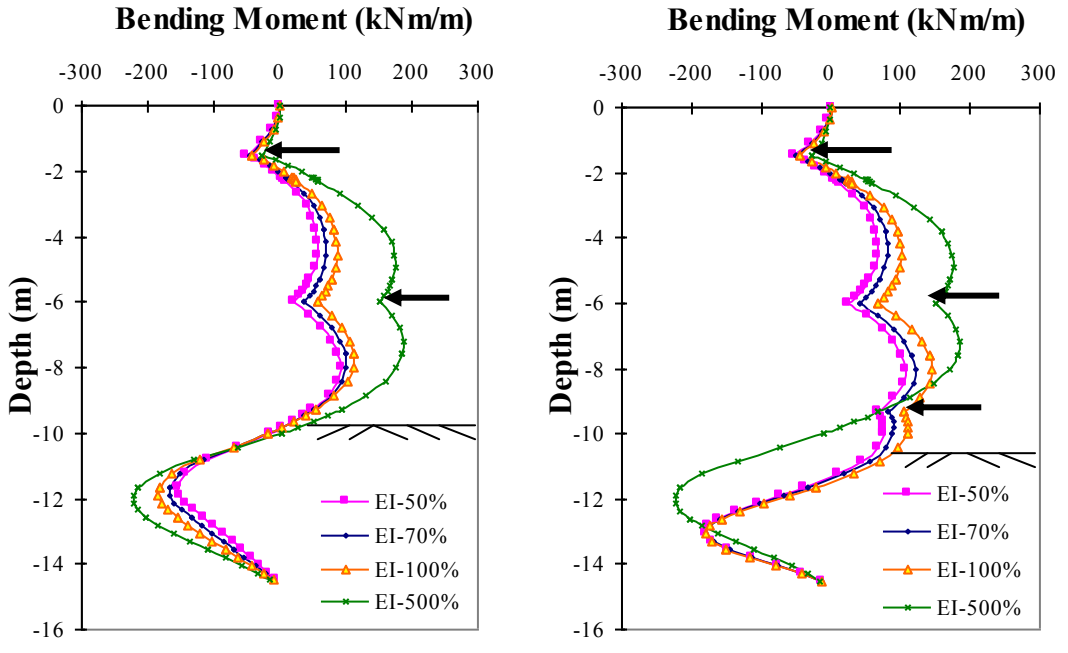

(c) Stage 6, H =10 m

(d) Stage 8, H = 11.65 m

Figure 5.30. Effect of Stiffness of Wall on Bending Moments at different Excavation Depth (Circle on Cavill)

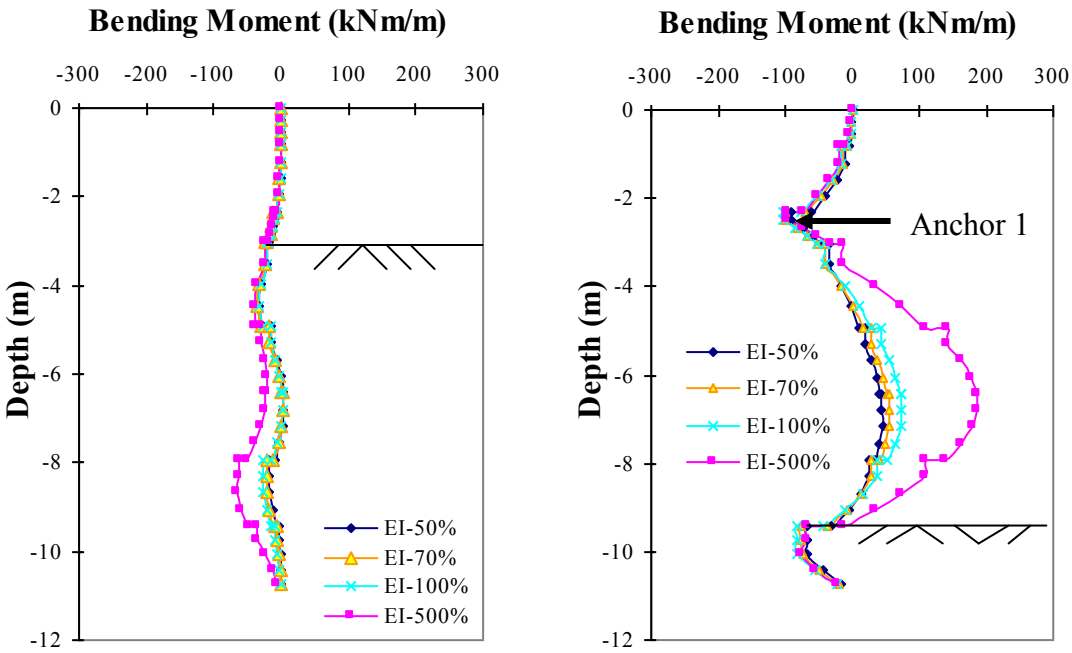

(a) Stage 2, H = 3.3 m (b) Stage 4, H = 9.7 m

Figure 5.31 Effect of Stiffness of Wall on Bending Moments at different Excavation Depth (Sundale)

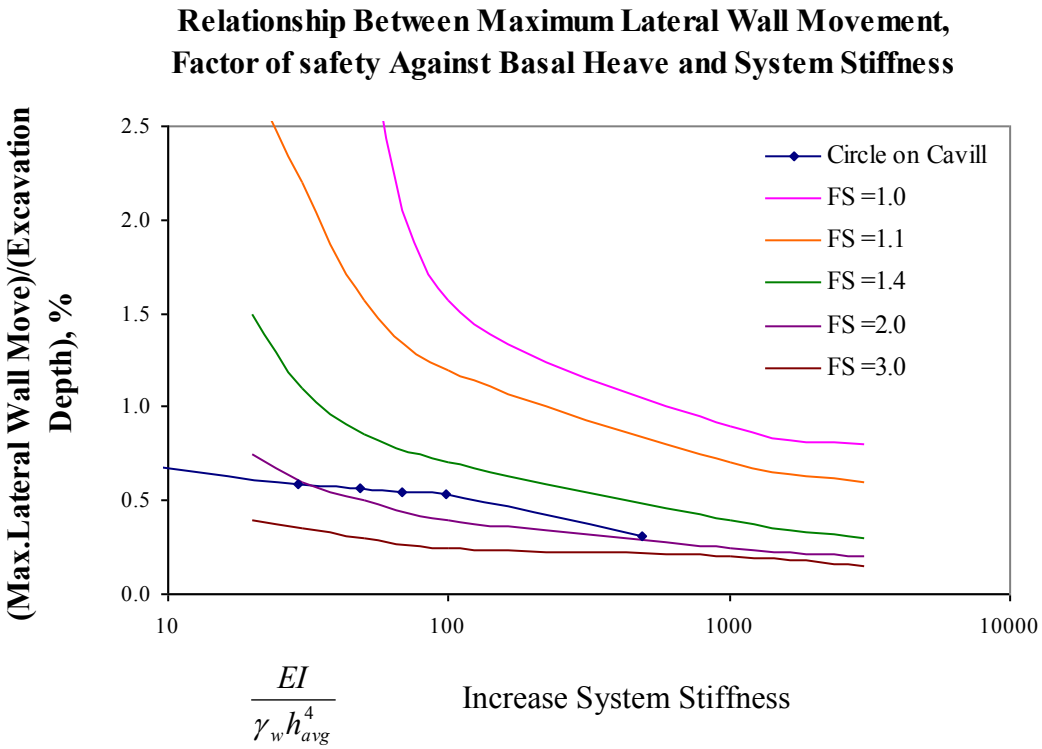

Figure 5.32. Relationship between Maximum Lateral Wall Movement, Factor of safety Against Basal Heave and System Stiffness (Circle on Cavill).

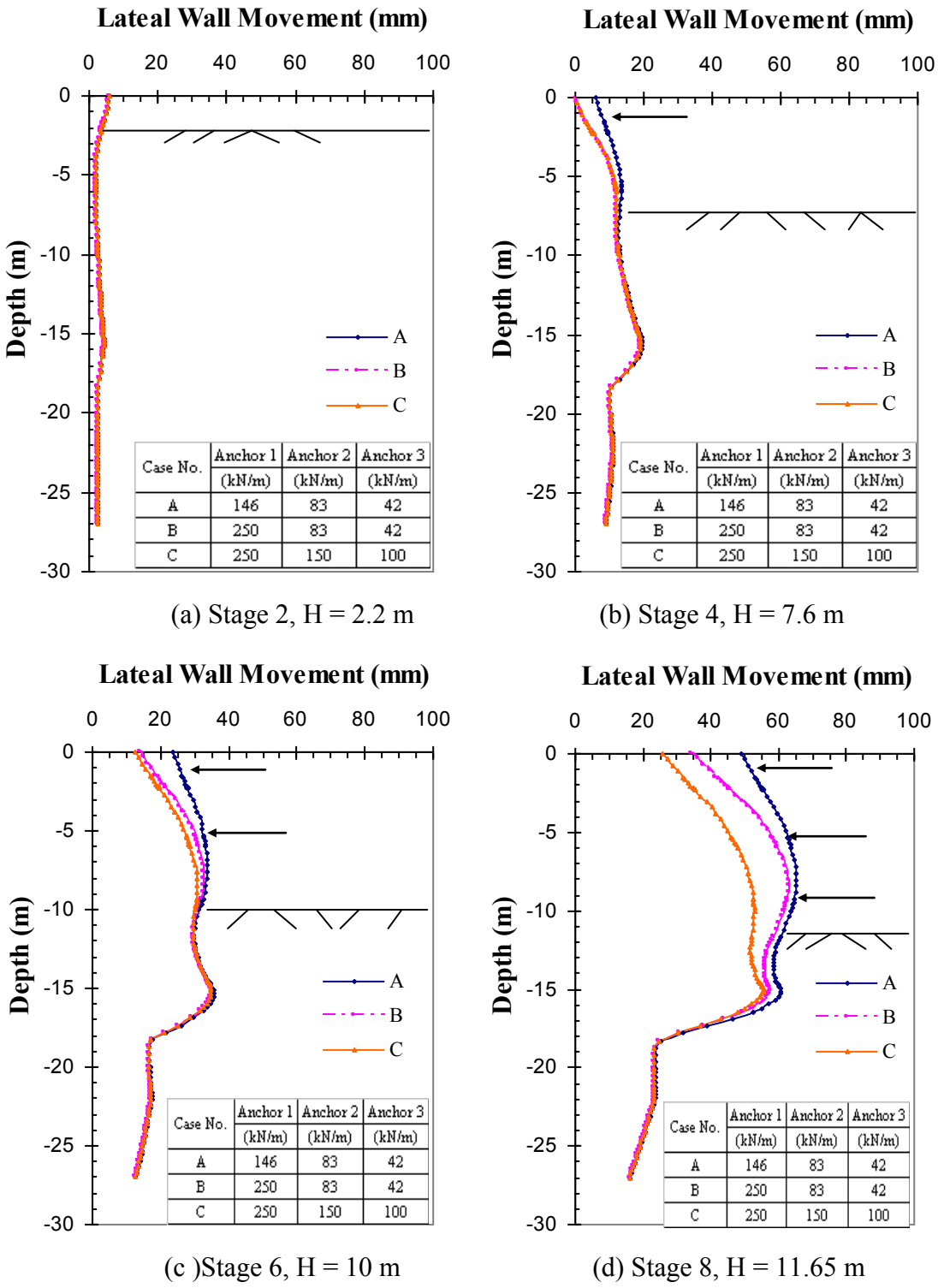

(a) Stage 2, H = 2.2 m

(b) Stage 4, H = 7.6 m

(c)Stage 6, H = 10 m

(d) Stage 8, H = 11.65 m

Figure 5.33(a) ~(d). Effects of Pre-stress of Anchors on Lateral Wall Movement at final stage (Circle on Cavill).

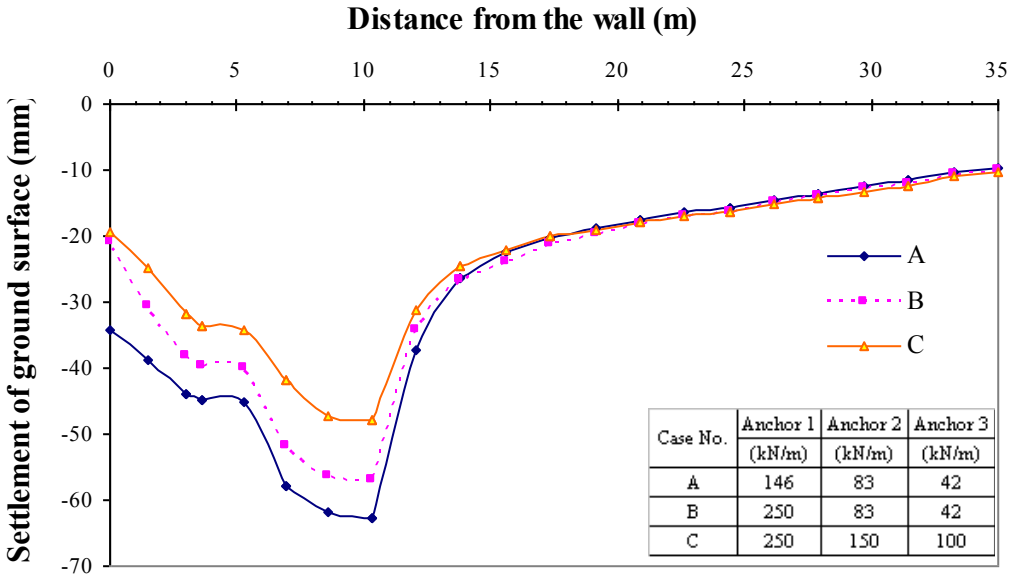

Figure 5.34 Effects of Pre-stress of Anchors on Settlement of Ground Surface at final stage (Circle on Cavill).

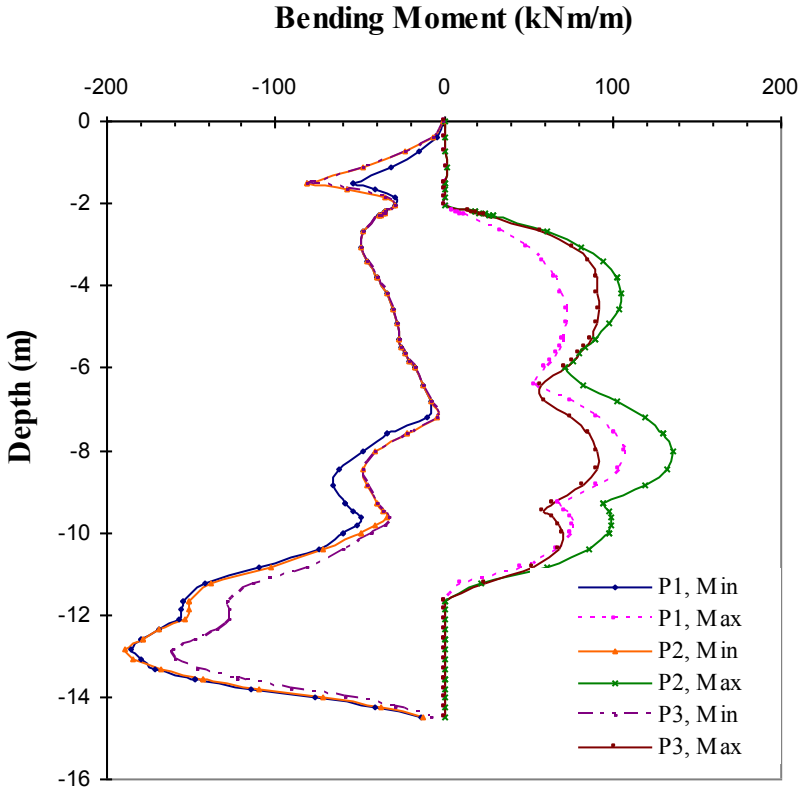

Figure 5.35. Effects of Pre-stress of Anchors on Envelopes of Bending Moments (Circle on Cavill).

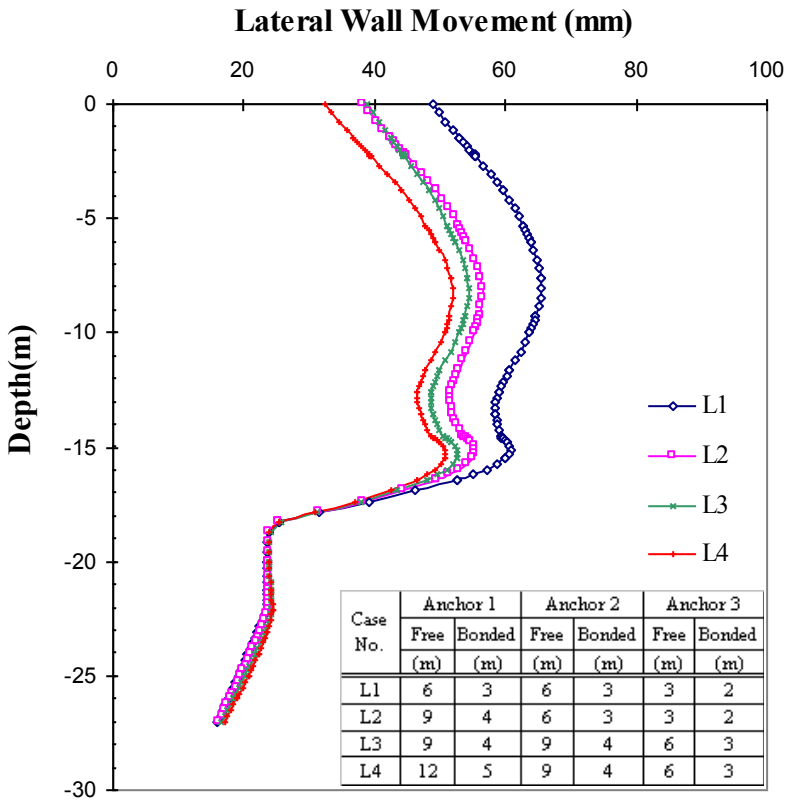

Case No.	Anchor 1		Anchor 2		Anchor 3	
	Free (m)	Bonded (m)	Free (m)	Bonded (m)	Free (m)	Bonded (m)
L1	6	3	6	3	3	2
L2	9	4	6	3	3	2
L3	9	4	9	4	6	3
L4	12	5	9	4	6	3

Figure 5.36. Effects of Anchor Length on Lateral Wall Movement (Circle on Cavill)

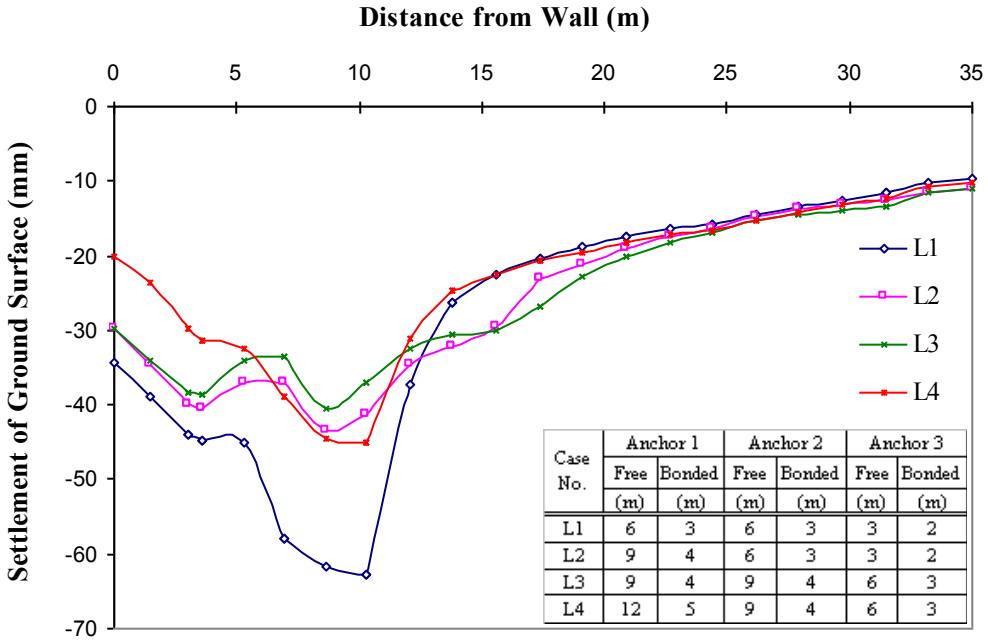

Case No.	Anchor 1		Anchor 2		Anchor 3	
	Free (m)	Bonded (m)	Free (m)	Bonded (m)	Free (m)	Bonded (m)
L1	6	3	6	3	3	2
L2	9	4	6	3	3	2
L3	9	4	9	4	6	3
L4	12	5	9	4	6	3

Figure 5.37. Effects of Anchor Lengths on Settlement of Ground Surface (Circle on Cavill).

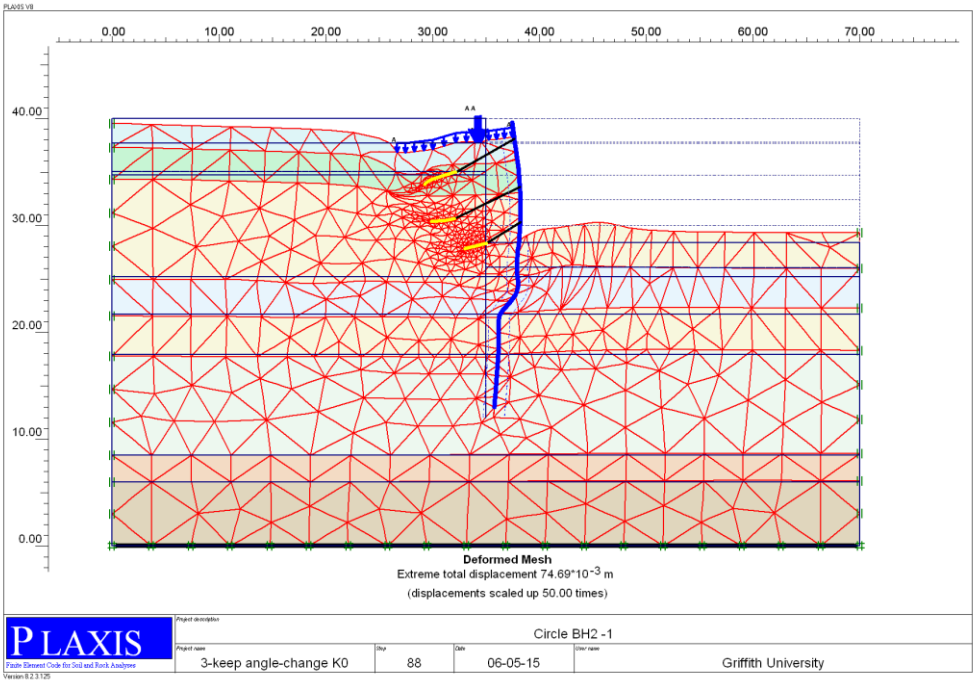

Figure 5.1a Deformed Mesh (Circle on Cavill)
(Topper Pile-1 is reinforced, and lower Pile-2 is only concrete pile)
(Extreme total displacement is 74.69 mm)

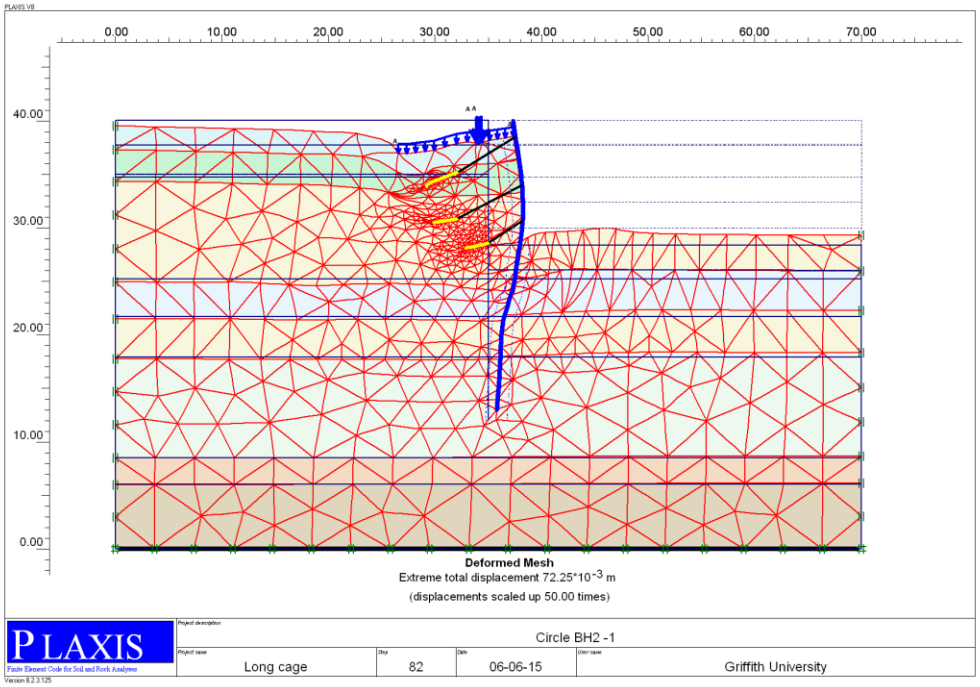

Figure 5.1a Deformed Mesh for whole-length reinforced wall (Circle on Cavill)
(Extreme total displacement = 72.25 mm)

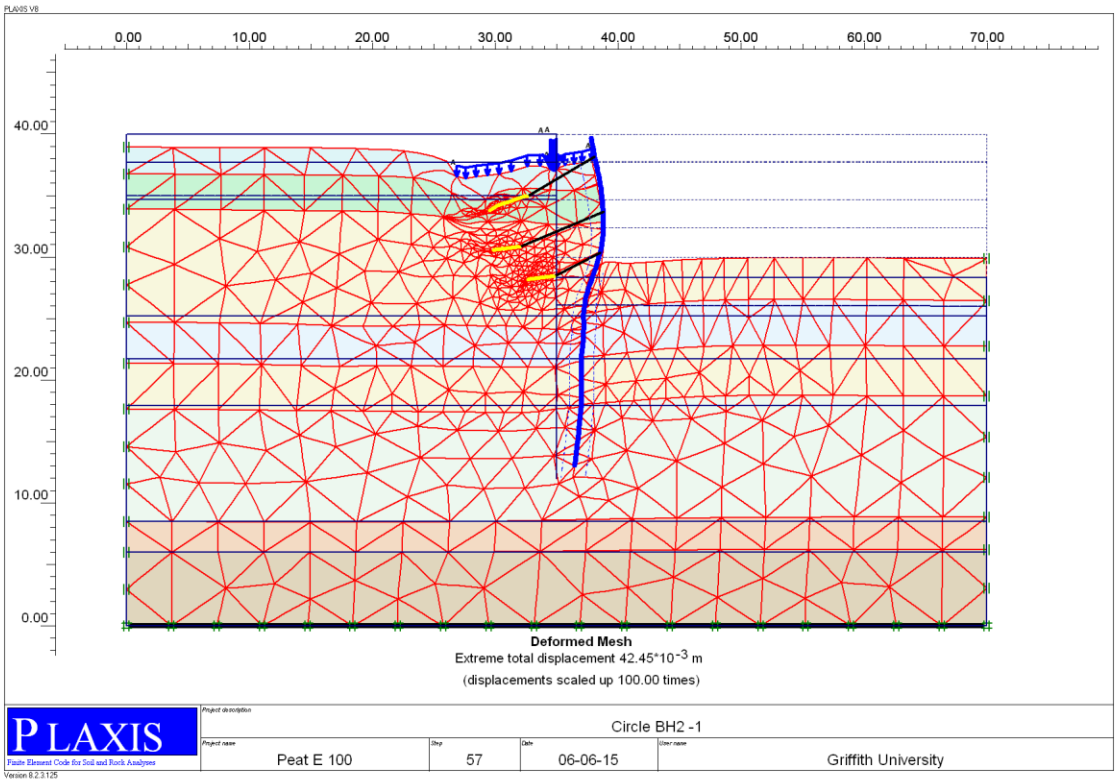

Figure . Deformed mesh when young's modulus of peat is 100 Mpa (Circle on Cavill)
(Topper Pile-1 is reinforced, and lower Pile-2 is only concrete pile)
(Extreme total displacement = 42.45 mm)

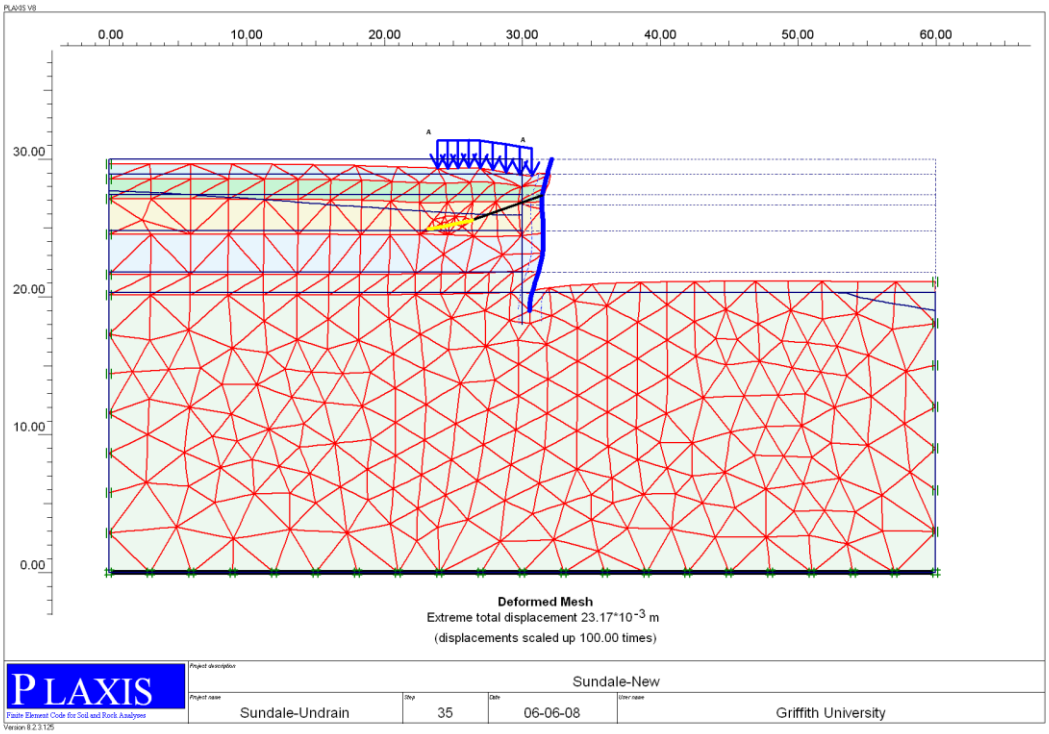

Figure 5.1b Deformed Mesh for Sundale project

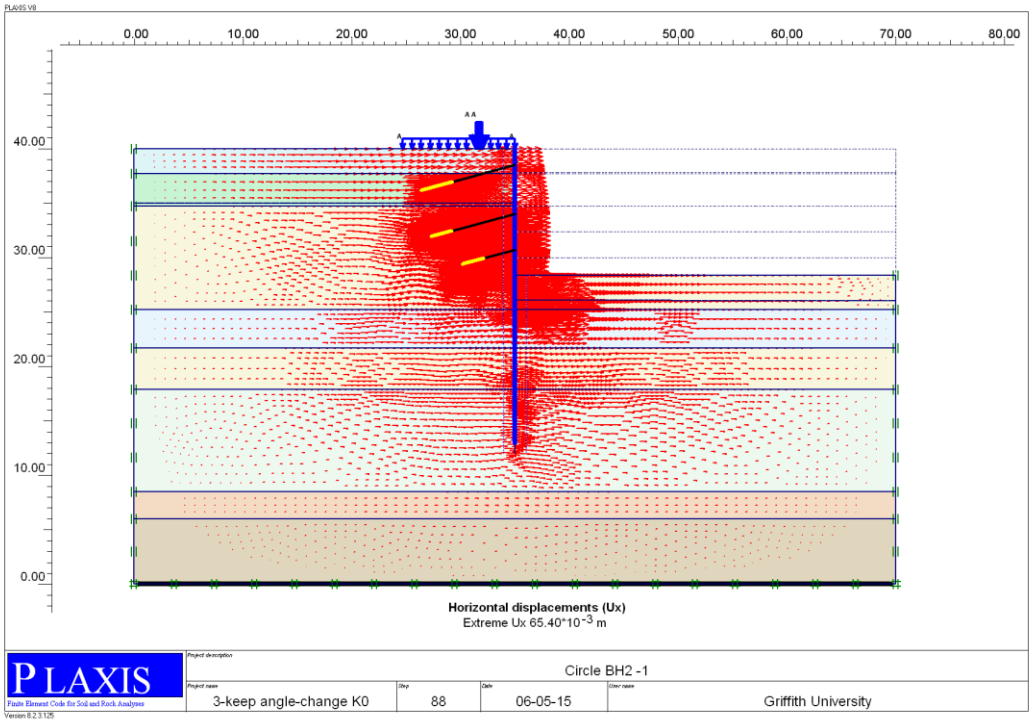

Figure 5.2a. Horizontal displacement for Circle on Cavill project

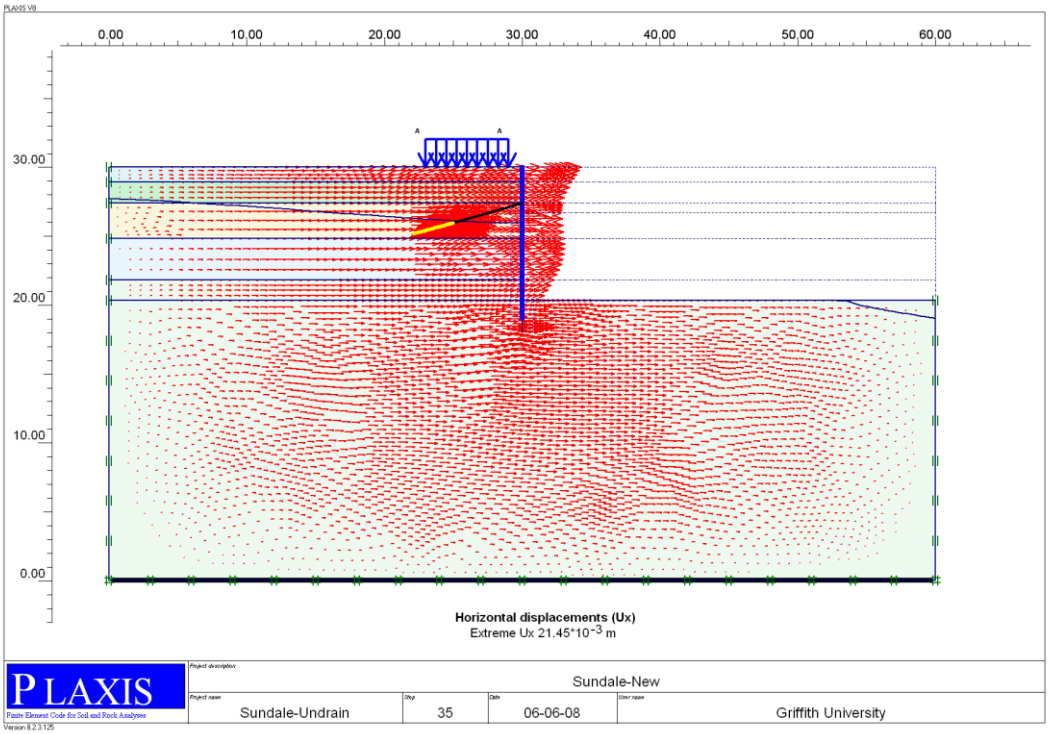

Figure 5.2b. Horizontal displacement for Sundale project.

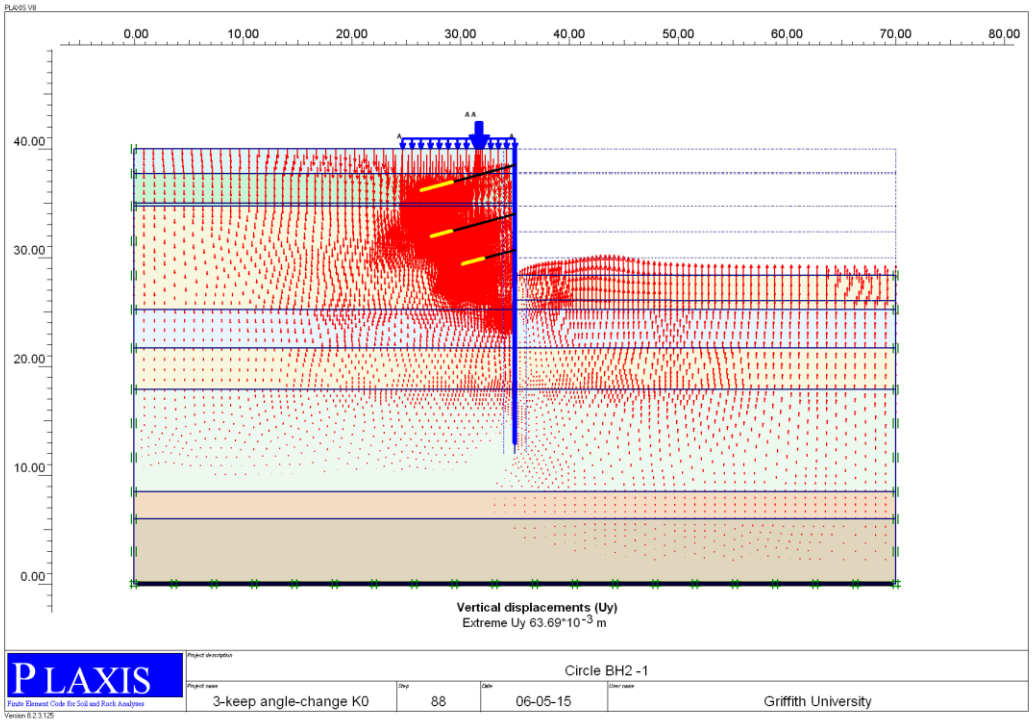

Figure 5.3a Vertical displacement for Circle on Cavill project.

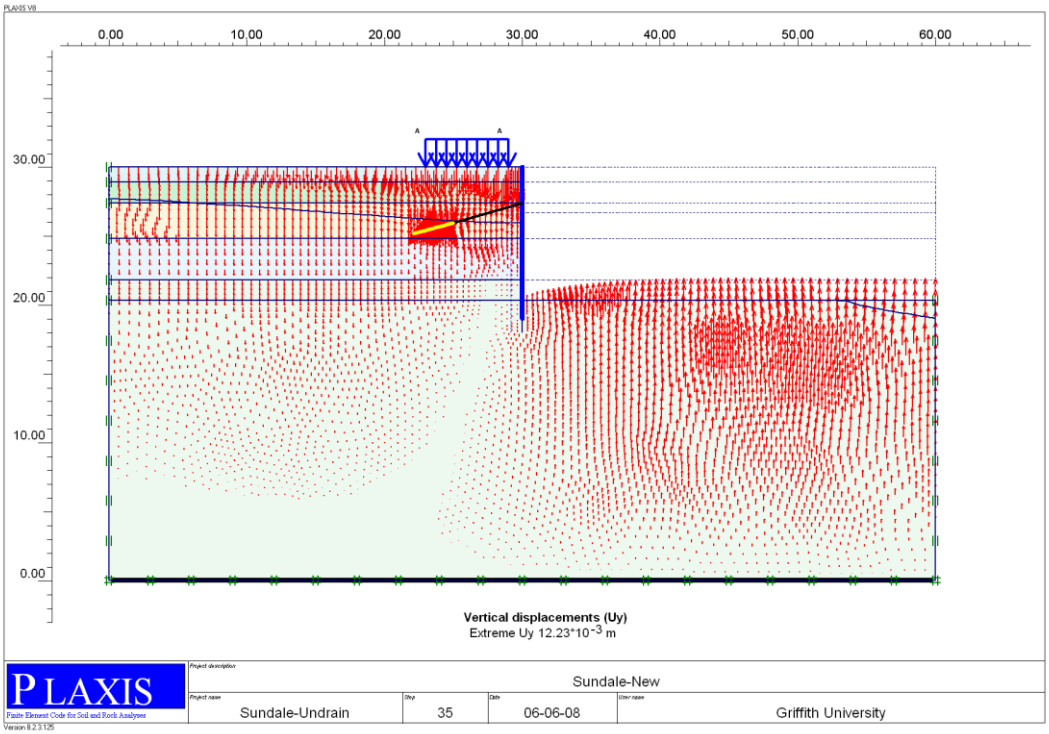

Figure 5.3b Vertical displacement for Sundale project.

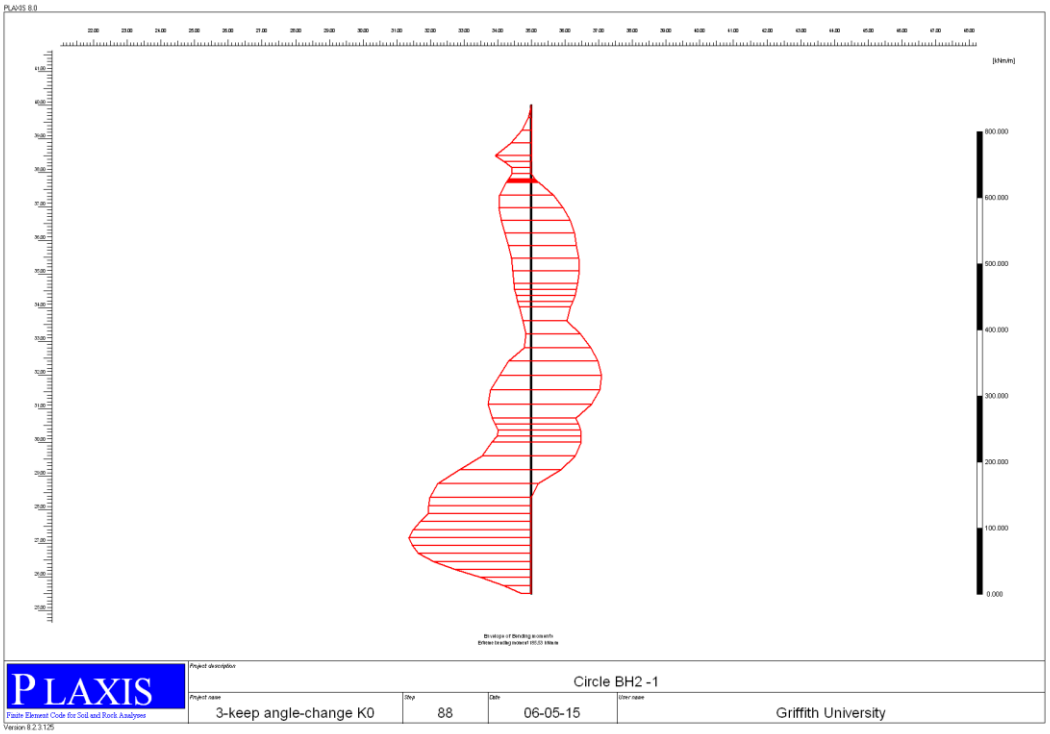

Figure 5.4a Envelopes of bending moments for Circle on Cavill
(Extreme bending moment = 185.53 kNm/m)

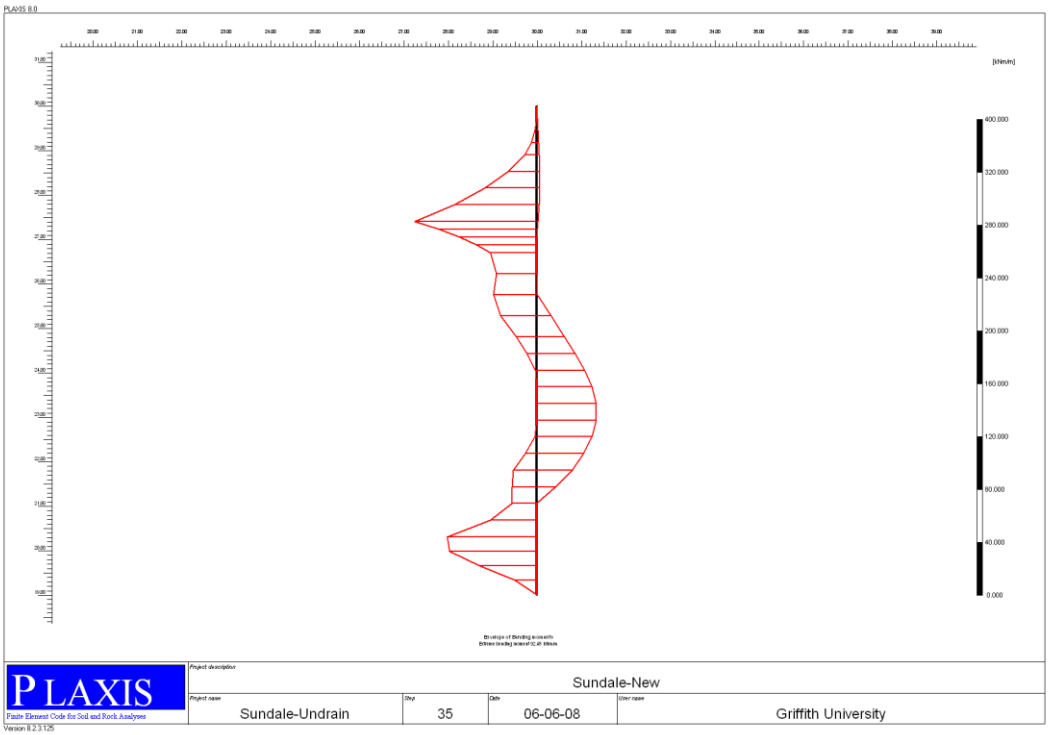

Figure 5.4b Envelopes of bending moments for Sundale
(Extreme bending moment = 92.48 kNm/m)

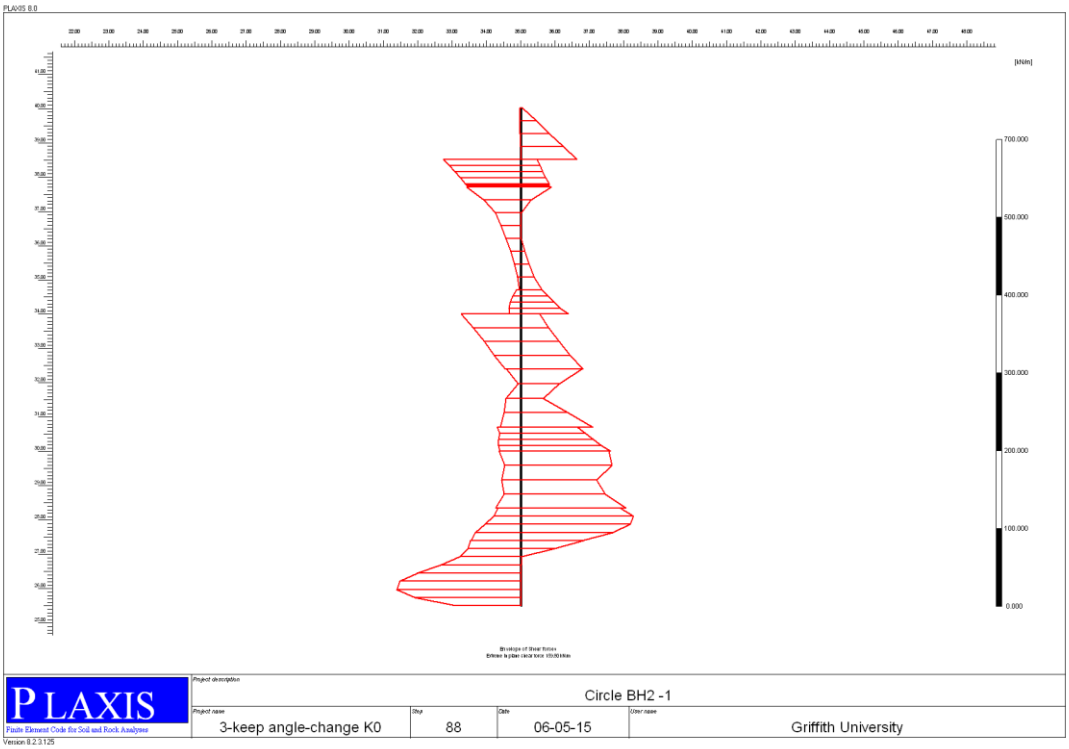

Figure 5.5a Envelopes of shear forces for Circle on Cavill
(Extreme shear force = 159.81 kN/m)

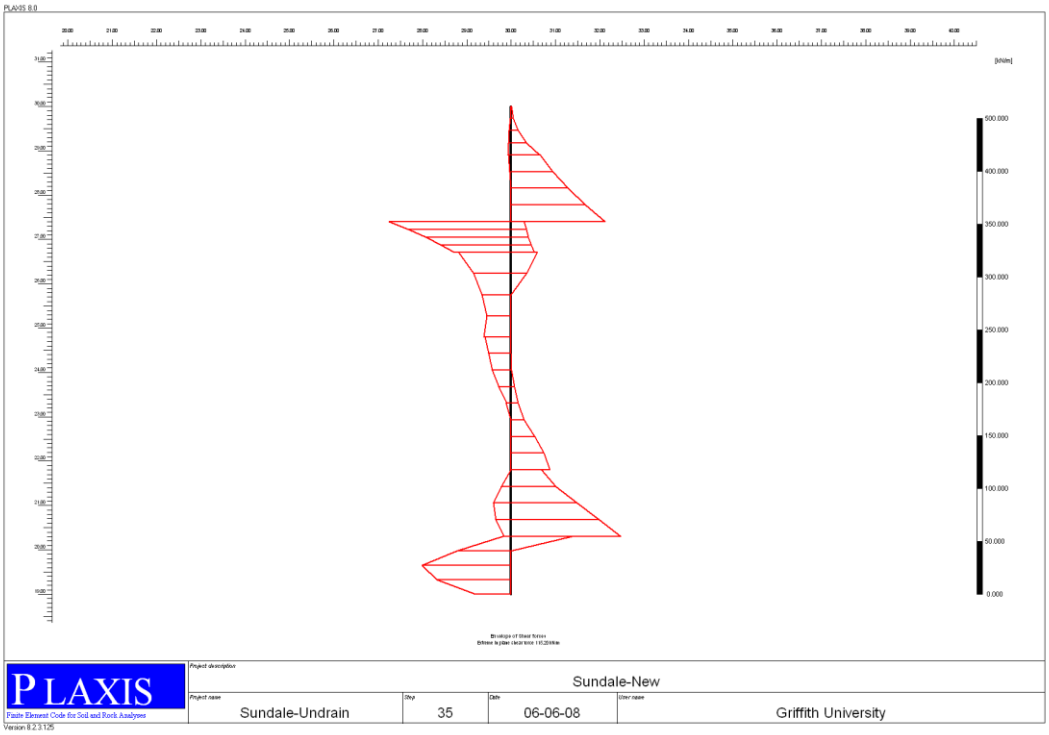

Figure 5.5b Envelopes of shear forces for Sundale
(Extreme shear force = 115.2 kN/m)

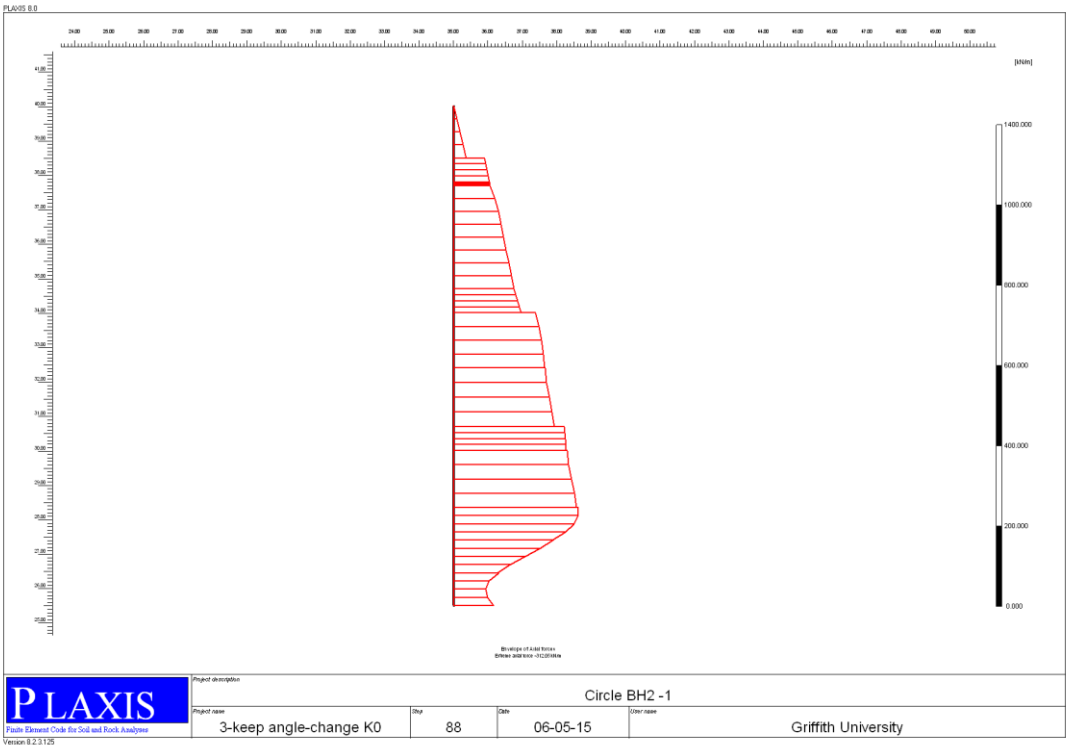

Figure 5.6a Envelopes of Axial Forces for Circle on Cavill

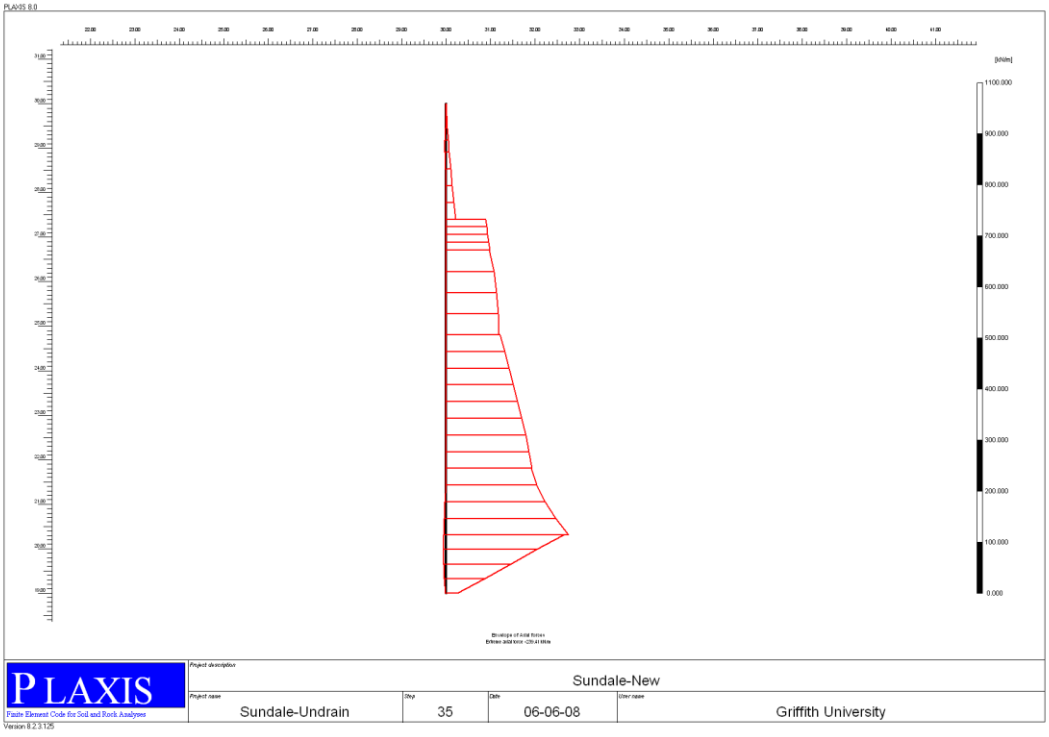

Figure 5.6b Envelopes of Axial Forces for Sundale
(Extreme Axial Force = - 239.41 kN/m)

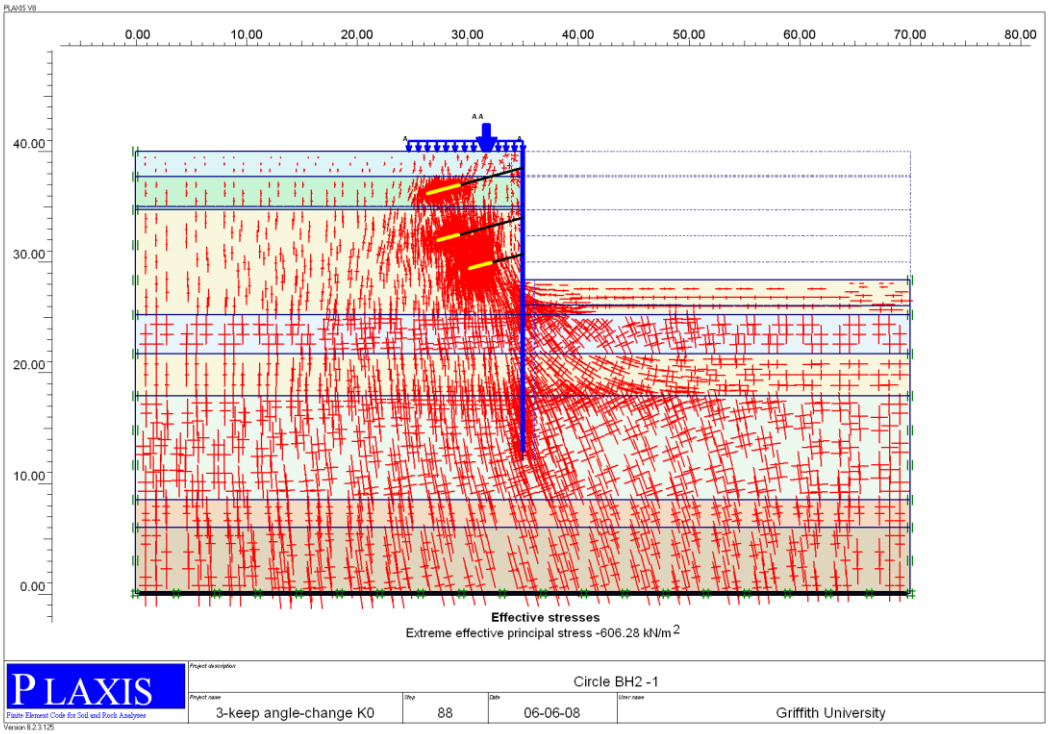

Figure 5.7a. Effective stress for Circle on Cavill
(Extreme effective stress = -606.28 kN/m^2)

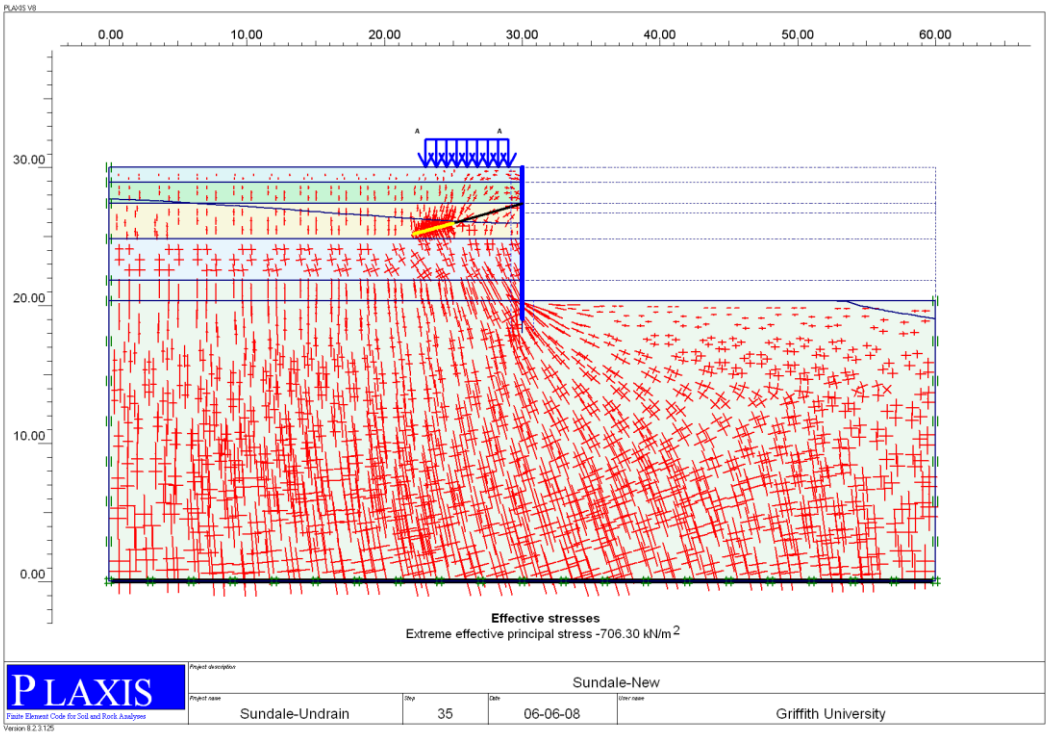

Figure 5.7b. Effective stress for Sundale project
(Extreme effective stress = -706.3 kN/m^2)

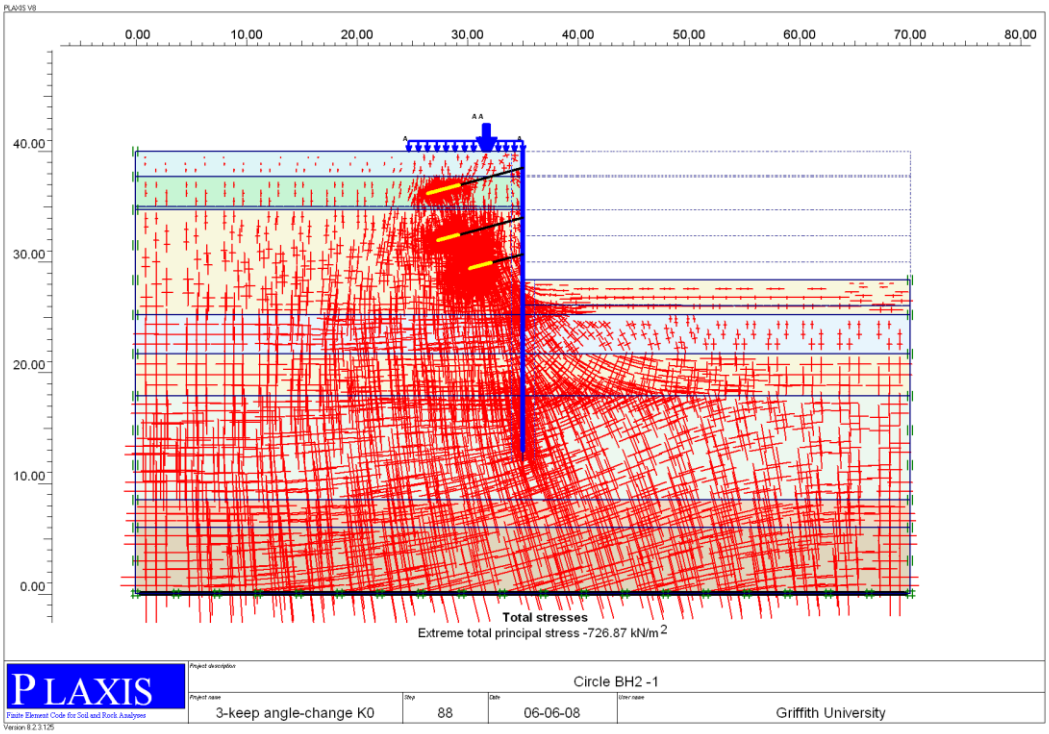

Figure 5.8a Total stresses for Circle on Cavill
(Extreme total principal stress = -726.87 kN/m^2)

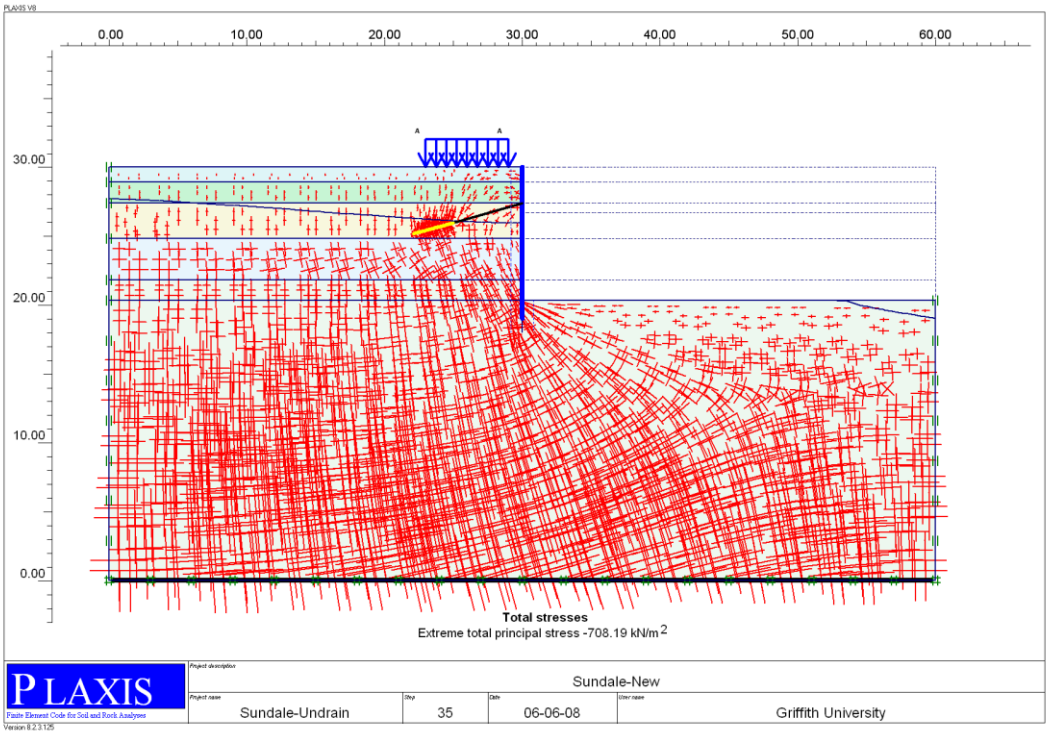

Figure 5.8b. Total stress distribution for Sundale project
(Extreme total principal stress = -708.19 kN/m^2)

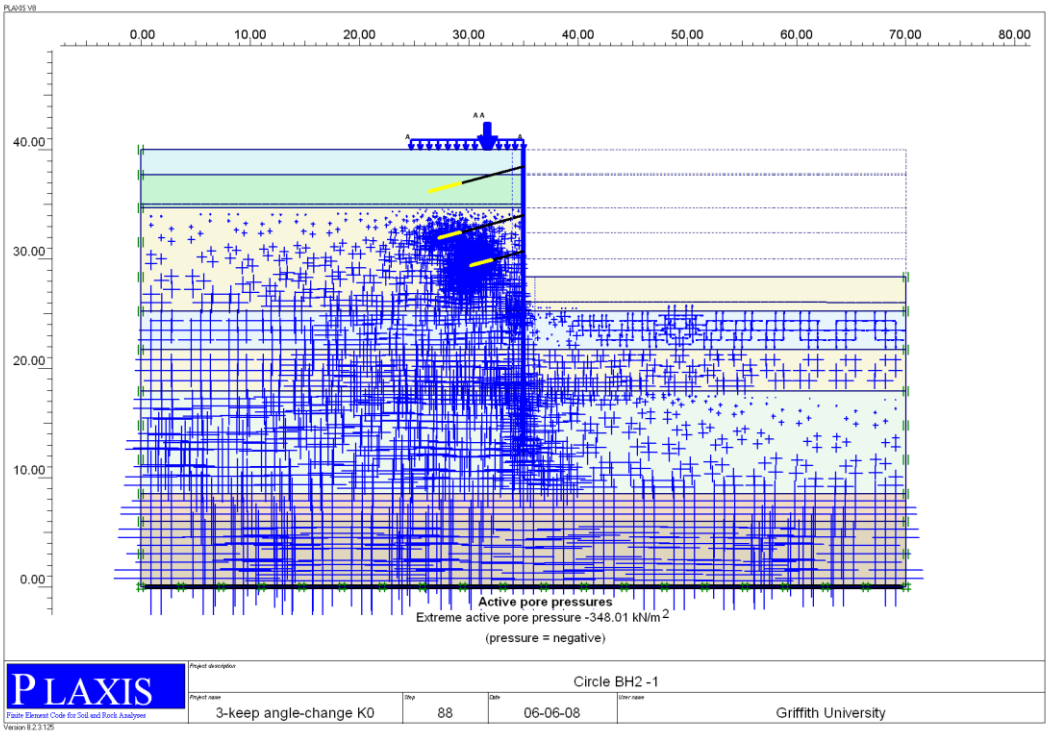

Figure 5.9a. Active pore pressures for Circle on Cavill
(Extreme active pore pressure = -348.01 kN/m^2)

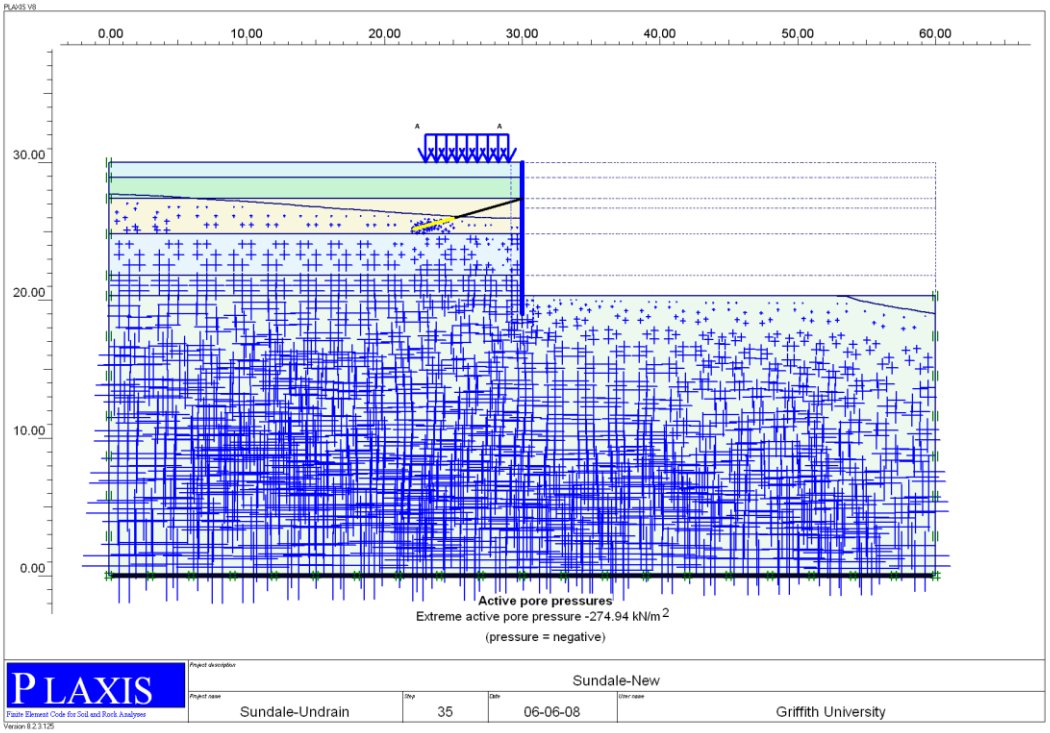

Figure5.9b. Active pore pressure for Sundale project
(Extreme active pressure = -274.94 kN/m^2)

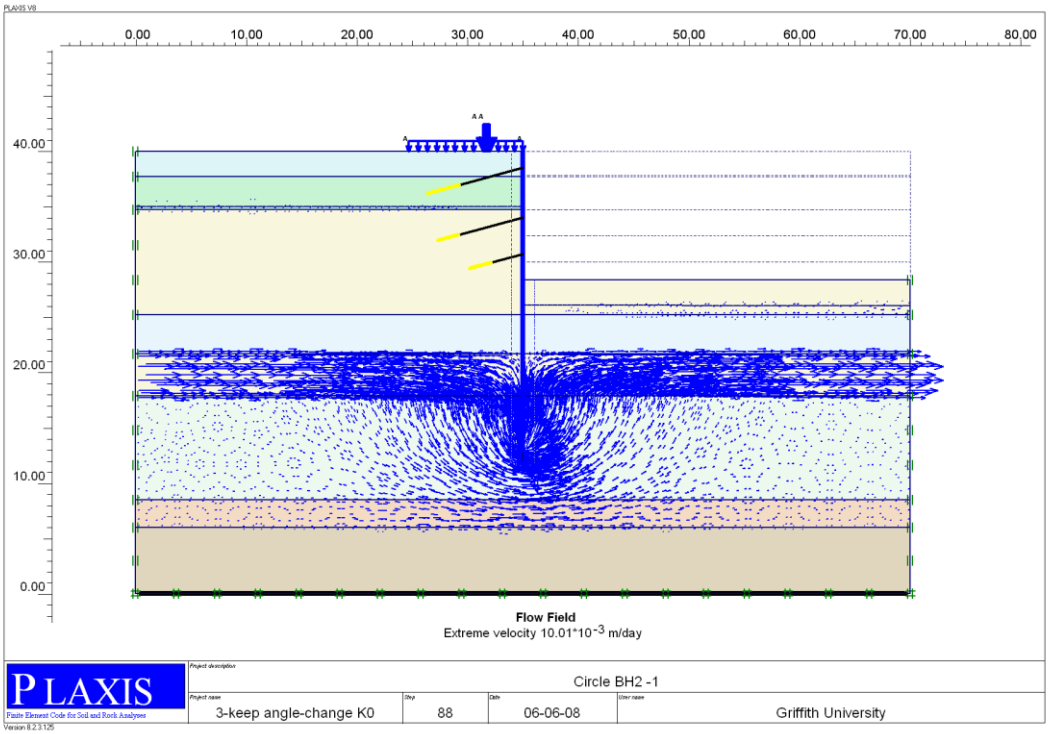

Figure 5.10a. Flow field for Circle on Cavill
(Extreme velocity = 10.01 mm/day)

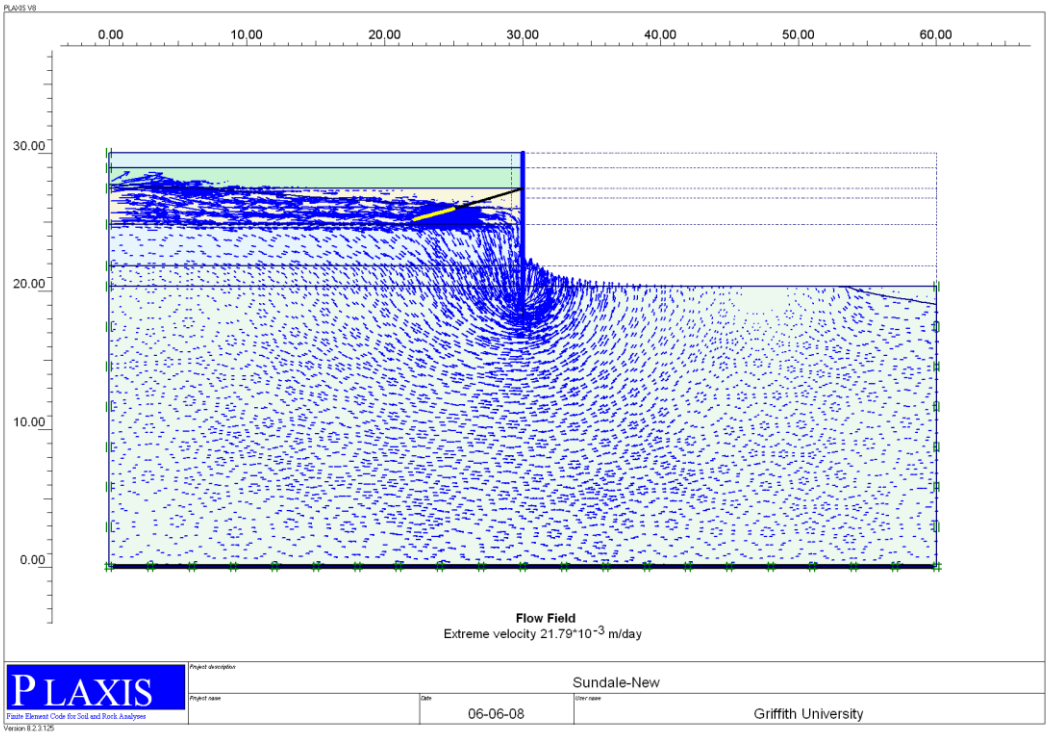

Figure10b. Flow field for Sundale project
(Extreme velocity = 29.47 mm/ day)